THE
PHYSICAL REVIEW
A journal of experimental and theoretical physics established by E. L. Nichols in 1893

VOL. 61, NOS. 9 AND 10 MAY 1 AND 15, 1942 SECOND SERIES

Multiple Secondary Effects of the Penetrating Cosmic Radiation at Sea Level

PIERRE AUGER* AND JEAN DAUDIN
University of Paris, France
(Received January 22, 1942)

The production of multiple secondary particles by cosmic rays under thick layers of lead has been studied with coincidence counters and with a cloud chamber. Part of the coincidences obtained under 15 cm of lead is attributed to groups of particles of atmospheric origin associated with extensive showers. The other part is due to a local effect produced in the lead by single penetrating particles. Among the particles emitted in these processes, some have the penetrating power of low energy mesons.

INTRODUCTION

IT is well known[1] that some showers contain penetrating particles and that showers can be produced by the penetrating part of the cosmic radiation observed in the low atmosphere. The tail of the Rossi curve is due to showers produced by particles which have penetrated more than ten centimeters of lead. Showers observed under ground have their direct or indirect origin in the penetrating component of cosmic rays. Nevertheless, the exact relation between penetrating rays and showers is not completely understood. Some information has been obtained in the following experiments by the use of simple geometrical arrangements of coincidence counters and of a cloud chamber.

It has been admitted here that the particles responsible for the counts were only electrons and mesons, and that the distinction between them had to be based on their absorption and their cascade shower production. An electron of high energy, which is able, for instance, to penetrate ten centimeters of lead, is always accompanied by a shower in the atmosphere as well as in lead, and is most probably associated with an extensive shower. On the contrary a meson generally has a high penetrating power without being associated with electrons in free air, and gives rise to showers, with an appreciable probability, only in dense media.

The principal aim here has therefore been the study of the "accompaniment" of the particles responsible for secondary effects, that is to say the number of electrons and photons arriving simultaneously in their close neighborhood (ordinary local showers) or at a distance of a few meters (extensive, or *A* showers).[2] The geometrical characteristics of the secondary effects produced have also been analyzed.

GENERAL ARRANGEMENTS

The counters had an argon-hydrogen filling, and an effective surface of about 100 cm² when

* Research Associate at the University of Chicago.

[1] See, for instance, P. Auger, P. Ehrenfest, A. Fréon, and R. Maze, J. de Phys. **10**, 1 (1939); G. Wataghin, M. D. de Souza Santos, and P. A. Pompeia, Phys. Rev. **57**, 61 (1940); L. Janossy and P. Ingleby, Nature **145**, 511 (1940); Josephson, Froman, and Stearns, Phys. Rev. **57**, 335 (1940); P. Auger and J. Daudin, Comptes rendus **212**, 24 (1941); etc.

[2] The extensive showers of the atmosphere will be referred to as *A* showers. See P. Auger, R. Maze, and T. Grivet-Meyer, Comptes rendus **206**, 1791 (1938); P. Auger, R. Maze, and A. Fréon, J. de Phys. **10**, 39 (1939).

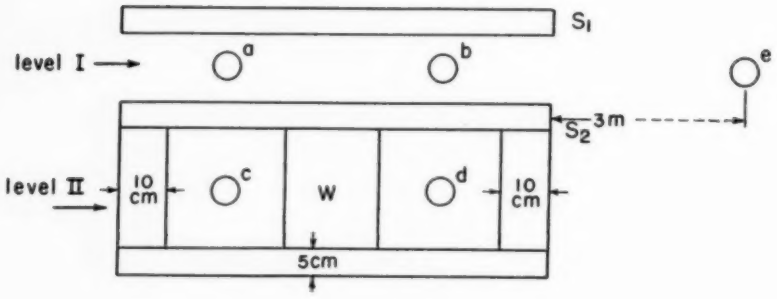

FIG. 1. Arrangement of counters and screens in the absorption measurements on local air showers and on A showers.

horizontal. The coincidence system was of the Maze type. The cloud chamber, originally devised by P. Ehrenfest, had a surface of 28×18 cm and a depth of 3 cm. Most of the experimental work was done by J. Daudin, and details will be published by him later on.

The counters were placed on two horizontal planes marked I and II (Fig. 1) separated by a vertical distance of 25 cm; lead screens could be placed above level I (screen S_1) and between I and II (screen S_2). Lateral protection and protection of the counters from below, on level II, was realized by walls 10 cm thick and by a bottom shield 5 cm thick. A lead wall W could be placed between the counters at level II. When A showers had to be counted, a supplementary unshielded counter was added at level I, from 3 to 5 meters distant. The surface of the counters was sometimes doubled by connecting two of them in parallel. This arrangement will be indicated by the symbol (×2). All these arrangements have been considerably modified in the last set of experiments here described.

ABSORPTION EXPERIMENTS. AIR SHOWERS

Experiments were first made on the penetrating part of ordinary local air showers and of A showers. These two kinds of showers were defined by the coincidences of two unshielded counters in level I, these counters being 5 cm to 20 cm distant (a, b) in one case or 5 m distant (a, e) in the other.

(a) A local shower being defined by the coincidences between the two unshielded counters a b in level I, the triple coincidences with counter c (×2) in level II were measured as a function of the thickness of the interposed screen S_2. The distance between a and b was 5 cm in series 1 and 20 cm in series 2 and 3. The results are shown in Table I and on Fig. 2, curves I, II, III, in which N_3 (number of triple coincidences per hour) is plotted on a logarithmic scale.[3]

(b) An A shower being defined by the coincidence of counters a, b with a third one, e (×2) placed at 3-meters distance, the quadruple coincidences with counter c in level II were measured as a function of the thickness of screen S_2. The results are given in Fig. 2, curve IV, where three separate series are indicated, and in Table II, where only the mean values of the three series are given.

(c) The correlation of the local showers which contain penetrating particles with A showers can

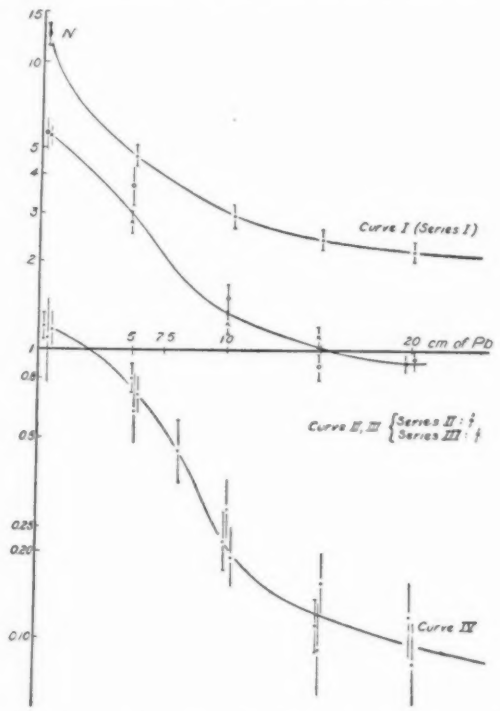

FIG. 2. Absorption curves for local air showers and for A showers. N is the number of coincidences per hour.

[3] The symbols N_3 and N_4 will mean, respectively, "triple coincidences per hour" and "quadruple coincidences per hour" in this paper.

TABLE I. Absorption of local air showers in lead.

Thickness of screen S_2(cm)		0	5	10	15	20
N_3 (a b c)	Series I	12.2±1	4.7 ±0.4	2.9 ±0.2	2.4 ±0.2	2.2 ±0.15
	Series II	5.6±0.8	3.7 ±0.5	1.52±0.18	0.91±0.1	0.95±0.07
	Series III	5.5±0.4	2.74±0.2	1.24±0.11	1.13±0.1	0.91±0.9

TABLE II. Absorption of A showers. Correlation with local air showers.

Thickness of screen S_2(cm)	0	5	10	15	20
N_4 (a b c e)	1.15±0.1	0.73±0.06	0.22±0.05	0.12±0.02	0.10±0.02
Ratio $\frac{N_4\ (a\ b\ c\ e)}{N_3\ (a\ b\ c)}$	0.22	0.23	0.17	0.12	0.09

TABLE III. Coincidences under lead. Correlation with A showers.

Thickness of screen S_2 (cm)	5	10	15
N_3 (a c d)	4.75±0.4	1.8±0.2	1.3±0.1
Ratio $\frac{N_4\ (a\ c\ d\ e)}{N_3\ (a\ c\ d)}$	0.11		0.03

be measured as a function of the minimum penetrating power of these particles, that is to say the thickness of the screen S_2. This correlation is given by the ratio of the number of quadruple coincidences $a\ b\ c\ e$ to the number of triple coincidences $a\ b\ c$. (See Table II, last line.)

Two conclusions can be drawn from these results:

(1) The local air showers, as measured by the triple counts $a\ b\ c$ are markedly more absorbed by the first five centimeters of lead than the single rays which exist at sea level. This shows that local showers contain a greater proportion of electrons and especially of low energy electrons than does the total cosmic radiation at sea level. The narrower showers are the richest in low energy electrons. When the screen S_2 is 20 cm thick, only mesons are responsible for the counts in counter c, directly or indirectly; in this experiment one sixth of the initial number of showers gave a count under that screen.

(2) The A showers, as measured by the quadruple counts $a\ b\ c\ e$, contain also a penetrating part.[2] For the first five centimeters of lead the absorption of A showers is about the same as for single rays at sea level and smaller than for narrow showers. Between 5 cm and 10 cm and even more markedly between 10 cm and 20 cm lead, the absorption is much larger for the A showers than for the ordinary ones. This is probably due to the existence in the A showers of a component of intermediate penetrating power. The nature of this component is complex. Electrons of very high energy are present, a point which has been noticed in our cloud-chamber photographs of A showers; but only slow mesons could explain the existence of particles requiring 20 cm of lead to be stopped.[4] The number of counts under such a screen is equal only to one-twelfth of the number without a screen, thus showing that the A showers contain a smaller proportion of penetrating mesons than the local air showers.

ABSORPTION EXPERIMENTS. SHOWERS UNDER LEAD

Consider now the shower production under lead, in level II. Two counters $c\ d$ are placed at this level, one counter a ($\times 2$) remaining at level I. The interposition of a screen of less than 5 cm brings about an increase of the counts due to the well-known cascade shower production. Between 5-cm and 10-cm screen the fall is quite pronounced, indicating the absorption of the highest energy electrons. After 10 cm the decrease is much smaller, as the mesons are probably the only shower producer able to penetrate these thick screens. Results are given in Table III.

The addition of a distant counter e ($\times 2$) gives an idea of the correlation of the particles responsible for the shower production under lead with A showers. Showers produced under 5 cm of lead give a count in the distant counter in 10 percent of the cases. That means that their producing particles are associated in about 20 percent of the cases with A showers. Showers under a shield of 15 cm show a much smaller association; this is due to the fact that penetrating mesons, which

[4] This points out an analogy of composition between the semi-penetrating part of the A showers in the low atmosphere, and the soft component of the total cosmic radiation at altitudes of 3 or 4 km. In both cases a considerable amount of slow mesons is added to the electrons of high energy.

TABLE IV. Coincidences under varying thickness of upper screen.

Thickness of screen S_1(cm)	0	1	2	5	10
N_3 $(a\,c\,d)$	1.30±0.06	1.33±0.2	1.55±0.15	1.47±0.15	1.28±0.2
Ratio $\frac{N_4\,(a\,b\,c\,d)}{N_3\,(a\,c\,d)}$	0.05	0.09	0.14	0.12	0.15

TABLE V. Coincidences for varying wall thickness.

Thickness of wall (cm)		0	0.5	2	5	10
N_3 $(a\,c\,d)$	Series 1	2.05±0.2	0.85±0.2	0.5 ±0.1	0.42±0.1	
	Series 2	—	—	0.67±0.08	0.47±0.06	
	Series 3	—	—	1.65±0.3	1.13±0.15	0.68±0.1

produce most of the showers under thick screens, are not numerous in A showers.

EXPERIMENTS ON THE PRODUCTION OF SECONDARY ELECTRONS

One of the important properties of the particles studied here is their capacity for electron production. This may be measured in the air by the association of a counter b near the counter a which is, in the preceding arrangement, sensitive to the particles producing showers under lead. The fourfold coincidences $a\,b\,c\,d$ have been actually measured with a geometrical disposition slightly different from that which gives the numbers in Table III, but the figures may well be compared if we try only to find a qualitative indication. The proportion between the quadruples $a\,b\,c\,d$ and the triples $a\,c\,d$ falls from 40 percent with a screen S_2 of 5-cm lead to 17 percent with a screen of 15 cm. The mesons, which play a greater role in the second case, are also less shower producing in air. They have a small accompaniment of electrons.

The capacity of shower production is easier to measure in a lead screen, and a long series of experiments has been made with the interposition of a variable screen S_1 above the counters in level I, the screen S_2 remaining constant (15 cm) and the counters c, d in level II being separated by a wall of 2-cm lead. For each value of the thickness of screen S_1 the triple counts $a\,c\,d$ with one counter at level I and two at level II, and the quadruple counts $a\,b\,c\,d$ with two counters in each level, have been measured. We give in Table IV the values for N_3 (triples $a\,c\,d$ per hour) and the ratio N_4/N_3 (quadruples $a\,b\,c\,d$/triples $a\,c\,d$). The interposition of screen S_1 favors the production of secondary electrons and photons by the primaries which are responsible for the showers in level II. The sensitivity of counter a, and *a fortiori* of two counters $a\,b$, for these primaries is increased; the effect is more marked with two counters in level I, and shows saturation for two centimeters lead (like the ordinary shower curve for penetrating rays).

Consider the number of counts $a\,c\,d$ obtained without shower-producing screen S_1. The addition of counter b (×2) at a distance of about 10 cm leaves 5 percent of the coincidences, showing thus a correlation with local showers which is of the same order of magnitude as the correlation with A showers. (See Table III.) As the mesons have a very poor accompaniment of electrons in free air, it is natural to attribute the quadruple counts $a\,b\,c\,d$ with $S_2=5$ cm lead to electrons of very high energy or to mesons coupled with a shower of electrons. Both of these events are likely to happen only within an A shower. In order to test this conclusion a fifth counter e (×2) has been added at a distance of three meters. This system records quintuple coincidences produced by A showers. The ratio of quintuple counts $a\,b\,c\,d\,e$ to quadruple counts $a\,b\,c\,d$ was as high as 0.50, a value which can be considered only as an order of magnitude because of the small number of counts per hour (0.3 for the quintuple counts with a 5-cm thick shield S_2).

The rate of production of secondary electrons in the screen S_2 by the penetrating radiation associated with showers in air may also be studied. If the air shower is an electronic cascade, the penetrating part will consist of high energy electrons, and will give rise to a dense shower all along its path in the lead. If, on the contrary, the air shower is secondary to a meson, this particle will constitute the penetrating part, and will remain generally single. The measurements were made by the same arrangement as before, with two unshielded counters $a\,b$ at level I and two counters $c\,d$ at level II separated by a wall

of 2-mm lead. The number N_3 of triple counts $a\,b\,c$ and the number N_4 of quadruple counts were measured for different values of the thickness of screen S_2. The ratio $N_4(a\,b\,c\,d)/N_3(a\,b\,c)$ gives the probability for the second counter under lead d to be touched by the penetrating part of the air shower detected by $a\,b$. This probability is as high as 0.25 with a 5-cm screen and decreases to 0.10 with a screen of 15 cm. If there is no screen S_2 at all, the ratio N_4/N_3 reaches 0.40. This value is a consequence of the high density of the air showers selected by a system of three counters. The important part played by the electronic penetrating showers in the case of small thicknesses of lead, and the prominent role of mesons in the shower production under 15-cm lead are clearly shown by these results.

ORIGIN OF THE SHOWERS UNDER LEAD

In the preceding analysis we have admitted that only two types of showers containing a penetrating part were present: electronic cascades of very high energy, associated with showers, and showers of electrons more or less directly produced by a meson. Another possibility, already suggested by different authors, would be found in the existence of showers of mesons, or at least pairs of mesons, created in the atmosphere or in the lead. In order to study the relative importance of these processes, several experiments were made with an arrangement of counters slightly more complicated. The level II was occupied by two chambers separated by a wall W and each containing two counters (Fig. 3). The influence of the thickness of the wall and of the screen S_2, of the disposition of counters in level II and in level I have been studied.

(A) Influence of Wall W

Three counters, a in level I, c and d in level II were used; the screen S_2 was 10 cm thick, and the thickness of the wall W could be varied from 0 to 5 cm. The results of three series of measurements are given in Table V. In series 3 the arrangement of counters was modified in order to increase the number of counts. The number of triple coincidences decreases very strongly when 5 mm of lead are interposed between the counters $c\,d$. This points out the existence of a large number of electrons of small energy emitted in very oblique directions, presumably in knock-on showers. The decrease continues when the wall thickness is increased to 2 cm showing the existence of electrons of higher energy; the role of the photons of 10^7 ev, which have a relatively high penetrating power, is also important in these circumstances. But the surprising fact is that an increase of the wall thickness up to 5 cm brings a diminution of about 30 percent of the counts, and that an additional 5 cm determines a reduction of the same order. This means that some of the oblique particles emitted have a penetrating power which is not compatible with an electronic or a photonic nature. The role of multiple penetrating particles coming from the air must be small. It is here limited to the production of the coincidences which are insensitive to the increase of thickness of the wall. They cannot be responsible for more than 25 percent of the effect observed with a 2-cm wall.

(B) Multiple Penetrating Particles from the Air

A fourth counter b ($\times 2$) was added on level I. When this counter was situated in b_2 just above d the arrangement could be considered as specially sensitive to parallel penetrating particles coming from the air. Table VI shows that the ratio of quadruple counts $a\,b_2\,c\,d$ to triple counts $a\,c\,d$ increases when the thickness of the wall is increased from 0 to 5 cm. When counter b was situated in b_1, thus necessitating three particles, the ratio $N_4(a\,b_1\,c\,d)/N_3(a\,c\,d)$ was notably reduced.

Since the number of quadruple counts per hour are very small in these arrangements, (0.2 with

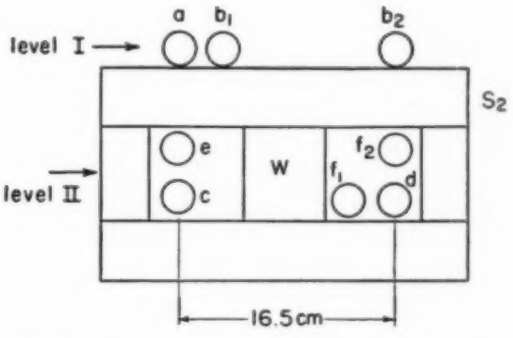

FIG. 3. Arrangement of counters for the detection of simultaneous penetrating particles.

TABLE VI. Ratio of triple and quadruple coincidences for varying wall thickness, and different counter arrangement.

Thickness of wall W (cm)	0	2	5
$N_4\,(a\,b_2\,c\,d)/N_3\,(a\,c\,d)$	0.14	0.20	0.45
$N_4\,(a\,b_1\,c\,d)/N_3\,(a\,c\,d)$			0.10

TABLE VII. Triple coincidences under varying screen thickness.

Thickness of screen S_2 (cm)	1	5	10	15
$N_3\,(c\,d\,e)$	12.1±1.5	3.95±0.25	2.88±0.15	2.74±0.12

TABLE VIII. Ratio of triple and quadruple coincidences with different counter arrangements.

Thickness of S_2 (cm)	1	5	10	15
$N_4\,(c\,d\,e\,f_1)/N_3\,(c\,d\,e)$			0.70	0.50
$N_4\,(c\,d\,e\,f_2)/N_3\,(c\,d\,e)$	0.62	0.40	0.34	0.28

the 2-cm wall), the results can be only considered as an indication of the existence of groups of penetrating particles coming from the air. The role of these particles is only important in the production of coincidences between counters under lead (10 cm) when the counters are not too near to one another (15 cm) and are separated by a wall of a few centimeters of lead. This conclusion is in agreement with the results of Wataghin and others [see bibliography, in Phys. Rev. **59**, 902 (1941)].

(C) Characteristics of the Multiple Secondary Effects in Lead

For this study the counters a and b were removed from level I and placed at level II (counters e and f, Fig. 3). First a series of triple counts ($c\,d\,e$) was made with a wall of 5 cm and a variable screen S_2. Table VII shows that after a very quick decrease, due to the absorption of the air showers, there remains a considerable number of coincidences under as much as 15-cm lead (the wall W being 5 cm thick). Also the increase of the wall from 5 to 10 cm, with a screen S_2 of 15 cm, brought a decrease of N_3 from 2.74±0.12 to 1.56±0.2 showing once again the existence of oblique particles with a strong penetrating power.

A fourth counter was then added which could be placed in two different positions f_1 and f_2. The first one was favorable to the detection of oblique particles; the second one was favorable to the counting of parallel vertical penetrating rays. In each case the number of quadruple coincidences $N_4(c\,d\,e\,f_1)$ and $N_4(c\,d\,e\,f_2)$ was compared to the number of triple counts $N_3(c\,d\,e)$. The thickness of the screen S was increased from 1 cm to 15 cm; the wall W was maintained 5 cm thick. (See Table VIII.) It can be noted that the proportion of quadruples which are due to vertical parallel rays decreases when the screen increases because of the relatively large absorbability of the high energy electrons which are the ordinary cause of the counts. The proportion of quadrupoles is larger when the counter arrangement is favorable to the detection of oblique particles. When the arrangement is suited for the detection of parallel vertical groups of particles the ratio of quadruple to triple counts decreases continuously when the screen S increases. However, the role of these vertical particles is still important with a screen of 10 cm as is shown by following experiments. The shield S being 10 cm thick, and counter f in position f_2, the thickness of the wall W was increased from 5 cm to 10 cm. The ratio N_4/N_3 increased from 0.29 to 0.77. In the last case most of the coincidences were probably due to showers of electrons of high energy from the air and associated with A showers. The high density of tracks in these showers explains the fact that the probability of the quadruple counts is almost as large as that of the triples.

(D) Evidence of the Existence of a Local Production of Penetrating Particles

The preceding experiments suggest that only one part of the coincidences between counters under lead is due to multiple penetrating particles arriving from the air. The other part would have to be attributed to a local production of multiple secondary particles. Some of them are more penetrating than electrons of reasonable energy and can be identified with slow mesons. These particles would diverge from one or from a few centers situated in the lead and their emission could be provoked by a meson or any other incident particles of high energy. The action of the first process would be related to the A showers where beams of very numerous parallel electrons of high energy are present. It would be favored by smaller thicknesses of the screen S, by greater thicknesses of the wall W, by larger horizontal distances between the counters under

lead, and by their disposition in vertical telescopes (superposition of two or more parallel counters). The second process would be related to more or less isolated particles of great energy, like mesons. It would be more important with thin walls W, thick screens S, when the counters are arranged at random and are not far from one another. The last section of this paper is devoted to the description of experiments especially devised for the study of this local production of secondary penetrating particles.

EXPERIMENTS ON THE PRODUCTION OF PENETRATING PARTICLES

(A) Counter Experiments

The counters were placed inside a large block of lead (Fig. 4) so that three of them constituted a vertical telescope ($b\ c_1\ d$), the fourth a being separated by a wall of 10 cm. This arrangement is favorable to the detection of groups of vertical particles. Then the middle counter of the telescope c was shifted to c_2 where it was outside of the solid angle determined by b and d, so that at least three vertical particles were necessary for a quadruple count. In each case the triple coincidences $a\ b\ d$ and the quadruples $a\ b\ c\ d$ were registered simultaneously and the values of the ratio N_4/N_3 obtained were found practically equivalent (Table IX). This fact, and also the high value of the ratio N_4/N_3, were confirmed by another measurement where the counter c was placed in position c_3.

TABLE IX. Effect of changed position of counter.

Position of counter c	c_1	c_2	c_3	c_4	c_5
$N_4\ (a\ b\ c\ d)/N_3\ (a\ b\ d)$	0.64	0.77	0.42	0.15	0.08

The counter c was then removed outside of the lead block, first in the immediate neighborhood (c_4) then at a distance of 3 m (c_5). The ratio N_4/N_3 fell to a smaller value in the first case, and to an even smaller one in the second (Table IX). These characteristics fit well with the hypothesis of a local secondary effect, as described above. On the other hand, the interpretation by multiple penetrating rays coming from the air would be difficult. These penetrating particles would have to exhibit two simultaneous properties: (1) A high density of tracks all over the area where the counters are situated, in order to explain the high value of the ratio N_4/N_3 in all positions of

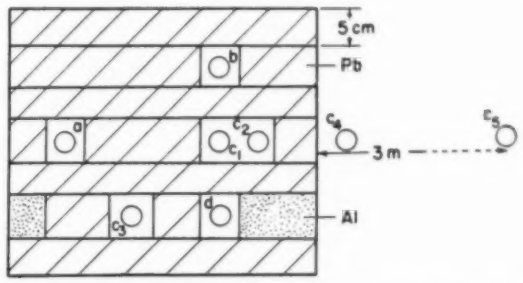

FIG. 4. Detection of local showers of penetrating particles.

counter c inside the lead. (2) A narrow localization in space in order to explain the decrease of the counts when c is displaced outside of the lead.

This localization has been proved also by the following experiment: Three counters are disposed as $a\ b\ c_1$ in Fig. 4. One of them, a, can be placed at a variable distance from its neighbor c_1(the distances are measured between the centers of the counters) and separated by a wall of 5-cm lead. When the distance between a and c_1 is increased from 10 to 16 cm, all other conditions remaining unchanged, the number of triple counts per hour decreases from 2 ± 0.2 to 1.1 ± 0.1. This could be explained only by a narrow beam of parallel particles or by a spread of particles diverging from a center situated in the neighborhood of the counters.

These two kinds of geometrical groupings of tracks are represented in the cascade showers of electrons as they are generally observed, in air and in the presence of a few masses of dense material. This fact explains why the geometrical properties of the effects in lead here described are strangely similar to those of ordinary showers, with the difference that the medium through which the particles move is air in the one case, lead in the other. An experiment in which the counters were arranged as in Fig. 4 but without any lead surrounding gave a counting rate ten times higher than with all the lead, but the ratio of the quadruple against the triple counts decreased from $N_4(a\ b\ c_1\ d)/N_3(a\ b\ d)=0.53$ to $N_4(a\ b\ c_2\ d)/N_3(a\ b\ d)=0.35$ when counter c was shifted. This ratio decreased again down to 0.12 when the distance of c was increased to a few meters.

(B) Cloud-Chamber Experiments

In order to obtain more direct information about the relation between the counts under lead

and the *A* showers, a vertical cloud chamber was placed sideways in close contact with the lead block containing the three coincidence counters which controlled the expansion. Here the counters were disposed vertically, as shown in Fig. 5 (in horizontal projection); they were separated by at least 5 cm of lead from one another and from the chamber; and a lead plate 10 cm thick covered them. No particle touching two of the counters could penetrate the chamber.

A series of 143 photographs was made with the chamber controlled, and a series of 83 was made at random in order to check the results. After a careful examination of the tracks recorded, the pictures could be classified as follows:

Type of pictures	Number of pictures: Controlled	Random
I Shower of more than 3 particles, not much inclined to the vertical	13	0
II One good track, nearly horizontal and crossing the lead block	11	1
One dubious track of the same type	7	7
A pair of tracks of the same type originating from the lead block	3	0
III Two, one, or no tracks of particles of ordinary type, distributed as follows:	109	75
Two tracks	10%	12%
One track	33%	33%
No track	57%	55%

The first type is due to concentrated air showers, probably parts of *A* showers, and their presence in the controlled photographs is a new evidence of the existence of a penetrating part in these showers.

The frequency of horizontal or of very oblique tracks (type II) is much higher when the chamber is controlled than it is in random operations. These tracks are due mostly to particles issuing from the lead block, and are associated with the secondary processes taking place in the lead and responsible for the controlling coincidence. The number of pictures of types I and II relative to the total of controlled records is in good agreement with the results of the counter experiments

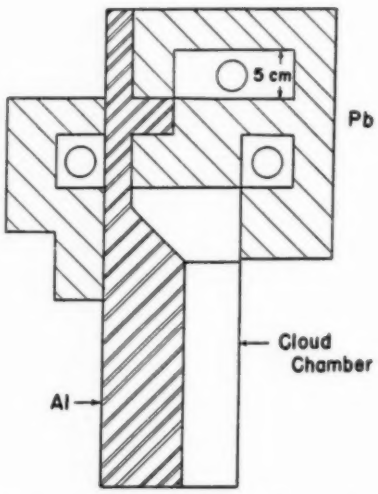

FIG. 5. Arrangement of cloud chamber and controlling counters, in vertical projection.

with counter c in position c_4, (Fig. 4), as given in Table IX. A direct experiment was also made with the chamber removed and replaced by a counter.

The pictures in the third group are identical in aspect and in relative numbers (records with one, two, or no tracks) in both series of controlled and random operations. The tracks recorded have generally nothing to do with the cause of the coincidence, and their number is due to the fact that the resolving power of the cloud chamber is much smaller than that of the counter set. So most of the coincidences between the three counters in the lead block are due to a local phenomenon taking place in the lead and probably caused by a single initial particle.

If the oblique tracks in group II are really due to some of the particles emitted in this local process and which have been able to emerge outside from the lead, it would be interesting to get some information about their nature. The fact that they appear single or in pairs of notable divergence suggests that they are mesons. This hypothesis is in agreement with the penetrating power of some of the oblique particles as measured in the wall *W*.

Cloud-Chamber Photographs at 4310 Meters Altitude

W. H. Bostick
Ryerson Physical Laboratory, University of Chicago, Chicago, Illinois
(Received December 1, 1941)

Cloud-chamber photographs taken at 4310 meters altitude give evidence for the existence of penetrating particles in air showers. Out of 2983 successful expansions 5.8 percent showed particles classified either as slow mesotrons or slow protons. 1.3 percent of the expansions show particles whose specific ionization increases markedly on passing through a 1.3-cm lead plate in the chamber. Twenty-seven photographs show penetrating pairs and thus indicate the production of penetrating secondaries at this altitude. Some photographs give evidence for nuclear processes associated with showers. Five photographs show electrons which may have come from the disintegration of mesotrons within the chamber.

IN connection with a cosmic-ray expedition sent from the University of Chicago to Mt. Evans in August, 1940, the author took a series of cloud-chamber photographs. It was hoped by these experiments to confirm the existence of penetrating particles believed from previous counter tube observations to be present in large air showers. It was also desired to obtain data on the number of heavily ionizing cosmic-ray particles and on the number of particles generated and stopped in a lead plate in the chamber.

The equipment consisted of a cloud chamber, counter controlled by any of the two-, three-, and fourfold coincidence arrangements of Geiger-Mueller counter tubes shown in Fig. 1 and indicated by the letters, A, B, $\cdots$ G. To aid in distinguishing particles of different types a lead plate 1.3 cm thick was placed in the middle of the chamber. With this procedure, some of the cosmic-ray particles can be identified on the basis of (a) the increase of ionization on passing through the lead plate, (b) the production of secondaries, and (c) the scattering of the particle in the lead plate.

The cloud chamber, 24 cm in diameter and 7 cm in illuminated depth, was used without magnetic field. The illumination was provided by four automobile headlight lamps, each having two 32-candle-power filaments. The lamps were mounted in parabolic reflectors and all the filaments were connected in series. Power for these lamps was provided by a 450-watt a.c. gasoline electric generator. The filaments were operated at a dull red except during expansions. The camera arrangement was stereoscopic. The counter circuit and cloud-chamber timing control were those used by Herzog[1] and Herzog and Bostick.[2]

(1) PENETRATING PARTICLES IN AIR SHOWERS

The fourfold coincidence arrangements D and F in Fig. 1 were used to photograph particles in air showers penetrating, respectively, 12.7 and 20 cm of lead. For electrons that traverse the 1.3-cm lead plate, under the conditions of the experiment, there is a probability of from 3 to 22 percent that no multiplication will occur.[3] If, as is actually the case, a much larger fraction of the particles traverse without multiplication, we may infer the presence of mesotrons or protons. This fraction traversing without multiplication is seen from Table II to be, respectively, 93 and 86 percent of the total number of traversing particles observed in the photographs triggered by air showers. This demonstrates the presence of penetrating particles (mesotrons or protons) in air showers.

The investigations of Janossy and Ingleby,[4] and

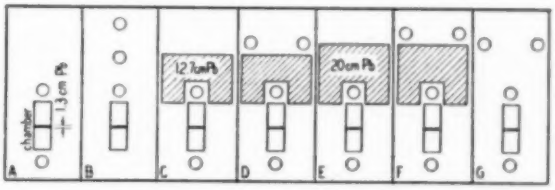

FIG. 1. Arrangement of counters.

[1] G. Herzog, Phys. Rev. **59**, 117 (1941).
[2] G. Herzog and W. H. Bostick, Phys. Rev. **59**, 122 (1941).
[3] According to Arley's calculation [Proc. Roy. Soc. **A168**, 525 (1938)] 3 percent of the electrons of energy above 2×10^8 ev traversing the lead plate should emerge as single particles. For electrons under 2×10^8 ev, this calculated fraction is 22 percent.
[4] L. Janossy and P. Ingleby, Nature **145**, 511 (1940).

TABLE I. Data on cloud-chamber photographs.

Counter Arrangement			A	B	C	D	E	F	G	Totals
(1) Total number of photographs			653	1430	593	58	89	80	80	2983
(2) Number of particles penetrating the 1.3-cm lead plate in the chamber without producing any secondaries			210	330	252	13	38	12	4	859 (29%)
(3) Number of particles producing secondaries in the 1.3-cm lead plate (excluding those cases where a large shower was seen in the chamber)			24	55	25	1	5	2	4	116 (3.9%)
(4) Number of particles penetrating the 1.3-cm lead plate in pairs without producing any secondaries			6	24	18	2	2	2	4	54 (1.8%)
(5) Number of particles judged by their specific ionization and range to be	Angle with the vertical	0°–30°	21	25	4	5	3	6	3	67
	slow mesotrons	30°–60°	2	7	4	2	0	2	1	18
		60°–90°	3	3	3	0	0	0	0	9 } 172
		0°–30°	5	18	8	1	1	2	0	35 (5.8%)
	slow protons	30°–60°	5	11	7	3	1	0	0	27
		60°–90°	5	6	0	3	1	0	1	16
(6) Number of particles showing marked increase in specific ionization on passing through 1.3 cm of lead in the chamber and their classification according to that appearance (see Figs. 8, 9, 10, and 11)	slow mesotrons		14	6	5	2	2	0	0	29 } 39
	slow protons		0	6	3	0	0	1	0	10 (1.3%)
(7) Number of particles produced in 1.3 cm of lead in the chamber by non-ionizing radiation, judged by their specific ionization and range to be (see Fig. 12)	slow mesotrons		5	16	3	4	2	2	2	34 } 51
	slow protons		2	10	4	1	0	0	0	17 (1.3%)
	fast particles		19	83	25	10	6	3	3	146
(8) Particles stopped in 1.3 cm of lead in the chamber judged by their specific ionization to be (see Fig. 9)	slow mesotrons		1	11	2	1	1	1	1	18 } 23
	slow protons		0	2	1	1	0	1	0	5 (0.8%)
	fast particles		7	37	9	1	3	5	4	66
(9) Number of large showers with greater than 50 particles in the chamber (see Fig. 4)			1	1	3	3	0	2	1	11 (0.4%)

of Wataghin, Pompeia, and Santos[5] demonstrate the existence of cosmic-ray particles in showers at sea level capable of penetrating 50 and 63 cm of lead. If the extremely high penetration of these showers is to be interpreted by the cascade theory, these showers would have been initiated at the top of the atmosphere by single particles with the unbelievably high energy of 10^{19} ev. Swann and Ramsey[6] report pairs of particles penetrating 4 to 18 cm of lead without any apparent production of secondaries. Auger[7] and also Hilberry[8] find the number of extensive showers at low altitudes considerably greater than the number predicted by the cascade theory. Finally, Hilberry and Regener,[9] working with extensive showers at Mt. Evans, and Wataghin,[5] using counter arrangements separated by 11 and 30 cm of lead, show that the reduction in the number of showers by lead absorbers is far less than expected from the cascade theory. The same discrepancy is shown in the contrast between rows 11 and 13 of Table II in this paper. In order to explain these departures from the cascade theory all of the above mentioned investigators suggest, in accord with the evidence just presented, that penetrating particles are present in air showers.

A possible explanation for the presence of such particles in air showers was suggested by Booth and Wilson[10] and also by Christy and Kusaka[11] who calculated the pair production of spin 1 mesotrons by γ-rays and found that at energies greater than 10^{14} ev mesotron pair production is more probable than pair production of electrons.

TABLE II. Photographs showing penetrating particles taken with counter arrangements *D* and *F* of Fig. 1.

	D	F
(1) Counter arrangement		
(2) Thickness of lead above the chamber	12.7 cm	20 cm
(3) Number of *photographs* taken with fourfold shower triggering of Table I	58	80
(4) Number of *photographs* in (3) with particles penetrating the 1.3-cm lead plate without multiplying	12	11
(5) Ratio, Item (4)/Item (3)	21%	14%
(6) Fraction of random expansions showing particles penetrating 1.3 cm of lead without multiplication	—	$4.6 \pm 2.7\%$
(7) Number of *particles* in (3) that penetrate the 1.3-cm lead plate without multiplication	13	12
(8) Number of *particles* in (3) penetrating the 1.3 cm of lead *with* multiplication (excluding particles in showers of greater than 50 particles in the chamber)	1	2
(9) The fractional number of particles in (3) penetrating without multiplication, i.e., $(7)/[(7)+(8)]$	93%	86%
(10) The fractional number of electrons (calculated by Arley) which would penetrate the plate without multiplication	3%–22%	3%–22%
(11) Item (4) per hour	0.43 ± 0.12	0.42 ± 0.12
(12) Accidental fourfold shower triggerings per hour	0.02	0.02
(13)* For purely cascade processes the relative numbers of showers penetrating the different thicknesses of lead to be expected in equal time intervals	1	10^{-4}
(14) Number of photographs in (3) showing large showers (more than 50 particles in the chamber)	3	2

* This calculation uses curves plotted by N. Hilberry from Serber's calculations [Phys. Rev. **54**, 317 (1938)] for the penetration of showers of a given energy, and a differential primary energy spectrum $dN = kE^{-2.5}dE$.

[5] G. W. Wataghin, M. D. Santos, and P. A. Pompeia, Phys. Rev. **57**, 61 (1940); **57**, 339 (1940); **59**, 902 (1941).
[6] W. F. G. Swann and W. E. Ramsey, Phys. Rev. **57**, 1051 (1940).
[7] P. Auger *et al.*, Rev. Mod. Phys. **11**, 289 (1939).
[8] N. Hilberry, Phys. Rev. **59**, 763 (1941).
[9] N. Hilberry and V. H. Regener, Phys. Rev. **59**, 471 (1941).
[10] F. Booth and A. H. Wilson, Proc. Roy. Soc. **A175**, 483 (1940).
[11] R. F. Christy and S. Kusaka, Phys. Rev. **59**, 403 (1941).

However, it is very doubtful that the mesotron possesses spin 1, and for mesotrons of spin 0 or $\frac{1}{2}$ the predicted pair production is practically negligible even at the highest γ-ray energies.

(2) ABUNDANCE OF HEAVILY IONIZING PARTICLES

The differentiation between a slow mesotron and a slow proton on the basis of measurements of range and estimates of ionization, though theoretically possible, is not very accurate. Nevertheless, some information can thus be obtained. The numbers of slow particles classified by this method are tabulated in Table I, row (5). The classification is divided according to the angles the tracks make with the vertical. The number of slow particles showing tracks with angles less than 30° with the vertical predominates for both mesotrons and protons. This leads to the belief that some of the slow protons and a large proportion of the slow mesotrons are produced not in nuclear evaporations, which would certainly give a more uniform angular distribution of the heavy particles than observed, but in events in which the vertical direction predominates.

Several investigators have obtained photographs of heavily ionizing cosmic-ray particles at various altitudes. A brief summary of their work is given in Table III. These results show a very marked increase in the number of heavily ionizing particles with height above sea level. As can be seen from Table I, row (5), the author obtained such tracks in 5.8 percent of the photographs taken at Mt. Evans, thus confirming these earlier results.

TABLE III. Summary of photographs of heavily ionizing particles.

AUTHOR	CLOUD CHAMBER	ALTITUDE OF OBSERVATIONS	NUMBER OF EXPANSIONS	NO. OF SLOW MESOTRONS	NO. OF SLOW PROTONS	TOTAL NO. OF TRACKS WITH IONIZATION>FAST E'S	NO. OF EXPANSIONS TOTAL NO. OF HEAVY TRACKS
Anderson[1] H = 7900 oersteds	15cm	14000ft.	9188			123	1 in 75
		sea level					1 in 885
Powell[2] H = 0	1cm Pb	14000ft.					1 in 80
Herzog[3] H = 708		15,000 to 29000 ft.	155	39	51	90	1 in 1.7
		10,000 to 15,000 ft.	29	0	3	3	1 in 10
Brode[4] H = 0		sea level	8500		21	80	1 in 106
Auger[5] H = ?	?	10,000ft.	with ordinary shower control				1 in 75
			with extensive shower control				1 in 8
Johnson[6] H = 0	?	sea level	4000		3	3	1 in 1300
Bostick H = 0		14000ft.	2983	94	78	172	1 in 18

[1] C. D. Anderson and S. H. Neddermeyer, Phys. Rev. **50**, 263 (1936).
[2] W. Powell, Phys. Rev. **58**, 474 (1940).
[3] G. Herzog, Phys. Rev. **59**, 117 (1941).
[4] R. B. Brode, Phys. Rev. **50**, 587 (1936).
[5] P. Auger, Rev. Mod. Phys. **11**, 289 (1939).
[6] T. H. Johnson, Barry, and Shutt, Phys. Rev. **57**, 1047 (1940).

(3) CLASSIFICATION OF PARTICLES SHOWING AN INCREASE IN SPECIFIC IONIZATION ON PASSING THROUGH THE LEAD PLATE

(a) A marked increase in ionization on passing through the 1.3-cm lead plate in the chamber was observed for 39 tracks (see Table I, row (6), and Figs. 8, 9, 10, and 11). These particles were classified as mesotrons or protons according to the curves A and B in Fig. 2, which show the expected increases in ionization for mesotrons and protons of various incident kinetic energies as they traverse the lead plate. These curves in Fig. 2 were calculated from the range curves for mesotrons and protons in lead (see Fig. 3, curves 5 and 6) and from the energy loss by ionization curves in argon, the gas in the chamber. The former were obtained by graphical integration of the Bloch formula for energy loss by ionization.* Figure 2 shows that a 10^8 ev proton entering the lead plate should exhibit an ionization in argon of 3.7 (curve A_P) in the units used in Fig. 2, and after traversing the plate should exhibit an ionization of 9.5 (curve B_P), which respresents an increase by a factor of 2.6. On the other hand, a mesotron which traverses the lead plate and exhibits an increase in ionization by a factor of 2.6, should enter with an ionization of only 1.55

* See Appendix A.

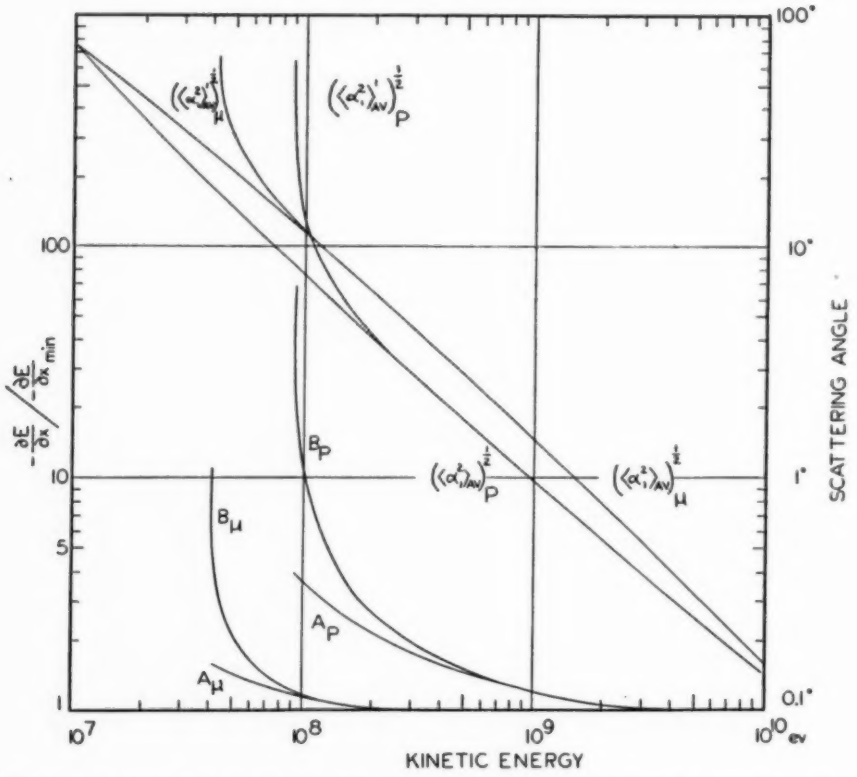

FIG. 2. The specific ionization in argon is expressed in terms of the minimum ionization that a particle can experience in argon. μ refers to a mesotron of mass $200m_e$ and P to a proton of mass $1840m_e$. A_μ is the specific ionization in argon by a mesotron entering the lead plate *vs.* its kinetic energy. B_μ is the specific ionization in argon by a mesotron as it leaves the lead plate *vs.* the kinetic energy it possessed *when it entered.* A_P and B_P are the corresponding curves for protons. $(\langle\alpha_1^2\rangle_{Av})_\mu^{\frac{1}{2}}$ is the root mean square scattering angle of a mesotron calculated from Williams (see Appendix B) for a finite nucleus and shielding, for 1.3 cm of lead, neglecting the loss of energy by ionization in the lead plate. $(\langle\alpha_1^2\rangle_{Av})_P^{\frac{1}{2}}$ is the corresponding curve for a proton. $(\langle\alpha_1^2\rangle_{Av}{}^1)_\mu^{\frac{1}{2}}$ is the root mean square scattering angle for a mesotron after energy loss in the plate has been considered. $(\langle\alpha_1^2\rangle_{Av}{}^1)_P^{\frac{1}{2}}$ is the corresponding curve for a proton.

(curve A_μ), and is thereby distinguishable from a proton. Finally, if a mesotron enters the lead plate with an ionization any higher than 1.56 it should stop in the lead plate. With this method, of the 39 tracks classified in row (6) of Table I, 29 were found to be slow mesotrons and 10 to be slow protons.

(b) Some of the 39 particles show a definite scattering in the lead plate. According to the theory of multiple scattering the mean scattering angle is a function of the kinetic energy. For the purposes of calculation this mean scattering angle was identified with the observed scattering angle, and the kinetic energies of the incident particles, assumed in turn to be mesotrons and protons, were computed.** Using this value of the kinetic energy of the incident particle, one can read from the curves A and B in Fig. 2 the expected increase in ionization as the particle passes through the lead plate. If the particles are assumed to be mesotrons, the expected increases of ionization thus calculated are not high enough to agree with the observed increases in any of the 39 tracks. On the other hand, if the particles are assumed to be protons, the expected increases of ionization are of the right order of magnitude, i.e., from a comparison of the increase in ionization with the scattering angle all 39 particles are identified as protons.

Although for protons the calculated increase of ionization is thus of the right order of magnitude, the calculated density of ionization by the protons as they enter the lead plate is in most

** See Appendix B.

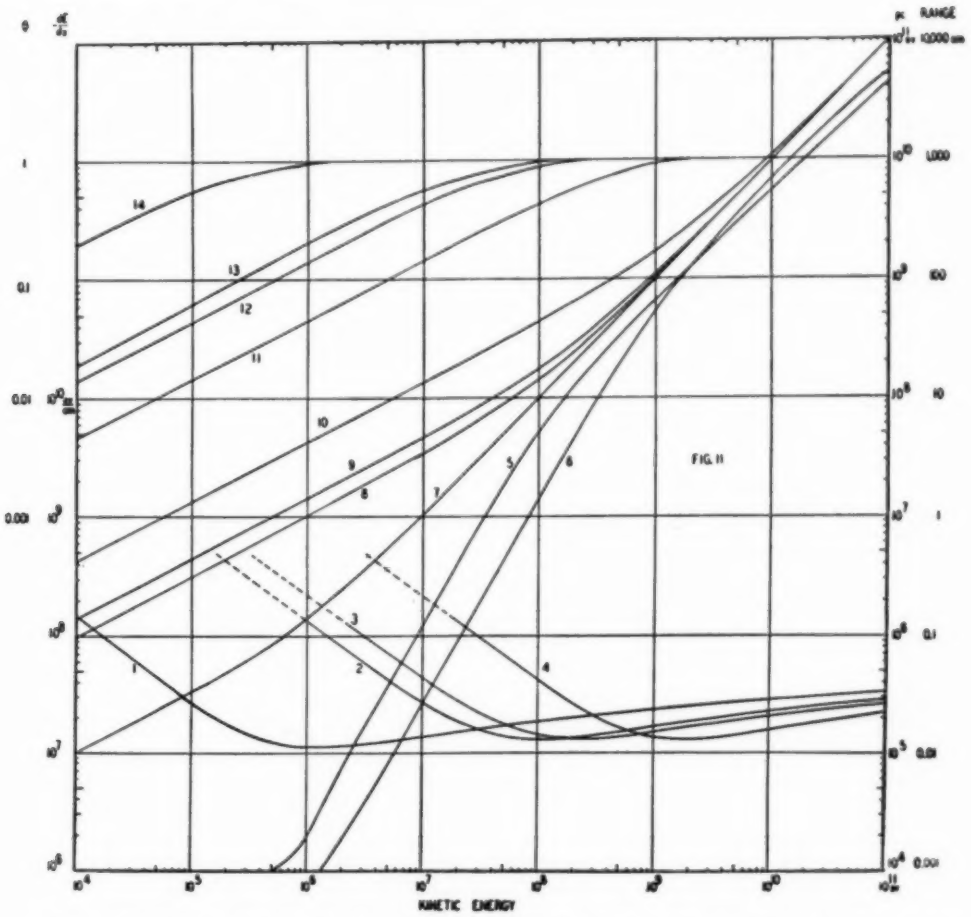

FIG. 3. Energy loss per cm by ionization is $-\partial E/\partial x$, pc is the momentum multiplied by c, β is v/c. $-\partial E/\partial x$ in lead *vs.* kinetic energy (1) for an electron; (2) for a mesotron of mass $100m_e$; (3) for a mesotron of mass $200m_e$; (4) for a proton of mass $1840m_e$.
Range in lead vs. kinetic energy (5) for a mesotron of mass $200m_e$; (6) for a proton of mass $1840m_e$.
pc *vs.* kinetic energy (7) for an electron; (8) for a mesotron of mass $100m_e$; (9) for a mesotron of mass $200m_e$; (10) for a proton.
β *vs.* kinetic energy (11) for a proton; (12) for a mesotron of mass $200m_e$; (13) for a mesotron of mass $100m_e$; (14) for an electron.

cases three times higher than the observed value. This indicates that the identification of these particles as protons by using the scattering angle and increase of ionization as criteria is doubtful. Since the kinetic energy was not measured by a direct method (such as deflection in a magnetic field), but was calculated in case (a) from the theory of ionization loss, and in case (b) from the combination of ionization increase and the theory of multiple scattering, both methods have limitations in identifying heavily ionizing particles in cloud chambers. The difference in the classification of the particles by the two methods may thus merely reflect the uncertainty in the estimates of the density of ionization.

(4) PAIRS OF PENETRATING PARTICLES

Row (4) of Table I shows twenty-seven cases in which pairs of particles penetrated the 1.3-cm lead plate without producing secondaries.[12, 13] In Fig. 5 a group of particles coming from the top (left) strike the plate, and two of them penetrate without multiplying. In Fig. 12 can be found a similar pair. All twenty-seven photographs show that penetrating particles can be produced in pairs or groups.

[12] H. J. J. Braddick and G. S. Hensby, Nature **144**, 1012 (1939), publish a photograph of a penetrating pair taken at sea level.

[13] W. Powell, Phys. Rev. **58**, 474 (1940), publishes a photograph of a penetrating pair obtained at Mt. Evans.

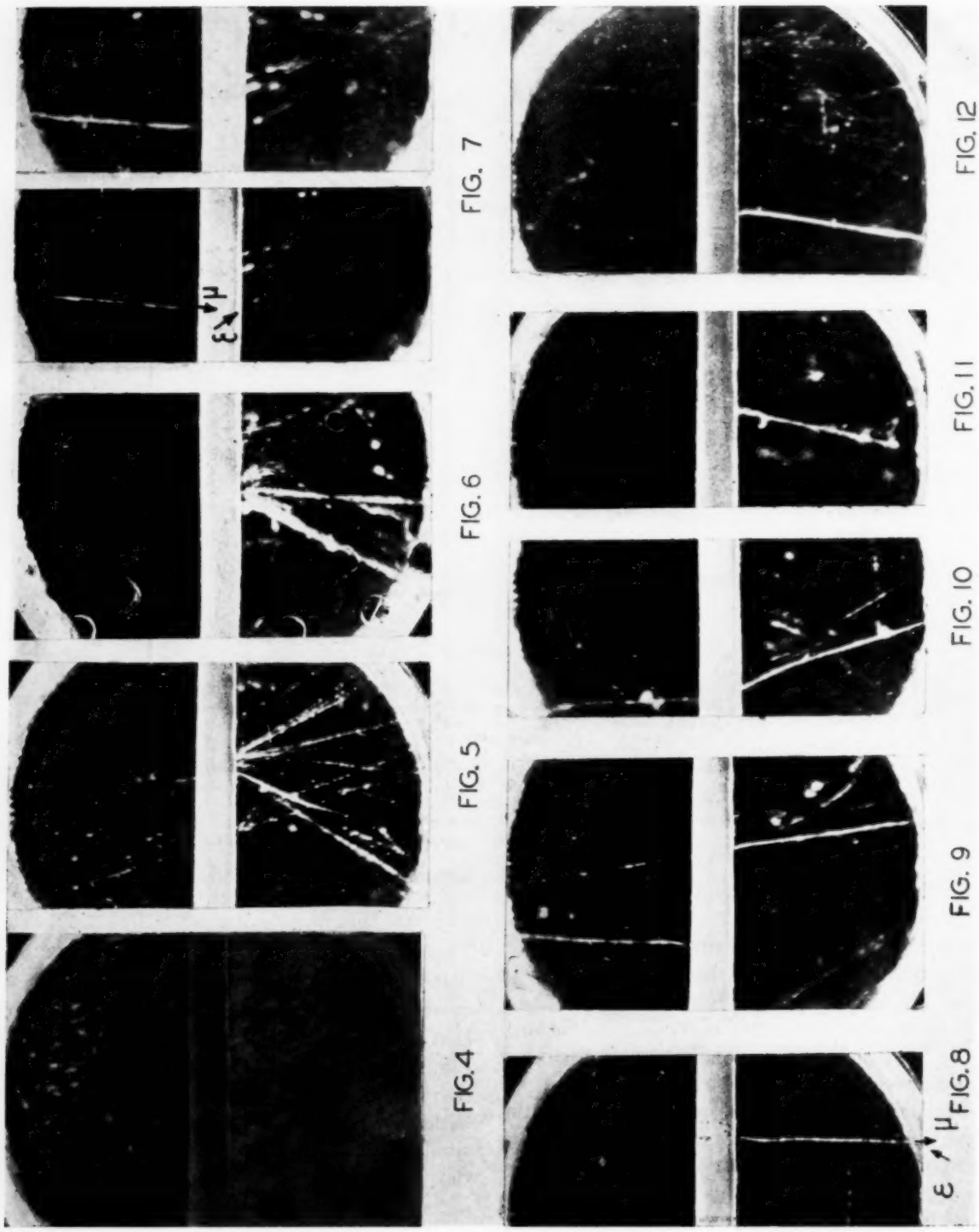

FIG. 4 FIG. 5 FIG. 6 FIG. 7

FIG. 8 FIG. 9 FIG. 10 FIG. 11 FIG. 12

CAPTIONS TO FIGURES ON OPPOSITE PAGE

Figure 4, triggered by the fourfold coincidence arrangement *F* in Fig. 1 with 20 cm of lead above the chamber, shows a large shower in the chamber.

Figures 5 and 6 taken with no lead above the chamber show showers containing particles with specific ionization high enough to be either slow mesotrons or slow protons. Figure 5 shows at least 2 particles passing obliquely through the 1.3-cm lead plate without producing secondaries. It is, therefore, probable that these particles are not electrons, but are a shower of mesotrons or protons.

Figure 7, the two stereoscopic views show a particle with the specific ionization of a slow mesotron or a slow proton entering the plate and a particle with the specific ionization of a fast electron coming out below at an angle of 40° with the direction of the first track. A possible interpretation is that a slow mesotron disintegrates and gives rise to the electron below.

Figure 8 was taken with 12.7 cm of lead above the chamber and was triggered with the fourfold shower arrangement shown in *D*, Fig. 1. It shows a particle with the appearance of a fast mesotron markedly increasing its ionization on passing through 1.3 cm of lead, and according to the curves A_μ and B_μ in Fig. 2 it is classified as a mesotron. It is possible that the track in the bottom of the chamber is the decay electron of the slow mesotron.

Figures 9, 10, and 11 are examples of tracks showing a marked increase in specific ionization on passing through the lead plate. Figures 9 and 10 were taken with 12.7 cm of lead above the chamber, Fig. 11 with no lead above the chamber.

Figure 12, taken with arrangement *B*, Fig. 1, shows the following events occurring in the same expansion: (a) Shower production in the lead plate by an electron, (b) shower production in the lead plate by a photon, (c) a pair of particles penetrating the lead plate without multiplication, and (d) the production in the lead plate of a heavy particle by non-ionizing radiation. This heavy particle with its delta-rays is very similar in appearance to a heavy particle photographed by Herzog[1] at 8,800 meters.

(5) HEAVILY IONIZING PARTICLES ASSOCIATED WITH SHOWERS

Figure 12 shows the photograph of a heavy particle produced in the lead plate by non-ionizing radiation. This occurs simultaneously with a cascade shower in the chamber. The heavy particle with its accompanying delta-rays is very similar in appearance to that photographed by Herzog[1] at 8,800 meters altitude. Other cases of the simultaneous occurrence of heavily ionizing particles and cascade showers are reproduced in Figs. 5 and 6. These photographs agree with Korff's[14] conclusions that protons (and also neutrons) can be produced by a process connected with the soft component.

(6) POSSIBLE CASES OF MESOTRON DECAY

In Figs. 7 and 8 are reproduced two of the five photographs which might be explained by a spontaneous decay of the mesotron. In four of these five photographs the particle assumed to be a decay electron originates from the stopping of a heavily ionizing particle in the lead plate (Fig. 7). Row (8) of Table I shows that 23 heavily ionizing particles and 66 particles with normal ionization were observed to stop in the lead plate. If all of these particles were mesotrons, we should expect more than the four observed disintegrations. The same infrequency of decay electrons was reported by Herzog and Bostick[2] where a 0.3-cm copper plate was placed in the middle of a cloud chamber carried to an altitude of 8,800 meters. Such results indicate that many of the heavily ionizing particles are protons, and that most of those of normal ionization which stop in the lead plate are electrons.

The author wishes to express his gratitude to Professor Compton for his advice on this work, to Dr. Gerhard Herzog whose cloud-chamber control system and Geiger counter circuit were used, to Dr. Marcel Schein who gave constructive criticisms of the paper, to Dr. Bruno Rossi who suggested the experiment, and to Dr. Norman Hilberry from whom were borrowed the curves on Serber's calculations.

APPENDIX A

The Bloch[15,16] formula for the energy loss per cm of a charged particle by ionization processes in passing through a substance of atomic number Z is

$$-\frac{\partial E}{\partial x}=2\pi\sigma Z r_0^2\frac{m_e c^2}{\beta^2}\left[\log_\epsilon\frac{m_e c^2\beta^2 W_m}{(1-\beta^2)I^2Z^2}+1-\beta^2\right]$$

where σ is the number of atoms per cc, $r_0=e^2/m_e c^2$, m_e is the mass of the electron, $\beta=v/c$, I is the mean ionization energy and is equal to 13.5 ev, e is the electronic charge, W_m is the maximum energy that can be imparted to an electron by a particle of Mass M.

$$\frac{W_m}{E_0-Mc^2}=\frac{2m_e M(\gamma+1)}{m_e^2+M^2+2m_e M\gamma},$$

where E_0-Mc^2 is the kinetic energy, M is the rest mass of the incident particle and $\gamma=(1-\beta^2)^{-\frac{1}{2}}$.

The quantity $-\partial E/\partial x$ for lead can be plotted *vs.* kinetic energy for particles of mass m_e, $100m_e$, $200m_e$, and $1840m_e$ as has been done in Fig. 3. When these curves are drawn it is possible to obtain the range of the particles as a function of their kinetic energies by a graphical integration as shown in Table IV.

APPENDIX B

E. J. Williams[17] has calculated $(\langle\alpha_1^2\rangle_{Av})^{\frac{1}{2}}$, the root mean square of the scattering angle, for a charged particle of

[14] S. A. Korff, Phys. Rev. **59**, 949 (1941).

[15] F. Bloch, Ann. d. Physik **16**, 285 (1933).

[16] H. J. Bhabha, Proc. Roy. Soc. **A164**, 270 (1938).

[17] E. J. Williams, Proc. Roy. Soc. **A169**, 531 (1938–39).

TABLE IV. Distance $d=(K_i-K_f)/-\langle\partial E/\partial x\rangle_{Av}$ is that traveled in lead when a particle of mass $200m_e$ and of an initial kinetic energy K_i loses by ionization an amount of energy equal to K_i-K_f, where K_f is the kinetic energy which the particle possesses after having traversed d. The average ionization loss per cm $-\langle\partial E/\partial x\rangle_{Av}$ is read from the curves in Fig. 3. The sum of the d's gives the range for a given K_i.

K_i (in ev)	K_f (in ev)	Av. $-\langle\partial E/\partial x\rangle_{Av}$ (in ev/cm)	d (in cm)	Range (in cm)
10^4	0	10^{10}	10^{-6}	10^{-6}
10^5	10^4	5.0×10^9	1.8×10^{-5}	$10^{-6}+1.8\times10^{-5}=1.9\times10^{-5}$
5×10^5	10^5	5.0×10^8	10^{-3}	1.02×10^{-3}
10^6	5×10^5	2.7×10^8	1.85×10^{-3}	2.87×10^{-3}
5×10^6	10^6	1.14×10^8	3.54×10^{-2}	3.83×10^{-2}
10^7	5×10^6	5.85×10^7	8.55×10^{-2}	0.125
2×10^7	10^7	3.41×10^7	0.294	0.419
—	—	—	—	—

mass M, where $\langle\alpha_1^2\rangle_{Av}+\langle\alpha_2^2\rangle_{Av}=\langle\theta^2\rangle_{Av}$ and θ is the total scattering angle, and α_1 and α_2 are the scattering angles projected in two perpendicular planes, each of which contains the track of the incident particle. Neglecting the energy loss by ionization in the scattering material, taking into consideration shielding by electrons, and using a finite nucleus with a radius of 10^{-12} cm, Williams obtains the following expression:

$$(\langle\alpha_1^2\rangle_{Av})^{\frac{1}{2}}=\left(\frac{\pi}{2}\right)^{\frac{1}{2}}[19.5-3.1\log_{10}Z]^{\frac{1}{2}}\frac{2(Nt)^{\frac{1}{2}}Ze^2(1-\beta^2)^{\frac{1}{2}}}{Mc^2\beta^2},$$

where W is the atomic weight, Z is the atomic number, t is the thickness, and N is the number of atoms per cc of the scattering material, and e is the electronic charge. The values of $(\langle\alpha_1^2\rangle_{Av})^{\frac{1}{2}}$ *vs.* the kinetic energy for both mesotrons and protons are plotted in Fig. 1.

It is now desired to calculate the corresponding values of $(\langle\alpha_1^2\rangle_{Av})^{\frac{1}{2}}$ when the energy loss in the plate is taken into account. Consider a particle of mass $200m_e$ entering the 1.3-cm lead plate with a kinetic energy of 8×10^7 ev. It will be seen from curve 5 of Fig. 3 that this particle will emerge with a kinetic energy of 6.1×10^7 ev. For the average between the energies 8×10^7 and 6.1×10^7 ev, the scattering angle $(\langle\alpha_1^2\rangle_{Av})^{\frac{1}{2}}$ was read from the curve in Fig. 2. If this value of $(\langle\alpha_1^2\rangle_{Av})^{\frac{1}{2}}$ is now plotted against the incident kinetic energy of 8×10^7, we obtain a point on the curve for $(\langle\alpha_1^2\rangle_{Av}{}^1)^{\frac{1}{2}}$. For lower kinetic energies the averaging process was made more precise by dividing the plate up into thin sections, numbered a, b, c, $\cdots$, and calculating the average kinetic energy of the particle in each section and in turn the resulting $(\langle\alpha_1^2\rangle_{Av}{}^1)^{\frac{1}{2}}$ in each section. The total $(\langle\alpha_1^2\rangle_{Av}{}^1)^{\frac{1}{2}}$ for the 1.3 cm of lead is given by

$$(\langle\alpha_1^2\rangle_{Av}{}^1)^{\frac{1}{2}}=[\langle\alpha_a^2\rangle_{Av}+\langle\alpha_b^2\rangle_{Av}+\langle\alpha_c^2\rangle_{Av}+\cdots]^{\frac{1}{2}}.$$

MAY 1 AND 15, 1942 PHYSICAL REVIEW VOLUME 61

Radioactive Isotopes of Praseodymium

J. W. DEWIRE,* M. L. POOL, AND J. D. KURBATOV
The Ohio State University, Columbus, Ohio

(Received March 3, 1942)

New nuclear reactions $Pr^{141}(d,p)$, $Ce^{142}(p,n)$, and $La^{139}(\alpha,n)$ yielding radioactive isotope Pr^{142} have been observed. The decay curves obtained for Pr^{142} after chemical purifications showed a half-life of 19.3 ± 0.1 hours, a value considered to be more exact than that previously reported. The negative beta-ray spectrum was measured with a recently constructed magnetic spectrometer of the 180° focusing type and was found to have an end point of 2.14 ± 0.02 Mev. A weak gamma-ray approximately 1.9 Mev was found associated with this period. The isotope Pr^{140} has been formed by the reaction: $Pr^{141}(n,2n)$. Its half-life was measured as 3.4 ± 0.1 minutes. Cloud-chamber measurements yield an upper limit of 2.40 ± 0.15 Mev for its positron spectrum.

I. INTRODUCTION

THE study of radioactivity in praseodymium began with the work of Fermi and coworkers, who produced periods of 5 minutes and 19 hours by bombarding praseodymium with neutrons.[1] They reported that the 19-hour period was sensitive to water and found a half-value thickness for its beta-rays of 0.12 g/cm² of aluminum. Marsh and Sugden[2] assigned the 19-hour period to Pr^{142}, and Pool and Quill[3] found that the shorter period was a 3.5-minute positron emitter and assigned it to Pr^{140}. Recently these assignments were confirmed by Wu and Segrè,[4] who reported that the half-life of Pr^{142} was 18.7 hours. They found that this isotope emitted only electrons with a continuous spectrum having an upper limit of 2 Mev.

* Now at Princeton University, Princeton, New Jersey.
[1] E. Fermi *et al.*, Proc. Roy. Soc. **149**, 522 (1935).
[2] J. K. Marsh and S. Sugden, Nature **136**, 102 (1935).
[3] M. L. Pool and L. L. Quill, Phys. Rev. **53**, 437 (1938).
[4] C. S. Wu and E. Segrè, Phys. Rev. **61**, 203 (1942).

In this study, other possible methods of formation of these two isotopes have been investigated. The electron spectrum of Pr^{142} has been measured by a magnetic spectrometer, the positron spectrum of Pr^{140} by a Wilson cloud chamber. A weak gamma-ray has been found associated with Pr^{142}; its energy has been measured by absorption in lead.

II. THE 19.3-HOUR PERIOD

A. Formation and Half-Life

Figure 1 shows an isotopic chart of the region studied. The stable isotopes are represented by rectangles, the unstable isotopes by ovals. The reactions which were studied in this work are shown by the heavy arrows. The values found for the radiations from Pr^{140} and Pr^{142} are given in heavy print.

The 19.3-hour period was formed by the action of deuterons and neutrons on praseodymium, protons on cerium, and alpha-particles on lanthanum. Hilger H.S. brand oxides were used in all the bombardments. A spectroscopic study, delivered by Hilger, revealed the following impurities in these materials:

Praseodymium oxide, Lab. No. 6782—Mg, 0.1 percent; Dy, 0.02 percent.

Cerium oxide, Lab. No. 6401—traces of Mg and Gd.

Lanthanum oxide, Lab. No. 6404—very slight traces of Na, Mg, Ca, Bi, Sm; Gd, 0.015 percent; Nd, 0.1 percent.

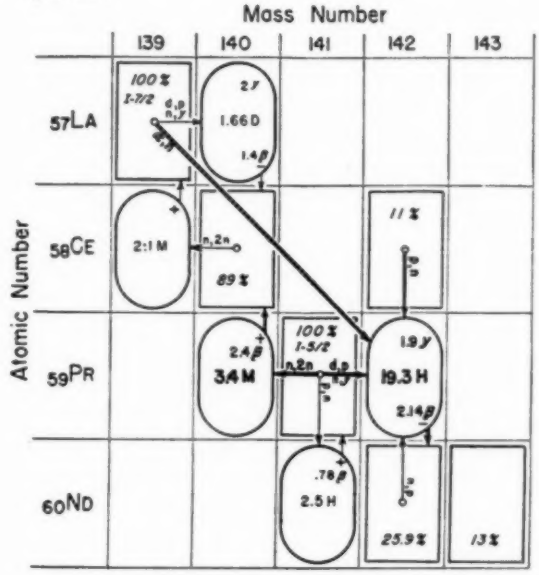

FIG. 1. Isotopic chart of praseodymium region.

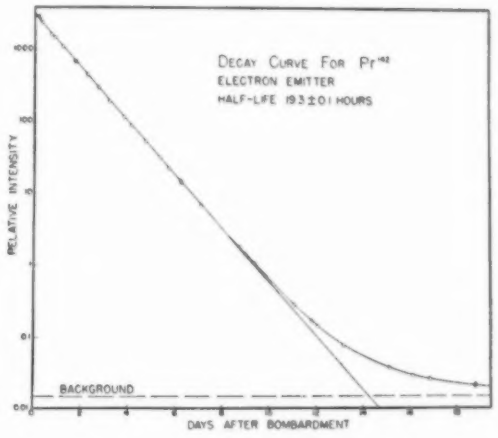

FIG. 2. Decay curve for Pr+*d*.

A study of the distribution of the stable isotopes in the praseodymium region leads to the conclusion that the reactions forming the 19.3-hour period assign the period to Pr^{142}. The chemical procedures of purification were arranged to remove all active impurities other than the rare earths, which might originate either from the target material or the bombarded sample. The same procedures were followed in all the bombardments leading to the 19.3-hour period. The bombarded sample was first dissolved in nitric acid and evaporated to dryness, the process being repeated several times to drive off all volatile active substances. Then the residue was again dissolved in nitric acid and filtered to remove any insoluble activity from the platinum target. After filtration, carriers were added, such as Cu, Ni, Co, Na, K, Cs, Ca, Ba, and Sr. The filtrate was then neutralized with ammonium hydroxide added in excess. This precipitated the rare earths and left the above shown impurities in solution. The rare-earths' precipitate was filtered, and afterward was redissolved in nitric acid. Other carriers such as Fe, Al, Cr, Ti, etc., were added, and the rare earths were precipitated by oxalic acid and filtered off. In case any of the filtrates showed activity when measured with an immersion type G-M tube, carriers were again added and the rare earths precipitated once more. The oxalates of the rare earths were finally converted to the oxides, whose activity was followed.

The activities were measured by an ionization chamber containing Freon at a pressure of two

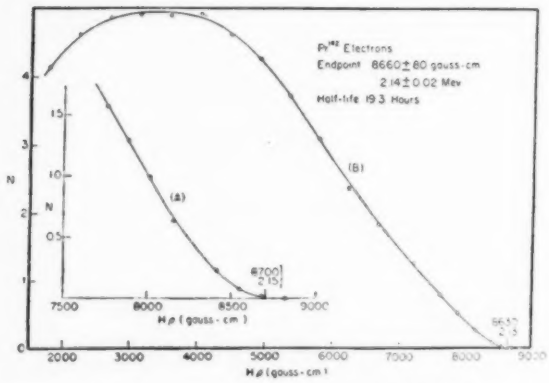

FIG. 3. Momentum distribution of the Pr^{142} electrons.

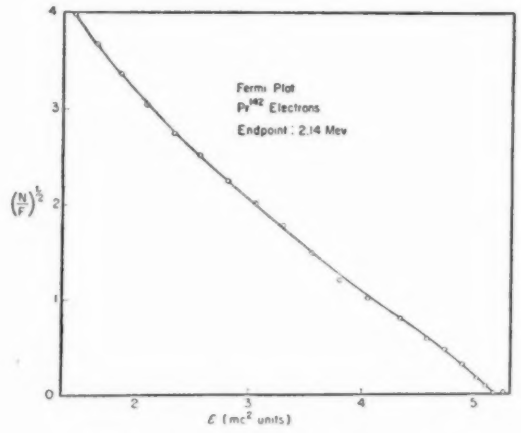

FIG. 4. Fermi plot of Pr^{142} electrons.

atmospheres and a Wulf unifilar electrometer. The sensitivity of this arrangement was determined for each point on the curves by a uranium standard.

Praseodymium oxide bombarded with 10-Mev deuterons yielded a strong rare-earth activity, whose intensity was followed from 200,000 times background to one-tenth background. This decay curve is shown in Fig. 2. From it the half-life was determined to be 19.3±0.1 hours.

The rare-earth fraction from the bombardment of lanthanum oxide with 20-Mev alpha-particles gave an activity, which was followed for 10 half-lives and gave a half-life of 19.2 hours. If any longer period was present, its initial intensity was less than 0.1 percent of the 19-hour period.

Cerium oxide was bombarded with 10-Mev deuterons and 5-Mev protons. From the deuteron bombardment no 19-hour period was found, but from the proton bombardment a 19.3-hour activity was derived.* This decay curve was followed for 12 half-lives. Longer periods, if present, had an initial relative intensity of less than 1 part in 1000.

B. Beta-Ray Spectrum

The beta-ray spectrum of Pr^{142} was measured by a newly constructed magnetic spectrometer of the 180° focusing type, having a radius of curvature of 16 cm. The source holder is similar to that described by Lawson and Tyler.[5] The geometry is determined by three defining slits and an exit slit (3×19 mm), which leads into a Geiger tube filled with hydrogen to a pressure of 8 cm of Hg. The magnetic field is determined by measuring the voltage developed by a small coil rotating at 1800 r.p.m. in the field.[6] The coil is driven by a synchronous motor and is connected through a two-segment commutator to a potentiometer. This method has proved reliable in many calibration tests made on the spectrometer. The magnetizing current is supplied by storage batteries and requires only an occasional adjustment to keep it constant to within 1 part in 1000. The calibration of the field has been checked by measuring the P^{32} electron spectrum and the Cu^{64} electron and positron spectra. These measurements are in excellent agreement with those reported by previous workers.

Figure 3 shows the momentum distribution of the Pr^{142} electrons as found by the magnetic spectrometer. The source was a sample of praseodymium oxide bombarded with deuterons. Impurities other than the rare earths were removed chemically, and a part of the rare-earth precipitate was spread in a thin layer on a strip of thin paper (1 mg/cm²) mounted on the source holder. Counting rates were corrected for counting losses, background counts, the variable H increments, and absorption and scattering by the counter window. Curve (A) shows the entire spectrum plotted from measurements taken thirty-two hours after bombardment. In this case, the maximum counting rate was about 700

* *Note added in proof:* The reaction $Ce^{142}(d, 2n)Pr^{142}$ has recently been obtained with deuteron bombardment of cerium. The 19.3-hour period was established after repeated chemical separations of praseodymium from cerium.

[5] J. L. Lawson and A. W. Tyler, Rev. Sci. Inst. 11, 6 (1940).

[6] R. H. Cole, Rev. Sci. Inst. 9, 215 (1938).

counts per minute. From the two curves, an end point of 2.14±0.02 Mev was found as compared with 2 Mev recently reported.[4]

This value was substantiated by the Fermi plot of curve (*B*) shown in Fig. 4. The points show a definite deviation from a straight line. A consideration of the half-life and the energy on the basis of the Fermi theory shows that the transition ($Pr^{142} \rightarrow Nd^{142}$) is first forbidden.

One gamma-ray was emitted for about every twenty-five beta-rays. This disagrees with the findings of Wu and Segrè,[4] who reported no gamma-rays associated with this period. The lead absorption coefficient for this gamma-radiation was 0.51 cm^{-1}, corresponding to an energy of 1.9 Mev. The decay curve for the gamma-rays gave a half-life of about 19 hours.

III. THE 3.4-MINUTE PERIOD

Praseodymium oxide bombarded with fast neutrons (Li+*d*) gave an activity whose decay curve is shown in Fig. 5. Subtraction of the

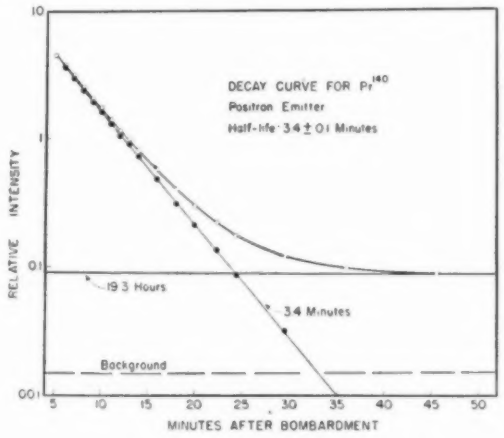

FIG. 5. Decay curve for Pr+fast *n*.

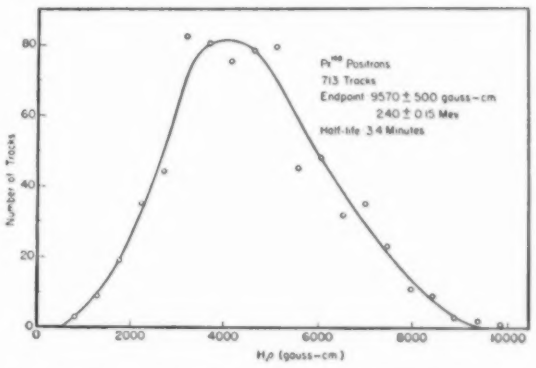

FIG. 6. Momentum distribution of the Pr^{140} positrons.

19.3-hour period, which was due to slow neutrons behind the lithium target, gave a half-life of 3.4±0.1 minutes. No chemical purification was done on this sample. The only positrons obtained from the fast neutrom bombardment were the positrons associated with 3.4-minute period, the 19.3-hour period being an electron emitter. Thus sources were prepared by fast neutron bombardment for a cloud-chamber study of the Pr^{140} positrons.

Figure 6 gives the momentum distribution for the positrons, derived from 713 measured tracks. The end point from this plot was found to be 2.40±0.15 Mev. From the consideration of this value and the half-life, it is probable that ($Pr^{140} \rightarrow Ce^{140}$) is an allowed transition.

It is a pleasure to acknowledge the support received from the University Development Fund and from Mr. Julius F. Stone. Valuable assistance through the W.P.A. cyclotron project No. 65-1-42-89 is also acknowledged. Construction of the spectrometer was supported by a grant-in-aid from the American Association for the Advancement of Science.

Theoretical Half-Lives of Forbidden β-Transitions

E. GREULING*
Department of Physics, Indiana University, Bloomington, Indiana
(Received March 9, 1942)

Fermi's theory of β-decay is extended to the "nth forbidden" approximation. Precise formulas for the distribution in energy of the emitted β-rays are derived for arbitrarily charged nuclei, according to the five possible invariant forms of interaction, the so-called scalar, polar vector, tensor, axial vector, and pseudo-scalar interactions, respectively. The nuclear matrix elements of the transitions, made up of the components of certain irreducible tensors, are constructed. The selection rules appropriate to these matrix elements are given in Table II. The magnitudes of the nuclear matrix elements are estimated by a simple averaging process depending only on the directional properties of the tensors from which they are constructed and the order of magnitude of the tensor components. Theoretical half-lives of the "forbidden" β-decays of RaE, P^{32}, K^{40}, and Rb^{87} are calculated by numerical integration of the energy dependent electron emission probabilities. Upon comparing with the experimental determinations of the half-lives, the most satisfactory agreement seems to be obtained with the tensor form of interaction. The evidence in favor of Gamow-Teller selection rules is somewhat inconclusive for the case of the K^{40} decay because of the uncertainty of the experimental determination of the maximum electron energy.

I. INTRODUCTION

IN order to explain the energy distribution of the β-particles from nuclei such as RaE and P^{32}, Konopinski and Uhlenbeck[1] extended the Fermi theory to the "forbidden" transitions. Upon comparing the theoretical distribution with the observed spectra, these authors were able to eliminate three of the five forms of interaction[2] which they considered. The invariant forms characterized as the scalar, axial vector, and pseudo-scalar interactions were shown to be inadequate to give the observed energy distributions of RaE and P^{32}. By assuming the nuclear spin changes, $J_i=2\rightarrow J_f=0$, for both RaE and P^{32} they found that the polar vector and tensor interactions were able to account satisfactorily for the observed distributions.

The above deductions will not be conclusive until not only the energy distributions of the β-particles emitted by radioactive nuclei are shown to agree with experimental determinations, but also the lifetimes characteristic of the decays are explained. A calculation of the half-lives may serve to verify the conclusions drawn from the theoretical treatment of the energy distributions, and furthermore may facilitate additional discrimination in the choice of interaction. Information concerning the nuclear spins of the initial and final nuclei is pertinent to these calculations. The "forbidden" transitions,

$$K^{40}(J_i=4)\rightarrow Ca^{40}(J_f=0)+\beta^-$$

and

$$Rb^{87}(J_i=3/2)\rightarrow Sr^{87}(J_f=9/2)+\beta^-,$$

having known spin changes,[3,4] are treated here in addition to RaE and P^{32}.

The theoretical half-lives of the four above-mentioned decays are calculated in detail according to the tensor and polar vector theories. For K^{40} the "allowed," "first," and "second forbidden" formulas derived in II are inadequate, in view of the fact that a spin change, $\Delta J=4$, requires at least the "third forbidden" approximation, and may entail the "fourth forbidden" formulas. The general formulas for "nth forbidden" transitions, calculated to the same degree of precision as those of II, are presented along with good approximations which are applicable to both heavy and light elements. The β-spectra of K^{40} and Rb^{87} are not of interest because their exact measurements are difficult; however, the more easily observed average electron energies are calculated.

The RaE and P^{32} lifetime problems are attacked for the first time in this paper. Good

* An abridgment of the dissertation to be submitted in partial fulfillment of the requirements for the Ph.D. degree at Indiana University.

[1] E. J. Konopinski and G. E. Uhlenbeck, Phys. Rev. **60**, 308 (1941)—to be referred to hereinafter as paper II.

[2] H. A. Bethe and R. F. Bacher, Rev. Mod. Phys. **8**, 82 (1936). The five invariant interactions are also listed in II.

[3] J. R. Zacharias, Phys. Rev. **60**, 168 (1941).

[4] M. Heyden and H. Kopfermann, Zeits. f. Physik **108** 3–4, 232 (1938).

TABLE I. Data on half-lives.

Emitter	Experimental half-life/sec.	W_0/mc^2	Theoretical half-life/sec.	$\overline{W}/mc^2$	$(f_{nX}t_{exp})$/sec.
RaE	$(4.3)10^6$	3.3			
$\Delta J=(2\rightarrow 0)$ "Yes"			$t_{1T}=(8)10^4$		$(3.4)10^4$
$\Delta J=(2\rightarrow 0)$ "No"			$t_{2T}=(5-13)10^6$		$(5-2.0)10^3$
			$t_{2V}=(1.9-3.4)10^6$		$(7-3.8)10^3$
P^{32}	$(1.2)10^6$	4.37			
$\Delta J=(2\rightarrow 0)$ "Yes"			$t_{1T}=(5.5)10^6$	2.4	$(13)10^2$
$\Delta J=(2\rightarrow 0)$ "No"			$t_{2T}=(0.54-11)10^7$	$(2.4-2.2)$	$(13-0.6)10^2$
			$t_{2V}=(0.27-4.2)10^7$	$(2.4-2.2)$	$(14-0.9)10^2$
K^{40}	$(4.5)10^{16}$				
$\Delta J=(4\rightarrow 0)$ "Yes"		2.4	$t_{3T}=(2.3)10^{17}$	1.6	$(1.2)10^3$
		3.6	$t_{3T}=(1.0)10^{15}$	2.2	$(2.7)10^5$
$\Delta J=(4\rightarrow 0)$ "No"		2.4	$t_{4T}=(0.23-13)10^{19}$	$(1.6-1.5)$	$(119-2.0)$
			$t_{4V}=(0.11-4.3)10^{19}$	$(1.6-1.5)$	$(120-3.1)$
		3.6	$t_{4T}=(1.1-32)10^{15}$	$(2.2-2.0)$	$(24-0.8)10^4$
			$t_{4V}=(0.55-11)10^{15}$	$(2.2-2.0)$	$(25-1.2)10^4$
Rb^{87}	$(2-6)10^{18}$	1.26			
$\Delta J=(3/2\rightarrow 9/2)$ "No"			$t_{2T}=(3.0)10^{15}$	1.13	$(4-12)10^8$
$\Delta J=(3/2\rightarrow 9/2)$ "Yes"			$t_{3T}=(0.3-13)10^{17}$	$(1.13-1.09)$	$(120-0.9)10^4$
			$t_{3V}=(0.14-3.3)10^{17}$	$(1.13-1.09)$	$(120-1.8)10^4$

agreement with the observed half-life of RaE[5] is obtained. Concurrently, the theoretical energy distribution predicted is in agreement with the well-defined experimental determinations of the shape of the spectra.[6-8] On the other hand, the calculated half-life of P^{32} differs considerably from its observed value. The shape of the P^{32} energy distribution calculated in II also varies somewhat from experimental determinations.

The half-life of K^{40} has been discussed by Bethe,[2] and recently was calculated by Marshak.[9] Both authors have shown that the "third forbidden" approximation is sufficient to explain its very long lifetime. Use of the K–U modification of the original Fermi theory (polar vector interaction) made it necessary for Bethe to assume $\Delta J=3$ which is in contradiction to the recent experimental data of Zacharias.[3] Marshak concludes that the K^{40} transition can be "third forbidden" if Gamow-Teller selection rules (tensor or axial vector interaction) are valid. The maximum β-ray energy, $W_0=3.6\,mc^2$, reported by Henderson,[10] as well as $W_0=2.4\,mc^2$, was used by Marshak. The former end-point energy yields a much smaller half-life than the latter. The results listed in Table I indicate that Marshak's conclusion is correct if the maximum energy is $2.4\,mc^2$, but if it amounts to as much as $3.6\,mc^2$, the half-life can be accounted for equally well by the "fourth forbidden" tensor or polar vector interactions. The uncertainty as to the end-point energy weakens the argument in favor of the Gamow-Teller rules based on K^{40}.

The lifetime of Rb^{87} (half-life, $t=(2-6)10^{18}$ sec.)[11,12] was discussed by Konopinski and Bethe.[13] They obtained a theoretical estimate of the mean-life, $\tau\approx 10^{10}$ yr., according to the "third forbidden" polar vector interaction, with $\Delta J=3$. The half-life of Rb^{87} listed in Table I is predicted within the experimental error by the "third forbidden" tensor or polar vector interaction. This is in substantial agreement with the calculations of Marshak.

II. THEORETICAL CALCULATIONS

The reciprocal half-life of a radioactive nucleus according to Fermi's theory of β-decay is given by

$$1/t_{nX}=(G^2/2\pi^3\ln 2)\times\int_1^{W_0} C_{nX}F_0(W,Z)pWq^2dW, \quad (1)$$

$$=(G^2/2\pi^3\ln 2)f_{nX}(W_0,Z). \quad (2)$$

[5] A. Pompei, J. de phys. et rad. **6**, 471 (1935).
[6] A. Flammersfeld, Zeits. f. Physik **112**, 727 (1939).
[7] E. M. Lyman, Phys. Rev. **51**, 1 (1937).
[8] G. J. Neary, Proc. Roy. Soc. **175**, 71 (1940).
[9] R. E. Marshak, Phys. Rev. **61**, 431 (1942).
[10] W. J. Henderson, Phys. Rev. **55**, 238 (1939).
[11] O. Hahn, F. Strassmann, and E. Walling, Naturwiss. **25**, 189 (1937).
[12] A. Hemmendinger and W. K. Smythe, Phys. Rev. **51**, 1052 (1937).
[13] E. J. Konopinski and H. A. Bethe, Phys. Rev. **53**, 679 (1938).

The subscript, $n=0, 1, 2, \cdots n$, designates an "allowed," "first," "second," or "nth forbidden" transition; $X=S, V, T, A, P$ denotes the form of interaction, scalar, polar vector, tensor, axial vector, or pseudo-scalar, respectively. G is the Fermi constant; to obtain the half-life t_{nX} in seconds the magnitude of $(2\pi^3 \ln 2/G^2)$ is taken to be about $(6)10^3$ sec. for the interactions T or A. The value $\approx(3)10^3$ sec. is more appropriate for the others.[14] The function, $F_0(W, Z)$, precisely defined by Eq. (15), represents the effect of the nuclear charge in the "allowed" energy distribution, F_0pWq^2dW. W is the electron's total energy in units[15] of mc^2; $p=(W^2-1)^{\frac{1}{2}}$ is the momentum of the electron, and $q=W_0-W$ is the energy taken by the neutrino. W_0 is the maximum energy available to the electron in the transition. The correction to the "allowed" formula which the "nth forbidden" transition requires is given by the factor,

$$C_{nX}=(2p^2F_0)^{-1}\int d\omega \sum_{jlm}\left|\int d\tau H_{nX}\right|^2, \quad (3)$$

in which H_{nX} has the invariant forms:

$$H_{nV}=[(V^*QU)(\psi^*\phi) - (V^*\boldsymbol{\alpha}^HQU)\cdot(\psi^*\boldsymbol{\alpha}\phi)]_n, \quad (4V)$$

$$H_{nT}=[(V^*\beta^H\boldsymbol{\sigma}^HQU)\cdot(\psi^*\beta\boldsymbol{\sigma}\phi) + (V^*\beta^H\boldsymbol{\alpha}^HQU)\cdot(\psi^*\beta\boldsymbol{\alpha}\phi)]_n. \quad (4T)$$

Only the polar vector and tensor interactions are presented here; however, the formulas for the correction factors, C_{nS}, C_{nA}, and C_{nP} are derived as well. $\int d\tau H_{nX}$ is the matrix element of the interaction between the nucleons of the parent nucleus and the electron-neutrino field. U and V are the wave functions of the initial and final nucleus. The operator Q by definition transforms a neutron into a proton. The square of the matrix element is integrated over the momentum and spin directions of the neutrino and summed over the spin and angular momentum quantum numbers, j, l, m, of the electron in the coulomb field. The Dirac electron wave functions ψ are to be normalized to one particle per sphere of unit radius.[16] ϕ is the four-component wave function of the neutrino. The operators $\boldsymbol{\sigma}$, $\boldsymbol{\alpha}$, and β, in (4) are the usual Dirac four-by-four matrices. The superscript H indicates that the operations are on the nuclear wave function.

The evaluation of the correction factors through "second forbidden" transitions was described in II. Briefly, the method is to expand the electron and neutrino wave functions in powers of their cartesian position coordinates x_i. The matrix elements will then contain, besides the vector operators $\boldsymbol{\sigma}$ and $\boldsymbol{\alpha}$, components x_i of the position vector $\mathbf{r}$. The final expressions must be invariant with respect to three-dimensional spacial rotations. Thus they must be expressible in terms of tensors made up of components of the vectors $\boldsymbol{\sigma}$ and $\boldsymbol{\alpha}$ in combination with the components x_i. For second and higher rank tensors formed in this way it becomes necessary to separate them into their irreducible representations. The irreducible tensors required through the "second forbidden" transitions, already constructed by Konopinski and Uhlenbeck (II), are designated in this paper as follows:

Scalars:

$$Q_0(s)=\int d\tau V^*sU, \quad (5)$$

where s may be any of the heavy particle scalar or pseudo-scalar operators,[17]

1, β, $(\boldsymbol{\sigma}\cdot\mathbf{r})$, $(\boldsymbol{\alpha}\cdot\mathbf{r})$, $\beta(\boldsymbol{\sigma}\cdot\mathbf{r})$, $\beta(\boldsymbol{\alpha}\cdot\mathbf{r})$, γ_5, or $\beta\gamma_5$.

Vectors:

$$Q_i(\mathbf{a})=\int d\tau V^*a_iU, \quad (6)$$

where $\mathbf{a}$ may be any of the vector operators, $\mathbf{r}$, $\boldsymbol{\sigma}$, $\boldsymbol{\alpha}$, $[\boldsymbol{\sigma}\times\mathbf{r}]$, or $[\boldsymbol{\alpha}\times\mathbf{r}]$, multiplied by any scalar operator.

Second-rank tensors:

$$Q_{ij}(\mathbf{a},\mathbf{r})=\int d\tau V^*[a_{(i}x_{j)}-\tfrac{1}{3}\delta_{(ij)}(\mathbf{a}\cdot\mathbf{r})]U, \quad (7)$$

where the a_i's are components of the vector

[14] E. J. Konopinski, *Advances in Nuclear Physics* (Interscience Publishers, Inc.), in press.

[15] The units used throughout this paper are: mc^2 = unit of energy, mc = unit of momentum, $\hbar/mc^2$ = unit of time, and $\hbar/mc$ = unit of length, where m is the rest mass of an electron.

[16] M. E. Rose, Phys. Rev. **51**, 484 (1937).

[17] The superscript H is dropped; all operators in the nuclear matrix elements are obviously heavy particle operators. The operator Q is also omitted from all the nuclear matrix elements.

TABLE II. Selection rules.

Interaction		"nth forbidden"	Completely "forbidden"
Scalar	Matrix	$Q_n(\beta\mathbf{r}, \mathbf{r})$	$\Delta J=(0\leftrightarrow n_{\text{even}})$ — yes
	ΔJ	$(n-1)', n$	$\Delta J=(0\leftrightarrow n_{\text{odd}})$ — no
	Parity Change	n_{odd} — yes, n_{even} — no	
Polar V.	Matrix	$Q_n(\mathbf{r}, \mathbf{r})$, $Q_n(\boldsymbol{\alpha}, \mathbf{r})$, $Q_{n-1}([\boldsymbol{\alpha}\times\mathbf{r}], \mathbf{r})$	
	ΔJ	$(n-1)', n$, $(n-1)', n$, $(n-1)$	$\Delta J=(0\leftrightarrow 0)$ — yes
	Parity Change	n_{odd} — yes, n_{even} — no	
Tensor	Matrix	$Q_n(\beta[\boldsymbol{\sigma}\times\mathbf{r}], \mathbf{r})$, $Q_n(\beta\boldsymbol{\alpha}, \mathbf{r})$, $Q_{n+1}(\beta\boldsymbol{\sigma}, \mathbf{r})$	
	ΔJ	n, n, $n', (n+1)$	None
	Parity Change	n_{odd} — yes, n_{even} — no	
Axial V.	Matrix	$Q_n([\boldsymbol{\sigma}\times r], \mathbf{r})$, $Q_{n+1}(\boldsymbol{\sigma}, \mathbf{r})$	
	ΔJ	n, $n', (n+1)$	$\Delta J=(0\leftrightarrow 0)$ — no
	Parity Change	n_{odd} — yes, n_{even} — no	
Pseudo-S.	Matrix	$Q_n(\beta\gamma_5\mathbf{r}, \mathbf{r})$	$\Delta J=(0\leftrightarrow n_{\text{even}})$ — no
	ΔJ	$(n-1)', n$	
	Parity Change	n_{odd} — no, n_{even} — yes	$\Delta J=(0\leftrightarrow n_{\text{odd}})$ — yes

operators given in (6). Q_{ij} is the irreducible tensor with zero spur.[18] The parentheses around the subscripts indicate that there is a term for each permutation of the indices. For "third" and "fourth forbidden" transitions, third-, fourth-, and fifth-rank tensors are required. The third-rank irreducible tensors are defined by

$$Q_{ijk}(\mathbf{a}, \mathbf{r})=\int d\tau V^*[a_{(i}x_jx_{k)} -1/5\delta_{(ij}a_{k)}r^2-2/5\delta_{(ij}x_{k)}(\mathbf{a}\cdot\mathbf{r})]U. \quad (8)$$

Similarly the fourth-rank tensors have the form

$$Q_{ijkl}(\mathbf{a}, \mathbf{r})=\int d\tau V^*[a_{(i}x_jx_kx_{l)} -3/7\delta_{(ij}x_kx_{l)}(\mathbf{a}\cdot\mathbf{r})-3/7\delta_{(ij}a_kx_{l)}r^2 +3/35\delta_{(ij}\delta_{kl)}(\mathbf{a}\cdot\mathbf{r})r^2]U. \quad (9)$$

All rank tensors are completely symmetric with respect to any permutation of their indices, and all "spurs" are zero; i.e.,

$$\sum_{\mu=1}^{3} Q_{\mu\mu kl\cdots m}=0. \quad (10)$$

"Fourth forbidden" tensor and axial vector interactions would require the fifth-rank tensor, $Q_{ijklm}(\boldsymbol{\sigma}, \mathbf{r})$. However, in the specific cases treated it will not be required.

The selection rules for which the various irreducible tensors are non-vanishing were given in II through the "second forbidden" approximation. Table II extends the spin and parity selection rules to the "nth forbidden" transitions.

The first column of Table II lists the five forms of interaction. For each form of interaction the second column contains the irreducible tensor matrix element appropriate to the "nth forbidden" approximation. The subscript n indicates that the tensor is of nth rank. There are tensors of lower rank in the "nth forbidden" transitions than those listed. The selection rules corresponding to these are already included in the "$(n-2)$ forbidden" degree. Therefore, it is seen that they constitute negligible corrections to the "$(n-2)$ forbidden" matrix elements. Beneath the matrix element is listed the spin changes for which the element is non-vanishing. The primes indicate that $|J_i|+|J_f|\geqslant J_{\max}$. As in II, "yes" means that the transition must be even↔odd; "no" indicates that the parities of initial and final nucleus must be the same. Particular combinations of spin and parity changes are completely "forbidden" in any approximation by four of the interactions. These cases are given in the last column. Table II is complete except for the "first" and "second forbidden" tensor and axial vector interactions. These omissions are certain scalars which are given in Konopinski and Uhlenbeck's Table I.[1]

[18] The tensors (7) are identified with those of paper II as follows:

$$Q_{ij}(\boldsymbol{\sigma}, \mathbf{r})\equiv B_{ij},\quad Q_{ij}(\boldsymbol{\alpha}, \mathbf{r})\equiv A_{ij},\quad Q_{ij}(\mathbf{r}, \mathbf{r})\equiv 2R_{ij}$$
$$Q_{ij}([\boldsymbol{\sigma}\times\mathbf{r}], \mathbf{r})\equiv T_{ij},\quad Q_{ij}([\boldsymbol{\alpha}\times\mathbf{r}], \mathbf{r})\equiv \mathcal{J}[\boldsymbol{\alpha}\times\mathbf{r}]_{(i}x_{j)}.$$

The notation used here is convenient for expression of the general nth-rank tensors, $Q_n(\mathbf{a}, \mathbf{r})$, introduced.

III. GENERAL FORMULAS FOR C_{nX}

The correction factors through "fourth forbidden" were derived for all the forms of interaction by the method outlined in the previous section. Upon inspection it was found that all the correction factors could be written in a generalized "nth forbidden" form.

$$C_{nS}=|Q_n(\beta\mathbf{r},\mathbf{r})/n!|^2\sum_{\nu=0}^{n}(A_{n\nu}q^{2(n-\nu)-2}M_\nu+2C_{n\nu}q^{2(n-\nu)-1}N_\nu+D_{n\nu}q^{2(n-\nu)}L_\nu),$$

$$\begin{aligned}C_{nV}=&|Q_n(\mathbf{r},\mathbf{r})/n!|^2\sum_{\nu=0}^{n}(A_{n\nu}q^{2(n-\nu)-2}M_\nu-2C_{n\nu}q^{2(n-\nu)-1}N_\nu+D_{n\nu}q^{2(n-\nu)}L_\nu)\\&+|Q_n(\boldsymbol{\alpha},\mathbf{r})/n!|^2\sum_{\nu=0}^{n}(A_{n\nu}q^{2(n-\nu)-2}L_\nu)+i[Q_n(\boldsymbol{\alpha},\mathbf{r})/n!\cdot Q_n^*(\mathbf{r},\mathbf{r})/n!-\text{c.c.}]\\&\times\sum_{\nu=0}^{n}(-A_{n\nu}q^{2(n-\nu)-2}N_\nu+C_{n\nu}q^{2(n-\nu)-1}L_\nu)+|Q_{n-1}([\boldsymbol{\alpha}\times\mathbf{r}],\mathbf{r})/(n-1)!|^2\\&\times\sum_{\nu=0}^{n-1}(A_{(n-1)\nu}q^{2(n-1-\nu)-2}M_\nu+2C_{(n-1)\nu}q^{2(n-1-\nu)-1}N_\nu+[D_{(n-1)\nu}-B_{(n-1)\nu}/n]q^{2(n-1-\nu)}L_\nu),\end{aligned}$$

$$\begin{aligned}C_{nT}=&|Q_n(\beta[\boldsymbol{\sigma}\times\mathbf{r}],\mathbf{r})/n!|^2\sum_{\nu=0}^{n}(A_{n\nu}q^{2(n-\nu)-2}M_\nu-2C_{n\nu}q^{2(n-\nu)-1}N_\nu\\&+[D_{n\nu}-B_{n\nu}/(n+1)]q^{2(n-\nu)}L_\nu)+|Q_n(\beta\boldsymbol{\alpha},\mathbf{r})/n!|^2\sum_{\nu=0}^{n}(A_{n\nu}q^{2(n-\nu)-2}L_\nu)\\&-[Q_n(\beta[\boldsymbol{\sigma}\times\mathbf{r}],\mathbf{r})/n!\cdot Q_n^*(\beta\boldsymbol{\alpha},\mathbf{r})/n!+\text{c.c.}]\sum_{\nu=0}^{n}(-A_{n\nu}q^{2(n-\nu)-2}N_\nu+C_{n\nu}q^{2(n-\nu)-1}L_\nu)\\&+|Q_{n+1}(\beta\boldsymbol{\sigma},\mathbf{r})/(n+1)!|^2\sum_{\nu=0}^{n}(B_{n\nu}q^{2(n-\nu)}L_\nu),\end{aligned}\tag{11}$$

$$\begin{aligned}C_{nA}=&|Q_n([\boldsymbol{\sigma}\times\mathbf{r}],\mathbf{r})/n!|^2\sum_{\nu=0}^{n}(A_{n\nu}q^{2(n-\nu)-2}M_\nu+2C_{n\nu}q^{2(n-\nu)-1}N_\nu\\&+[D_{n\nu}-B_{n\nu}/(n+1)]q^{2(n-\nu)}L_\nu)+|Q_{n+1}(\boldsymbol{\sigma},\mathbf{r})/(n+1)!|^2\sum_{\nu=0}^{n}(B_{n\nu}q^{2(n-\nu)}L_\nu).\end{aligned}$$

C_{nP} is the same as C_{nS} except that $Q_n(\beta\gamma_5\mathbf{r},\mathbf{r})$ replaces $Q_n(\beta\mathbf{r},\mathbf{r})$. $|Q_n/n!|^2$ is the sum of the squares of the absolute values of the components of the tensors, the summation sign over the n indices being omitted. The quantities, $A_{n\nu}$, $B_{n\nu}$, $C_{n\nu}$, and $D_{n\nu}$, are the numerical coefficients:

$$\begin{aligned}A_{n\nu}&=\frac{(n-\nu)2^{n-2\nu}(2\nu+1)!}{(2n-2\nu)!(\nu!)^2},\quad B_{n\nu}=\frac{2^{n-2\nu}(2\nu+1)!}{(2n-2\nu+1)!(\nu!)^2},\\C_{n\nu}&=\frac{(n-\nu)2^{n-2\nu}(2\nu+1)!}{(2n-2\nu+1)!(\nu!)^2},\quad D_{n\nu}=\frac{2^{n-2\nu}(\nu+1)(2\nu)!}{(2n-2\nu+1)!(\nu!)^2}.\end{aligned}\tag{12}$$

L_ν, M_ν, and N_ν are combinations of the radial part of the electron wave functions evaluated at $r=\rho$, the nuclear radius.

$$\begin{aligned}L_\nu&=(2p^2F_0)^{-1}(g_\nu^2+f_{-(\nu+2)}^2)\rho^{-2\nu},\\M_\nu&=(2p^2F_0)^{-1}(f_\nu^2+g_{-(\nu+2)}^2)\rho^{-2(\nu+1)},\\N_\nu&=(2p^2F_0)^{-1}(f_\nu g_\nu-f_{-(\nu+2)}g_{-(\nu+2)})\rho^{-2\nu-1}.\end{aligned}\tag{13}$$

Expanding the radial functions in ascending powers of ρ, one obtains the first approximation formulas for L, M, and N.

$$L_\nu=(F_\nu/F_0)\left(\frac{2^\nu\nu!}{(2\nu+1)!}p^\nu\right)^2\frac{\nu+1+S_\nu}{2\nu+2},$$

$$M_\nu=(F_\nu/F_0)\left(\frac{2^{\nu+1}\nu!}{(2\nu+2)!}p^\nu\right)^2\left[\frac{2\nu+2}{\nu+1+S_\nu}\left(\frac{\alpha Z}{2\rho}\right)^2+\left(\frac{S_\nu}{2S_\nu+1}p^2/W-\frac{(2\nu+1)(\alpha Z)^2W}{(2S_\nu+1)(\nu+1+S_\nu)}\right)\left(\frac{\alpha Z}{\rho}\right)\right.$$
$$\left.+\frac{(\nu+1)(S_\nu-\nu)S_\nu}{(2S_\nu+1)^2}\left(1-\frac{4S_\nu+3}{S_\nu(S_\nu+1)}(\alpha Z)^2\right)p^2+\left(1+\frac{\nu(4S_\nu+3)}{(S_\nu+1)(\nu+1+S_\nu)}(\alpha Z)^2\right)\left(\frac{\alpha Z}{2S_\nu+1}\right)^2\right], \tag{14}$$

$$N_\nu=-(F_\nu/F_0)\left(\frac{2^\nu\nu!}{(2\nu+1)!}p^\nu\right)^2\frac{1}{\nu+1}\left[\left(\frac{\alpha Z}{2\rho}\right)+\frac{S_\nu}{2S_\nu+1}p^2/W-\frac{2(\alpha Z)^2}{2S_\nu+1}W\right],$$

where

$$F_\nu(W,Z)=\left(\frac{(2\nu+2)!}{\nu!}\right)^2(2p\rho)^{2(S_\nu-\nu-1)}\exp(\pi y)\,|\,\Gamma(S_\nu+iy)\,|^2/\Gamma^2(1+2S_\nu) \tag{15}$$

and

$$S_\nu=[(\nu+1)^2-(\alpha Z)^2]^{\frac{1}{2}},\quad y=\alpha ZW/p.$$

For positron emission $-Z$ replaces Z; $\alpha=1/137$ is the fine structure constant. Formula (14) was used for RaE; however, for lighter elements, $A<100$, simplifications valid for $\alpha Z\ll 1$ are sufficient. In these cases $S_\nu\approx\nu+1$ and $F_\nu\approx F_0$ for any ν. L, M, and N then reduce to the simple expressions

$$L_\nu=a_\nu{}^2p^{2\nu},\quad M_\nu=a_{\nu+1}{}^2p^{2\nu}\left[b_\nu{}^2\left(\frac{\alpha Z}{2\rho}\right)^2+b_\nu\left(\frac{\alpha Z}{\rho}\right)p^2/W+p^2\right],\quad N_\nu=-a_\nu{}^2p^{2\nu}\left[b_\nu\left(\frac{\alpha Z}{2\rho}\right)+p^2/W\right], \tag{16}$$

where a_ν, and b_ν are the numerical factors, $a_\nu=2^\nu\nu!/(2\nu+1)!$, $b_\nu=(2\nu+3)/(\nu+1)$. The correction factors given above are complete except for C_{1T}, C_{1A}, and C_{2T}. The omitted terms apply only to $0\leftrightarrow 0$ transitions and are given in II. The characteristic features of the correction factors (11), have been discussed by Konopinski and Uhlenbeck in their effect on the shape of the spectra.

The evaluation of the lifetimes requires some estimate of the size of the nuclear matrix elements, (5) to (9), inclusive. An exact evaluation will not be possible until more is known concerning nuclear states. The comparable problem was met in the case of the "allowed" transitions by assuming the order of magnitude unity for the square of the matrix elements, $|\,Q_0(1)\,|^2$ and $\sum_i|\,Q_i(\beta\boldsymbol{\sigma})\,|^2$, which is consistent with normalized nuclear wave functions. In the "forbidden" case the situation is complicated by the fact that the irreducible tensors Q_n were constructed without regard to normalization. In symmetrizing them the $n!$ permutations of their indices introduce many terms. The spurious effect of this repetition of terms may be removed by introducing the normalization factors, $1/n!$, as is done in the formulas (11).

In order to obtain a more conservative estimate of the order of magnitude of the nuclear matrix elements, a method of averaging the tensor directions over a sphere may be adopted. To do this, the tensor $Q_{ij}([\boldsymbol{\sigma}\times\mathbf{r}],\mathbf{r})$, for example, is treated as if it were made up of ordinary independent vectors, $(\mathbf{r})$ and $(\boldsymbol{\sigma})$, having the magnitudes ρ and (σ), respectively. This procedure is at least consistent with the above-mentioned treatment of the "allowed" matrix elements. Two of the "first forbidden" tensor interaction matrix elements estimated in this way are $\sum_i|\,Q_i(\beta\boldsymbol{\alpha})\,|^2\approx(\beta)^2(\alpha)^2$ and $\sum_i|\,Q_i(\beta[\boldsymbol{\sigma}\times\mathbf{r}])\,|^2\approx\frac{2}{3}(\beta)^2(\sigma)^2\rho^2$. The normalized second- and higher-rank tensors may be estimated

by applying step by step the identities:

$$\sum_{ij}|Q_{ij}(\mathbf{a},\mathbf{r})/2!|^2=\sum_{ij}\left|\int d\tau V^*a_ix_jU\right|^2-\tfrac{1}{2}\sum_i|Q_i([\mathbf{a}\times\mathbf{r}])|^2-\tfrac{1}{3}|Q_0(\mathbf{a}\cdot\mathbf{r})|^2,$$

$$\sum_{ijk}|Q_{ijk}(\mathbf{a},\mathbf{r})/3!|^2=\sum_{ijk}\left|\int d\tau V^*a_ix_jx_kU\right|^2-\tfrac{2}{3}\sum_{ij}|Q_{ij}([\mathbf{a}\times\mathbf{r}],\mathbf{r})/2!|^2-\tfrac{3}{5}\sum_i|Q_i((\mathbf{a}\cdot\mathbf{r})\mathbf{r})|^2$$
$$+\tfrac{1}{5}\sum_i[Q^*{}_i((\mathbf{a}\cdot\mathbf{r})\mathbf{r})\cdot Q_i(\mathbf{a}r^2)+\text{c.c.}]-\tfrac{2}{5}\sum_i|Q_i(\mathbf{a}r^2)|^2, \tag{17}$$

$$\sum_{ijkl}|Q_{ijkl}(\mathbf{a},\mathbf{r})/4!|^2=\sum_{ijkl}\left|\int d\tau V^*a_ix_jx_kx_lU\right|^2-\tfrac{3}{4}\sum_{ijk}|Q_{ijk}([\mathbf{a}\times\mathbf{r}],\mathbf{r})/3!|^2$$
$$-\tfrac{5}{7}\sum_{ij}|Q_{ij}((\mathbf{a}\cdot\mathbf{r})\mathbf{r},\mathbf{r})/2!|^2+\tfrac{3}{7}\sum_{ij}[Q^*{}_{ij}((\mathbf{a}\cdot\mathbf{r})\mathbf{r},\mathbf{r})\cdot Q_{ij}(\mathbf{a}r^2,\mathbf{r})+\text{c.c.}]/(2!)^2$$
$$-\tfrac{5}{7}\sum_{ij}|Q_{ij}(\mathbf{a}r^2,\mathbf{r})/2!|^2-\tfrac{3}{10}\sum_i|Q_i([\mathbf{a}\times\mathbf{r}]r^2)|^2-\tfrac{1}{5}|Q_0((\mathbf{a}\cdot\mathbf{r})r^2)|^2.$$

Upon applying the above method one obtains the following estimated magnitudes for the square of the normalized matrix elements:

$$|Q_n(s\mathbf{r},\mathbf{r})/n!|^2\approx N_n(s)^2\rho^{2n}$$

where

$$N_n=2^n(n!)^2/(2n)! \tag{18}$$

and (s) is the order of magnitude of the scalars (β), 1, and $(\beta\gamma_5)$ for the scalar, polar vector, and pseudo-scalar interactions, respectively.

$$|Q_n(s\boldsymbol{\sigma},\mathbf{r})/n!|^2\approx(2n+1)/3n\cdot N_n(s)^2(\sigma)^2\rho^{2n-2}. \tag{19}$$

Here, $(s)=1$ for the axial vector interaction and $(s)=(\beta)$ for the first term of $(4T)$, $(s)=(\beta\gamma_5)$ for the second term, and $(s)=(\gamma_5)$ for the second term of $(4V)$.[19] Finally, the matrix elements involving the components of the vector products, $[\boldsymbol{\sigma}\times\mathbf{r}]$ and $[\boldsymbol{\alpha}\times\mathbf{r}]=\gamma_5[\boldsymbol{\sigma}\times\mathbf{r}]$, have the magnitudes:

$$|Q_n(s[\boldsymbol{\sigma}\times\mathbf{r}],\mathbf{r})/n!|^2\approx(n+1)/3n\cdot N_n(s)^2(\sigma)^2\rho^{2n}. \tag{20}$$

Cross products of the matrix elements of the type

$$i[Q_n(\boldsymbol{\alpha},\mathbf{r})/n!\cdot Q^*{}_n(\mathbf{r},\mathbf{r})/n!-\text{c.c.}]$$

and

$$[Q_n(\beta[\boldsymbol{\sigma}\times\mathbf{r}],\mathbf{r})/n!\cdot Q^*{}_n(\beta\boldsymbol{\alpha},\mathbf{r})/n!+\text{c.c.}],$$

appearing in C_{nV} and C_{nT}, vanish upon applying the method of evaluation described above. One would expect such interference terms to be very small on the basis that the phases of the individual terms of the sum are random; i.e., the presence of both positive and negative terms would tend to cancel each other and result in negligible values for their sum.

In estimating the sizes of the matrix elements (18), (19), and (20), the order of magnitudes of $(\beta)^2$, $(\sigma)^2$, $(\gamma_5)^2$ and $(\beta\gamma_5)^2$ must be introduced. It was assumed that $(\beta)^2=(\sigma_i)^2\approx1$ for the usual reason that the operators β and σ_i cause the large components of the nuclear wave functions to be multiplied together. Accordingly the magnitude, $(\sigma)^2=(\sigma_1)^2+(\sigma_2)^2+(\sigma_3)^2\approx3$, emerges. On the other hand, the operators γ_5 and $\beta\gamma_5$ mix the large and small components of the wave functions resulting in values of $(\gamma_5)^2$ and $(\beta\gamma_5)^2$ smaller by a factor of $\approx(v/c)^2$, where v is the order of magnitude of the velocity of nuclear particles. One would expect v to be about 1/10 the velocity of light. Critchfield[20] obtained $(\beta\gamma_5)^2\approx0.1$ by assuming special (s and p) nuclear wave functions; however, his introduction of such wave functions led to a much smaller magnitude for $(\gamma_5)^2$ alone: namely, $(\gamma_5)^2\approx10^{-5}W_0^2$. A similar small magnitude was obtained by Marshak who made use of the quantum-kinematical relation, $\int d\tau V^*\boldsymbol{\alpha}U=iW_0\int d\tau V^*\mathbf{r}U$. This yields the value, $(\alpha)^2=(\gamma_5)^2(\sigma)^2\approx W_0^2\rho^2$. This relation is applicable only if the coulomb energy differences

[19] The operator $\boldsymbol{\alpha}$, appearing in the second terms of (4), may be written $\boldsymbol{\alpha}=\gamma_5\boldsymbol{\sigma}$ where $\gamma_5=-i\alpha_1\alpha_2\alpha_3$.

[20] C. L. Critchfield, Phys. Rev. 61, 249 (1942).

between the initial and final nuclei are ignored. For most of the decays treated the coulomb energy difference is larger than the electron's maximum energy. In this paper the magnitudes, $(\beta\gamma_5)^2 \approx (\gamma_5)^2 \approx (v/c)^2$, are assumed. $(v/c)^2$ is considered as a parameter having the range of values $(v/c)^2 \approx ((W_0\rho)^2 - 0.1)$. The value of the nuclear radius, $\rho = 0.004A^{\frac{1}{3}}$, which is roughly five percent larger than that used by Marshak, is assumed in the cases treated here.

In deriving the formulas (11), it was tacitly assumed that transitions involving a spin change, $\Delta J = |J_i - J_f|$, could lead to $2\Delta J+1$ degenerate magnetic states of the electron plus neutrino. This is in effect what is assumed when the sum over the quantum numbers m is performed as indicated in Eq. (3). Marshak has shown that if $J_i > J_f$ only one value of the electron-neutrino total magnetic quantum number, $\mu = k = \Delta J$ is permitted. $k = \Delta J$ is the value of the electron-neutrino total angular momentum that gives the largest contribution to the transition probability. Larger values of k that are possible yield probabilities smaller by a factor of $\approx (W_0\rho)^2$ and are ignored by both methods of treatment. Consequently half-lives calculated from Eq. (1) should be multiplied by $2\Delta J+1$ if $J_i > J_f$.

The relation between the nuclear matrix elements (18), (19), and (20), and those used by Marshak (constructed from spherical harmonics) was investigated. It was found that the half-life formulas were identical if Marshak's normalized matrix elements $|M_n|^2$, $|M_{n-1}'|^2$, and $|M_{n-1}''|^2$ were evaluated by the averaging process just discussed. Performing these averages we find the values $|M_n|^2 \approx |M_{n-1}'|^2 \approx 1$ for $(\gamma_5)^2 \approx (W_0\rho)^2$, $(\sigma)^2 = 3$. Those matrix elements containing the components of $[\sigma \times \mathbf{r}]$ are slightly smaller. By averaging, the values, $|M_{n-1}''|^2 \approx (n+1)/(2n+1)$, were obtained.

Aside from the difference in form of the nuclear matrix elements a more serious difference between Marshak's calculations and those presented here appears in the cases of unfavorable parity change from the tensor or polar vector interaction. He ignores the terms linear in $(\alpha Z/\rho)$ and independent of $(\alpha Z/\rho)$ which appear in the formula (16) for M_ν, and completely ignores L_ν and N_ν, on the basis that $(\alpha Z) \ll 1$. This approximation is good only as long as the maximum kinetic energy of the electron is very small in comparison to the coulomb energy difference $(\alpha Z/\rho)$. The energy dependent factors multiplying $(\alpha Z/\rho)$ in M_ν and N_ν contain the energy to one degree higher than in the factor multiplying $(\alpha Z/\rho)^2$. In the case of Rb^{87} $(W_0 - 1 = 0.26,\ (\alpha Z/\rho) = 15.2)$ the error introduced is insignificant; however, for K^{40} $(W_0 - 1 = 1.4 - 2.6,\ (\alpha Z/\rho) = 10.1)$ dropping all except the terms in $(\alpha Z/\rho)^2$ increases the calculated "fourth forbidden" half-life by a factor of 2 on the basis of Marshak's values of ρ and (α). The discrepancy is aggravated when the larger values of ρ and (α) used in this paper are applied. (See Table I.)

IV. COMPARISON WITH EXPERIMENT

The theoretical half-lives of RaE, P^{32}, K^{40}, and Rb^{87} listed in Table I were calculated by numerical integration of Eq. (1) for the tensor and polar vector interactions. The values $(6)10^3$ sec. and $(3)10^3$ sec. were assumed for $(2\pi^3 \ln 2/G^2)$ for the tensor and polar vector interactions, respectively.[14] The calculated half-lives listed for the cases of unfavorable parity change correspond to the range of values, $(v/c)^2 = [0.1 - (W_0\rho)^2]$. The shape of the electron energy distribution is very sensitive to changes in (v/c) as can be seen from the calculated average electron energies. The spin and parity change for each transition is listed in the first column. The $(f_{nX}t_{\exp})$ values listed in the last column give the order of magnitude of $(2\pi^3 \ln 2/G^2)$ that would yield the experimental half-life.

RaE

Previous to the work of Konopinski and Uhlenbeck[21] it was generally supposed that the half-life of RaE could be accounted for by the "first forbidden" approximation. However, these authors have shown that the distribution in energy of the emitted β-rays could be predicted only by assuming $\Delta J = (2 \to 0)$, "no," which requires the "second forbidden" approximation.

[21] The results for RaE presented here are based on the numerical calculations performed by Konopinski and Uhlenbeck. I am greatly indebted to Dr. Konopinski for access to the numerical tables of the RaE correction factors. The nuclear radius, $\rho = 0.027$, used in paper II for RaE is also used here in estimating the magnitudes of the nuclear matrix elements.

It remained to be shown that the half-life could also be obtained in this approximation.

For an element as heavy as RaE the formulas (14) are required. Using the estimated values of the matrix elements given by Eqs. (19) and (20), one obtains in the "first" and "second forbidden" approximations:

$$f_{1T}(3.3, 83) \approx (7.9)10^{-2}, \quad (21)$$

$$f_{2T}(3.3, 83) \approx [4.1+79(v/c)^2]10^{-3}, \quad (22)$$

$$f_{2V}(3.3, 83) \approx [8.2+79(v/c)^2]10^{-3}. \quad (23)$$

The half-life given by the "first forbidden" calculation (21) is too small by a factor of only $\frac{1}{5}$. Thus the evidence of the calculated half-life alone does not eliminate the possibility of accounting for the RaE decay in the "first forbidden" approximation. However, the "second forbidden" formulas (22) and (23) yield calculated half-lives equally satisfactory. Moreover, the fact that the shape of the energy distribution can be reproduced accurately only by the "second forbidden" approximation, indicates that by either Gamow-Teller or Fermi selection rules the transition involves no change of parity with a spin change of $\Delta J=(2\rightarrow 0)$. The value of (v/c) that yields the best reproduction of the electron energy distribution according to the tensor interaction is $(v/c)\approx 0.16$. Using this value of (v/c) one obtains $(f_{2T}t_{\exp})=(2\pi^3 \ln 2/G^2)$ $\approx(2.6)10^3$ sec. as compared to the value, $\approx(6)10^3$ sec., appropriate for "allowed" transitions.[14]

A slightly better energy distribution can be obtained by including the cross products of the matrix elements as is done in paper II. There the ratio, $Q_{ij}(\beta\boldsymbol{\alpha}, \mathbf{r})/Q_{ij}(\beta[\boldsymbol{\sigma}\times\mathbf{r}], \mathbf{r})\approx -5.8$, was used in order to obtain the best spectrum. On the other hand, this procedure is equivalent to a different evaluation of the nuclear matrix element, $Q_{ij}(\boldsymbol{\alpha}, \mathbf{r})$. If one assumes the ordinary vector $(\boldsymbol{\alpha})$ perpendicular to $(\mathbf{r})$ and $(\boldsymbol{\sigma})$ and of magnitude $(\alpha)=(\sigma)(v/c)$, one may obtain such a non-vanishing interference term. The ratio used in paper II corresponds to the magnitude, $(v/c)=0.16$, which yields an (ft) value of $(6.4)10^3$ sec.

Although the inclusion of the interference term is thus seen to give an excellent account of the observed half-life and energy distribution, its inclusion is not essential. The fact that the cross term contributes more than half of the probability of electron emission, when the ratio, -5.8, is assumed, perhaps indicates that its inclusion is not to be preferred over the simpler evaluations that lead to vanishing interference terms.

P^{32}

The best reproduction of the observed energy spectrum of P^{32} was obtained in II by adjusting the ratio of the nuclear matrix elements, $Q_{ij}(\beta\boldsymbol{\alpha}, \mathbf{r})/Q_{ij}(\beta[\boldsymbol{\sigma}\times\mathbf{r}], \mathbf{r})\approx -2.2$, and including the cross term. Using the same method of evaluation of these matrix elements as mentioned in the previous paragraph, one obtains for $\Delta J=(2\rightarrow 0)$, "no" and $W_0=4.37$[22] a theoretical half-life too large by a factor of 100. The observed half-life of P^{32} is 14.07 ± 0.01 days.[23]

An equally good reproduction of the energy distribution can be obtained with the simpler assumptions used in evaluating the matrix elements. [See Eqs. (19) and (20).] For the tensor and polar vector interactions one obtains:

$$f_{1T}(4.37, 15) \approx (1.1)10^{-2}, \quad (24)$$

$$f_{2T}(4.37, 15) \approx [1.9+(1.1)10^3(v/c)^2]10^{-5}, \quad (25)$$

$$f_{2V}(4.37, 15) \approx [3.9+(1.1)10^3(v/c)^2]10^{-5}. \quad (26)$$

The best energy distribution is given by $C_{2T}F_0pWq^2dW$ when $(v/c)\approx 0.029$ is assumed, which is considerably less than the minimum value $W_0\rho$ used in Table I. However, the half-life predicted is ≈ 200 times too large. In order to obtain the correct half-life, one must assume $(v/c)=0.67$ in (25), which is unreasonably large.

The "first forbidden" half-life listed in Table I is too small by a factor of only $\frac{1}{2}$, while f_{2V} and f_{2T} give half-lives at least two and four times too large, respectively. The energy distribution for these three alternative cases is practically the same; it deviates somewhat from the observed spectra.[22] In view of the fact that the energy distribution favors only slightly the "second forbidden" approximation the evidence of the half-life indicates that P^{32} is probably a

[22] J. L. Lawson, Phys. Rev. **56**, 131 (1939).
[23] D. Mulder, G. W. Hoeksema, and G. J. Sizoo, Physica **7**, 849 (1940).

"first forbidden" transition according to Gamow-Teller selection rules with $\Delta J=(2\rightarrow 0)$, the transition being from the P^{32} state of odd parity to the ground state of S^{32} which has even parity.

K^{40}

The known spin change[3] of K^{40} requires at least the "third forbidden" approximation if Gamow-Teller selection rules are to be preferred to Fermi rules. In substantial agreement with the calculations of Marshak,[9] it was found that the observed half-life,[24] $t_{\exp}=(4.5\pm 0.9)10^{16}$ sec., could be given by the "third forbidden" tensor interaction if the maximum energy has approximately the value $W_0\approx 2.4$, used here. On the other hand, if the end-point energy[10] amounts to as much as $3.6\,mc^2$, the "third forbidden" half-life calculated is too small by a factor $\approx 1/50$, and the "fourth forbidden" tensor or polar vector interactions yield results even better than the "third forbidden" approximation with $W_0=2.4$.

The average energy quoted by Bramley and Brewer,[24] $\bar{E}=0.35$ Mev, is in good agreement with the "third forbidden" value calculated with $W_0=2.4$. For $W_0=3.6$ the average energy according to the "fourth forbidden" tensor or polar vector interactions is at least 0.5 Mev which is considerably higher than previously reported.

Until more precise values of the end-point and average electron energies are determined, the argument in favor of Gamow-Teller selection rules presented by the K^{40} decay will remain somewhat doubtful.

[24] A. Bramley and A. K. Brewer, Phys. Rev. **53**, 502 (1938).

Rb^{87}

The low maximum energy[25] of the Rb^{87} electrons, $W_0=1.26$, accounts for its very long half-life. Experimental determinations of the half-life vary somewhat; $(2-4)10^{18}$ sec. is reported by Hemmendinger and Smythe,[12] while $(6-12)10^{18}$ sec. is the value found by Hahn, Strassmann, and Walling.[11] The latter authors indicate that the shorter half-life, $(6)10^{18}$ sec., is probably the best.

The "third forbidden" approximations yield half-lives of the correct order of magnitude, while the "second forbidden" calculations result in a value too small by a factor of 1/1000. It should be noticed that the average kinetic energy of the decay electrons corresponding to the best calculated half-life is roughly $\frac{1}{3}$ their maximum kinetic energy.

V. CONCLUSIONS

For the four cases treated, the tensor interaction seems consistently to give the best results. The good agreement with experimental determinations obtained for RaE can, of course, be given equally well by the polar vector interaction. However, the polar vector interaction fails to account for the half-life of P^{32}. It likewise is inadequate for K^{40} if the lower end-point energy of K^{40} is more nearly correct than the larger value reported by Henderson.

The author wishes to thank Dr. E. J. Konopinski under whose valuable guidance this work was done, for suggesting the lifetime problems treated, and for criticizing the work in preparation.

[25] W. F. Libby and D. D. Lee, Phys. Rev. **55**, 245 (1939).

Beta-Ray Spectra of Scandium

GAIL P. SMITH*
Randall Laboratory of Physics, University of Michigan, Ann Arbor, Michigan
(Received February 20, 1942)

The positron spectrum of Sc^{44}, and the electron spectrum of Sc^{48} have been measured by a spectrometer of high resolution. A Kurie plot of the spectra shows that neither satisfies the Fermi distribution for an "allowed disintegration." The maximum energy of the positrons is 1.45 ± 0.01 Mev, and of the electrons 640 ± 4 kev. Other activities in scandium were too weak to be measured. The spectra have been corrected for width of the slits of the spectrometer, and an experimental check on the accuracy of the correction obtained. The positron decay curve may be resolved into two components, of 4-hr. and 52-hr. half-life, due to a 52-hr. γ-ray transition to the 4-hr. Sc^{44} positron-emitting level. The conversion coefficient of the γ-ray is 0.070 ± 0.012, corresponding to a change of angular momentum of 3 units in the transition. The excitation energy of the γ-ray for deuteron bombardment has been obtained as 4.0 ± 0.2 Mev.

THE well-known Fermi theory of β-decay[1] gives an explicit expression for the shape of the β-spectrum of radioactive disintegrations for allowed transitions. The distribution function is seen to be rather sensitively dependent upon the maximum energy of the radioactive transition. Recently, Uhlenbeck and Konopinski[2] have been able to formulate the theory for forbidden transitions, which is given in the form of a correction factor to the Fermi distribution function. To be able to classify a given radioactive disintegration as allowed, or forbidden, it is then necessary to measure both the shape of the spectrum, and its upper end point with the maximum precision possible.

An isotope of scandium was one of the first elements to be formed by an artificial disintegration due to bombardment,[3] and a considerable amount of work in the identification and classification of the radioactive isotopes of scandium has already been reported. Scandium is interesting in that it has only one stable isotope, Sc^{45}, whereas the latest systematic classification gives it at least seven radioactive ones, of weights 41, 42, 43, 44, 46, 48, 49.[4,5] Where measured at all, the spectra had been observed by cloud-chamber methods. It seemed worth while to re-examine the spectra more exactly, namely by the β-ray spectrometer. Preliminary results have been reported previously.[6] The instrument used is a high resolution 180° focusing type, with radius of curvature of the β-particles 12 cm and has previously been described.[7]

Preliminary deuteron bombardments of calcium, alpha-particle bombardments of potassium and calcium, and irradiation of titanium with neutrons from the (Be-n) reaction, showed that the calcium-deuteron reactions were the only ones which gave intensities of radioactive spectra great enough to be measured accurately in the beta-ray spectrometer. No bombardments were made of scandium because of the requirement of a very thin sample for the spectrometer. No activities were found which conflict with the final assignments of the isotopes made by Walke.[4]

Calcium, in the form of the metal, or the oxide or hydroxide, was bombarded with 9.5 Mev deuterons at average beam currents of 8–10 microamperes, irradiations lasting for as long as 175 microampere hours. The entire sample was dissolved in a minimum of concentrated HCl, and after a preliminary filtering to remove any traces of dust and other impurities which were not acted on by the HCl; 0.1 mg carrier was added, and the scandium deposited as the hydroxide by filtering through a funnel whose base, held tightly against a filter paper, was formed into a slit of the desired size. The filter paper weighed about 3 mg/cm². The active

* Now with Corning Glass Works, Corning, New York.
[1] E. Fermi, Zeits. f. Physik **88**, 161 (1934).
[2] G. E. Uhlenbeck and E. J. Konopinski, Phys. Rev. **60**, 308 (1941).
[3] M. Zyw, Nature **134**, 64 (1934).
[4] H. Walke, Phys. Rev. **57**, 163 (1940).
[5] L. D. P. King and D. R. Elliot, Phys. Rev. **59**, 168A (1941).
[6] G. P. Smith, Phys. Rev. **59**, 937A (1941).
[7] J. L. Lawson and A. W. Tyler, Rev. Sci. Inst. **11**, 6 (1940).

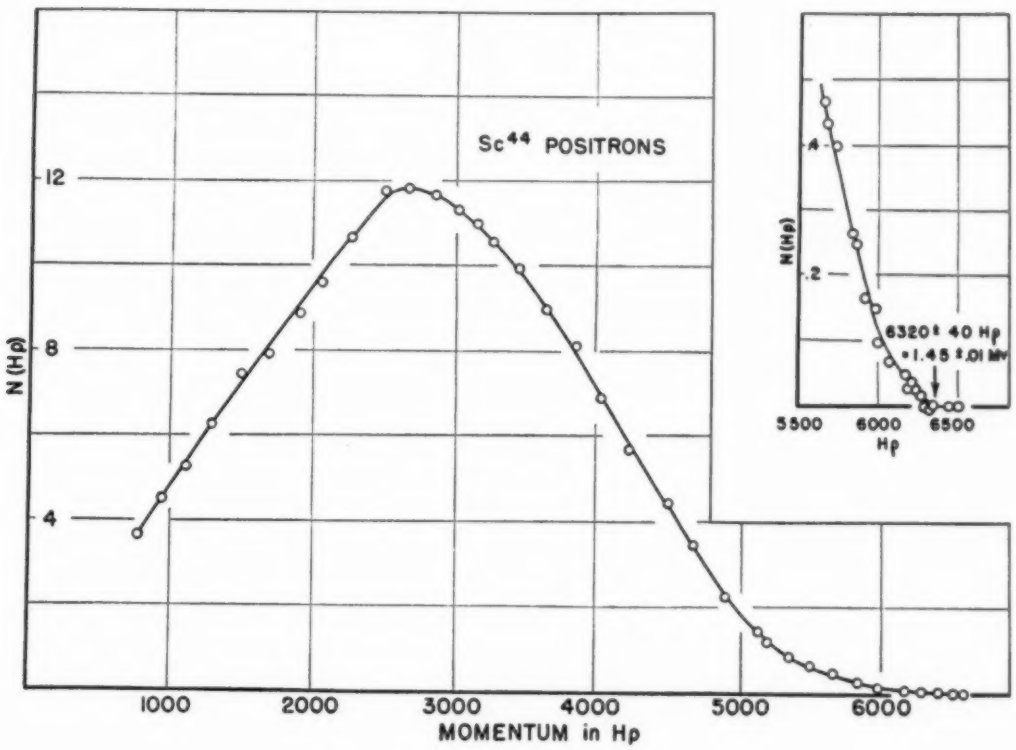

FIG. 1. The positron spectrum of Sc^{44}.

scandium deposit was covered with a very thin layer (<0.05 mg/cm²) of collodion, and placed in the spectrometer. Experiments of Lawson[8] have shown that the scattering due to the filter paper and collodion is probably negligible.

When examined in the spectrometer, both electron and positron spectra were found, along with a line of conversion electrons. They are shown in Figs. 1 and 2. Each has been corrected for background counting rate, efficiency of the counter, absorption in the counter window, counting losses in the scale-of-64 recording circuit, and decay of the source during observation. Decay curves of the various components of the observed spectra are shown in Fig. 3.

THE SPECTRUM OF Sc^{44}

The positron spectrum of the separated scandium has an end point at 1.45±0.01 Mev, and by measuring the activity as a function of time for a particular value of $H\rho$, a decay curve with two components, 4.1±0.1 hr., and 52±2 hr., was obtained. To identify these two components, previously suggested to be isomers,[4,9] several tests were made, from which the following conclusions may be drawn:

1. The shape of the observed spectrum does not change with energy of the bombarding deuterons. This indicates that there is only one responsible isotope; the excitation functions of two different isotopes are almost certainly widely different, and the shape of the spectrum, if complex, should change with bombardment energy.

2. The shape of the decay curves taken for several different values of $H\rho$ remains the same. If there were two superposed spectra, with presumably different half-lives and different maximum energies, the decay rate would be dependent on the $H\rho$ of the point considered.

3. The upper end point was also constant with time. Within the statistical fluctuations of the very weak activity near the maximum energy, the end-point energy is the same for the 4.1-hr. and the 52-hr. periods.

Since, therefore, the 4.1-hr. and the 52-hr.

[8] J. L. Lawson, Phys. Rev. **56**, 131 (1939).

[9] J. M. Cork and R. L. Thornton, Phys. Rev. **53**, 866 (1938).

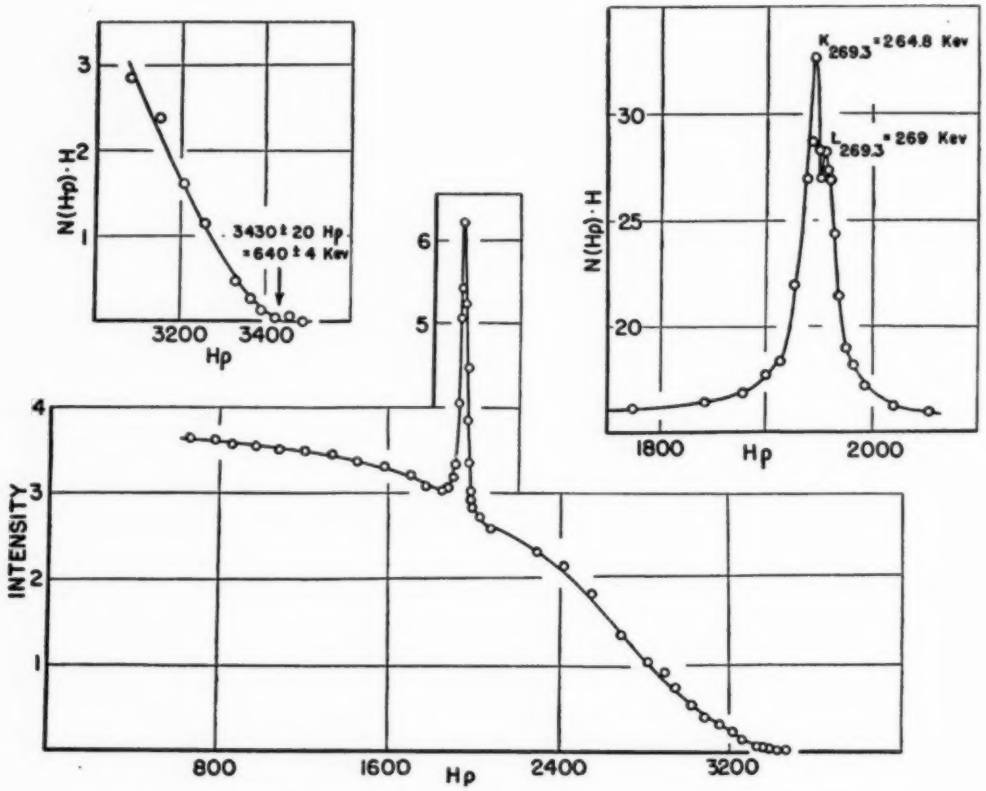

FIG. 2. The electron spectrum of Sc^{48}, and the conversion electrons from the γ-ray in Sc^{44}.

spectra have the same shape, and the same maximum energy, independent of the energy of the deuterons producing them, it may be concluded that they are identical. The presence of a 52-hr. gamma-ray allows the conclusion that the 4.1-hr. period is to be associated with the Sc^{44} level. After the active atoms originally on the Sc^{44} level have all decayed, the level is still being supplied with Sc^{44} atoms from the γ-ray transition with a 52-hr. half-life from Sc^{*44}, 269 kev above the Sc^{44} level. Since Sc^{44} has a relatively short half-life the positrons then appear with the half-life of the parent, 52 hours. Intensities extrapolated to the end of bombardment of the 52-hr. and 4.1-hr. components indicate that both scandium levels are formed in the bombardment.

INTERNAL CONVERSION OF THE GAMMA-RAY

After all the excited nuclei originally on the Sc^{44} level have disintegrated with the 4.1-hr. period, every positron which appears should have been produced by a γ-transition, and so for each γ, a β^+-ray should appear. Counting the total number of β^+-particles (by integrating under the spectrum) should then be equivalent to counting the γ-rays, which would be more difficult. By the same method of integration, the conversion electrons from the γ-ray can be counted, and hence the internal conversion coefficient for the γ-ray obtained. Three samples gave 0.064 ± 0.015, 0.10 ± 0.02, and 0.077 ± 0.010, of which the last is seen to be the most accurate.[10]

Hebb and Uhlenbeck,[11] and others[12] have calculated the probability that a γ-ray of given energy in a transition between two states whose angular momentum difference is known, will be

[10] A. C. Helmholz [Phys. Rev. **60**, 415 (1941)] has estimated the conversion coefficient of this γ-ray by comparing the number of conversion electrons with the number of photoelectrons from lead. He obtained $\alpha=0.5$ corresponding to $l=4$. The half-life of the radiation does not agree with computed λ's for any l, and hence cannot be used to determine uniquely the spin change.

[11] M. H. Hebb and G. E. Uhlenbeck, Physica **7**, 605 (1938).

[12] S. M. Dancoff and P. Morrison, Phys. Rev. **55**, 122 (1939).

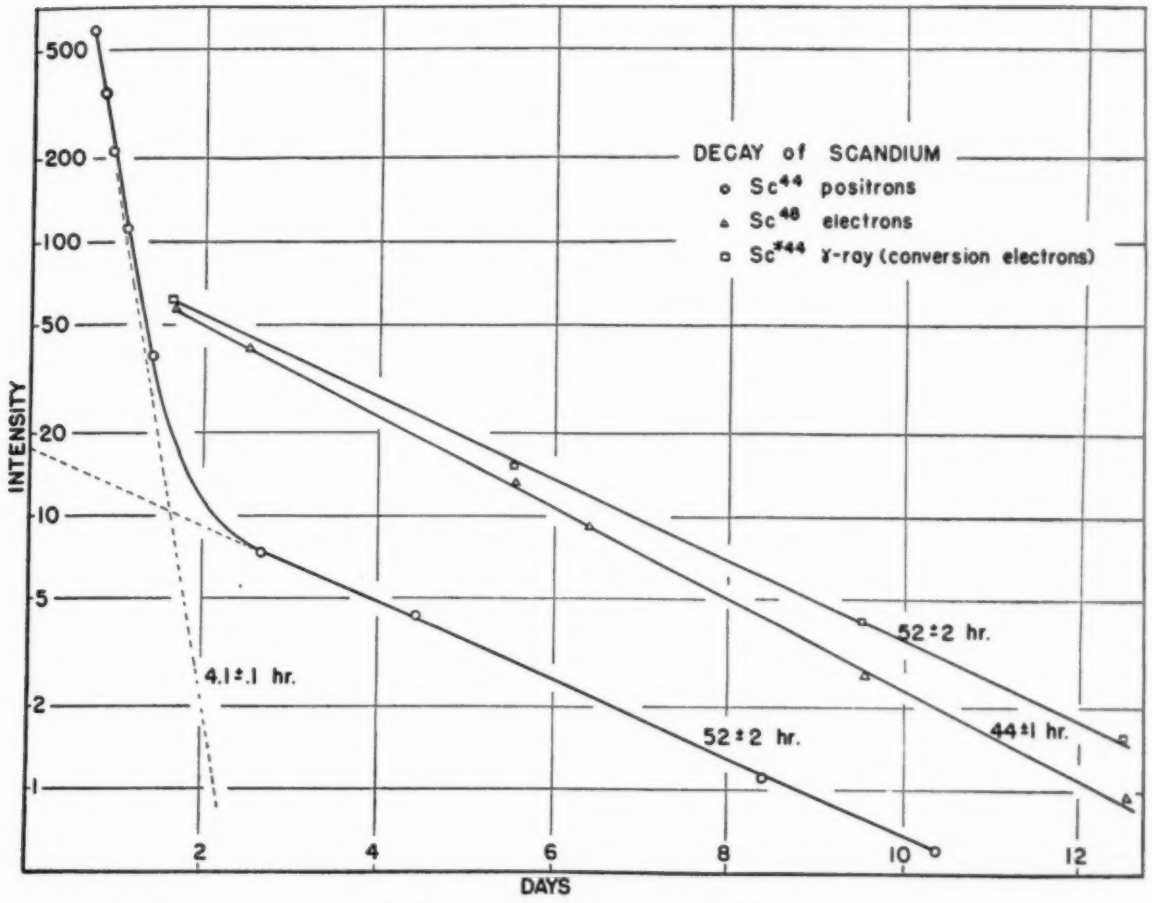

FIG. 3. Decay curves of the scandium isotopes.

internally converted. For light nuclei, up to $Z \sim 30$, the probability may be computed non-relativistically. For scandium, $Z=21$, and for a γ-ray transition between two states of energy difference 269.3 kev, the expected ratio of electrons to γ-ray quanta depends on the change in angular momentum in the following way:

l	1	2	3	4
N_e/N_q	0.00084	0.0047	0.084	0.308

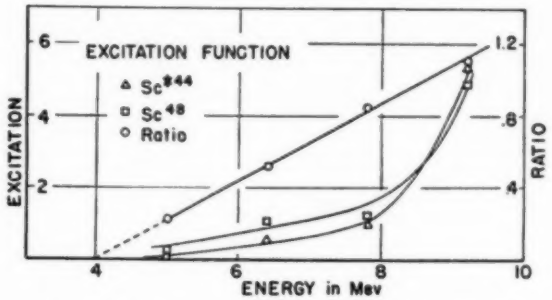

FIG. 4. Excitation energy of the 269-kev γ-ray.

for conversion in the K shell only. Conversion in the L shell must be added to this, which would increase the ratio somewhat. Curves drawn by Hebb and Nelson give for a γ-ray of 269 kev in scandium, the ratio $\alpha_K/\alpha_L=11$, with a possible error of 10–20 percent, and almost independent of the angular momentum change. From the known shape of electron conversion lines in the spectrometer, the observed conversion electron spectrum may be approximately resolved into two components due to conversion in the orbital electron shells. This gives $\alpha_K/\alpha_L=8\pm50$ percent, in fair agreement with theory. The corrected experimental value of N_e/N_q is then 0.070 ± 0.012, which when compared with the values given in the table above, indicates that this is an electric octopole radiation; change of angular momentum $=3$.

EXCITATION ENERGY OF THE γ-RAY

The spectrometer affords an accurate method of measuring the excitation energy of the Sc^{*44}

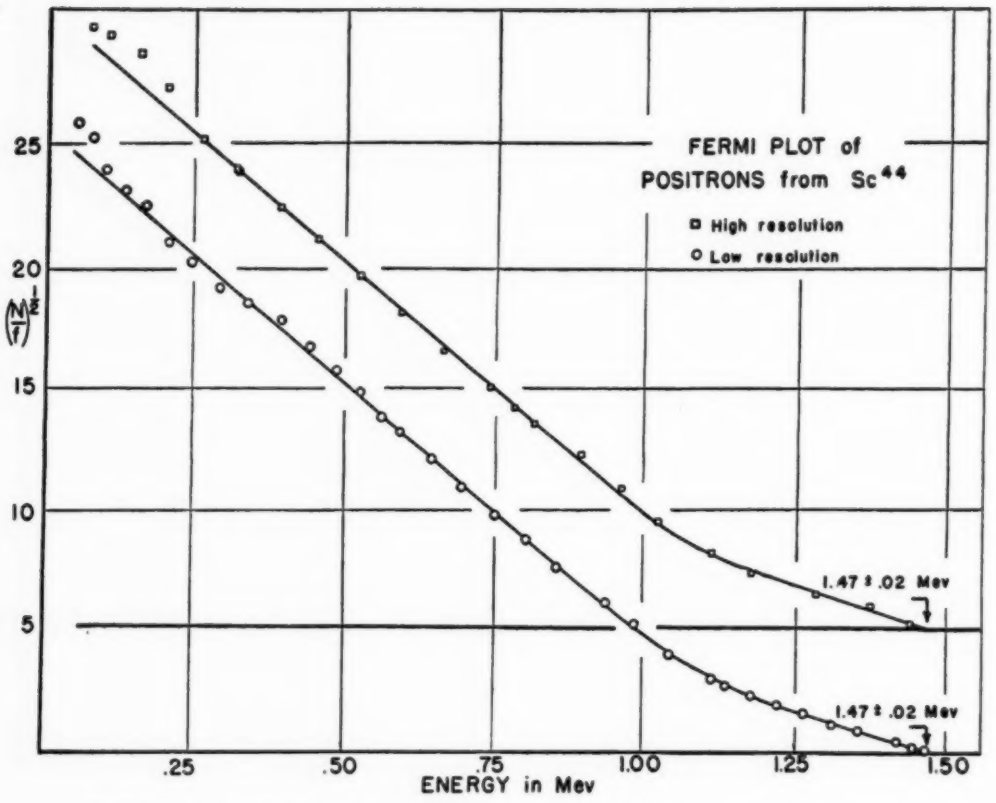

FIG. 5. The Fermi plot of the positron spectrum of Sc^{44}. The upper curve has been raised 5 units to avoid confusion of points.

level. An attempt to measure the total yield (or, what amounts to the same thing, the counting rate at a given time after bombardment) per deuteron always contains in the results all the uncertainties of interrupted bombardments, and of the efficiency of measurement, and of the efficiency of the chemical separation. However, in the spectrometer, the γ-ray of the Sc^{*44}—Sc^{44} transition appears superposed on the continuous spectrum of Sc^{48}. In measuring the two spectra, the same uncertainties, (and of the same amount and sign) are present in both. The ratio of the two then results in considerably more significant data than either taken separately, especially as the general excitation energy curve goes to zero somewhat asymptotically. Figure 4 shows the counting rate per microampere hour of bombardment, for Sc^{*44}, Sc^{44}, and their ratio. The indicated energy of excitation by deuterons for the Sc^{*44} level is seen in Fig. 4 to be 4.0 ± 0.2 Mev. The bombarding energy was changed by either changing the wave-length of the oscillators of the cyclotron, or by interposing foils of aluminum in the deuteron beam. The energy was computed from the range-energy curves in air for protons given by Livingston and Bethe;[13] a deuteron of energy $2E$ having twice the range of a proton of energy E.

EFFECT OF SLIT WIDTH ON THE SHAPE OF THE SPECTRUM

The observed spectra have also been corrected for the effect of a finite slit width, by choosing a suitable average radius of curvature of the particles. To test this quantitatively, sources were prepared for a slit width of 3 mm and of 1 mm and the positron spectra of each measured separately in the spectrometer. The positrons were measured, rather than the electrons, because of their greater intensity. However, it was impossible to get a source strong enough for the 1 mm slit to give results statistically as good as

[13] M. S. Livingston and H. A. Bethe, Rev. Mod. Phys. 9, 268 (1939).

for low resolution. The Kurie plot of the two spectra appears in Fig. 5. The two curves have been displaced by one unit on the graph to show more clearly the points on each. They are seen to be parallel, and to have the same extrapolated upper end point, indicating that the effect of a finite slit width may be satisfactorily corrected for in obtaining the true shape of the spectrum.

THE SPECTRUM OF Sc^{48}

The electron spectrum has an upper end point of 3430 ± 30 $H\rho$, corresponding to an energy of 640 ± 4 kev. A plot of the Kurie approximation to the Fermi function gives the curve shown in the Fig. 6. The decay in the spectrometer shows a single half-life 44 ± 2 hr. No electrons of energy greater than 650 kev, either from a continuous spectrum or a converted γ-ray were found.[14] The observed conversion electrons from the K shell occur at 1943 $H\rho$, or 264.8 kev. The conversion in the L shell is seen to be incompletely resolved from the K conversion electrons, but an approximate separation in which the known shape of a conversion line in the spectrometer is used gives for the electrons from the L shell, $H\rho=1962$, or $E=269.2$ kev. .By adding the binding energies of the K and L electrons obtained from x-ray data, 4.5 and 0.5 kev, respectively, one obtains the energy of the γ-ray as 269.3 ± 1 kev. By subtracting the continuous electron background (which decays with a different half-life) from the conversion electrons, the half-life of the electron line, and hence of the γ-ray, is found to be 52 ± 2 hr.

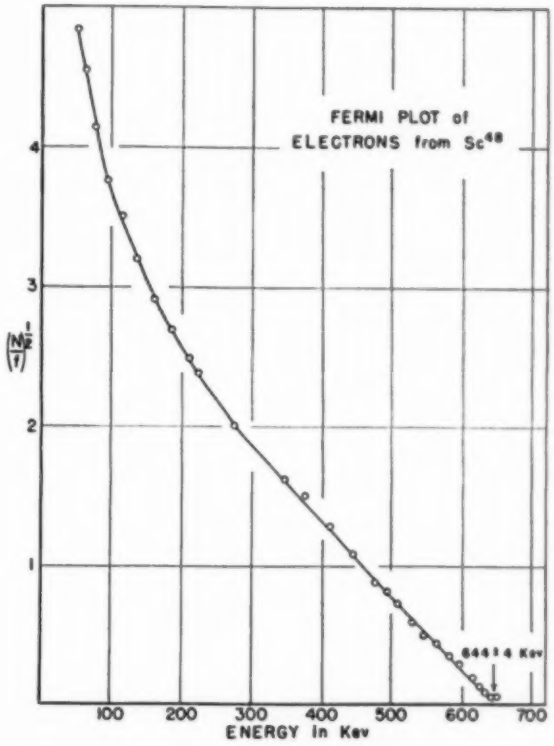

FIG. 6. The Fermi plot of the electron spectrum of Sc^{48}.

I wish to acknowledge the cooperation of Professor J. M. Cork, under whose direction this research was carried out. I am grateful for helpful discussions of theory with Professor G. E. Uhlenbeck. Mr. R. J. Bessey has performed some of the calculations.

[14] Compare H. Walke, reference 4.

Theory of the Continuous X-Ray Spectrum

ROBERT WEINSTOCK
Stanford University, Stanford University, California

(Received January 6, 1942)

The theory of continuous x-radiation from thin targets—relativity and retardation of potential neglected—is completed by the incoherent integration of the single process transition probabilities over the unit sphere. This is carried out by means of series expansion. Comparison with the absolute intensity determination of Smick-Kirkpatrick gives a result too large by a factor of greater than 2.5. The theory compares satisfactorily with the absolute measurement of Clark-Kelly and the relative measurements of Harworth-Kirkpatrick.

I. INTRODUCTION

THE theory of the continuous x-ray spectrum —relativity and retardation of potential neglected—was worked out by Sommerfeld[1] in 1931. It is Sommerfeld's work upon which the present paper is directly based. One computes the probability that an electron moving toward an atom with velocity v_1 be deflected through a given angle θ with asymptotic velocity v_2, having experienced an energy loss $h\nu$. The dipole matrix elements of the single process have been rigorously computed by Sommerfeld, but the incoherent integration over all polar angles (θ, φ) of scattering of the incident electron has not in general been calculated in closed form.

Sauter[2] has given a non-relativistic treatment which makes use of the Born approximation, $Ze^2/hv_{1,2} \ll 1$, for incident and emergent electron. Unfortunately, this condition is not met in a large number of experiments. When it is satisfied, on the other hand, the electron velocities are comparable with the velocity of light, so that the problem then requires a detailed relativistic treatment.

Elwert[3] has worked out an ingenious method for integration over all θ, φ of Sommerfeld's result, breaking off his series expansion under the assumption $(Ze^2/hv_2)-(Ze^2/hv_1) \ll 1$.

The present author employs a straightforward method whose accuracy is curtailed only by the physical limitations of the original Sommerfeld theory—in the main, the assumption of a pure Coulomb field as seen by the electron during the emission process. This is only strictly justified for an electron whose de Broglie wave-length is small compared with the radius of the K shell of the scattering atom. For $Z=28$ and $V=15$ kilovolts, for example, these lengths are of the same order of magnitude, so that at best the assumption of a pure Coulomb field is only approximate—the higher the voltage and the smaller Z, the better the approximation. The extreme difficulty associated with a more rigorous treatment of the field, plus the success in assuming a pure Coulomb field in numerous other problems (e.g., characteristic x-radiation, form of the Compton line from atomic electrons, etc.), justifies its assumption here. In addition, there is the question of what to assume for the value of Z, even once a Coulomb field is assumed. The procedure herein is to assign to Z the full atomic number of the scatterer. At worst, this may be an error of two parts in Z, since in general the electron wave-length is small compared with the L-shell radius of the scatterer. In the case of 15 kilovolt electrons incident upon nickel $(Z=28)$ and $\lambda=1.431$A, computations employing $Z=28$ and $Z=26$, the extreme values of effective nuclear charge, have yielded absolute intensity results differing by 15 percent. It turns out, however, that the discrepancy between experiment and theory in this single case is too great to be accounted for by merely an error in the choice of Z.

[1] A. Sommerfeld, Ann. d. Physik **11**, 257 (1931).
[2] F. Sauter, Ann. d. Physik **18**, 486 (1933).
[3] G. Elwert, Ann. d. Physik **34**, 178 (1939). The present work was undertaken before the author had complete knowledge of the significance or justification of Elwert's results. The latter's work is indeed elegant and provides a more rapidly convergent expansion in most cases; numerical work therefrom, however, requires computation of the Γ-function and its logarithmic derivative for imaginary argument. (There are tables of $\Gamma(z)$ for imaginary z for $|z| \leqslant 1$.) Also, Elwert computes merely $\mathfrak{M}_y^2 (=\mathfrak{M}_z^2)$, and uses the Sommerfeld-Maue result (Section II.D) for $\mathfrak{M}^2$ to determine $\mathfrak{M}_x^2 = M^2 - 2\mathfrak{M}_y^2$. He thereby loses the advantage of having the numerical check set forth in Section II.D.

II. ANALYTICAL TREATMENT

Sommerfeld finds for the elementary dipole moments (unnormalized) for a single electron incident in the x direction upon a bare nucleus of charge $+Ze$:

$$M_x = -A\{[1+n_1-(1+n_2)\cos\theta]F - 2\sin^2\tfrac{1}{2}\theta(1-\xi)F'\}, \tag{1}$$

$$\left.\begin{matrix} M_y \\ M_z \end{matrix}\right\} = A\sin\theta\left\{\begin{matrix} \cos\varphi \\ \sin\varphi \end{matrix}\right\}\{(1+n_2)F-(1-\xi)F'\}. \tag{2}$$

Here $F = F(1+n_1, 1+n_2, 1, \xi)$, the hypergeometric function of indicated parameters, where

$$F(a,b,c,\xi) = \sum_{\nu=0}^{\infty}\frac{\Gamma(a+\nu)\Gamma(b+\nu)\Gamma(c)}{\Gamma(a)\Gamma(b)\Gamma(c+\nu)\nu!}\xi^\nu, \quad \text{for } |\xi|<1; \tag{3}$$

$$\xi = -\frac{4n_1n_2}{(n_1-n_2)^2}\sin^2\frac{\theta}{2}; \quad n_{1,2} = \frac{Z}{ik_{1,2}a} = \frac{\alpha Z}{i\beta_{1,2}}; \quad \begin{cases} hk_{1,2} = mv_{1,2}; & \beta_{1,2} = v_{1,2}/c \\ a = h^2/me^2; & \alpha = e^2/hc \end{cases}$$

$$A = -\frac{16\pi k_1k_2\exp -i\pi n_1}{(k_1+k_2)^2(k_1-k_2)^4}\left(\frac{k_1+k_2}{k_1-k_2}\right)^{n_1+n_2}.$$

The unnormalized eigenfunctions used in the calculation of the moments are

$$\psi_1 = \exp(ik_1x)L_{n_1}(ik_1(r-x)), \quad \psi_2 = \exp(ik_2x')L_{-n_2}(-ik_2(r+x')),$$

where

$$L_n(u) = \sum_{\nu=0}^{\infty}(-1)^\nu\binom{n}{\nu}\frac{u^\nu}{\nu!},$$

and x' is the coordinate measured along the asymptotic direction of the emerging electron.

In the event that $\xi_0 = -[4n_1n_2/(n_1-n_2)^2] < -1$, it is not permissible to employ the above (3) series development of F, which is valid only within the unit circle. We therefore use the analytic continuation:[5]

$$F(a,b,c,\xi) = (1-\xi)^{-a}F[a, c-b, c, \xi/(\xi-1)]. \tag{4}$$

Expansion of the second factor on the right in powers of $w = \xi/(\xi-1)$ according to (3) gives a series convergent for $-\infty < \xi < \frac{1}{2}$—in particular for all non-positive values of ξ.

A. Calculation of $\mathfrak{M}_x^2 = \int_0^{2\pi} d\varphi \int_0^{\pi} |M_x|^2 \sin\theta d\theta$

From the relation $\xi = \xi_0\sin^2\frac{1}{2}\theta$, (1) becomes

$$M_x = -(A/\xi_0)\{\xi_0(n_1-n_2)F + 2\xi[(1+n_2)F-(1-\xi)F']\}$$
$$= (2n_1A/\xi_0)\{BF-F_1\},$$

---

[4] A. Sommerfeld and A. W. Maue, Ann. d. Physik **23**, 589 (1935). In this paper, the authors introduce wave functions which differ slightly from those used in the 1931 work. The results (1) and (2) above, somewhat different from the expressions derived in 1931, are merely stated in the later paper. The physical results are of course unchanged, the reason for the altered procedure being one of better visualization.

[5] This is readily verified by substitution in the differential equation (Whittaker and Watson, *Modern Analysis*, fourth edition, p. 283) for $F(a, b, c, \xi)$, which the right-hand member of (4) is seen to satisfy. One then notes that the two members behave identically in the neighborhood of $\xi=0$. Equation (4) is actually a mere expression of the identity (p. 207, reference 5):

$$(1-\xi)^{-a}P\left\{\begin{matrix} 0 & \infty & 1 & \\ 0 & a & 0 & \xi \\ 1-c & b & c-a-b & \end{matrix}\right\} = P\left\{\begin{matrix} 0 & 1 & \infty & \\ 0 & 0 & a & \xi/(\xi-1) \\ 1-c & b-a & c-b & \end{matrix}\right\},$$

so long as the indentical behavior about $\xi=0$ (or any other point) is established.

where $F_1=F(n_1, 1+n_2, 1, \xi)$, $B=(n_1+n_2)/(n_1-n_2)$, as one obtains directly through use of the easily verified relations:

$$F'(a, b, c, \xi)=(ab/c)F(a+1, b+1, c+1, \xi), \tag{5}$$

$$cF(a, b, c, \xi)-a(1-\xi)F(a+1, b+1, c+1, \xi)=(c-a)F(a, b+1, c+1, \xi), \tag{6}$$

$$(b\xi/c)F(a, b+1, c+1, \xi)=F(a, b, c, \xi)-F(a-1, b, c, \xi),$$

plus the fact that $\xi_0=-4n_1n_2/(n_1-n_2)^2$;

$$\therefore \quad |M_x|^2=\left|\frac{2n_1A}{\xi_0}\right|^2\{B^2|F|^2+|F_1|^2-2B\Re FF_1^*\}, \qquad \text{since } B \text{ is real.}$$

According to (4),

$$\left.\begin{aligned} F&=(1-\xi)^{-1-n_1}G_1; \quad G_1=F(1+n_1, -n_2, 1, w)\\ F_1&=(1-\xi)^{-n_1}G_2; \quad G_2=F(n_1, -n_2, 1, w)\end{aligned}\right\} w=\frac{\xi}{\xi-1}.$$

Since n_1 is pure imaginary and $(1-\xi)^{-1}=(1-w)$ is real,

$$|M_x|^2=\left|\frac{2n_1A}{\xi_0}\right|^2\{B^2(1-w)^2|G_1|^2+|G_2|^2-2B(1-w)\Re G_1G_2^*\}.$$

Also, since $\sin^2\frac{1}{2}\theta=\xi/\xi_0$,

$$2\cos\tfrac{1}{2}\theta\sin\tfrac{1}{2}\theta d\theta=\sin\theta d\theta=\frac{2d\xi}{\xi_0}=-\frac{2}{\xi_0}\frac{dw}{(1-w)^2}.$$

$$\therefore \quad \mathfrak{M}_x^2=-\frac{4\pi}{\xi_0}\left|\frac{2n_1A}{\xi_0}\right|^2\left\{B^2\int_0^{w_0}|G_1|^2dw+\int_0^{w_0}\frac{|G_2|^2}{(1-w)^2}dw-2B\Re\int_0^{w_0}\frac{G_1G_2^*}{1-w}dw\right\}; \quad w_0=\frac{\xi_0}{\xi_0-1}.$$

Since $0<w_0<1$, it is permissible to expand G_1 and G_2 in powers of w. As a result, upon term by term integration:

$$\mathfrak{M}_x^2=-\frac{4\pi}{\xi_0}\left|\frac{2n_1A}{\xi_0}\right|^2\left\{B^2\sum_{r=0}^{\infty}\frac{s_rw_0^{r+1}}{r+1}-\xi_0+\sum_{r=1}^{\infty}t_r[(1-\xi_0)w_0^r-rI_{r-1}]-2B\sum_{r=0}^{\infty}I_r\Re u_r\right\}; \tag{7}$$

$$s_r=\sum_{\nu=0}^{r}g_{1\nu}g^*_{1,r-\nu}, \quad t_r=\sum_{\nu=0}^{r}g_{2\nu}g^*_{2,r-\nu}, \quad u_r=\sum_{\nu=0}^{r}g_{1\nu}g^*_{2,r-\nu},$$

where we have written $G_\sigma=\sum_{\nu=0}^{\infty}g_{\sigma\nu}w^\nu$, and where, according to (3):

$$g_{1\nu}=\frac{\Gamma(\nu+1+n_1)\Gamma(\nu-n_2)}{\Gamma(1+n_1)\Gamma(-n_2)\nu!\nu!}, \quad g_{2\nu}=\frac{\Gamma(\nu+n_1)\Gamma(\nu-n_2)}{\Gamma(n_1)\Gamma(-n_2)\nu!\nu!};$$

$$I_r=\log(1-\xi_0)-\sum_{k=1}^{r}\binom{r}{k}\frac{(w_0-1)^k-(-1)^k}{k}.^{*} \tag{8}$$

B. Calculation of $\mathfrak{M}_y^2=\mathfrak{M}_x^2=\int_0^{2\pi}d\varphi\int_0^{\pi}|M_y|^2\sin\theta d\theta$

By application of (5), (6), and (4) to (2) above, we obtain

$$M_y=-An_1(1+n_2)\cos\varphi\sin\theta(1-w)^{1+n_1}F(1+n_1, -n_2, 2, w),$$

* *Note added in proof:* P. C. Rosenbloom has pointed out that $I_r=\int_0^{w_0}\frac{w^r}{1-w}dw$ may be evaluated more simply in the form $I_r=\log(1-\xi_0)-\sum_{\nu=1}^{r}\frac{w_0^\nu}{\nu}$.

whence
$$|M_y|^2=(4/\xi_0^2)|An_1(1+n_2)|^2\cos^2\varphi[\xi_0 w(w-1)-w^2]|G_3|^2,$$
where
$$G_3=F(1+n_1,\ -n_2,\ 2,\ w).$$
$$\therefore\quad \mathfrak{M}_y^2=\mathfrak{M}_z^2=\frac{8\pi}{\xi_0^3}|An_1(1+n_2)|^2\int_0^{w_0}\left\{\frac{\xi_0 w}{1-w}+\frac{w^2}{(1-w)^2}\right\}|G_3|^2dw$$
$$=\frac{8\pi}{\xi_0^3}|An_1(1+n_2)|^2\sum_{r=0}^{\infty}p_r\{(\xi_0-r-2)I_{r+1}+(1-\xi_0)w_0{}^{r+2}\},\qquad(9)$$

as one finds on expansion of G_3 and term by term integration. Here,

$$p_r=\sum_{\nu=0}^{r}g_{3\nu}g^*_{3,r-\nu},\quad\text{and}\quad g_{3\nu}=\frac{\Gamma(\nu+1+n_1)\Gamma(\nu-n_2)}{\Gamma(1+n_1)\Gamma(-n_2)\nu!(\nu+1)!},$$

while I_r is the quantity defined in (8) above.

C. Normalization

The question of normalization is treated in detail by Sommerfeld.[1] We may accomplish his result by means of a slightly different viewpoint, however. Namely, we employ the usual artifice of limiting the system to a finite volume Ω, sufficiently large that only the first term in the asymptotic expansions of the wave functions is needed in computing the integrals over Ω of the absolute squares. The continuous range of energy levels is approximated by a discrete set whose separation goes to zero as Ω increases without limit. This is accomplished in the usual manner of requiring periodicity with Ω as the fundamental interval of volume. As usual, Ω drops out, and the result is that which we should obtain as Ω increases to infinity. In short, $\mathfrak{M}_x^2$, $\mathfrak{M}_y^2$, $\mathfrak{M}_z^2$ must be multiplied by the following factors in order to bring the result to the units, "ergs per unit solid angle per unit frequency range per bombarding electron per atom-per-square-centimeter of target area":

(i) Normalization of the final state eigenfunction:
$$\frac{1}{\Omega}\frac{2\pi i n_2}{1-\exp(-2\pi i n_2)}.$$

(ii) Reduction of bombarding current to one electron per second per square centimeter incident upon one atom per square centimeter:
$$\frac{2\pi i n_1}{1-\exp(-2\pi i n_1)}\frac{m}{\hbar k_1}.$$

(iii) Number of states in volume Ω in unit range of k_2:
$$\frac{\Omega}{(2\pi)^3}k_2^2.$$

(iiii) Conversion from "per unit k_2 interval" to "per unit frequency range":
$$2\pi m/\hbar k_2.$$

(iiiii) Factors arising in formula for dipole radiation:
$$\frac{e^2}{2\pi c^3}\frac{\hbar^4}{(2m)^4}(k_1^2-k_2^2)^4.$$

If we call the product of the above five factors (i to iiiii) N^2, we find the result:

$$N^2|A|^2=\frac{1}{(1-\exp(-2\pi i n_2))(\exp(2\pi i n_1)-1)}\left(\frac{Z}{a}\right)^2\frac{e^2}{8\pi c^3}\left(\frac{h}{m}\right)^2\frac{\xi_0^2}{k_1^2}. \quad \left(a=\frac{h^2}{me^2}\right).$$

That is, the "components" of radiation associated with the three moments $\mathfrak{M}_x$, $\mathfrak{M}_y$, $\mathfrak{M}_z$ are:

$$I_\nu^{(x,y,z)}=\frac{1}{(1-\exp(-2\pi i n_2))(\exp(2\pi i n_1)-1)}\left(\frac{Z}{a}\right)^2\frac{e^2}{8\pi c^3}\left(\frac{h}{m}\right)^2\frac{\xi_0^2}{k_1^2}\frac{\mathfrak{M}^2_{x,y,z}}{|A|^2},$$

where, for the direction of observation making an angle Θ with the (x-) direction of bombardment, the absolute intensity is given by:[6]

$$I_\nu^{(\Theta)}=I_\nu^{(x)}\sin^2\Theta+I_\nu^{(z)}\cos^2\Theta+I_\nu^{(y)}$$

ergs per unit solid angle per unit frequency range per bombarding electron per atom-per-square-centimeter of target area.

In particular, for 90° (z direction) observation,

$$I_\nu^{(90°)}=\frac{1}{(1-\exp(-2\pi i n_2))(\exp(2\pi i n_1)-1)}\left(\frac{Z}{a}\right)^2\frac{e^2}{8\pi c^3}\left(\frac{h}{m}\right)^2\frac{\xi_0^2}{k_1^2}\frac{(\mathfrak{M}_x^2+\mathfrak{M}_y^2)}{|A|^2}.$$

D. Numerical Check

Since, in the numerical calculation, the series expansions (7) and (9) are broken off after a finite number of terms, it is desirable to have a check which permits an estimation of the error thus involved. Such a check is available through the work of Sommerfeld and Maue,[4] who have been able, by ingenious application of the differential equation for the hypergeometric function, to express $\mathfrak{M}^2=\mathfrak{M}_x^2+\mathfrak{M}_y^2+\mathfrak{M}_z^2$ in closed form. According to their work,

$$\mathfrak{M}^2=\frac{8\pi}{\xi_0}|A|^2\frac{d}{d\xi_0}|\mathfrak{F}|^2,$$

where $\mathfrak{F}=F(-n_1,\ -n_2,\ 1,\ \xi_0)$.

For $\xi_0<-1$, we use the analytic continuation of the hypergeometric function:[7]

$$F(-n_1,\ -n_2,\ 1,\ \xi_0)=\frac{\Gamma(n_1-n_2)}{n_1\Gamma(n_1)\Gamma(-n_2)}(-\xi_0)^{n_1}G_4+\frac{\Gamma(n_2-n_1)}{n_2\Gamma(n_2)\Gamma(-n_1)}(-\xi_0)^{n_2}G_5, \tag{10}$$

where

$$G_4=F(-n_1,\ -n_1,\ 1+n_2-n_1,\ \xi_0^{-1}), \quad G_5=F(-n_2,\ -n_2,\ 1+n_1-n_2,\ \xi_0^{-1}).$$

Whence, on expanding in powers of ξ_0^{-1} and performing the differentiation, we obtain:

$$\mathfrak{M}^2=-\frac{8\pi}{\xi_0}|A|^2\left\{\left|\frac{\Delta}{n_1}\right|^2\sum_{r=1}^{\infty}rq_r\xi_0^{-r-1}+\left|\frac{\Delta}{n_2}\right|^2\sum_{r=1}^{\infty}rl_r\xi_0^{-r-1}\right.$$
$$\left.-2\Re\left\{\frac{\Delta^2}{n_1n_2}(-\xi_0)^{n_1-n_2}\left[\sum_{r=1}^{\infty}rj_r\xi_0^{-r-1}-(n_1-n_2)\sum_{r=0}^{\infty}j_r\xi_0^{-r-1}\right]\right\}\right\},$$

[6] Here the y direction is taken perpendicular to both the direction of incident electron and direction of observation.

[7] Whittaker and Watson, reference 5, p. 289. Since the text suffers a typographical error, we restate the result:

$$\frac{\Gamma(a)\Gamma(b)}{\Gamma(c)}F(a,\ b,\ c,\ z)=\frac{\Gamma(a)\Gamma(b-a)}{\Gamma(c-a)}(-z)^{-a}F(a,\ 1-c+a,\ 1-b+a,\ z^{-1})+\frac{\Gamma(b)\Gamma(a-b)}{\Gamma(c-b)}(-z)^{-b}F(b,\ 1-c+b,\ 1-a+b,\ z^{-1}),$$

where $|\arg(-z)|<\pi$.

where

$$\Delta=\frac{\Gamma(n_1-n_2)}{\Gamma(n_1)\Gamma(-n_2)};\quad q_r=\sum_{\nu=0}^{r} g_{4\nu}g^*_{4,r-\nu};\quad l_r=\sum_{\nu=0}^{r} g_{5\nu}g^*_{5,r-\nu};\quad j_r=\sum_{\nu=0}^{r} g_{4\nu}g^*_{5,r-\nu},$$

and the $g_{s\nu}$ are the expansion coefficients of the G_s:

$$g_{4\nu}=\frac{\Gamma(\nu-n_1)\Gamma(\nu-n_1)\Gamma(1+n_2-n_1)}{\Gamma(-n_1)\Gamma(-n_1)\Gamma(\nu+1+n_2-n_1)\nu!};\quad g_{5\nu}=\frac{\Gamma(\nu-n_2)\Gamma(\nu-n_2)\Gamma(1+n_1-n_2)}{\Gamma(-n_2)\Gamma(-n_2)\Gamma(\nu+1+n_1-n_2)\nu!}.$$

For $\xi_0\ll-1$, this expansion converges quite rapidly and thereby provides a splendid check for the numerical work by comparison with the sum of the individually computed quantities $\mathfrak{M}_x^2$, $\mathfrak{M}_y^2$, $\mathfrak{M}_z^2$.

III. NUMERICAL EVALUATION

In all cases it was found sufficient to neglect all but the first nine or ten terms in each of the infinite series in order to obtain the accuracy stated below. The procedure lends itself well to compactness, so that with the aid of computing machine the time needed for each complete calculation is reasonably short. It is possible to obtain more rapid convergence if one uses for part of the interval in ξ the expansion in w (4), and for the remainder the expansion (10) in ξ^{-1} employed in the Sommerfeld-Maue check calculation of $\mathfrak{M}^2$. In this case, however, the evil of employing two different representations is by far greater than that of the somewhat slower convergence. Originally, in the $Z=28$, $\lambda=1.431$A, $V=15$ kilovolts computation of $\mathfrak{M}_y^2$, this procedure was followed; the result merely served later as a check in the calculation of $\mathfrak{M}_y^2$ as set forth in Section IIB.

For all computations, the hypergeometric coefficients were computed with the aid of the following recursion formulae:

$$g_{2,\nu+1}=\frac{\nu^2-n_1n_2+\nu(n_1-n_2)}{(\nu+1)^2}g_{2\nu};\quad (g_{s0}=1)$$

$$g_{1\nu}=\left(1+\frac{\nu}{n_1}\right)g_{2\nu};\quad g_{3\nu}=\frac{1}{\nu+1}g_{1\nu}.$$

Since only two or three terms per series were required in the calculation of $\mathfrak{M}^2$ as check, the coefficients $g_{4\nu}$ and $g_{5\nu}$ were calculated directly.

The following detailed remarks concern the computations for $Z=13$, $\lambda=0.474$A, $V=31.7$ kilovolts. The various parameters were found to be: $in_1=0.269$, $in_2=0.647$, $\xi_0=-4.87$, $w_0=0.830$. Although $(1-w_0)^2\ll1$, it was found inadvisable to neglect $(1-w_0)^k$ for $k>1$ in the computation of $I_r(8)$; wholesale cancellations in the alternating series for I_r render these terms significant. A table of the values of I_r so obtained follows:

$r=$	0	1	2	3	4	5	6	7	8	9
$I_r=$	1.769	0.939	0.595	0.404	0.285	0.206	0.152	0.113	0.085	0.064

The results for the unnormalized moments are: $\mathfrak{M}_x^2=0.691|A|^2$, $\mathfrak{M}_y^2=\mathfrak{M}_z^2=0.059|A|^2$, and $\mathfrak{M}_x^2+\mathfrak{M}_y^2+\mathfrak{M}_z^2=0.809|A|^2$. The latter is within about two percent of the Sommerfeld-Maue check result of $\mathfrak{M}^2=0.826|A|^2$. An assumed total arithmetic error of at most four percent is, therefore, by no means an unreasonable claim of accuracy.

IV. COMPARISON WITH EXPERIMENT

In order that the foregoing theory be applied to the conditions of any given experiment, the x-radiation upon which measurement is made must originate from a thin target. The requirement is necessary for the reason that we have assumed both initial direction and energy of the electron to be known. For a target to be acceptable as "thin," therefore, the occurrence of all processes altering the direction or energy of the electron before it radiates must be negligibly frequent. A number of experiments have been performed recently with targets sufficiently thin for comparison with the theory to be valid.

Smick and Kirkpatrick,[8] bombarding a nickel target (thickness ~500A) with 15 kilovolt electrons, observed a narrow frequency range of the continuous spectrum centered about 1.431A at an angle negligibly less than 90° (~88°).

[8] E. Smick and P. Kirkpatrick, Phys. Rev. **60**, 162 (1941).

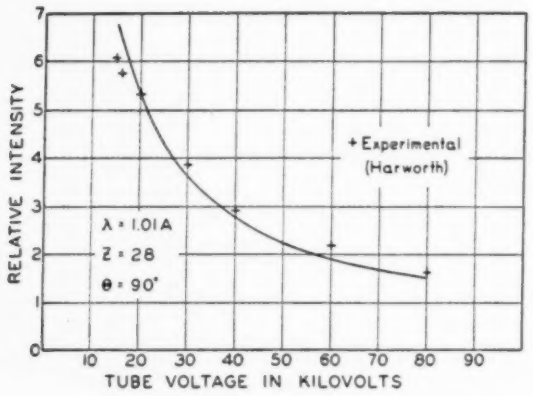

FIG. 1.

These investigators obtained the absolute intensity measurement of 2.2×10^{-50} erg per unit solid angle per unit frequency range per bombarding electron per atom-per-square-centimeter of target area. Using the full atomic number, 28, of nickel, we have, by the method given above, arrived at a much too high value of 6.09×10^{-50} in the same units. In the extreme case of assumed complete screening by the nickel K electrons ($Z=26$), the result is somewhat better, 5.27×10^{-50} erg, etc., yet still too large by a factor of greater than two. Although it does not seem likely that deviation from the Coulomb field should cause so large a discrepancy, it has been suggested the experiment be repeated with somewhat harder electrons and/or target of lower atomic number, whereupon this difficulty may drop out. At present, such a repetition is in prospect at Stanford.

The only other investigation of absolute intensity from a thin target known to the author fulfills this requirement, and here the agreement between theory and experiment is quite satisfactory. Employing 31.7-kilovolt electrons and an aluminum target, Clark and Kelly[9] have observed a narrow band of the continuous spectrum centered about 0.474A at an angle (Θ) of 60°. Their result, in the proper units, is 6.17×10^{-51} erg, etc., with a stated error of about ±33 percent. Our computations give 4.23×10^{-51} erg, etc., which does fall within the experimental error of the Clark-Kelly result. It may be significant that the agreement occurs in a region where the theory should rigorously hold, and the disagreement in a region in which the uncertainties due to deviation from the Coulomb field render its strict application somewhat hazardous.

The final comparison with experiment, and by far exhibiting the best agreement to date, is with the relative intensity measurements of Harworth and Kirkpatrick.[10] The results are given in Fig. 1. Since the measurements are merely relative, normalization is necessary; this is done by fitting the results at 20 kilovolts. This not only gives the best fit, but also finds justification in that below 20 kilovolts screening has its greatest effect; above, the relativistic effects are greater. As in the case of the Smick-Kirkpatrick measurement, the computation has been made assuming an observation angle of 90°, whereas the actual mean angle was 93.5°. The error thus involved is of course negligible. The good agreement may be in part attributed to the thinness of the target (nickel) used. It was about 200A thick.

V. ACKNOWLEDGMENT

The author wishes to express sincere appreciation of the assistance and stimulation given by the members of the Physics Department at Stanford University. In particular, he owes hearty thanks to Professor Paul Kirkpatrick, but for whose keen interest this work would never have been undertaken; to Messrs. Howard R. Kelly, Keith Harworth, and David B. Nicodemus for various aid, and especially to Professor Felix Bloch, for suggesting this problem and for valuable discussions.

Finally, his thanks go to the National Youth Administration and to their patient, untiring Miss Dorothy Pearson, whose careful computation forms the largest part of the numerical results obtained.

[9] J. Clark and H. Kelly, Phys. Rev. **59**, 220 (1941). Here the result is reported as being a factor of 20 larger than predicted by the Sauter (note 2) theory. The greatness of the discrepancy was due merely to an oversight in that the experimental result was not reduced to the proper units for comparison. This fact has been discovered and corrected by Clark and Kelly themselves in a personal communication.

[10] K. Harworth and P. Kirkpatrick, Phys. Rev. **60**, 163 (1941). Among others, the results represented in the figure are to be published in a forthcoming paper by Harworth and Kirkpatrick.

The First Spark Spectrum of Caesium (Cs II)

MARSHALL A. WHEATLEY* AND RALPH A. SAWYER
University of Michigan, Ann Arbor, Michigan

(Received February 13, 1942)

With an electrodeless discharge in a quartz tube the first spark spectrum of caesium has been rephotographed in the region λ2954.07–λ1857.45 by means of three sizes of quartz spectrographs. The classifications made by Laporte, Miller, and Sawyer and by Olthoff and Sawyer have been confirmed by additional transitions and used as a basis for extending the classification. Four missing terms in the blended $5p^5(^2P_{1\frac{1}{2}})7d$, $8s$; $5p^5(^2P_{\frac{1}{2}})6d$, $7s$ configurations have been found, two of these giving rise to resonance lines. The proposed blended configurations $5p^5(^2P_{1\frac{1}{2}})8d$, $9s$; $5p^5(^2P_{\frac{1}{2}})7d$, $8s$ contain thirteen terms; the $5p^5(^2P_{1\frac{1}{2}})10s$, one term, also giving a resonance line; the $5p^5(^2P_{1\frac{1}{2}})7p$, six terms; the $5p^5(^2P_{\frac{1}{2}})7p$, three terms; and the $5p^5(^2P_{1\frac{1}{2}})nf$, eight terms. In all, 37 levels have been established and 189 lines have been classified. It has also been possible, through the discovery of f terms, to separate the d terms from the s terms of the $5p^5(^2P_{1\frac{1}{2}})6d$, $7s$ configuration because of the failure of the f and s terms to combine. The classifications, assignment of inner quantum numbers, and the identification of levels agree with the theoretical considerations as well as with the predictions from the Xe I classification.

I. INTRODUCTION

THE work of Sommer[1] laid the foundation for the classification of the first spark spectrum of caesium. He photographed the spectrum in the region λ3267–λ7280 and arranged 51 lines as transitions between three groups of terms—lower, middle, and upper. Laporte, Miller, and Sawyer,[2] from hollow cathode spectra made with a one-meter spectrograph, discovered eight resonance lines between λ962 and λ612. These ultraviolet lines were identified as transitions between the $5p^5(5d, 6d, 6s, 7s)$ configurations and the $5p^6\ ^1S_0$ ground term and so established the relative term values of Sommer's level diagram.

The work of Olthoff and Sawyer[3] extended the classification of Laporte, Miller, and Sawyer, established 23 new terms in the $5p^5(^2P_{1\frac{1}{2}})6s$, $7s$, $8s$, $6p$, $5d$, $6d$, $7d$ and $5p^5(^2P_{\frac{1}{2}})6s$, $7s$, $6p$, $6d$ configurations, and classified 92 lines, mostly newly observed. Laporte, Miller and Sawyer, as well as Olthoff and Sawyer found it impossible to distinguish the mingled s and d terms, and to separate the $6d$, $7s$; and $7d$, $8s$ term groups because of their close proximity. Had it been possible to obtain f terms, the d and s terms might then have been separated because of the failure of f terms to combine with s terms. However, from the approximate value of the $^1S_0$ term given by Laporte, Miller, and Sawyer, it can be calculated that the $s-f$ transitions should lie below the ultraviolet limit imposed on the measurements by the transmission limit of the Corex bulb used by Olthoff and Sawyer for their electrodeless discharge.

The present research was undertaken to extend the classification of the first spark spectrum of caesium by obtaining more d, s, and p terms and by locating f terms to make it possible to separate some of the d and s terms.

II. EXPERIMENTAL

For the present work, the light source was an electrodeless discharge in a quartz tube about 28 cm long and 2.5 cm in diameter, with a clear quartz window in one end. Pure caesium was distilled in vacuum into the tube, as in the work of Olthoff and Sawyer. The tube was placed in an electric oven and excited by a Tesla discharge through a winding of 20 turns of braided copper wire. The spectrum was photographed in the region from λ2955 to λ1857, with three sizes of Hilger quartz spectrographs and with exposure times varying from 5 minutes to 7 hours. For the longer wave-lengths, iron arc lines were used as reference standards. Since accurate measurements on iron arc lines in the region below λ2375 were not available, Shenstone's[4] measurements on silver spark lines were used down to λ1932.88,

* Now at Wayne University, Detroit, Michigan.
[1] L. A. Sommer, Ann. d. Physik **75**, 163 (1924).
[2] Laporte, Miller and Sawyer, Phys. Rev. **39**, 458 (1932).
[3] Olthoff and Sawyer, Phys. Rev. **42**, 766 (1932).
[4] A. G. Shenstone, Phys. Rev. **31**, 321 (1928).

TABLES I–VI. Classification of the lines of Cs II.

TABLE I.

$5p^5(^2P_{1\frac{1}{2}})5d,\ 6s$			$5p^6$	$5p^5(^2P_{1\frac{1}{2}})6p$						$5p^5(^2P_{\frac{1}{2}})6p$			
			$^1S_0$	1_1	2_2	3_3	4_1	5_2	6_0	7_1	8_1	9_2	10_0
	J		0	1	2	3	1	2	0	1	1	2	0
		Relative Term Value	00.00	*126,518.54	*128,089.83	*129,107.65	*129,989.72	*130,766.00	*133,153.54	*141,555.59	*143,352.12	*143,394.19	*144,523.45
$1°_3$	3	*105,949.74			*22,139.77(2) 0.30	*23,157.78(0) 0.13		*24,816.59(0) −0.33				*37,444.50(1) −0.05	
$2°_1$	1	*106,222.77		*20,295.73(1) 0.04	*21,867.31(3) −0.25			*24,542.83(1) 0.40		*35,332.52(2) 0.30		*37,171.83(2) −0.41	*38,300.69(0) −0.01
$3°_2$	2	*107,392.33		*19,126.12(8) 0.09	*20,697.48(6) 0.02	*21,715.33(10) −0.01	*22,597.42(2) −0.03	*23,373.78(9) −0.11		*34,163.16(0) 0.10	*35,959.78(1) 0.01		
$4°_0$	0	*107,563.14		*18,955.52(4) −0.08			*22,426.92(3) −0.34			*33,992.66(7) −0.21	*35,789.21(2) −0.23		
$5°_1$	1	*107,905.01	*107,905(20) 0.01	*18,613.42(6) 0.11	*20,184.84(6) −0.02		*22,084.85(7) −0.14	*22,861.10(6) −0.11	*25,248.63(5) −0.10	*33,650.61(5) −0.03	*35,447.19(2) −0.08	*35,489.04(4) 0.14	*36,618.32(1) 0.12
$6°_2$	2	108,304.19			19,785.91(3) −0.27		21,685.97(2) −0.44	22,461.66(1) 0.15			35,047.37(8) 0.56	35,090.24(3) −0.24	
$7°_1$	1	*110,945.18	*110,946(20) −0.82	*15,573.14(2) 0.22	*17,144.51(6) 0.14		*19,044.61(6) −0.07	*19,820.81(6) 0.01	*22,208.49(7) −0.13	*30,610.40(7) 0.01	*32,406.84(1) 0.10	*32,448.92(2) 0.09	*33,578.17(1) 0.10
$8°_4$	4	112,236.53				16,871.12(5) 0.00							
$9°_2$	2	*112,795.08			*15,294.63(4) 0.12	*16,312.38(4) 0.19	*17,194.57(3) 0.07	*17,970.87(7) 0.05		*28,760.70(0) −0.19	*30,557.09(5) −0.05	*30,599.05(7) 0.06	
$10°_3$	3	*113,716.61			*14,373.12(4) 0.10	*15,390.96(3) 0.08		*17,049.36(1) 0.03				*29,677.65(7) −0.07	
$5p^5(^2P_{\frac{1}{2}})5d,\ 6s$													
$11°_2$	2	*119,665.41								*21,890.25(3) −0.07	*23,686.83(0) −0.12	*23,728.67(6) 0.11	
$12°_2$	2	*120,404.87								*21,150.58(1) 0.14	*22,947.39(0) −0.14	*22,989.36(0) −0.04	
$13°_0$	0	*122,365.51								*19,189.95(2) 0.13	*20,986.61(5) 0.00		
$14°_1$	1	*122,866.03	*122,872(20) −5.97							*18,689.34(3) 0.22	*20,486.32(0) −0.23	*20,528.06(6) 0.10	*21,657.19(3) 0.23
$15°_1$	1	*123,636.44	*123,645(20) −8.56							*17,919.29(0) −0.14	*19,715.72(0) −0.04	*19,757.88(3) −0.13	*20,886.87(3) 0.14

TABLE II.

	$5p^5(^2P_{1\frac{1}{2}})6d$, $7s$		$5p^6$	$5p^5(^2P_{1\frac{1}{2}})6p$					
			$^1S_0$	1_1	2_2	3_3	4_1	5_2	6_0
	J		0	1	2	3	1	2	0
		Relative Term Value		*126,518.54	*128,089.83	*129,107.65	*129,989.72	*130,766.00	*133,153.54
$16°_2$	2	*149,212.25		*22,693.82(7) −0.11	*21,122.47(4) −0.05	*20,104.64(5) −0.04		*18,446.14(5) 0.11	
$17°_1$	1	*149,605.33	*149,604 (12) 1.33	*23,086.95(4) −0.16	*21,515.53(5) −0.03		*19,615.46(4) 0.15	*18,839.20(3) 0.13	*16,451.65(2) 0.14
$18°_1$	1	*152.172.11	*152,172 (5) 0.11	*25,653.67(7) −0.10	*24,082.27(4) 0.01		*22,182.32(2) 0.07	*21,406.02(4) 0.09	*19,018.53(0) 0.04
$19°_2$	2	*152.791.49		*26,273.12(6) −0.17	*24,701.59(4) 0.07	*23,683.75(3) 0.09	*22,801.61(5) 0.16	*22,025.41(6) 0.08	
$20°_2$	2	*153,302.27		*26,783.83(2) −0.10	*25,212.38(6) 0.06	*24,194.54(2) 0.08	*23,312.46(7) 0.09	*22,536.21(0) 0.06	
$21°_3$	3	*153,556.54			*22,466.74(6) −0.03			*22,790.50(0) 0.04	
$22°_3$	3	*153,678.17			*25,588.30(4) 0.04	*24,570.52(6) 0.00		*22,912.15(9) 0.02	
$23°_1$	1	*156,399.31	*156,392 (12) 7.31		*28,309.51(0) −0.03		*26,409.65(5) −0.06	*25,633.22(0) 0.09	*23,245.86(6) −0.09

and Eder's[5] measurements, corrected to conform to Shenstone's, down to λ1855.67. The plates were measured by a Gaertner comparator and the wave-lengths computed by the Hartmann formula. The errors in wave number measurements are about 0.04 cm^{-1} in the region λ2900–λ2450, 0.08 cm^{-1} in the region λ2450–λ2000, and 0.10 cm^{-1} in the region below λ2000. Measurements were made on 850 lines covering the region λ2954.08–λ1857.45; of these, 193 had been previously classified; 302 were below the limit of Olthoff and Sawyer's observations in the ultraviolet.

III. RESULTS

In Tables I–VI are given the results of the classification of the spectrum of Cs II. In the first column are given the electronic configurations of the odd terms and spectroscopic notations of the levels. The terms have been numbered since L and S values cannot be assigned. The second column gives the J value of the odd levels, and the third, the relative term value referred to $5p^6\ ^1S_0$. In the remaining columns are given the J values, the electronic configurations, the spectroscopic notation, and the relative term values of the even terms, to which are assigned numbers instead of their undetermined L and S values. The body of the table contains the wave numbers of the classified lines, together with their intensities in parentheses. Below each wave number is the discrepancy (calculated value minus observed value) between the wave number as calculated from the assigned term values and the observed wave numbers. Asterisks mark the terms and transitions from previous researches. Figure 1 is the energy level diagram of Cs II.

Four of the newly measured lines appear as transitions between previously established Cs II levels. A search of the unpublished vacuum-spectrograph data of Laporte, Miller, and Sawyer revealed five lines (ν164,480, ν165,850, ν169,180, ν173,809, ν177,225) which were thought to be possible transitions to the $5p^6\ ^1S_0$ term and for which sufficient confirming transitions to the known terms were found among the new lines to establish the reality of the corresponding new odd terms. Additional new odd terms were found by looking for lines with the wave number differences of the known $5p^5(^2P_{1\frac{1}{2}})5d$, $6s$ and $6d$, $7s$ terms. A group of six such terms, between ν155,965 and ν157,743 appear, from their location, to be $5p^5(^2P_{1\frac{1}{2}})7p$ terms, and three, νν166,096–168,525, to be $5p^5(^2P_{\frac{1}{2}})7p$. Another group of eight terms, νν188,791–200,407, because

[5] J. M. Eder, in Kayser's *Handbuch der Spectroscopie*, Vol. 5.

TABLE III.

$5p^5(^2P_{1\frac{1}{2}})7d$, $8s$ $5p^5(^2P_{\frac{1}{2}})6d$, $7s$			$5p^6$	$5p^5(^2P_{1\frac{1}{2}})6p$						$5p^5(^2P_{\frac{1}{2}})6p$			
			$^1S_0$	1_1	2_2	3_3	4_1	5_2	6_0	7_1	8_1	9_2	10_0
	J		0	1	2	3	1	2	0	1	1	2	0
		Relative Term Value		*126,518.54	*128,089.83	*129,107.65	*129,989.72	*130,766.00	*133,153.54	*141,555.59	*143,352.12	*143,394.19	*144,523.45
$24°_2$	2	*158,717.91			*30,628.61(1) −0.53	*29,610.16(0) 0.10		*27,951.81(0) 0.10			*15,365.59(1) 0.20		
$25°_0$	0	*162,352.92		*35,834.32(3) 0.06			*32,363.01(1) 0.19			*20,797.53(1) −0.20			
$26°_3$	3	*162,388.96			*34,299.37(3) −0.24			*31,623.10(0) −0.14				*18,994.53(0) 0.24	
$27°_0$	0	*163,024.80		*36,505.69(6) 0.57						*21,469.12(3) 0.02	*19,672.70(2) −0.02		
$28°_1$	1	*163,180.20	*163,180(7) 0.20	*36,662.16(0) −0.50	*35,090.18(1) 0.19		*33,190.44(2) 0.04		*30,026.58(2) 0.08	*21,624.51(4) 0.10	*19,828.56(1) −0.48	*19,785.91(3) 0.10	*18,656.65(0) 0.10
$29°_2$	2	*164,444.88		*37,926.67(0) −0.33	*36,355.02(8) 0.03	*35,337.24(2) −0.01		*33,678.55(2) 0.33			*21,092.66(5) 0.10	*21,050.61(2) 0.08	
$30°_1$	1	164,456.70	164,480(1) 14.30		36,376.32(15) 0.45		34,475.65(8) 0.33			22,909.97(0) 0.14		21,070.71(1) 0.80	19,942.67(1) −0.42
$31°_1$	1	*164,656.77	*164,655(3) 1.77		*36,567.26(2) −0.32		*34,666.98(2) 0.07	*33,890.73(5) 0.04	*31,503.30(1) −0.07	*23,101.13(2) 0.05	*21,304.73(1) −0.08	*21,262.55(5) 0.03	
$32°_1$	1	*165,813.70			*37,723.92(3) −0.05			*35,047.74(0) −0.04	*32,659.85(1) 0.31	*24,257.90(4) 0.21	*22,461.66(1) −0.08	*22,419.35(3) 0.16	*21,290.55(1) −0.30
$33°_1$	1	165,843.10	165,850(1) 6.90	39,324.52(1) 0.04	37,752.26(10) 1.01		35,854.36(10) −0.98					22,448.36(3) 0.55	
$34°_2$	2	*165,890.08		*39,371.06(2) 0.48	37,800.37(5) −0.12	36,782.78(1) −0.35	*35,900.36(1) 0.00	*35,124.31(4) −0.23		*24,334.53(0) 0.06	*22,538.01(4) −0.05	*22,495.94(2) −0.05	
$35°_3$	3	166,117.72			38,028.19(2) −0.30	37,009.76(4) 0.31		35,351.42(00) 0.30				22,723.52(4) 0.01	
$36°_2$	2	*166,131.11		39,612.92(4) −0.35	*38,041.11(2) 0.17		*36,141.39(2) 0.00	*35,365.28(0) −0.17		*24,575.44(6) 0.08	*22,779.08(2) −0.09	*22,736.88(3) 0.04	
$37°_3$	3	*166,600.74			*38,510.97(1) −0.06	*37,493.20(0) −0.11		35,834.32(10) 0.42				*23,206.44(1) 0.11	
$38°_2$	2	166,687.09		40,168.85(1) −0.30	38,597.16(10) 0.10	37,579.42(5) 0.02	36,697.04(10) 0.33			25,131.18(5) 0.32	23,334.88(0) 0.09	23,292.59(3) 0.31	

TABLE IV.

$5p^5(^2P_{1\frac{1}{2}})8d$, $9s$ $5p^5(^2P_{\frac{1}{2}})7d$, $8s$			$5p^6$	$5p^5(^2P_{1\frac{1}{2}})6p$						$5p^5(^2P_{\frac{1}{2}})6p$			
			$^1S_0$	1_1	2_2	3_2	4_1	5_2	6_0	7_1	8_1	9_2	10_0
	J		0	1	2	3	1	2	0	1	1	2	0
		Relative Term Value		*126,518.45	*128,089.83	*129,107.65	*129,989.72	*130,766.00	*133,153.54	*141,555.59	*143,352.12	*143,394.19	*144,523.45
$39°_2$	2	166,961.57		40,442.82(1) 0.21	38,871.79(2) −0.05	37,854.33(3) −0.41	36,971.98(3) −0.13	36,195.37(8) 0.20			23,609.43(5) 0.02	23,567.33(2) 0.05	
$40°_2$	3	167,015.97			38,926.58(10) −0.44	37,908.58(8) −0.26		36,249.97(7) 0.00				23,621.81(6) −0.03	
$41°_1$	1	167,434.91		40,916.85(5) −0.48	39,345.40(3) −0.32		37,445.01(10) 0.18	36,668.91(0) 0.00			24,082.27(4) 0.52	24,039.74(4) 0.98	
$42°_0$	0	168,721.56		42,203.45(0) −0.43			38,732.34(0) −0.50			27,165.46(2) 0.51	25,370.24(3) −0.80		
$43°_1$	1	169,183.40	169,180(3) 3.40	42,664.86(8) 0.00	41,094.04(5) −0.47		39,193.94(7) −0.26			27,627.54(0) 0.27	25,831.40(2) −0.12		24,660.32(3) −0.37
$44°_2$	2	169,588.87		43,070.33(10) 0.00	41,499.06(0) −0.02	40,480.48(0) 0.74		38,822.27(3) 0.60		28,033.82(0) −0.54			
$45°_1$	1	170,363.90		43,845.70(4) −0.24	42,273.76(10) 0.31		40,374.38(10) −0.20	39,597.70(0) 0.20	37,210.74(10) −0.38				
$46°_2$	2	170,504.28		43,985.74(0) 0.00	42,414.72(0) −0.27	41,396.65(8) −0.02		39,738.09(10) 0.19				27,109.91(2) 0.18	
$47°_3$	3	172,544.21			44,454.34(0) 0.04			41,778.25(15) −0.04				29,150.51(0) −0.49	
$48°_3$	3	172,826.52			44,737.40(0) −0.71	43,718.01(5) 0.86		42,060.52(0) 0.00				29,432.78(0) −0.45	
$49°_0$	0	173,244.21		46,725.50(2) 0.17			43,254.99(0) −0.50			31,689.09(1) −0.47	29,891.31(0) 0.78		
$50°_1$	1	173,837.00	173,809(1) 28	47,318.87(5) −0.41			43,846.85(4) 0.43	43,070.33(10) 0.67	40,682.42(1) 1.04	32,281.44(1) −0.03			
$51°_1$	1	175,951.42		49,432.88(0) 0.00	47,861.15(8) 0.44			45,185.66(0) −0.24	42,796.91(00) 0.97		32,599.88(5) −0.58		31,428.22(2) −0.25
$5p^5(^2P_{1\frac{1}{2}})10s$													
$52°_1$	1	177,243.50	177,225(3) 18.50	50,720.99(3) 3.97	49,153.64(0) 0.03		47,254.01(0) −0.23		40,091.84(3) −1.88		33,890.73(5) 0.65		

TABLE V.

$5p^5(^2P_{\frac{1}{2}})5d$, $6s$			$5p^5(^2P_{\frac{1}{2}})7p$						$5p^5(^2P_{\frac{3}{2}})7p$		
			11_1	12_2	13_2	14_2	15_1	16_0	17_1	18_1	19_2
	J		1	2	3	2	1	0	1	1	2
		Relative Term Value	155,965.45	156,115.18	156,513.16	156,757.30	157,062.46	157,743.28	166,096.39	167,453.71	168,525.71
$1°_2$	3	*105,949.74				50,807.58(2) −0.02					
$2°_1$	1	*106,222.79					50,841.17(2) −1.48				
$3°_2$	2	*107,392.33	48,572.89(3) 0.23	48,723.19(0) −0.34	49,120.56(7) 0.27	49,365.51(5) −0.54					
$4°_0$	0	*107,563.14									
$5°_1$	1	*107,905.01	48,060.36(8) 0.08			48,851.72(00) 0.57		49,838.47(00) −0.20			
$6°_2$	2	108,304.19	47,660.15(0) 1.11		48,209.00(1) −0.03	48,454.48(00) −1.37					
$7°_1$	1	*110,945.18	45,020.65(9) −0.38	45,170.35(5) −0.35		45,812.18(5) −0.06	46,117.32(3) −0.04	46,797.94(3) 0.16			
$8°_4$	4	112,236.53			44,276.77(12) −0.14						
$9°_2$	2	*112,795.08	43,170.56(6) −0.19	43,319.64(5) 0.46	43,718.01(5) 0.07	43,962.15(0) 0.07	44,266.38(5) 1.00				
$10°_3$	3	*113,716.61		42,398.53(5) 0.04	42,796.91(00) −0.40						
$5p^5(^2P_{\frac{3}{2}})5d$, $6s$											
$11°_2$	2	*119,665.41					37,396.69(6) 0.36		46,430.86(0) 0.14	47,786.57(8) 1.73	48,860.11(00) 0.19
$12°_2$	2	*120,404.87		35,711.31(10) −1.00		36,355.02(8) −2.59			45,692.22(3) −0.70	47,048.32(0) 0.32	48,120.99(8) −0.15
$13°_0$	0	*122,365.51					*34,697.72(15) −0.72			*45,089.68(3) −1.48	
$14°_1$	1	*122,866.03	33,098.95(2) 0.47	33,248.89( ) 0.26		33,890.73(5) 0.54		34,877.12(8) 0.13	43,230.48(0) −0.12	44,588.16(2) −0.48	45,658.84(10) 0.84
$15°_1$	1	*123,636.44	32,328.90(5) 0.11	32,478.53(1) 0.21			33,425.57(2) 0.45	34,107.07(20) −0.23	42,459.94(10) 0.01	43,817.26(00) 0.01	44,889.26(00) 0.01

TABLE VI.

$5P^5(^2P_{\frac{1}{2}})6d$, $7s$			$5p^5(^2P_{\frac{1}{2}})nf$							
			20_3	21_4	22_3	23_3	24_2	25_3	26_2	27_2
	J		3	4	3	3	2	3	2	2
		Relative Term Value	200,406.90	197,675.63	*197,642.3	192,530.62	192,475.51	191,103.04	191,002.05	188,791.09
16^0_2	2	*149,212.25								
17^0_1	1	*149,605.33		43,070.33(10) −0.03					41,396.65(8) 0.07	39,185.9(10) −0.14
18^0_1	1	*152,172.11		40,504.42(3) −0.90			40,303.75(6) −0.35		38,830.27(10) −0.33	36,618.28(5) 0.70
19^0_2	2	*152,791.49	47,615.21(4) 0.20	39,883.78(1) 0.36	44,851.60(10) −0.79	39,738.4(10) 0.73	39,683.67(00) 0.35	38,310.97(15) 0.58	38,210.96(10) −0.40	35,999.48(15) 0.12
20^0_2	2	*153,302.27	47,104.41(1) 0.02	39,372.51(10) 0.85	44,340.38(15) −0.35	39,228.08(2) 0.27	39,173.21(2) 0.03	37,800.37(5) 0.40	37,700.31(12) −0.53	35,489.02(20) −0.20
21^0_3	3	*153,556.54	46,850.56(0) −0.20		44,085.62(20) 0.14	38,974.38(1) −0.30	38,918.69(15) 0.28	37,545.84(1) 0.66	37,445.01(10) 0.50	35,234.79(00) −0.24
22^0_3	3	*153,678.17			43,965.05(20) −0.92	38,853.06(30) −0.61	38,797.12(10) 0.22	37,425.67(4) −0.80		35,112.06(3) 0.86
23^0_3	1	*156,399.31								

TABLE VII. Wave-length of the Cs II lines not previously classified.

Intensity	λ in air	ν (vac)	Classification
3	vac 564.25	177,225	$5p^6\ ^1S_0 - 52^\circ_1$
1	575.34	173,809	$5p^6\ ^1S_0 - 50^\circ_1$
3	591.08	169,180	$5p^6\ ^1S_0 - 43^\circ_1$
1	602.95	165,850	$5p^6\ ^1S_0 - 33^\circ_1$
1	607.98	164,480	$5p^6\ ^1S_0 - 31^\circ_1$
2	1966.26	50,841.17	$15_1 - 2^\circ_1$
2	1957.66	50,807.58	$14_2 - 1^\circ_2$
3	1970.92	50,720.92	$1_3 - 52^\circ_1$
00	2005.83	49,838.47	$16_0 - 5^\circ_1$
0	2022.29	49,432.88	$1_1 - 51^\circ_1$
5	2025.05	49,365.51	$14_2 - 3^\circ_2$
0	2033.78	49,153.64	$2_3 - 52^\circ_1$
7	2035.15	49,120.56	$13_3 - 3^\circ_2$
00	2046.00	48,860.11	$19_2 - 11^\circ_2$
00	2046.25	48,851.72	$14_2 - 5^\circ_1$
0	2051.75	48,723.19	$12_2 - 3^\circ_2$
3	2058.10	48,572.89	$11_1 - 3^\circ_2$
00	2063.13	48,454.48	$14_2 - 6^\circ_2$
1	2073.60	48,209.00	$13_3 - 6^\circ_2$
8	2077.43	48,120.99	$19_2 - 12^\circ_2$
8	2080.05	48,060.36	$11_1 - 5^\circ_1$
8	2088.71	47,861.15	$2_2 - 51^\circ_1$
8	2091.97	47,786.57	$18_1 - 11^\circ_2$
0	2097.52	47,660.15	$11_2 - 6^\circ_2$
4	2099.50	47,615.21	$20_3 - 19^\circ_2$
5	2112.65	47,318.87	$1_1 - 50^\circ_1$
0	2115.55	47,254.01	$4_1 - 52^\circ_1$
1	2122.27	47,104.41	$20_3 - 20^\circ_2$
0	2124.80	47,048.32	$18_1 - 12^\circ_2$
0	2133.77	46,850.56	$20_3 - 21^\circ_3$
3	2136.17	46,797.94	$16_0 - 7^\circ_1$
2	2139.48	46,725.50	$1_1 - 49^\circ_0$
0	2153.06	46,430.86	$17_1 - 11^\circ_2$
3	2167.70	46,117.32	$15_1 - 7^\circ_1$
5	2182.14	45,812.18	$14_2 - 7^\circ_1$
3	2187.87	45,692.22	$17_1 - 12^\circ_2$
10	2189.47	45,658.84	$19_2 - 14^\circ_1$
0	2212.40	45,185.66	$5_2 - 51^\circ_1$
5	2213.15	45,170.35	$12_3 - 7^\circ_1$
3	2217.91	45,089.68	$18_1 - 13^\circ_0$
9	2220.51	45,020.65	$11_1 - 7^\circ_1$
00	2227.01	44,889.26	$19_2 - 15^\circ_1$
10	2228.88	44,851.60	$22_3 - 19^\circ_2$
0	2234.57	44,737.40	$2_2 - 48^\circ_3$
2	2242.05	44,588.16	$18_1 - 14^\circ_1$
0	2248.80	44,454.34	$2_2 - 47^\circ_3$
15	2254.58	44,340.38	$22_3 - 20^\circ_2$
12	2257.82	44,276.77	$13_3 - 8^\circ_4$
5	2258.35	44,266.38	$15_1 - 9^\circ_2$
3	2267.29	44,091.84	$6_0 - 52^\circ_1$
20	2267.61	44,085.62	$22_3 - 21^\circ_3$
0	2272.76	43,985.74	$1_1 - 46^\circ_2$
20	2273.83	43,965.05	$22_3 - 22^\circ_3$
0	2273.98	43,962.15	$14_2 - 9^\circ_2$
4	2279.96	43,846.85	$4_1 - 50^\circ_1$
		43,845.70	$1_1 - 45^\circ_1$
00	2281.50	43,817.26	$18_1 - 15^\circ_1$
5	2286.68	43,718.01	$3_3 - 48^\circ_3$
			$13_3 - 9^\circ_2$
5	2307.71	43,319.64	$12_2 - 9^\circ_2$
0	2311.16	43,254.99	$4_1 - 49^\circ_0$
0	2312.47	43,230.48	$17_1 - 14^\circ_1$
6	2315.68	43,170.56	$11_1 - 9^\circ_2$
10	vac 2321.07	43,070.33	$21_1 - 17^\circ_1$
			$1_1 - 44^\circ_2$
			$5_2 - 50^\circ_1$
00	2335.90	42,796.91	$6_0 - 51^\circ_1$
			$13_3 - 10^\circ_3$
8	2343.13	42,664.86	$1_1 - 43^\circ_1$
10	2354.44	42,459.94	$17_1 - 15^\circ_1$
0	2356.95	42,414.72	$2_2 - 46^\circ_3$
5	2357.85	42,398.53	$12_2 - 10^\circ_3$
10	2364.81	42,273.76	$2_2 - 45^\circ_1$
0	2368.75	42,203.45	$1_1 - 42^\circ_0$
0	2376.80	42,060.52	$5_2 - 48^\circ_3$
15	2392.86	41,778.25	$5_2 - 47^\circ_3$
0	2408.96	41,499.06	$2_2 - 44^\circ_2$
8	2414.89	41,396.65	$26_2 - 17^\circ_1$
			$3_2 - 46^\circ_2$
5	2432.71	41,094.04	$2_2 - 43^\circ_1$
5	2443.24	40,916.85	$1_1 - 41^\circ_1$
1	2457.32	40,682.42	$6_0 - 50^\circ_1$
3	2468.12	40,504.42	$21_1 - 18^\circ_1$
0	2469.58	40,480.48	$3_3 - 44^\circ_2$
1	2471.88	40,442.82	$1_1 - 39^\circ_2$
10	2476.07	40,374.38	$4_1 - 45^\circ_1$
6	2480.41	40,303.75	$24_2 - 18^\circ_1$
1	2488.74	40,168.85	$1_1 - 38^\circ_2$
1	2506.53	39,883.78	$21_1 - 19^\circ_2$
10	2515,72	39,738.09	$23_3 - 19^\circ_2$
			$5_2 - 46^\circ_2$
00	2519.17	39,683.67	$24_2 - 19^\circ_2$
4	2523.66	39,612.92	$1_1 - 36^\circ_2$
0	2524.64	39,597.70	$5_2 - 45^\circ_1$
10	2539.08	39,372.51	$21_1 - 20^\circ_2$
3	2540.83	39,345.40	$2_2 - 41^\circ_1$
1	2542.18	39,324.52	$1_1 - 33^\circ_1$
2	2548.43	39,228.08	$23_3 - 20^\circ_2$
7	2550.65	39,193.94	$4_1 - 43^\circ_1$
10	2551.17	39,185.9	$27_2 - 17^\circ_1$
2	2552.00	39,173.21	$24_2 - 20^\circ_2$
1	2565.02	38,974.38	$23_3 - 21^\circ_3$
10	2568.17	38,926.58	$2_2 - 40^\circ_3$
15	2568.69	38,918.69	$24_2 - 21^\circ_3$
2	2571.79	38,871.79	$2_2 - 39^\circ_2$
30	2573.03	38,853.06	$23_3 - 22^\circ_3$
10	2574.54	38,830.27	$26_2 - 18^\circ_1$
3	2575.07	38,822.27	$5_2 - 44^\circ_2$
10	2574.74	38,797.12	$24_2 - 22^\circ_2$
0	2581.05	38,732.34	$4_1 - 42^\circ_0$
10	2590.09	38,597.16	$2_2 - 38^\circ_2$
15	2609.44	38,310.97	$25_3 - 19^\circ_2$
10	2616.27	38,210.96	$26_2 - 19^\circ_2$
2	2628.86	38,028.19	$2_2 - 35^\circ_3$
8	2637.14	37,908.58	$3_3 - 40^\circ_3$
3	2640.92	37,854.33	$3_3 - 39^\circ_2$
5	2644.69	37,800.37	$25_3 - 20^\circ_3$
			$2_2 - 34^\circ_2$
10	2648.07	37,752.26	$2_2 - 33^\circ_1$
12	2651.71	37,700.31	$26_2 - 20^\circ_2$
5	2660.24	37,579.42	$3_3 - 38^\circ_2$
1	2662.62	37,545.84	$25_3 - 21^\circ_3$
10	2669.79	37,445.01	$26_2 - 21^\circ_2$
			$4_1 - 41^\circ_1$
4	2671.17	37,425.67	$25_3 - 22^\circ_3$
6	2673.24	37,396.69	$15_1 - 11^\circ_2$
10	vac 2686.60	37,210.74	$6_0 - 45^\circ_1$
4	2701.19	37,009.76	$3_3 - 35^\circ_2$
3	2703.95	36,971.98	$4_1 - 39^\circ_2$
1	2717.86	36,782.78	$3_3 - 34^\circ_2$
10	2724.21	36,697.04	$4_1 - 38^\circ_2$
0	2726.30	36,668.91	$5_2 - 41^\circ_1$
5	2730.07	36,618.28	$27_2 - 18^\circ_1$
15	2748.23	36,376.32	$2_2 - 30^\circ_1$
8	2749.84	36,355.02	$14_2 - 12^\circ_2$
7	2757.81	36,249.97	$5_2 - 40^\circ_3$
8	2761.97	36,195.37	$5_2 - 39^\circ_2$
15	2776.99	35,999.48	$27_2 - 19^\circ_2$
10	2788.24	35,854.36	$4_1 - 33^\circ_1$
10	2789.80	35,834.32	$5_2 - 37^\circ_2$
10	2799.41	35,711.31	$12_2 - 12^\circ_2$
20	2816.94	35,489.04	$27_2 - 20^\circ_2$
00	2827.91	35,351.42	$5_2 - 35^\circ_3$
00	2837.28	35,234.79	$27_2 - 21^\circ_3$
3	2847.24	35,112.06	$27_2 - 22^\circ_4$
3	2848.96	35,090.24	$9_2 - 6^\circ_2$
8	2852.42	35,047.37	$8_1 - 6^\circ_2$
8	2866.37	34,877.12	$16_0 - 14^\circ_1$
15	2881.19	34,697.72	$15_1 - 13^\circ_0$
8	2899.75	34,475.65	$4_1 - 30^\circ_1$
20	2931.09	34,107.07	$16_0 - 15^\circ_1$
5	2949.80	33,890.73	$8_1 - 52^\circ_1$
			$14_2 - 14^\circ_1$
2	2990.85	33,425.57	$15_1 - 15^\circ_1$
	3006.75	33,248.89	$12_2 - 14^\circ_1$
2	3020.37	33,098.95	$11_1 - 14^\circ_1$
5	3066.60	32,599.88	$8_1 - 51^\circ_1$
1	3078.07	32,478.53	$12_3 - 15^\circ_1$
5	3092.31	32,328.90	$11_1 - 15^\circ_1$
1	3095.86	32,281.44	$7_1 - 50^\circ_1$
1	3154.75	31,689.09	$7_1 - 49^\circ_0$
2	3180.94	31,428.22	$10_0 - 51^\circ_1$
0	3345.00	29,891.31	$8_1 - 49^\circ_0$
0	3396.60	29,432.78	$9_2 - 48^\circ_3$
0	342.49	29,150.51	$9_2 - 47^\circ_3$
0	3566.11	28,033.82	$7_1 - 44^\circ_2$
0	3618.55	27,627.54	$7_1 - 43^\circ_1$
2	3680.10	27,165.46	$7_1 - 42^\circ_0$
2	3687.64	27,109.91	$9_2 - 46^\circ_2$
2	3870.16	25,831.40	$8_1 - 43^\circ_1$
5	3978.00	25,131.18	$7_1 - 38^\circ_2$
3	4053.96	24,660.32	$10_0 - 43^\circ_1$
4	4151.27	24,082.27	$8_1 - 41^\circ_1$
10	4158.61	24,039.74	$9_2 - 41^\circ_1$
6	4232.19	23,621.81	$9_2 - 40^\circ_3$
5	4234.41	23,609.43	$8_1 - 39^\circ_2$
2	4241.97	23,567.33	$9_2 - 39^\circ_2$
0	4284.23	23,334.88	$8_1 - 38^\circ_2$
3	4292.01	23,292.59	$9_2 - 38^\circ_2$
0	4363.69	22,909.97	$7_1 - 30^\circ_1$
4	4399.50	22,723.52	$9_2 - 35^\circ_3$
1	4450.79	22,461.66	$5_2 - 6^\circ_2$
3	4453.44	22,448.36	$9_2 - 33^\circ_1$
2	4609.99	21,685.97	$4_1 - 6^\circ_2$
1	4744.60	21,070.71	$9_2 - 30^\circ_1$
1	5012.98	19,942.67	$10_0 - 30^\circ_1$
3	5052.70	19,785.91	$2_2 - 6^\circ_2$
5	5925.65	16,871.12	$3_3 - 8^\circ_4$

of their position and because of their combining with only part of the odd terms appear to be f terms which would combine feebly, if at all, with s terms.

From the differences between the relative term values of the $6p$ terms, 12 new odd terms were found, in addition to those previously mentioned. The highest of the new odd terms has been tentatively assigned to the $5p^5(^2P_{1\frac{1}{2}})10s$ configuration, while the others are thought to be a mixture of $5p^5(^2P_{1\frac{1}{2}})8d$, $9s$ and $5p^5(^2P_{\frac{1}{2}})7d$, $8s$ both of which groups can be predicted to be in this region. The two groups should contain 16 terms. Of the missing three, one with $j=4$ will be difficult to locate because it has but one transition to each group of p terms. The same is true of the term with $j=4$ which is the only term missing in the blended configurations $5p^5(^2P_{1\frac{1}{2}})7d$, $8s$ and $5p^5(^2P_{\frac{1}{2}})6d$, $7s$. The term, ν112,236.53, has been assigned as the term with $j=4$ in the $5p^5(^2P_{1\frac{1}{2}})5d$, $6s$ configuration because the expected transitions, to $6p$ and to $7p$, are strong and have small deviations.

It has proved possible to separate d and s terms only in the configuration $5p^5(^2P_{1\frac{1}{2}})6d$, $7s$. Here two terms, ν149,212.25 and ν156,399.31,

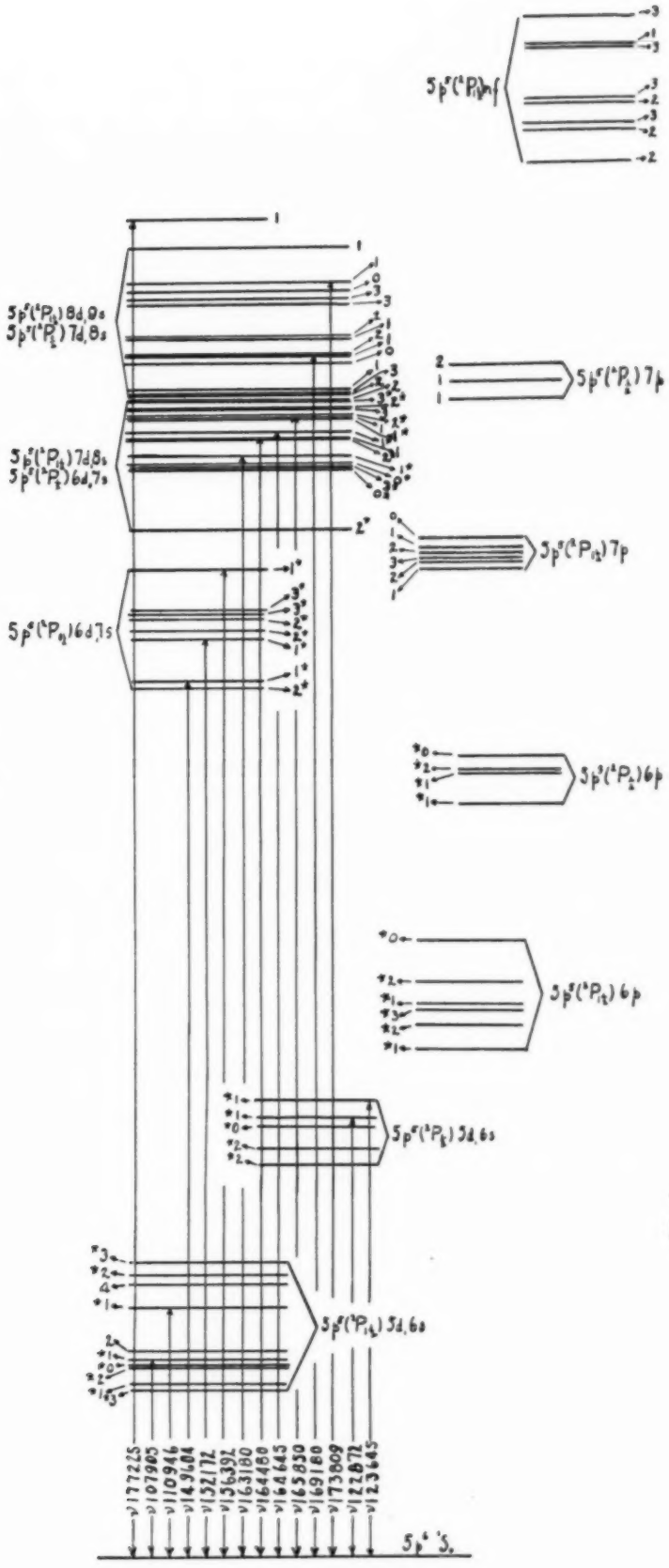

FIG. 1. Energy level diagram for Cs II.

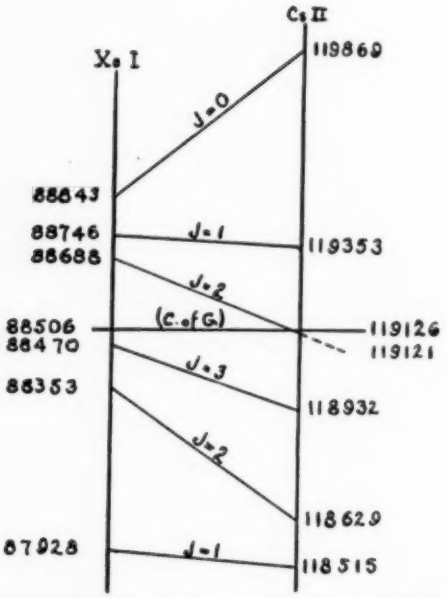

FIG. 2. The $5p^5(^2P_{1\frac{1}{2}})7p$ terms of Xe I and Cs II referred to their center of gravity and reduced in the caes of Cs II by multiplying by 10540/13870 the ratio of the relativistic doublets $5p^5$.

having J values of 2 and 1, respectively, are clearly not d terms and must be classified as s terms, since there are no transitions from f terms to the s terms. The classification by Laporte, Miller, and Sawyer as $^3P_2$ and $^3P_1$, for the terms ν149,212.25 and ν149,650.33, respectively, was based on calculations involving these two terms and two terms similarly situated in the $5p^5(^2P_{1\frac{1}{2}})5d$, $6s$ configuration. These pairs of terms seemed quite widely separated from other terms in the configuration and appeared to be s terms. Olthoff and Sawyer, however, found several other terms in the $5p^5(^2P_{1\frac{1}{2}})5d$, $6s$ configuration very close to these and hence these pairs of terms could not so easily be characterized as s terms. The present investigation shows that one of these terms (ν149,650.33) is a d term. Transitions between the f terms and the lower s and d terms lie out of the range of this work.

The h.f.s. measurements of Kopfermann[6] showed that the term ν107,563.14 has a J value of 0, instead of 2, as given by Olthoff and Sawyer; hence it was necessary to omit the term ν108,245.86 with an indicated J value of 0, since this configuration can have only one term with a J value of 0. A search for a term with a J value of 2 led to term ν108,304.19 which has five confirming transitions. Of the terms proposed by R. Ricard[7] and his collaborators, ν197,642.3 and ν163,024.80 are the only two which can be fitted with certainty into the present classification, the former appears to be an f term and the latter was found by Boyd and Sawyer to have a J value of 0 and it, therefore, has been included in the blended configurations $5p^5(^2P_{1\frac{1}{2}})7d$, $8s$ and $5p^5(^2P_{\frac{1}{2}})6d$, $7s$. Boyd and Sawyer, in the accompanying paper, have proposed ν122,365.51 as a member of the configuration $5p^5(^2P_{\frac{1}{2}})5d$, $6s$ having a J value of 0. This term has been substituted for ν119,465.41, proposed by Olthoff and Sawyer. The substitution has been made on the basis of h.f.s. measurements, intensity of the lines, deviation from the calculated values and comparison with the order of the terms of Xe I.

In further proof of the validity of the $5p^5(^2P_{1\frac{1}{2}})7p$ terms, the six terms of Xe I[8] are drawn in Fig. 2, referred to their center of gravity, and beside them the six terms of Cs II, likewise referred to their center of gravity but reduced by multiplication with 10,540/13,870, the ratio of the relativistic doublets in the two cases. The close correlation of the Xe I terms with those of Cs II is evidence for the correctness of the Cs II analysis. A similar comparison of the $5p^5(^2P_{\frac{1}{2}})7p$ is impossible since no data are available for this configuration in Xe I.

Table VII contains a list of the lines of Cs II classified in this research. The data in the visible are supported by nine transitions which exhibit hyperfine structure, as explained in the accompanying paper by Boyd and Sawyer. No violations in the selection rules were expected and none found. It is hoped that the classification can be further extended by using the many remaining unclassified lines, after measurements of wave-lengths are obtained in the ultraviolet region below λ1850.

[6] H. Kopfermann, Zeits. f. Physik **73**, 437 (1931).

[7] R. Ricard, Comptes rendus **206**, 905 (1938). Ricard, Givoid, and George, Comptes rendus **205**, 1229 (1937).

[8] Meggers, de Bruin, and Humphreys, J. Research Bur. Stand. **3**, 731 (1929).

The Hyperfine Structure of Cs II

ROBERT A. BOYD AND RALPH A. SAWYER
University of Michigan, Ann Arbor, Michigan

(Received February 13, 1942)

The first spark spectrum of caesium was photographed in the visible region with equipment including an electrodeless discharge, a Fabry-Perot interferometer, and a glass Littrow-type spectrograph. The hyperfine structure of thirteen lines was measured and twelve of the patterns were analyzed and identified as being caused by transitions between the $5p^5(^2P_{\frac{1}{2}})6p$ terms and the $5p^5(^2P_{\frac{1}{2}})5d$, $6s$, $6d$, $7s$, and $5p^5(^2P_{1\frac{1}{2}})7d$, $8s$ terms of the energy level scheme established by Sawyer, Olthoff, and others. This analysis verified the J values of seven levels given by Olthoff and Sawyer, determined the interval factors for nine energy levels, established one new energy level, and fixed the J value for one of the levels suggested by Ricard. A tentative identification of the two terms with the largest interval factor as $5p^5(^2P_{\frac{1}{2}})6s\,^1P_1$ and $5p^5(^2P_{\frac{1}{2}})7s\,^1P_1$ leads to 202,263 cm^{-1} as an approximate value of $5p^6\,^1S_0$.

INTRODUCTION

THE first accurate measurements of the h.f.s. in Cs II were made by Kopferman[1] on nine lines that involved transitions from four $5p^56p$ levels to four $5p^55d$, $6s$ levels. The results of Kopferman's experiment indicated that for caesium the nuclear moment is 7/2, and established interval factors and J values for the eight levels.

The present work was undertaken with a view to distinguishing the s levels from the d levels, to establishing more definitely the J values of known energy levels, and to locating undiscovered energy levels.

EXPERIMENTAL PROCEDURE

In this research, as in the work described in the preceding paper, an electrodeless discharge was used as a source. The discharge tube, 10 inches long and about 1 inch in diameter, wound with 20 turns of woven-wire braid, was placed in an electrically heated transite box and arranged for end-on observation. The exciting current was provided by a Tesla discharge. The discharge in the tube was started at a temperature of approximately 180°C and continued intermittently for 25 seconds in each minute; longer operating periods caused excessive heating of the quartz tube.

To minimize relative vibrations, the Fabry-Perot interferometer and the Hilger E1 glass spectrograph were supported by a heavy cast-iron frame work. To reduce temperature and pressure fluctuations, the interferometer, equipped with invar separators, a 50-cm focal length collimating lens, and a 60-cm focal length achromatic converging lens, was enclosed in an airtight box. The temperature of the air in this compartment was kept constant to within two tenths of a centigrade degree. As is well known, the fringe shift owing to change of temperature is negligible, provided the separators are made of invar. Variations in pressure, however, produce serious fringe shifts and therefore must be avoided.

The quartz interferometer plates, 6 cm in diameter, were supported in a cylindrical frame so designed that pressure could be applied to the plates at three symmetrically located points by three independent T-shaped springs. The plates were silvered by an evaporation method in a chamber large enough to allow a maximum distance of 15 cm from the filament to each mirror. For the most part, a point source was

TABLE I. Lines and h.f.s. intervals.

λ(air)	h.f.s. intervals (cm^{-1})				
4158.610	0.531	0.440	0.389	0.284	
4616.13	0.758	0.586			
4623.091	0.589	0.457	0.152		
4656.538	0.606	0.471			
4763.616	0.225	0.174			
4870.024	0.288	0.370	0.376	0.302	
4879.95	0.211	0.540	0.405	0.412	0.143
5059.866	0.146	0.203	0.265	0.316	
5081.773	0.171	0.228			
5209.58	0.473	0.612			
5349.16	0.275	0.333	0.240	0.497	
5358.53	0.497	0.657			
5579.033	0.447	0.590			

[1] H. Kopferman, Zeits. f. Physik **73**, 437 (1931).

used for the evaporation of the silver but in a few cases a symmetrically located ring filament was used to greater advantage.

The caesium discharge was photographed throughout the visible region with intermittent exposure times equivalent to as much as two hours and with interferometer separators of 2, 3, 5, 7.5, and 10 mm. Eastman spectroscopic plates N, F, and O of types II, III, 144, and IV were used and were developed in Eastman D19

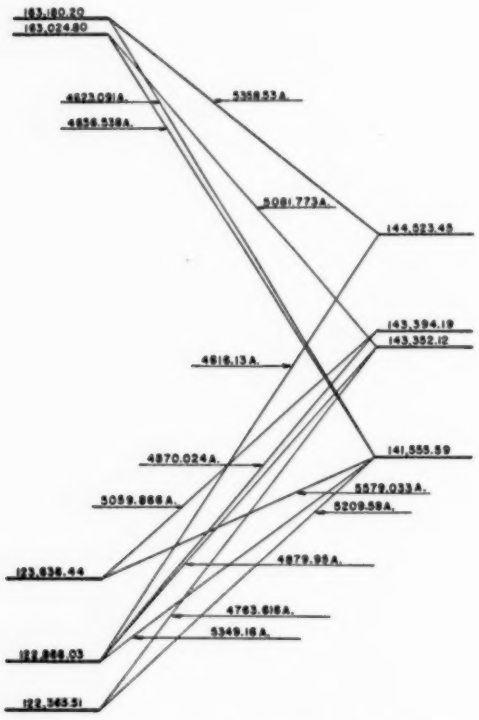

FIG. 1. Partial energy level diagram of Cs II.

developer. It was found expedient when using N and F plates in the 6000A region to hypersensitize them with ammonium hydroxide.

RESULTS

In Table I are listed the lines and the hyperfine structure intervals as measured in this research. The h.f.s. intervals are tabulated so that the wave-length decreases from left to right. Figure 1 is a partial energy-level diagram showing how these lines fit into the energy-level scheme of the preceding paper. The term values as given are based on the $5p^6\ ^1S_0$ level.

All the lines analyzed will be seen to involve transitions with the four $5p^5(^2P_{\frac{1}{2}})6p$ terms found by Olthoff and Sawyer.[2] The reality of these $6p$ terms and the correctness of the assigned J values are definitely established by the results. The hyperfine structure of the combinations of all four of these terms with the term ν122,866 has been measured, as well as that of two of them to the term ν122,365. These terms, both classified as $J=1$ terms in the group $5p^5(^2P_{\frac{1}{2}})5d$, $6s$, are thereby corroborated. So also is the term ν163,180, in the $5p^5(^2P_{\frac{1}{2}})7d$, $8s$—$5p^5(^2P_{\frac{1}{2}})6d$, $7s$ group, for which two transitions to the $(^2P_{\frac{1}{2}})6p$ group have been analyzed. From these six lines the interval factors of the four $(^2P_{\frac{1}{2}})6p$ terms have been determined, as given in Table II.

The intervals and separations measured for the lines, 5209A and 4656A, indicate that these lines are combinations of levels having $J=0$ with the level, ν141,555. In the same way, the lines 5081A and 4763A are also seen to be combinations of the level, ν143,352, with two levels with $J=0$, and, in fact, with the same two levels as in the preceding case.

Of the two levels thus confirmed, the higher, ν163,024 was first given by Ricard.[3] This level and ν197,642, included in the preceding paper, are the only two of the nineteen levels suggested by Ricard and his associates that have been confirmed in the present researches. Ricard suggested for this level the configuration $5p^46s6p$. It falls, however, among the levels assigned in the previous work in this laboratory to the configurations $5p^5(^2P_{1\frac{1}{2}})7d$, $8s$ and $5p^5(^2P_{\frac{1}{2}})6d$, $7s$ and has been so included in the classification by Wheatley and Sawyer.

TABLE II. Interval factors.

Level	J value	Interval Factor
141,555.59	1	0.137
143,352.12	1	−0.049
143,394.19	2	0.064
144,523.45	0	0
122,866.03	1	0.168
123,636.44	1	0.0117
163,024.80	0	0
163,180.20	1	0.144
122,365.51	0	0

[2] J. Olthoff and R. A. Sawyer, Phys. Rev. **42**, 6 (1932).
[3] R. Ricard, Comptes rendus **206**, 905 (1938); R. Ricard, M. Givoid, and F. George, Comptes rendus **205**, 1229 (1937).

The other $J=0$ level, $\nu 122{,}365$ is new. It falls in the group of $5p^5(^2P_{\frac{1}{2}})5d$, $6s$ levels, and has displaced in this group the former $J=0$ level, which was less well established. Wheatley and Sawyer found two additional combinations of this level with the levels of the $7p$ group which give it additional support.

Six of the lines measured are clearly transitions between levels having J values of 0 and 1; three being from $J=0$ to $J=1$, and three from $J=1$ to $J=0$. In these cases, since the nuclear moment is known to be 7/2, the $J=0$ level has one hyperfine level for which $F=7/2$, and the $J=1$ level has three, for which $F=9/2$, 7/2, and 5/2, by virtue of the rule that F can take on values of $J+I$, $J+I-1$, $\cdots$ $J-1$. The hyperfine structure pattern of such a transition accordingly has three components which, following the interval rule, should have spacings of $9/2\,A$ and $7/2\,A$, where A is the interval factor for the $J=1$ level, and should have intensities in the ratio 5 : 4 : 3.

These conditions were very well satisfied by the patterns obtained for the above-mentioned lines. In the case of lines 4616A and 4763A where the measurements were made on patterns from interferometer separators of three different values, 2, 3, and 5 mm for line 4616A, and 3, 5, and 7.5 mm for line 4763A—the ratio of the large interval to the small interval did not differ from the theoretical ratio of 9/7 by more than $1\frac{1}{2}$ percent.

The analysis of the remaining six lines, indicated in Fig. 1, which involve levels with J values other than zero, was aided by the use of Fisher-Goudsmit[4] analysis diagrams. Figure 2 is the analysis diagram for a transition between levels with $J=1$. In the use of this diagram to interpret h.f.s. patterns, if both terms have normal h.f.s. and obey the interval rule, there are three F levels of 9/2, 7/2, and 5/2 in each term separated by distances of $9/2\,A$ and $7/2\,A$ in the upper term and by distances of $9/2\,B$ and $7/2\,B$ in the lower term, where A and B are the interval factors for the upper and lower terms, respectively. Upon application of the selection rules, i.e., $\Delta F=\pm 1$, 0 (0→0 excluded) and use of $Y=A/B$, the displacements of the lines from the line representing the transition 7/2 to 7/2 are,

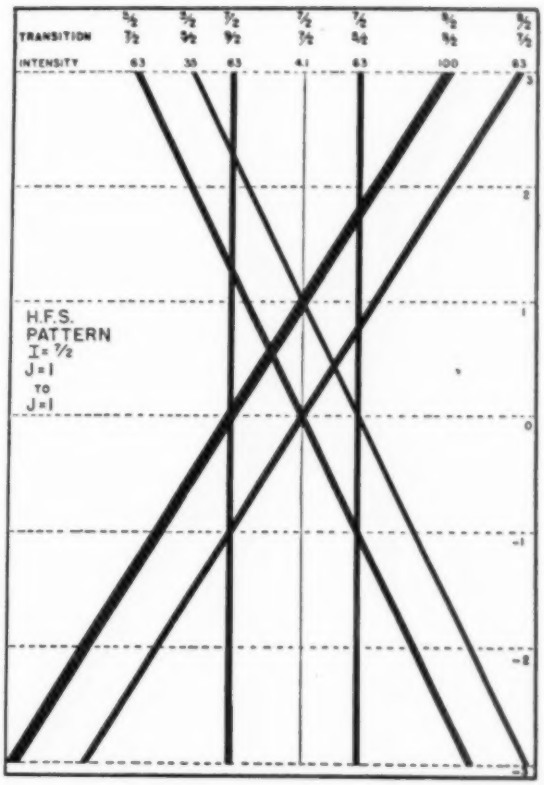

FIG. 2. Fisher-Goudsmit diagram for analysis of h.f.s. The case shown is that for a transition between two terms with $J=1$ when $I=7/2$.

$-9/2\,B$ for 7/2 to 9/2, $+7/2\,B$ for 7/2 to 5/2, $+9/2\,B(Y-1)$ for 9/2 to 9/2, $+9/2\,BY$ for 9/2 to 7/2, $-7/2\,BY$ for 5/2 to 7/2, and $-7/2\,B(Y-1)$ for 5/2 to 5/2. If one of the two terms is inverted, i.e., the largest F value lying deepest, Y has a negative value. When the displacements are plotted against positive and negative values of Y a straight line results for each transition. The relative intensities of these lines, as given by the intensity rules of Hill,[5] are written above the transition values and are also approximately represented by the width of the straight lines.

In the case of the line 5349A, the pattern has five components, with estimated intensities of 2, 2, 4, 1, and 6, and separations of 0.275, 0.333, 0.240, and 0.497 cm^{-1}, respectively. This transition if correctly assigned involves two of the $J=1$ levels for which the interval factors have been evaluated from their combinations with $J=0$ levels. The h.f.s. pattern should then be

[4] R. A. Fisher and S. A. Goudsmit, Phys. Rev. **37**, 1057 (1931).

[5] E. L. Hill, Proc. Nat. Acad. Sci. **16**, 68 (1930).

found on Fig. 2 and the spacings in the pattern can be calculated with the aid of the interval rule and the known interval factors. The pattern is found on Fig. 2 at $Y \leqq 0.8$ and it is seen that it is completely resolved except for the 7/2 to 5/2 and 9/2 to 7/2 components, which very nearly have the same displacement. The component due to the 7/2 to 7/2 transition is not observed because of its extremely low intensity. The interval 0.275 cm represents the difference between the transition 7/2 to 9/2 and the transition 5/2 to 7/2 and, therefore, according to the interval rule, is equal to $4/5 \times 0.168 - 3.5 \times 0.137$, where 0.168 cm^{-1} and 0.137 cm^{-1} are the interval factors previously determined for the lower and upper energy levels, respectively. The calculated value of the interval, 0.2765 cm^{-1} is in very good agreement with the observed value. The second interval in the observed pattern of 0.333 cm^{-1} is the difference between the transition 5/2 to 7/2 and the transition 9/2 to 9/2 and therefore should be $3.5 \times 0.137 - 4.5(0.168 - 0.137)$ or 0.340 cm^{-1}. By continuing in the same manner for the remaining two intervals, the complete calculated pattern is obtained. These calculated intervals and the observed intervals are shown for comparison in Fig. 3. Also in Fig. 3 are recorded the

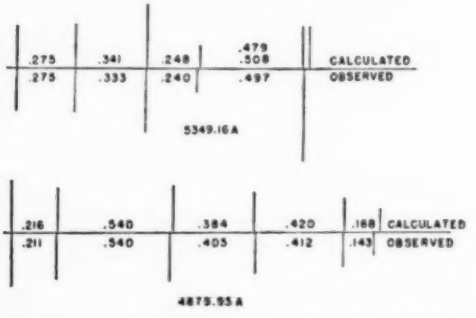

FIG. 3. Comparison of calculated and observed h.f.s. for lines 5349.16A and 4879.95A.

observed and calculated intervals for a pattern that was completely resolved 4879A. In general, the agreement between calculated and observed intervals for all of the h.f.s. patterns measured was very good.

In addition to the six 3-component patterns mentioned above as $J=0$ and $J=1$ transitions, one other h.f.s. pattern was measured that had three components. This pattern is the one belonging to line 5579A and is the result of a transition between two levels with $J=1$. The interval factor for one of these levels is approximately one-tenth of the interval factor of the other and therefore this pattern is found on Fig. 2 as an unresolved one near the axis $Y=0$. The intervals between the centers of gravity of the unresolved components were calculated as 0.459 cm^{-1} and 0.591 cm^{-1}, which are in good agreement with the observed intervals of 0.447 cm^{-1} and 0.590 cm^{-1}.

In Table II are listed the interval factors as obtained from h.f.s. measurements, together with the energy-level terms and their J values. All of the F levels of the energy levels involved in the measured transition are normal with the exception of those in term 143,352.12 cm^{-1} which are inverted.

In addition to the twelve h.f.s. patterns that were measured and satisfactorily assigned to transitions between known energy levels, a graded series h.f.s. pattern having five components was measured for 4158.6A. The wave number of this transition fits fairly well in two places in the present energy-level diagram but the h.f.s. pattern does not meet the requirements of the transition characteristics. The assignment of this line is therefore in doubt.

It is expected from the theory, and has been verified for arsenic by Tolansky,[6] that the terms based on $^2P_{\frac{1}{2}}$ should have a wider structure than those based on $^2P_{1\frac{1}{2}}$ of the same configuration. This prediction is verified in the present work; the $^2P_{\frac{1}{2}}(6p)$ terms, $\nu\nu$141,555.59, 143,352.12, and 143,394.19 have been found to have considerably larger interval factors than those found by Kopferman for the $^2P_{1\frac{1}{2}}(6p)$ terms, which were all of the order of 0.03 cm^{-1}.

Among the odd terms, those arising from an s electron should have wider structure than those arising from a d electron. The two levels, $\nu\nu$122,866.03 and 163,180.20, with the largest intervals yet found in the Cs II spectrum and, each with $J=1$, may be expected to arise, respectively, from the configurations $5p^5(^2P_{\frac{1}{2}})6s$ and $5p^5(^2P_{\frac{1}{2}})7s$ or $5p^5(^2P_{1\frac{1}{2}})8s$, rather than from the d levels blended with these groups.

The tentative calculated value of the term of the normal caesium ion was given by Laporte,

[6] S. Tolansky, Proc. Roy. Soc. **A137**, 541 (1932).

Miller, and Sawyer[7] as 189, 244 cm^{-1}. If the two levels $\nu\nu$122,866.03 and 163,180.20 are the $^1P_1$ terms of the configurations $5p^5(^2P_{\frac{1}{2}})6s$ and $5p^5(^2P_{\frac{1}{2}})7s$, respectively, then application of the Rydberg formula gives a value of 202,263 cm^{-1} for the $^1S_0$ term. This new value is preferable since all the terms in the preceding paper are then positive when referred to $^1S_0$.

[7] O. Laporte, G. R. Miller, and R. A. Sawyer, Phys. Rev. **39**, 458 (1932).

MAY 1 AND 15, 1942 PHYSICAL REVIEW VOLUME 61

On the Spectra of Hg II and Hg III

S. Mrozowski
*Ryerson Physical Laboratory, University of Chicago, Chicago, Illinois**

(Received February 3, 1942)

The structure of many lines of ionized mercury in the region 6000–2200A has been investigated by means of apparatus of high resolving power. Many of the lines have been found to possess complex structure. The structures found are presented in the form of graphs, in which approximate distances and intensities of components are given. In a few cases more exact values of the distances are indicated. From the data collected in Table I and Fig. 2 the isotope shifts in 47 energy levels of Hg II and the hyperfine structure splittings in ten of them have been roughly determined (Table II). The isotope shift and hyperfine splitting are very small for levels of the configuration $5d^{10}nx$ (where nx designates electronic orbits higher than $6s$), and quite considerable for levels of the type $5d^96snx$. In the latter case shifts of about 0.3 cm^{-1} between consecutive even isotopes Hg 200 and 202, and hyperfine splittings amounting to from 0.4 to 1.3 cm^{-1}, have been found. Some levels of the configuration $5d^{10}nx$ show perturbation in the isotope shift; the levels $15°_{3/2}$ and $25°_{5/2}$ reveal a strong perturbation of the same kind. The data collected in Table III, Fig. 3, and Fig. 4 present the results in the cases of lines for which no correct classification seems to be known. They belong, mostly at least, to Hg II, and possibly some of them to Hg III. The results show the necessity of rejecting the existing classification of these lines (Hg II and Hg III) and some of the term values previously given for Hg II by Paschen, by Naude, and by Venkatesachar and Subbaraya. A discussion taking into account also the conditions of excitation reveals many doubts about the correctness of an extension of the analysis of the spectrum of Hg III reported by Johns. The most interesting among the lines studied are lines with isotope shifts which are the highest among all known spectra, and most of which at the same time possess no observable hyperfine structure. Since a discussion shows that probably they do not belong to Hg III, their presence furnishes evidence for the existence of two previously unknown sets of levels in Hg II, belonging to configurations $5d^96s^2nx$ and $5d^9nxn'x'$, by which the presence of a considerable number of hitherto unclassified lines can be understood.

INTRODUCTION AND EXPERIMENTAL

SPECTRA of most of the elements have been investigated for hyperfine structure and isotope shift. Astonishingly enough, the spectra of singly and multiply ionized mercury have not been studied, although the spectrum of neutral mercury has been the object of many studies. Only in the singly ionized mercury spectrum has the structure of a few lines (λ7945; 6150, 4797, 3984, 2848, and 2262) been reported before. This lack of data was undoubtedly connected with the difficulty of obtaining these spectra with high intensity. On the other hand, the study of line structures in these spectra is interesting not only for itself, but is promising also as a means of determining the classification of lines of unknown origin.

The present writer in the spring of 1939 succeeded in obtaining at the Institute of Theoretical Physics, Joseph Pilsudski University, a spectrum of singly ionized mercury of extremely high intensity. The source of light consisted of a hollow cathode discharge tube operated at a very low pressure of helium. The details of the construction of this tube have been described fully in a former paper[1] in which results of other experiments carried out with the same tube have been reported. By using different Fabry-Perot etalons,

* A great part of the experimental work was done at the Institute of Theoretical Physics, Joseph Pilsudski University, Warsaw (Poland).

[1] S. Mrozowski, Phys. Rev. **58**, 332 (1940).

the structures of a considerable number of lines of Hg II in the region λ6000–2200 were observed. The relative intensities and distances of components in all the lines were hastily and roughly evaluated at the time; because of lack of time, the structure of only three of them, λ2815, 2848, and 3984A, were measured exactly. In view of the considerable interest of the hyperfine structure of a forbidden line of a quadrupole type (λ2815) the results of the analysis of these three lines were published in a separate paper two years ago.[2] This paper contains details concerning the operation of the source and a description of the apparatus used. It should be mentioned that, although completeness in references to former work of other investigators was attempted, a paper by Venkatesachar and Sibaiya[3] was unfortunately overlooked. This omission has been pointed out in a recent letter by Dr. Sibaiya.[4] The relation of the results of Venkatesachar and Sibaiya to mine has recently been discussed.[5]

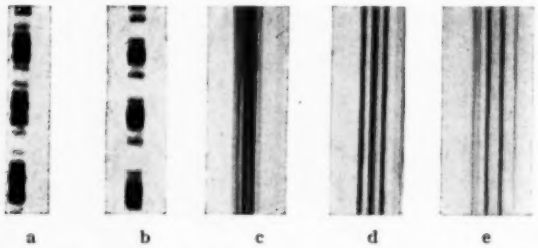

FIG. 1. (a) λ2916.37 Fabry-Perot etalon, 4.2-mm spacer (comp. Fig. 2); (b) λ2935.92 Fabry-Perot etalon, 4.2-mm spacer (comp. Fig. 2); (c) λ3549.42 Second order of 30-foot grating (comp. Fig. 2); (d) λ3090.60 Second order of 30-foot grating (comp. Fig. 4, type B); (e) λ3312.31 Second order of 30-foot grating (comp. Fig. 4, type B*).

At first the publication of all other data obtained for the spectrum of ionized mercury was postponed to the time when exact measurement would be made. But in the meantime a critical analysis, carried out here in Chicago, of the data available at present revealed several points of interest (especially the probable existence of two hitherto unknown sets of levels in Hg II). The exact values of distances of the components (to one percent) are important only for the calculation of the exact energy level separation; all important conclusions concerning the general problems of classification of levels can in this case be obtained just as well from the approximate as from the exact data.[6] The original plates were left at the Institute of Theoretical Physics in Warsaw, and there is little hope that the exact measurements can be carried out in the near future. In view of this situation the author decided to present in this paper all results obtained up to now, although he is fully aware of the incompleteness of this work. In a few cases more exact data have been obtained, and are inserted in the corresponding figures. For the lines λ2916 and λ2936, the measurements were performed on two enlargements made in Warsaw from plates taken with etalons of 4.2 and 7-mm separation (the first one is reproduced in Fig. 1, a and b). A few other lines have been photographed in the first order (λ4797, 5128, and 5210) and in the second order (λ2481, 2572, 2809, 2982, 3091, 3110, 3312, 3385, 3452, 3549, and 3557) of the 30-foot Chicago grating (resolving power in the second order around 300,000). Unfortunately, the relatively low intensity of the source did not

TABLE I. Classified lines of Hg II without structure.

Line	Classification	Width in 10^{-3} cm^{-1}	Line	Classification	Width in 10^{-3} cm^{-1}
2224.71	$6^3P^\circ_{1\frac{1}{2}} - 6^3D_{2\frac{1}{2}}$	D	3006.57	$6^3D_{2\frac{1}{2}} - 7^3F^\circ_{3\frac{1}{2}}$	*
2252.78	$6^3P^\circ_{1\frac{1}{2}} - 6^3D_{1\frac{1}{2}}$	D	3191.03	$7^3P^\circ_{1} - 9^3D_{1\frac{1}{2}}$	*
2260.26	$7^3S_{1\frac{1}{2}} - 6^3P^\circ_{1}$	D	3277.87	$16^\circ_{3\frac{1}{2}} - 4_{3\frac{1}{2}}$	*
2339.37	$5^\circ_{4\frac{1}{2}} - 3_{3\frac{1}{2}}$	~70	3317.30	$7^3P^\circ_{1} - 10^3S_{1}$	~120
2345.55	$6^\circ_{1\frac{1}{2}} - 4_{2\frac{1}{2}}$	D	3524.19	$6^3D_{1\frac{1}{2}} - 6^3F^\circ_{2\frac{1}{2}}$	*
2407.35	$7^\circ_{3\frac{1}{2}} - 4_{3\frac{1}{2}}$	~70	3605.80	$\left\{\begin{matrix} 6^3D_{2\frac{1}{2}} - 6^3F^\circ_{3\frac{1}{2}} \\ 7^3P^\circ_{1\frac{1}{2}} - 9^3D_{2\frac{1}{2}} \end{matrix}\right\}$	*
2414.13	$8^\circ_{2\frac{1}{2}} - 4_{2\frac{1}{2}}$	~85	3806.38	$7^3P^\circ_{1} - 8^3D_{1\frac{1}{2}}$	*
2514.79	$7^3S_{1\frac{1}{2}} - 9^3P^\circ_{1}$	*	4404.86	$5^3F^\circ_{3\frac{1}{2}} - 9^3G$	~150
2545.33	$11^\circ - 5_{2\frac{1}{2}}$	*◇	4454.33	$5^3F^\circ_{2\frac{1}{2}} - 9^3G$	~150
2691.13	$6^3D_{1\frac{1}{2}} - 8^3F^\circ_{2\frac{1}{2}}$	*	4552.89	$6^3D_{1\frac{1}{2}} - 8^3P^\circ_{1}$	~180
2732.60	$6^3D_{2\frac{1}{2}} - 8^3F^\circ_{3\frac{1}{2}}$	*	4762.22	$5^3F^\circ_{2\frac{1}{2}} - 8^3G$	~200
2749.83	$7^3P^\circ_{1} - 11^3D_{1\frac{1}{2}}$	*	5222.81	$5^3F^\circ_{3\frac{1}{2}} - 7^3G$	$\lesssim 80^z$
2788.40	$\left\{\begin{matrix} 7^3P^\circ_{1} - 12^3S_{1\frac{1}{2}} \\ 11^\circ - 4_{3\frac{1}{2}} \end{matrix}\right\}$	*	5677.17	$6^3D_{2\frac{1}{2}} - 5^3F^\circ_{2\frac{1}{2}}$	†
2909.36	$7^3P^\circ_{1} - 10^3D_{1\frac{1}{2}}$	~130	7944.66	$7^3P^\circ_{1} - 7^3S_{1\frac{1}{2}}$	‡
2955.13	$6^3D_{1\frac{1}{2}} - 7^3F^\circ_{2\frac{1}{2}}$	~180			

^{D} Width equal to the Doppler width.
* Total width of the line $\leq 100 \times 10^{-3}$ cm^{-1}. Not investigated with higher resolving power.
† Overlapped with a neighboring line. Width uncertain, studied only with lower resolving power.
‡ Not studied in this work. Data taken from H. Schüler and E. G. Jones, Zeits. f. Physik **76**, 14 (1932). Width not given by them.
^{z} On both sides of the line there are wings visible which undoubtedly belong to hyperfine structure. It shows an anomalously great splitting of one of the levels involved in this transition.
◇ Classified by Jones in Hg III as 11 −22°.

[2] S. Mrozowski, Phys. Rev. **57**, 207 (1940).
[3] B. Venkatesachar and L. Sibaiya, Proc. Ind. Acad. Sci. **1**, 8 (1934). They investigated the lines λ3984, 2848, and 2262.
[4] L. Sibaiya, Phys. Rev. **58**, 925 (1940).
[5] S. Mrozowski, Phys. Rev. **59**, 104 (1941).
[6] These are exact probably to around 5 percent, the errors are certainly smaller than 10 percent.

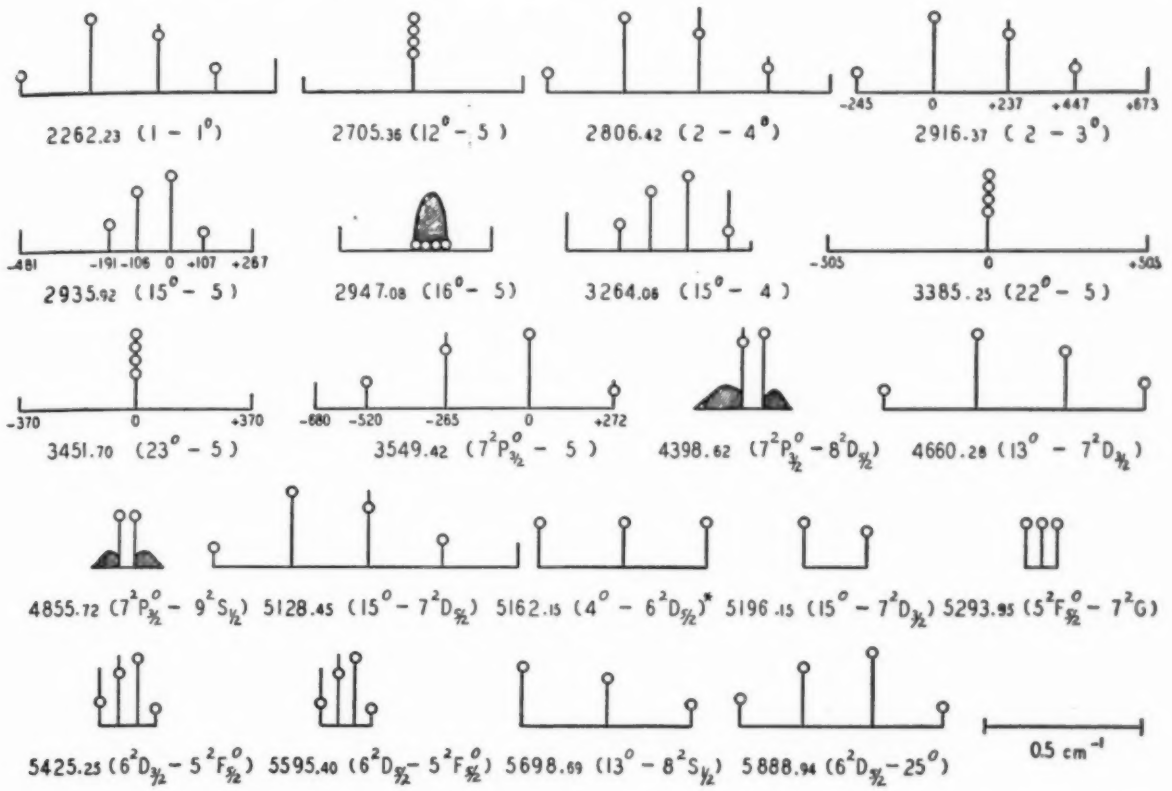

FIG. 2. Structure of classified lines of Hg II. The correlation of components to even isotopes is indicated by circles. The height of lines below the circles corresponds to relative concentration of isotopes Hg^{198}~10 percent, Hg^{200}~24 percent, Hg^{202}~29.5 percent, Hg^{204}~7 percent. In cases where the direction of the correlation is not certain, all circles are indicated on the same level. For λ5162.15 only the first of two alternate classifications proposed by McLennan, McLay, and Crawford (reference 8) has been adopted, since the second one $16°-7^2D_{5/2}$ leads to an isotope shift in $7^2D_{5/2}$ incompatible with the structure of λ5128.45 (see Table II).

permit getting particularly good pictures and extending the investigations to other weaker lines. The reason for the failure of the hollow cathode used here to give intense spectrum was its horizontal position. The presence of the drop of liquid mercury at the end of the cathode axis in the older arrangement[2] seems to make possible the running of the discharge at much lower pressures of helium, thus giving a much brighter spectrum of Hg II. Some of the pictures obtained with the grating are reproduced in Fig. 1.

RESULTS

Structure of Classified Lines of Hg II

In Table I are collected all formerly classified lines found to be single, use of which has been made in determination of the isotope shifts of levels in Hg II (Table II). The classification of the Hg II lines has been taken from the papers by Paschen[7] (the $5d^{10}nx$ set of levels) and by McLennan, McLay, and Crawford[8] (the $5d^96snx$ set of levels and the intercombinations). In Fig. 2 are presented in the form of graphs the structures found for all classified lines; these data have been used in preparation of Table II. In most of the cases the correlation of components to the even isotopes of mercury (198–204) can be found easily by inspection. The odd isotopes (199 and 201) possess in most cases an observable hyperfine splitting; according to the unsymmetrical position of their centers of gravity additional components appear outside of the lightest mercury isotope line (198), the other components being overlapped with the lines belonging to heavier even isotopes. The components belonging to even

[7] F. Paschen, Ber d. Preuss. Akad. d. Wiss. **32**, 536 (1928).

[8] J. C. McLennan, A. B. McLay, and M. F. Crawford, Proc. Roy. Soc. **134**, 41 (1932).

TABLE II. Isotope shifts and hyperfine separations in the levels of Hg II.

Level		Configuration	Isotope shift Hg^{200}–Hg^{202} in 10^{-3} cm^{-1}	H.f.s. Hg^{199} in 10^{-3} cm^{-1}
$6^2S_{\frac{1}{2}}$	0	$6s$	+226	+1358
$1_{2\frac{1}{2}}$	35514	$5d^9{}_{\frac{3}{2}}6s_{\frac{1}{2}}$	+508	+118
$2_{1\frac{1}{2}}$	50554	$5d^9{}_{\frac{1}{2}}6s_{\frac{1}{2}}$	+530	+183
$6^2P^o_{\frac{1}{2}}$	51485	$6p_{\frac{1}{2}}$	0	
$6^2P^o_{1\frac{1}{2}}$	60608	$6p_{1\frac{1}{2}}$	assumed 0	+49
$1^o{}_{2\frac{1}{2}}$	79704	$5d^9{}_{\frac{3}{2}}6s_{\frac{1}{2}}6p_{\frac{1}{2}}$	+295	~+700
$3^o{}_{2\frac{1}{2}}$	84834	$5d^9{}_{\frac{3}{2}}6s_{\frac{1}{2}}6p_{\frac{1}{2}}$	+290	~+780
$4^o{}_{1\frac{1}{2}}$	86177	$5d^9{}_{\frac{3}{2}}6s_{\frac{1}{2}}6p_{\frac{1}{2}}$	+290	~+780
$5^o{}_{4\frac{1}{2}}$	92566?	$5d^9{}_{\frac{3}{2}}6s_{\frac{1}{2}}6p_{1\frac{1}{2}}$	≈ +310 or +290*	
$6^o{}_{1\frac{1}{2}}$	94091	$5d^9{}_{\frac{1}{2}}6s_{\frac{1}{2}}6p_{\frac{1}{2}}$	+310	
$7^o{}_{3\frac{1}{2}}$	95186	$5d^9{}_{\frac{3}{2}}6s_{\frac{1}{2}}6p_{1\frac{1}{2}}$	+290	?
$8^o{}_{2\frac{1}{2}}$	95302	$5d^96s6p$	+285	?
$7^2S_{\frac{1}{2}}$	95714	$7s_{\frac{1}{2}}$	0	~+320
11^o	100859	$5d^96s6p$	~+300	
$12^o{}_{1\frac{1}{2}}$	103183	$5d^96s6p$	+290	~+1150
$13^o{}_{\frac{1}{2}}$	103872	$5d^96s6p$	+290	(~0?)
$6^2D_{1\frac{1}{2}}$	104983	$6d_{1\frac{1}{2}}$	0	
$6^2D_{2\frac{1}{2}}$	105543	$6d_{2\frac{1}{2}}$	0	
$15^o{}_{1\frac{1}{2}}$	106085	$5d^96s6p$	+190	~−400
$16^o{}_{2\frac{1}{2}}$	106213	$5d^9{}_{\frac{3}{2}}6s_{\frac{1}{2}}6p_{1\frac{1}{2}}$	+320	~+880
$7^3P^o_{\frac{1}{2}}(19^o{}_{\frac{1}{2}})$	108298	$7p_{\frac{1}{2}}$†	~0	
$22^o{}_{1\frac{1}{2}}$	110603	$5d^96s6p$†	~+295	~+1300
$23^o{}_{2\frac{1}{2}}$	111172	$5d^96s6p$†	~+295	~+1120
$7^3P^o_{1\frac{1}{2}}(24^o{}_{1\frac{1}{2}})$	111970	$7p_{1\frac{1}{2}}$†	+25	
$8^2S_{\frac{1}{2}}$	121416	$8s_{\frac{1}{2}}$	+30	
$25^o{}_{2\frac{1}{2}}$	121959	$5d^96s6p$†	+220	(~0?)
$5^3F^o_{3\frac{1}{2}}$	123152	$5f_{3\frac{1}{2}}$	~0	
$5^3F^o_{2\frac{1}{2}}$	123409	$5f_{2\frac{1}{2}}$	+60	
$7^3D_{1\frac{1}{2}}$	125324	$7d_{1\frac{1}{2}}$	0	
$7^3D_{2\frac{1}{2}}$	125578	$7d_{2\frac{1}{2}}$	−50	
$8^3P^o_{\frac{1}{2}}$	126954	$8^3p_{\frac{1}{2}}$	±50	
$9^3S_{\frac{1}{2}}$	132559	$9^3s_{\frac{1}{2}}$	+50 ±25	
$6^3F^o_{3\frac{1}{2}}$	133268	$6f_{3\frac{1}{2}}$	~0	
$6^3F^o_{2\frac{1}{2}}$	133350	$6f_{2\frac{1}{2}}$	~0	
$8^3D_{1\frac{1}{2}}$	134562	$8d_{1\frac{1}{2}}$	~~0	
$8^3D_{2\frac{1}{2}}$	134698	$8d_{2\frac{1}{2}}$	+90	
$3_{3\frac{1}{2}}$	135299	$5d^9{}_{\frac{3}{2}}6s_{\frac{1}{2}}7s_{\frac{1}{2}}$	≈ +290 or +310*	
$9^3P^o_{\frac{1}{2}}$	135467	$9p_{\frac{1}{2}}$	0	
$4_{2\frac{1}{2}}$	136712	$5d^96s_{\frac{1}{2}}7s_{\frac{1}{2}}$	+310	~+880
$10^3S_{\frac{1}{2}}$	138434	$10s_{\frac{1}{2}}$	~±30	
$7^3F^o_{3\frac{1}{2}}$	138793	$7f_{3\frac{1}{2}}$	~0	
$7^3F^o_{2\frac{1}{2}}$	138812	$7f_{2\frac{1}{2}}$	±50	
7^3G	139042	$7g$	+10	
$9^3D_{1\frac{1}{2}}$	139627	$9d_{1\frac{1}{2}}$	~~0	
$9^3D_{2\frac{1}{2}}$	139695	$9d_{2\frac{1}{2}}$	~+25	
$5_{4\frac{1}{2}}$	140135	$5d^96s_{\frac{1}{2}}7s_{\frac{1}{2}}$	+295	~+420
$8^3F^o_{3\frac{1}{2}}$	142127	$8f_{3\frac{1}{2}}$	~0	
$8^3F^o_{2\frac{1}{2}}$	142131	$8f_{2\frac{1}{2}}$	~0	
8^3G	142293	$8g$	0	
$10^3D_{1\frac{1}{2}}$	142660	$10d_{1\frac{1}{2}}$	~±30	
9^3G	144402	$9g$	±30	
$11^3D_{1\frac{1}{2}}$	144653	$11d_{1\frac{1}{2}}$	~~0	

Remarks: All isotope shifts have been determined under the assumption of zero isotope shift for the level $6^3P^o{}_{3/2}$. Of the two classifications given for the line λ2788.40 (Table I) only the second one has been adopted, as no traces of the next line in the series $7^3P^o_{\frac{1}{2}}-13^3S_{\frac{1}{2}}$ have been observed. Use of both classifications of λ3605.80 has been made, although it is very probable, that only one of them is correct (single structure of this line). The isotope shifts in 5° and 3 have been obtained by assuming for one of these levels a reasonable value of the shift and then calculating for the other level the corresponding shift from the width of the line λ2339.37. Two equally reasonable assumptions can be made (*). The values of hyperfine structure separations in the levels $7^3S_{\frac{1}{2}}$ and 2 have been calculated from the formulas of Goudsmit (reference 10). The latter has been used in evaluation of the splittings in the levels 3° and 4°. The absence of any hyperfine structure in the strong lines λ2407.35 and 2414.13 is rather strange. Therefore in the case of the levels 7° and 8° interrogation marks have been inserted. The absence of hyperfine structure in the lines λ4660.28 and 5888.94 indicates a very small hyperfine separation of the levels 13° and 25°, which seems rather improbable. It seems possible however that the structures observed are incomplete.

† Correlation to electronic configuration not given in the paper of McLennan, McLay, and Crawford, reference 8.

isotopes are marked on the top with small circles. For a few weak lines, whose structure has been obtained very incompletely in view of insufficient exposure, the direction of the correlation is not certain, and this uncertainty has been made visible by putting all circles at the same level.

From the data of Table I and Fig. 2 isotope shifts of levels for the isotope 200 relative to 202, and the approximate hyperfine structure separation of levels in the isotope 199 have been determined and are presented in Table II. The level designations and the corresponding electronic configurations are taken from the paper of McLennan, McLay, and Crawford.[8] Data formerly obtained by the author[2] for a few levels in Hg II have been included. For the isotope shifts the level $6^2P^o{}_{3/2}$ has been chosen as reference level and its isotope shift has been assumed to be equal to zero. From this level all given levels (with the exception of two levels 5° and 3) can be reached by way of lines observed with instruments of high resolving power. In several cases very good cross checking was possible, as for instance in the case

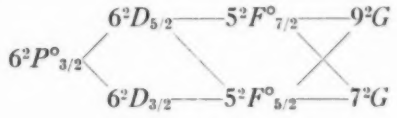

and

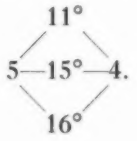

For some lines with uncertain direction of shift (Fig. 2 and broad lines of Table I) the more probable correlation has been chosen, except when the direction of the shift could be determined by cross checking (which was possible for example in the case of the line $16^o{}_{7/2}-5_{5/2}$). In general the possible limits of error probably do not exceed 10 percent; for the levels in which shifts can be obtained in several ways and for intermediate levels the values are a little more reliable. The relative shifts in the levels $6^2S_{\frac{1}{2}}$, $1_{5/2}$, $6^2P^o{}_{3/2}$, $7^2S_{\frac{1}{2}}$, $7^2P^o_{\frac{1}{2}}$, $7^2P^o{}_{3/2}$, and $5_{5/2}$ are determined with highest degree of precision. Some values possess a considerable uncertainty due to a

possible accumulation of errors. Especially in cases when use has been made of single lines with unknown width (Table I), there is a possibility of a larger error. Such cases are marked with one or two signs ~ according to the number of such single lines involved in evaluation of the shifts given.

The results are in best agreement with the currently accepted explanation of isotope shifts. These shifts are caused by the differences in the distribution of electric fields in the neighborhood of the nuclei of different isotopes and are proportional to the density of electrons in the immediate vicinity of the nucleus. Therefore the most important contribution to the isotope shift originates from the *s* electrons. The total isotope shifts are quite considerable, but they cannot be determined; since we are only interested in changes produced by the outer electrons we will choose as a reference configuration the configuration of the ground level of Hg III $5d^{10}$. In Hg II then only very small positive shifts are expected for levels belonging to the configuration $5d^{10}nx$, where nx designates electronic orbits higher than 6*s*. In Table II a zero shift has been adopted for the level $5d^{10}6p$; this means, that in order to get shifts relative to the configuration $5d^{10}$, a constant positive number Δ has to be added to all values given in Table II. According to the theory, the shift produced by the 7*s* electron (the shifts for 7*s* and 6*p* are equal, see Table II) has to be about 4.2 times smaller than in the case of 6*s* (the ratio has to be equal to $(n'_{\text{eff}}/n''_{\text{eff}})^3$). This means that $(226+\Delta)/\Delta = 4.2$ and $\Delta \leqq 70$. This value seems to be quite reasonable, since in this case all negative shifts would disappear from Table II. Köhler[9] claims that in the case of Tl II the relative contributions of the electrons in higher *s* orbits have been shown to be in agreement with theory. This seems to be not well founded, since his statement about the non-influence of the perturbing state $5d^{10}6p^{2}{}^{1}S_0$ is untenable. This state has a considerably smaller isotope shift than the series of states $5d^{10}6sns$ investigated by Köhler ($n = 7, 8, 9$), probably around 200 units (10^{-3} cm^{-1}) less, because of the absence of an electron in the 6*s* orbit. The increasing interaction with the term $6p^{2}{}^{1}S_0$ tends to lower the shift in levels $6sns\,{}^{1}S_0$ with increasing n. How a big part of the observed decrease must be ascribed to this perturbation is at present impossible to evaluate, but the investigations of Hg II show (1) that perturbations give rise to considerable changes in isotope shift, which would be entirely sufficient to explain the whole effect found by Köhler; (2) there is no evidence of a $1/n_{\text{eff}}{}^3$ decrease of shift in the series of levels $5d^{10}ns$ ($n = 7, 8, 9, 10$) in Hg II (however the decrease could be masked by increasing effect of possible perturbations by high $5d^96snx$ terms). Therefore, since the theoretical proportionality to $1/n_{\text{eff}}{}^3$ has not yet been checked experimentally in any of the spectra of heavy elements, there is no basis for the assumption $\Delta \leqq 70$ in Hg II. But if the value -50 of the shift found for $7^2D_{5/2}$ is right, at least Δ should not be smaller than $+50$. We therefore adopt the value $\Delta = 50$ in the following, with a possible error of ± 30.

For all the levels belonging to the configuration $5d^{10}nx$ shifts ranging from 0 to 140 are obtained. Among them the higher values are probably caused by perturbations, as will be explained below. For most of the levels belonging to the configuration $5d^96snx$ the isotope shifts obtained lay in the range 335–370 (two exceptions 15° and 25° are caused probably by perturbations), almost the whole shift is due to the contribution of the 6*s* electron. The increase by around 60 units of the shift caused by the 6*s* electron in comparison with the configuration $5d^{10}6s$ ($226+\Delta = 275$) is connected with the absence of one 5*d* electron and a consequent increase of the strength of binding of the 6*s* electron. The two sets of levels $5d^{10}nx$ and $5d^96snx$ perturb each other; it is easy to see that the perturbations can only result in an increase of the shift in perturbed $5d^{10}nx$ levels and a corresponding decrease in perturbed $5d^96snx$ levels. According to this we understand in principle the occurrence of exceptionally high shifts in some of the $5d^{10}nx$ levels and abnormally low shifts in the levels 15° and 25°. The set of levels $5d^96snx$ is known very incompletely, and therefore it is not possible to study these perturbations in detail. In the case of the level 25° the perturbation is probably caused by the level $5^2F_{5/2}$ and vice versa, but the case of the level 15° is obscure, as there are no appropriate levels of the configuration $5d^{10}nx$ in the neighborhood. The relatively high shifts in the levels $6^2P^\circ_{3/2,1}$ are also difficult to understand. The levels $7^2P^\circ_{3/2,1}$ show also relatively high shifts

[9] P. Köhler, Zeits. f. Physik **113**, 306 (1939).

which are probably caused by perturbation, but this perturbation is by far not as great as predicted by McLennan, McLay, and Crawford[8] and not so great as to make the correlation with the configuration $5d^{10}nx$ doubtful.

The values of the hyperfine structure separations of levels in Table II are far less accurate than the isotope shifts. Both isotopes of mercury 199 and 201 have many hyperfine structure components and only the strongest ones have been obtained on the plates. The adopted method of evaluation of splittings of levels has been the following: It has been assumed that the strong component lying outside of the sequence of the even isotopes at the side of lower masses belongs to the more abundant isotope 199. From the approximate distance of this component from the center of gravity (situated between Hg^{198} and Hg^{200}, very close to the first one), and the separation of one of the levels involved, the separation of the other level could be found. The applicability of the formulas of Hill for relative intensities in a hyperfine structure multiplet had to be assumed. Naturally, such procedure gives only very rough values. The separations in $6^2S_{\frac{1}{2}}$, $1_{5/2}$, and $6^2P^\circ_{3/2}$ were exactly determined and the calculated value for $7^2S_{\frac{1}{2}}$ roughly checked by the author previously.[2] Since the value found for $1_{5/2}$ is exactly equal to the value computed from the formula of Goudsmit,[10] the separation of the level $2_{3/2}$ has been calculated using the same formula. This last value was the starting point for evaluation of splitting in levels 3° and 4°. The hyperfine structure of the perturbed level 15° is inverted, as the structure of the line λ2936 shows; the value of splitting finds a very good check in the chain $7^2P^\circ_{3/2}(\sim 0) \leftrightarrow 5_{5/2}(\sim 420) \leftrightarrow 15^\circ_{3/2}(\sim -400) \leftrightarrow 7^2D_{5/2}(\sim 0)$. It can be hoped that the rough values of hyperfine separations here reported will help to correlate definite j values to different electrons in different levels of the configuration $5d^9 6snx$.

TABLE III. Unclassified lines of Hg II (or Hg III) without structure.*

2263.64	3315.93[7]	3776.26[14]
2467.62[1]	3358.78[8]	4140.38
2525.98	3402.77[9]	4227.29[15]
2552.87[2]	3420.04[10]	4230.13[16]
2574.86[3]	3492.77[11]	4261.88
2627.90[4]	3532.63	4264.65[17]
2781.93[5]	3606.92	4282.75
2796.13[6]	3630.61	4284.70[18]
2797.43	3638.39[12]	4825.62[19]
2873.24	3684.91	5204.78
2939.03	3774.52[13]	

* Total width of the line $\leqslant 100 \times 10^{-3}$ cm^{-1}, if not stated otherwise in a reference below. Unit for shift and width in references is 10^{-3} cm^{-1}.

[1] Classified by Naudé as $2_{1\frac{1}{2}} - {}^4P_{\frac{1}{2}}$ (expected isotope shift of ~230 or more). Existence of $^4P_{\frac{1}{2}}$ level doubtful (see reference 8).

[2] Classified by Naudé as $^4P_{5/2} - {}^4D^2_{5/2}$, (expected isotope shift of ~0), but existence of the level $^4D^2_{5/2}$ doubtful (see reference 8).

[3] Classified by Naudé as $15^\circ_{1\frac{1}{2}} - {}^4D^3_{\frac{1}{2}}$ (expected isotope shift of ~100 or less). Existence of level $^4D^3_{\frac{1}{2}}$ doubtful (see reference 8).

[4] Wide line (~800) without structure. Classified by Paschen as $13^\circ_{\frac{1}{2}} - 11^2S_{\frac{1}{2}}$ (expected total isotope shift ~300). Level $11^2S_{\frac{1}{2}}$ doubtful (see text below).

[5] Classified by Johns as 13 −36° of Hg III (expected isotope shift of ~400).

[6] Classified by Paschen as $13^\circ_{\frac{1}{2}} - 9^2D_{1\frac{1}{2}}$ (expected isotope shift of ~300).

[7] Total width of ~300.

[8] Two components in distance of ~1000. Probably two independent single lines.

[9] Total width of ~200. Classified by Naudé as $12^\circ_{1\frac{1}{2}} - 9^2S_{\frac{1}{2}}$ (expected isotope shift of ~230).

[10] Classified by Johns as 84° −37 of Hg III.

[11] Classified by Naudé as $^4F_{\frac{1}{2}} - 6^2D_{2\frac{1}{2}}$ (expected isotope shift ~300).

[12] Classified by Venkatesachar and Subbaraya as $1^\circ_{2\frac{1}{2}} - {}^2D^2_{5/2}$ (expected isotope shift ~0), but the existence of the level $^2D^2_{5/2}$ doubtful (see text below).

[13] Classified by Naudé as $2_{1\frac{1}{2}} - {}^4P_{5/2}$ (expected isotope shift ~230 or more). Existence of level $^4P_{5/2}$ doubtful (see reference 8).

[14] Two components in distance of ~800. Probably two independent single lines. Classified by Paschen and McLennan, McLay, and Crawford as $15^\circ_{1\frac{1}{2}} - 9^2S_{\frac{1}{2}}$ (expected isotope shift ~140); by Venkatesachar and Subbaraya as $1^\circ_{2\frac{1}{2}} - 6T$ (expected isotope shift ~300 for a transition $5d^9 6s6p - 5d^9 6p^2$).

[15] Classified by Johns as 82° −34 of Hg III (expected isotope shift ~0).

[16] Classified by Johns as 82° −33 of Hg III (expected isotope shift ~0).

[17] Classified by Johns as 15 −81° of Hg III (expected isotope shift ~100).

[18] Classified by Venkatesachar and Subbaraya as $1^\circ_{2\frac{1}{2}} - {}^2D^2_{2\frac{1}{2}}$ (expected isotope shift ~0), but existence of the level $^2D^2_{2\frac{1}{2}}$ doubtful (see text below).

[19] Total width of ~120.

Structure of Unclassified Lines of Hg II and Possibly Hg III

In Table III and Figs. 3 and 4 are presented results obtained for all remaining lines studied which have not been classified yet or for which the proposed classification seems to be in error. As can be seen, the results have given for Hg II in general a confirmation of the analysis of Paschen[5] (the $5d^{10}nx$ set of levels) and a very good one of the work of McLennan, McLay, and Crawford.[8] There are only some doubts about the level $11^2S_{\frac{1}{2}}$ (in Paschen's notation 6S), since all three lines observed λ2628, 2974, and 3338 in which this level is involved, are shown to be classified incorrectly. All in all the classification of only 2 lines by McLennan, McLay, and Crawford, and of 11 lines by Paschen has to be discarded. The classification of 9 lines by Naudé[11] has been proven to be incorrect, 6 of them involving levels whose existence has been put into doubt by the work of McLennan, McLay, and Crawford.[8] In

[10] S. Goudsmit, Phys. Rev. **43**, 636 (1933).

[11] S. M. Naudé, Ann. d. Physik **3**, 1 (1929).

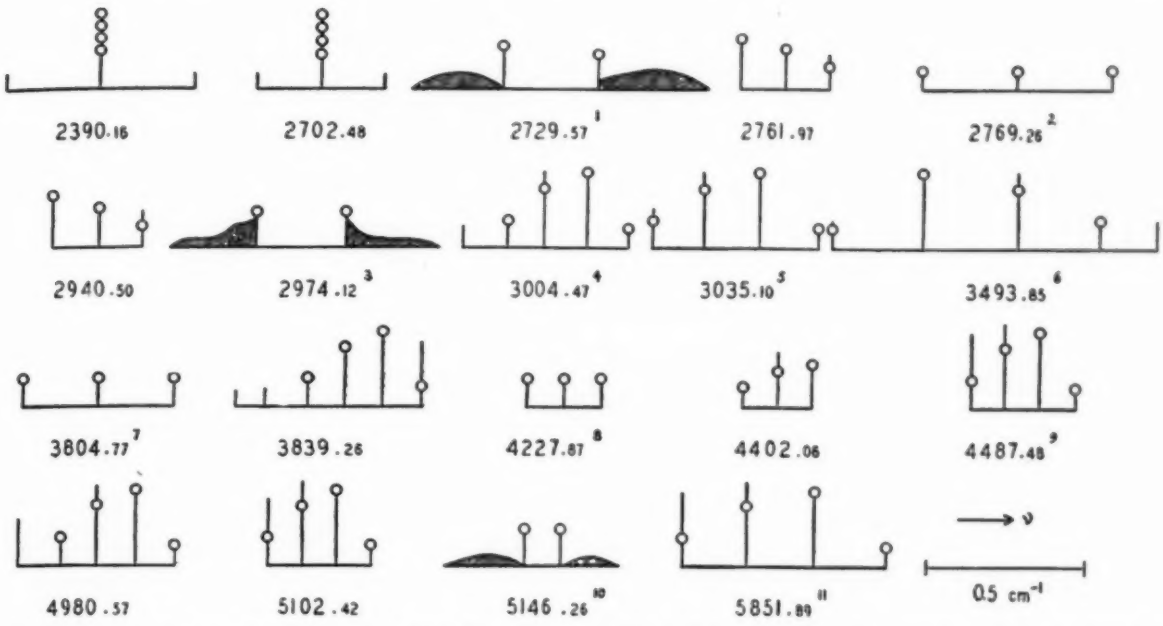

FIG. 3. Structure of unclassified lines of Hg II (possibly partly Hg III). The correlation of components to the even isotopes is marked similarly to the Fig. 2. (1) Classified by Paschen as $15°-10^2D_{5/2}$, the structure found would require an isotope shift in $10^2D_{5/2}$ of ~ -100. (2) If the wave-length of this line is correct the classification of McLennan, McLay, and Crawford as $14°-5$ is untenable (the isotope shift in 14° would be ~ 0). There remains the possibility however, that the structure observed belongs to λ2770.88 (the author was not able to check it once more on the original plate). (3) Classified by Paschen as $7^2P_{\frac{1}{2}}-11^2S_{\frac{1}{2}}$, or $15°-9^2D_{5/2}$, in the first case the line should be single, in the second the isotope shift should be ~ 200 thus considerably smaller than observed. (4) Classified by Naudé as $4°-{}^4D^2_{\frac{1}{2}}$, the isotope shift in ${}^4D^2_{\frac{1}{2}}$ would be ~ 420, which seems much too high. The existence of the level ${}^4D^2_{\frac{1}{2}}$ is doubtful (see reference 8). (5) Classified by Naudé as $7^2P_{3/2}-{}^4D^3_{\frac{1}{2}}$, the isotope shift in ${}^4D^3_{\frac{1}{2}}$ would be ~ 200, which seems possible, but the existence of the level ${}^4D^3_{\frac{1}{2}}$ is doubtful (see reference 8). (6) Classified by Paschen and McLennan, McLay, and Crawford as $15°-8^2D_{5/2}$, but the isotope shift seems to be too big (~ 280 instead of ~ 100). (7) Classified by Naudé as $8^2P-{}^4D^2_{3/2}$, the isotope shift in ${}^4D^2_{3/2}$ would be $\sim 240\pm 50$ which seems possible, but the existence of the level ${}^4D^2_{3/2}$ is doubtful (see reference 8). (8) Classified by Johns as 81°−33 in Hg III (expected isotope shift ~ 0). (9) Classified by Venkatesachar and Subbaraya as $1°-{}^2D^3_{3/2}$, the isotope shift in ${}^2D^3_{3/2}$ would be ~ 410, which seems too high. The existence of the level ${}^2D^3_{3/2}$ is doubtful (see text). (10) Classified by Johns as 10–12° in Hg III (expected isotope shift ~ 750). (11) Classified by Paschen as $25°-6^2G$, but the direction of the observed isotope shift is opposite to the expected. Classified by Johns as 21–82° in Hg III (expected isotope shift ~ 0).

view of such good agreement of my data with the results of McLennan, McLay, and Crawford three other lines classified by Naudé,[11] but involving levels in their opinion not well established have been included in Table II and Figs. 3 and 4, although the classification of Naudé is not in disagreement with the structure observed. Several new term values have been reported by Venkatesachar and Subbaraya,[12] but of all of them only one seems to be well established and is included in Table II ($1°_{5/2}$). Their new term ${}^2\bar{D}_{3/2}$ of the configuration $5d^96s6p$, the terms ${}^2D_{3/2}{}^2$, ${}^2D_{5/2}{}^3$ and ${}^2D_{3/2}{}^3$ of $5d^96s7s$, the term ${}^4\bar{P}_{\frac{1}{2}}$ of $5d^96s6d$ and the terms $6T$ and $7T$ of $5d^96p^2$ if correct would possess on the basis of the present results isotope shifts incompatible with shifts expected for such configurations (even taking into account possible large perturbations). The remaining 5 new terms, although one of them would show a reasonably great isotope shift, in view of the very poor agreement of calculated and measured frequencies and of the use of doubtful terms previously reported by Naudé (see above) should also be discarded.

The big number of relatively strong lines of Hg II for which no classification could be found up to now is rather striking. Of all the 132 lines investigated only 54 have been hitherto classified correctly. Among the unclassified lines a whole group of lines has been found (Fig. 4), which in view of their extremely high isotope shift (the biggest shifts till now observed in any spectrum with the exception of H and B II only), cannot be fitted into the two known sets of levels of Hg II.

[12] B. Venkatesachar and T. S. Subbaraya, Zeits. f. Physik **73**, 412 (1931).

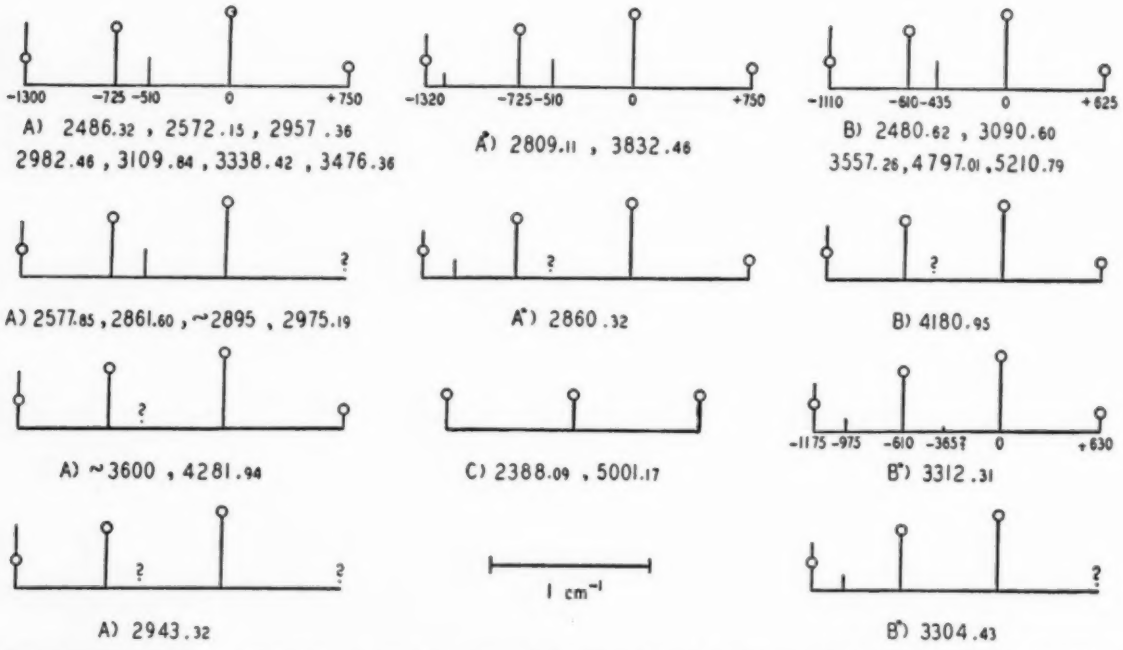

FIG. 4. Structure of unclassified lines, probably belonging to transitions of the type $5d^86s^2nx \rightarrow 5d^96pnx$ in Hg II. The correlation of components to different isotopes is marked similarly to the Fig. 2. All lines fall into three types *A*, *B*, and *C*, according to the magnitude of the isotope shift, the lines with evidence of hyperfine structure splitting are marked by asterisks. In view of the extremely high isotope shift, all previous attempts of classification should be discarded, with the possible exception of the two lines λ3312 and λ3557 classified by Johns in Hg III. λ2388, classified by Johns as 11–23° in Hg III. Expected isotope shift ~400. λ2480 classified by Naudé as $4P_{5/2}-{}^4D^2_{3/2}$. Level ${}^4D^2_{3/2}$ is doubtful (see reference 8). λ2957, classified by Naudé as $4P_{5/2}-{}^4D^2_{3/2}$. Level ${}^4D^2_{7/2}$ is doubtful (see reference 8). Classified also by Johns as 10−16° in Hg III; expected isotope shift ~400. λ2982 classified by Paschen as $21°-10^2D_{5/2}$, and by Naudé as ${}^4\bar{D}_{\frac{1}{2}}-5$. This line was not classified by McLennan, McLay, and Crawford, as was erroneously stated in my former paper, reference 2. λ3090, classified by Paschen as $15°-10^2S_{\frac{1}{2}}$. λ3304, classified by Venkatesachar and Subbaraya as ${}^4F_{7/2}-{}^2D^3_{5/2}$. λ3312, classified by Paschen as 15°−A, also by Johns as 1°−13 in Hg III (in the last case expected isotope shift ~700, which seems to be right). λ3338, classified by Paschen as $7^2P_{3/2}-11^2S_{\frac{1}{2}}$. λ3557, classified by Venkatesachar and Subbaraya as $1°-{}^2D^2_{3/2}$. Also classified by Johns as 2°−13 in Hg III (in the last case expected isotope shift ~700, which seems to be right). λ3832, classified by Venkatesachar and Subbaraya as ${}^2D^3_{5/2}-6^2F_{7/2}$. λ4281, classified by Venkatesachar and Subbaraya as ${}^4D_{\frac{1}{2}}-{}^4\bar{P}_{\frac{1}{2}}$. λ5210, classified by Johns as 28−87° in Hg III. Expected isotope shift ~100.

Therefore, the question arises, if they do belong to Hg II at all. All unclassified lines investigated by the author have been reported previously by Naudé[11] and included by him in a table of observed lines of Hg II (with the exception of the two new lines here reported at ~λ2895 and ~λ3600, whose exact wave-length the author, not having the original plates at his disposal, was not able to determine). But since Ellis and Sawyer[13] have shown, that in the case of Tl, higher spark spectra (Tl III and Tl IV) appear weakly in a hollow cathode discharge in He, the appearance of relatively strong higher spark spectra of mercury in the experiments of Naudé and of the author in discharges in pure mercury vapor at very low pressures seems possible.

A few years ago a considerable extension of the analysis of the spectrum of Hg III was published by Johns,[14] where also a part of the lines from the table of Naudé have been included. But of the 13 lines classified by Johns and observed in this work, only 5 have a structure compatible with the type of transition assigned by Johns. Some of the levels involved belong to highly excited levels of Hg III according to Johns, but at the same time several of the stronger lines emitted from lower levels of Hg III are definitely absent in my spectrograms (for instance λ2724.39 6−10° and λ4973.49 6−5°). Many of the lines classified by Johns as $d^8s^2-d^9p$ transitions are not reported by him to possess a wide structure, although extremely high isotope shifts are expected (see

[13] C. B. Ellis and R. A. Sawyer, Phys. Rev. **49**, 145 (1936).

[14] W. M. Johns, Can. J. Research **15**, 193 (1937).

below). In view of these inconsistencies which cast doubts upon Johns' extension of the term scheme of Hg III it seemed to be interesting to forget Johns' classification for a while and to try to fit at least the lines with extremely high shifts into the level scheme of Hg III independently. From the direction of the isotope shift in these lines (Fig. 4) it is clear that the big shifts belong to the upper levels; these upper levels can belong only to the configuration $5d^86s^2$ of Hg III or $5d^86s^2nx$ of Hg II, as can be seen from Table IV, where the approximate isotope shifts for different configurations are collected (configurations involving $5d^7$ are much less probable in the case of the excitation used, see footnote 15). The lower levels of the lines mentioned should have very small isotope shift (around zero) in the case of lines of type *A*, and in the case of lines type *B* these levels should belong to the same type of configuration, but should be perturbed (shift increased by around 115 units). In Hg III the lowest levels of the type, $5d^96p$ have been known for a long time and are well established. But trials revealed that no new differences of frequencies could be found among the lines of Fig. 4 which would be equal to the distance of the levels in question ($5d^96p$). The only two lines classified by Johns as transitions $5d^86s^2 \rightarrow 5d^96p$ in Hg III (λ3312 and 3557) emitted according to him from the same upper level (13_2), show a difference in behavior: the first one is fairly intense in a discharge in helium and has been reported by Paschen,[7] the second one is absent in presence of larger amounts of helium, and its intensity increases very rapidly with removal of the helium from the discharge tube (see the table in Naudé's work[11]). All the difficulties mentioned above seem to point out that the lines of Fig. 4 actually belong to Hg II. Their upper levels should belong to the configuration $5d^86s^2nx$.[15] Since transitions to the levels of the configuration $5d^{10}nx$ are forbidden (this being also the reason why they are not broadened by autoionization), their final levels should be of the type $5d^96pnx$. This would explain why all attempts to find a classification for these lines failed: Two till now unknown sets of levels in Hg II are involved. In order to extend the analysis of the spectrum of Hg II, to remove the uncertainty concerning the origin of these lines with high isotope shifts and concerning the level scheme of Hg III given by Johns, investigations of the Zeeman effect seem to be necessary. It should be very helpful to re-measure at the same time the wave-lengths of all the lines in question, since the data reported previously seem to be not very accurate.

TABLE IV. Electronic configurations and approximate isotope shifts (in 10^{-3} cm^{-1}) in mercury. The values in parenthesis are extrapolations.

Hg IV	$5d^76s^2$	(~1200)	$5d^86s$	(~500)	$5d^9$	(~0)
Hg III	$5d^76s^2nx$	(~1200)	$5d^86s\ nx$	(~500)	$5d^9nx$	~0
	$5d^86s^2$	~775	$5d^86s$	~350	$5d^{10}$	=0 assumed
Hg II	$5d^86s^2nx$	~775	$5d^86s\ nx$	~350	$5d^{10}nx$	~0
	$5d^96s^2$	~560	$5d^{10}6s$	~275		
Hg I	$5d^96s^2nx$	~560*	$5d^{10}6s\ nx$	~275		
	$5d^{10}6s^2$	~450				

* The isotope shift in such terms has not been investigated, the value given is a prediction.

It is a pleasure to me to take this opportunity to thank Professor C. Bialobrzeski in Warsaw for his great interest in this work.

[15] The excitation of these levels in the discharge tube proceeds partly by excitation of a $5d$ electron in a metastable Hg^+ ion ($5d^96s^2$), but the main process is the direct excitation of one $5d$ electron accompanied by the ejection of a second $5d$ electron from the neutral Hg atom. The results of W. Bleakney [Phys. Rev. **35**, 139 (1930)] seem to indicate that the probability of the first process for the probable average velocities of electrons in the low pressure discharge used is about 7 times bigger than for the second process. However, the low concentration of metastable ions makes the second process predominant. The excitation of the states $5d^76s^2nx$ of HgIII or $5d^76s^2$ of HgIV, to be of importance, requires electrons of considerably higher velocity which are probably present in this kind of discharge only in very small numbers.

Order in the Alloy Cu_3Au[1]

L. H. GERMER, F. E. HAWORTH, AND J. J. LANDER
Bell Telephone Laboratories, New York, New York

(Received March 25, 1942)

Electron diffraction by the transmission method has been used to investigate superstructure as produced in the alloy Cu_3Au by various heat treatments. Thin films of this composition, which have never been heated and are not thoroughly mixed, become homogenized and develop unmistakable order when heated at 169°C for 16 hours, but films heated only at lower temperatures for 16 hours do not yield certain evidence of order. Sharper superstructure rings are produced by films which have been annealed at higher temperatures, and from the evidence of the diffraction patterns we estimate that perfect order is developed by heating at 270°C for 16 hours. Diffraction patterns from films which have been quenched from temperatures above 400°C exhibit, in addition to rings of the disordered face-centered cubic structure, a very diffuse band inside the (111) ring. A similar diffuse diffraction feature is obtained from films while at various elevated temperatures up to 560°C. When an initially ordered specimen is heated to progressively higher temperatures, the originally sharp (100) and (110) superstructure rings becomes gradually broader and less well-defined, merging finally into a single diffuse band. Increase in breadth of the rings becomes noticeable first, for a film in equilibrium, at a temperature a little above 325°C. At about 370°C these rings have become very poorly resolved; but the resolution continues to become poorer, although at a much less rapid rate, up to 560°C which is the limit of our observations. There seems to be no sudden change in the diffraction pattern corresponding to the alleged Curie point of order.

ON account of its great sensitivity to small amounts of material the electron diffraction technique has been applied chiefly to problems which are not readily studied by means of x-rays; in most cases the relative slightness of the penetrating power of electrons has been essential to the investigation. We believe, however, that the limitation of electron diffraction to the study of surface phenomena only is not justified. It is one of the purposes of the work described in this paper to extend the field of usefulness of electron diffraction by applying it to material which has been studied for many years by means of x-rays.

The alloy Cu_3Au was chosen for this investigation because it has been studied for a great many years, because it presents problems still unsolved, because in the superlattice which is formed one can readily distinguish between the copper and gold atoms by their widely different scattering powers, and because the alloy is fairly resistant to corrosion. It seems to us probable that the methods of this research can be applied to other alloys and to mixtures of metal salts.

PREPARATION OF TEST SAMPLES

Test specimens of Cu_3Au for examination by the transmission method have been prepared in the form of films 300A or 400A in thickness. These are made by vaporizing an alloy of the correct composition upon a sheet of lucite, which is subsequently dissolved away in ethylene dichloride to leave the very thin metal film. This is caught across such a supporting slit as we often employ,[2] and is then ready for experimentation. It has been found that 400A alloy films are sturdy and easily handled, but that 300A films are very fragile. Most of the experiments reported here were made upon films 400A thick. (The pattern of Fig. 5 is the only one from a 300A film which is reproduced in this paper.)

The way in which films are prepared necessarily differs somewhat from that described earlier[2] because in the present experiments the films are to be heated and must, therefore, be freed from the supporting foil of plastic material. In order to accomplish this the metal is vaporized from a V-shaped tungsten ribbon upon a relatively thick sheet of lucite about 3 cm on a side, which is supported by a glass microscope slide or by wires at its edges and is located 30 cm above the tungsten ribbon. This composite sheet of lucite plus metal is later cut up into pieces 2 or 3 mm on a side, each of which, after dissolving the lucite, can be used in a single experiment or series of experiments. Lucite is used as support, rather than the Formvar of earlier experiments, because it was found that Formvar cannot be dissolved after metal has been vaporized upon it. The lucite films (thicker than 10^{-4} cm) are prepared from ethylene dichloride solution in the same way the very much thinner films of Formvar and Resoglaz were prepared. Although lucite is satisfactory for the purposes of

[1] Brief abstracts of parts of this work have been published; see L. H. Germer and F. E. Haworth, Phys. Rev. **56**, 212 (1939); **57**, 354 (1940); L. H. Germer, F. E. Haworth, and J. J. Lander, Phys. Rev. **61**, 93 (1942).

[2] L. H. Germer, Phys. Rev. **56**, 58–71 (1939), Fig. 1.

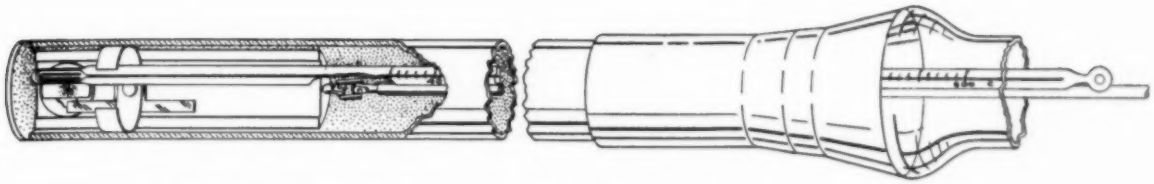

FIG. 1. Sketch of copper tube in which alloy films have been heat-treated in vacuum.

the present experiments, it has the one disadvantage of not being very resistant to heat, so that care has always been necessary to avoid rupturing or deforming the film during the vaporization process.

A further modification of earlier technique applies to the material of which the supporting slits are made. Because these are heated in the present experiments it was necessary to make them of molybdenum and to fasten the three parts together by welding, whereas in the earlier experiments the slits were made of a copper-beryllium alloy and the parts were soldered together.

Films of the composition Cu_3Au were made from an alloy containing 75.0 atomic percent copper supplied to us by Dr. F. C. Nix and prepared by him from Hilger spectroscopically standardized copper (H.S. brand) and Handy and Harman spectroscopic standard gold. Several films were prepared from this alloy, one by vaporizing 73 mg and the others by vaporizing 98 mg, in each case upon a lucite film at a distance $l=30$ cm. Thicknesses of these films are calculated (from the formula $t=0.45M/l^2\delta$, reference 2, page 59) to be 299A and 401A, respectively.

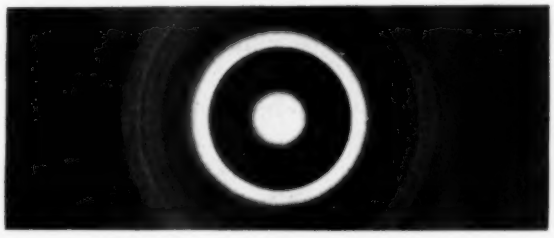

FIG. 2. Diffraction pattern from an unhomogenized 400A film, before heat treatment.

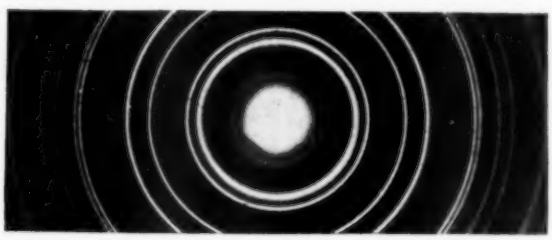

FIG. 3. Pattern from a film which has been heated in vacuum to 450°C and quenched from that temperature.

HEAT TREATED ALLOY FILMS

Alloy films have been heat treated in high vacuum in a glass tube about 45 cm long. The molybdenum slit holding the film is placed in this tube near its closed end, and a thermometer is located within the tube with its bulb close to the film. After the open end of the tube has been sealed to a diffusion pump and the tube has been exhausted, it is heated by a furnace which is placed over it. In some experiments we have wished to cool the alloy film very rapidly from a high temperature, and in these tests we have used the copper tube represented in the sketch of Fig. 1. This copper tube can be cooled very suddenly by removing the furnace and pouring water upon the tube. The slit, which supports the film, is pressed firmly against a copper block which in turn fits the inner wall of the tube closely and is held against it by springs. Thus good thermal contact is maintained between the film and the tube, and when the latter is cooled suddenly from a high temperature by means of water, the temperature of the film also is lowered very rapidly.

The diffraction patterns of Figs. 2 and 3 were produced by 400A films, the former by a film which had not been heated and the latter by an identical film after heat treatment. The pattern of Fig. 2 is made up of broad bands having sharp heavy edges, the bands being those of a face-centered cubic structure with inner and outer edges corresponding, respectively, to unit cells of the sizes of those of gold and of copper. It is clear that the film which produced the pattern of Fig. 2 was made up of randomly oriented crystals of gold and of copper and of alloys having various compositions intermediate between gold and copper. This result could have been predicted from casual examination of the film before removal of the lucite backing; in reflected light the side of the film adjacent to the

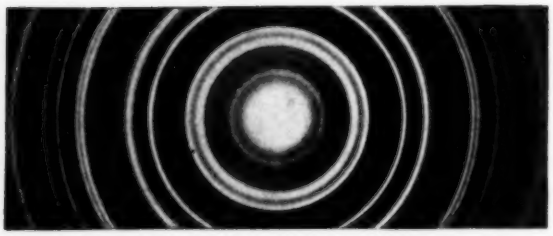

FIG. 4. Pattern from the same film after it had been heated for 16 hours at 194°C, showing imperfect order.

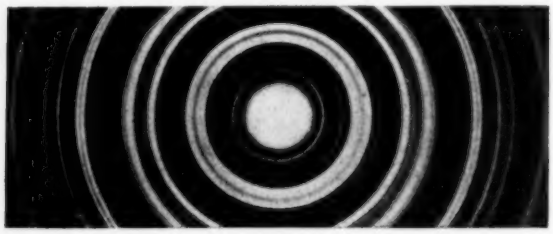

FIG. 5. Pattern from a 300A film in which the individual crystals had been almost perfectly ordered by annealing for 2 hours at 350°C and cooling rather slowly.

lucite had the appearance of slightly tarnished copper and the other side the color of gold.

The pattern of Fig. 3 was obtained from a film which had been heated in vacuum to 450°C and quenched from this temperature in the manner described above. There are on this pattern several extremely weak rings which are apparently due to a very small amount of a corrosion product or some foreign substance deposited upon the film during the heat treatment. If these are neglected, the estimated intensities and measured diameters of the 9 smallest rings are written down in the second and third columns of Table I. All of the sharp rings correspond to the Miller indices, given in the first column, appropriate to a face-centered cubic structure with edge of the unit cell equal, within the experimental error of the measurements, to the lattice constant of the alloy Cu_3Au. In addition to these there is a diffuse ring of diameter 12.3 mm. From ordered crystals of the alloy Cu_3Au, each of which can be thought of as a face-centered cubic arrangement in which gold atoms are located at the corners of a cubic array and copper atoms at the centers of the faces, superlattice diffraction rings will be produced at positions corresponding to mixed Miller indices (i.e., neither all odd nor all even). The diffuse ring of diameter 12.3 mm corresponds in position to (100) reflections from the ordered alloy, which according to theory should form the strongest of the superlattice rings.

If this diffuse ring in Fig. 3 is really made up of (100) reflections from Cu_3Au crystals, then the ordered arrangement of copper and gold atoms in these crystals, which the existence of these reflections implies, must either have existed at 450°C or have developed in the very short interval of time during which the alloy was being cooled from this temperature. In an attempt to distinguish between these possibilities, comparisons were made between diffraction patterns from films quenched at different rates, and from the temperatures 425° and 450°C. In all of these patterns the ring corresponding to (100) reflections is present and, as well as we can judge, its intensity relative to that of stronger rings is the same in all patterns. These observations suggest that the quenching rate was always sufficiently rapid to maintain the state which existed at the high temperature before quench. In order to clear up the matter it seemed, however, that we must obtain diffraction patterns from uncorroded films while they are actually at high temperature, above the alleged Curie point of order. Experiments in which this has been accomplished are described in a later section, and it is there established that the diffuse ring is actually characteristic of the condition of the alloy above the Curie point. It is interesting to point out that on some of the patterns from quenched films there seem to be indications of the superstructure rings (110), (210), and (211), but of this we cannot be certain. In a later section it is reported that some patterns obtained above 400°C seem also to show traces of these other rings having mixed indices.

TABLE I. Diffraction pattern of Cu_3Au alloy quenched from 450°C (Fig. 3).

Miller indices *hkl*	Estimated intensities	Diameters (mm) Measured	Diameters (mm) Calculated $(12.28)(h^2+k^2+l^2)^{-\frac{1}{2}}$
(100)	4	12.3	(12.3)
111	10	21.3	21.3
200	8	24.5	24.6
220	8	34.6	34.7
311	10	40.7	40.7
222	3	42.5	42.6
400	2	49.1	49.1
331	7	53.7	53.5
420	7	55.0	54.9

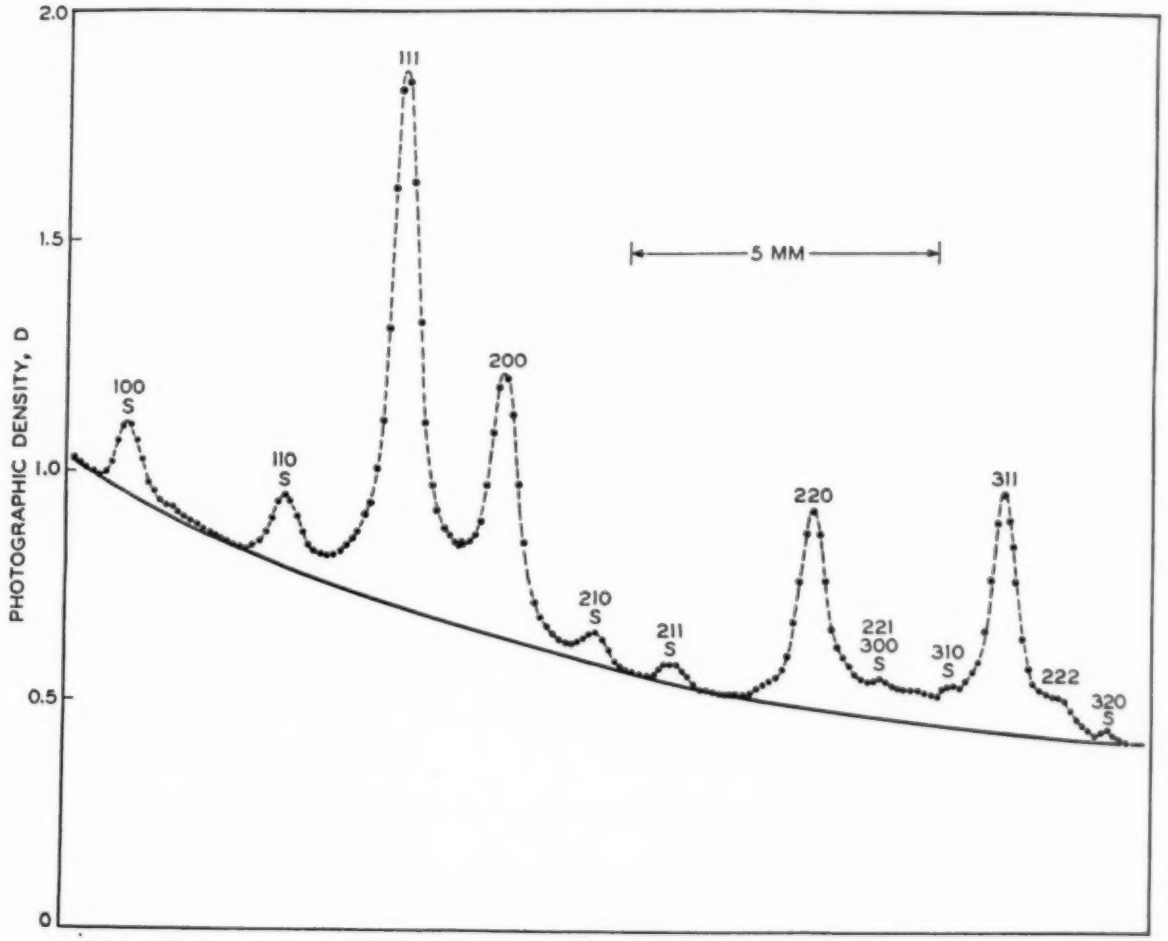

FIG. 6. Microphotometer curve of the pattern of a well-ordered film, prepared by heating for 16 hours at 270°C.

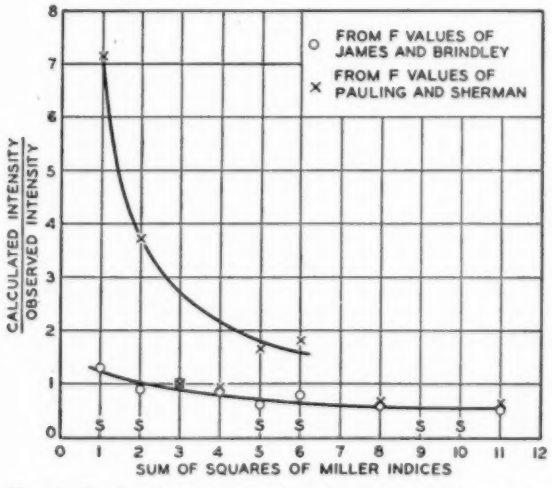
FROM F VALUES OF JAMES AND BRINDLEY
FROM F VALUES OF PAULING AND SHERMAN
CALCULATED INTENSITY / OBSERVED INTENSITY
SUM OF SQUARES OF MILLER INDICES
0 1 2 3 4 5 6 7 8 9 10 11 12
S S S S S S

FIG. 7. Ratio of the intensities of diffraction rings calculated for perfect order to the observed values obtained from Fig. 6, plotted against the sum of the squares of the Miller indices of the rings. Abscissas marked *S* are those of superstructure rings.

Whatever may be the interpretation of the ring of diameter 12.3 mm in Fig. 3 it is certain that the alloy which produced this pattern was at most only slightly ordered. To discover the effect of annealing upon this film it was heated in vacuum, in the glass tube described above, for 16 hours at 135°C and then for 16 hours at 194°C. After the first heating a diffraction pattern was produced which is not observably different from that of Fig. 3, but in the pattern of Fig. 4, obtained after heating at 194°C, the rings (100), (110), (210), and (211) are plainly seen. From this we conclude that annealing at 194°C produced ordering.

A higher degree of order, as evidenced by narrower superstructure rings, can be produced by heating at somewhat higher temperatures. For example, order which we judge to be almost

perfect was produced in a film by heating for 16 hours at 270°C, and in a different film by heating for 2 hours at 350°C and cooling rather slowly. A pattern from the latter film is reproduced as Fig. 5, and a microphotometer trace of a pattern from the former and data relating to this trace are given in Figs. 6 and 7 and in the second and third columns of Table II. (The pattern of Fig. 5 was much too heavily exposed to permit of microphotometer measurements of density at the maxima of its strongest rings, while the pattern from which Figs. 6 and 7 and Table II were obtained was too lightly exposed to reproduce well.)

The breadths of diffraction rings at half maximum, given in the second column of Table II, are the same within the error of measurements. This must be taken to indicate that the crystals which produced the diffraction pattern contained no out-of-phase domains, because the existence of more than one domain per crystal would certainly have caused the superstructure rings, marked S in the first column of Table II and on Figs. 6, 7, and 11, to be broader than the normal rings of the face-centered cubic structure. The crystal size C is about 60A as calculated from the half breadths by means of the Scherrer formula in the form $C=L\lambda/\Delta R$; here $L\lambda=2.3\times10^{-7}$ mm^2 and ΔR is the measured half breadth reduced by 0.2 mm to allow for primary beam size.

To get evidence as to whether or not order was perfect within the single domain of each crystal, we have compared the observed relative intensities of normal and superstructure rings with those calculated for perfect order. Measured intensities of the third column of Table II are simply the relative areas[3] of the peaks of Fig. 6, taking the area of the (111) peak as 10. The calculated intensities of the last two columns are proportional to values of $S^2p/(h^2+k^2+l^2)^3$ where p is the number of contributing planes, and $S=(Z-F)_{Au}+3(Z-F)_{Cu}$ for normal rings and $(Z-F)_{Au}-(Z-F)_{Cu}$ for superstructure rings. Here $(Z-F)_{Au}$ is the difference between the atomic number of gold and the x-ray structure factor, and $(Z-F)_{Cu}$ the corresponding difference for copper. Intensities have been calculated from values of F given by James and Brindley, column 4, and from values given by Pauling and Sherman, column 5[4]. In Fig. 7 is plotted the ratio of the calculated to the observed intensity for the two sets of values of the former. We are not concerned here with the fact that the points do not lie along a horizontal line, but only with a comparison of the points corresponding to superstructure rings with the points corresponding to normal rings. It is evident that all of the points fall on one curve when calculated from the structure factor values of James and Brindley, but the points for the superstructure rings and the normal rings fall on two different curves for the Pauling and Sherman values. We must conclude that if the former values of structure factor are correct the crystals are well ordered, whereas the order is very imperfect if the other set of values is right. It is, of course, true that one cannot draw from the experiments the two conclusions: (1) the crystals are perfectly ordered, and (2) the values of electron structure factor $(Z-F)$ of gold and of copper obtained from F

TABLE II. Diffraction pattern of well-ordered alloy.

Miller indices *hkl*	Breadths of diffraction rings at half max. (Fig. 6) (mm)	Relative intensities of rings		
		Measured (Fig. 6)	Calculated for perfect order: James and Brindley	Calculated for perfect order: Pauling and Sherman
100 *S*	0.50	1.0	1.3	7.1
110 *S*	0.60	1.1	1.0	4.1
111	0.58	10.0	10.0	10.0
200	0.62	5.0	4.3	4.6
210 *S*		0.67	0.41	1.1
211 *S*		0.39	0.30	0.70
220	0.55	3.4	2.0	2.3
221/300 *S*			0.19	0.30
310 *S*			0.12	0.18
311	0.54	3.7	1.9	2.4
222			0.53	0.67
320 *S*			0.08	0.09

[3] In earlier work [L. H. Germer and A. H. White, Phys. Rev. **60**, 447–454 (1941)] it was reported that calibration of an Eastman process plate showed that photographic density D and intensity I are related by $D=\text{const.}\ I^{1.2}$ for D in the range 0.05 to 1.3. For the present work a number of process plates, like those upon which the patterns reported here were recorded, were calibrated and it was found that the exponent in the equation connecting D and I is approximately 1.0 and not 1.2. Thus photographic density can be used for intensity directly.—The (111) peak of Fig. 6 extends considerably above the range $0.05<D<1.3$. Thus corrections should be applied in obtaining the intensity and the breadth at half maximum of the (111) ring from its peak in Fig. 6. No very great change in intensity or breadth is to be expected, however, and we have not made the corrections.

[4] R. W. James and G. W. Brindley, Phil. Mag. **12**, 81 (1932); L. Pauling and J. Sherman, Zeits. f. Krist. **81**, 1 (1932).

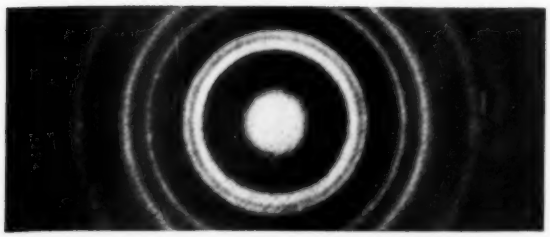

FIG. 8. Pattern from a film which had been heated for 16 hours at 148°C, without previous heat treatment.

values given by James and Brindley are correct (at least except perhaps for a common angle factor). One can, however, say that the data are consistent with such conclusions, and they seem altogether reasonable and likely. This view is supported by the fact that we have found superstructure rings of approximately the relative strengths of those of Figs. 5–7 from many different films, but stronger rings have never been obtained.

We pointed out above that a very considerable increase in order is produced in an initially homogenized and quenched film by heating for 16 hours at 194°C (see Fig. 4). We did not, however, intend to imply that this temperature is the lowest at which ordering goes on at an appreciable rate. Tests to discover this lowest temperature cannot readily be carried out upon quenched films because it appears that such films have initially a degree of order which is not inappreciable (see Fig. 3). We have modified the experimental procedure by heating new unhomogenized films, which are in the condition indicated by the pattern of Fig. 2, for considerable lengths of time at various low temperatures. After a great many such tests we find that all of the significant results which were obtained can be given by reporting four of the tests only. These four were made upon three newly prepared unhomogenized films which were heated for the first time, respectively, for 16 hours at temperatures of 127, 148, and 160°C; the third film was then heated for a further period of 16 hours at 169°C.

The film which had been heated at 127°C gave a diffraction pattern characteristic of a face-centered cubic structure with no certain indication of superstructure as evidenced by rings having mixed indices. All of the rings are rather broad and those of large diameter are broader than the smaller rings. From the increase of breadth with diameter we conclude that not all of the crystals in the film had unit cells of exactly the same size, and that therefore the film was *not* perfectly homogenized; the crystals were furthermore very small.

The pattern from the film heated at 148°C, reproduced as Fig. 8, appears to be very similar to that from the film heated at 127°C, but differs from it in the fact that, as far as we can detect, all rings have about the same widths; again there is no clear indication of superstructure rings. We conclude that the heat treatment which this film received was adequate to produce almost perfect mixing of the copper and gold atoms but did not bring about observable ordering.

Patterns from the film heated at 160°C appear qualitatively like that of Fig. 8, but there is now an indication of superstructure rings of which we cannot, however, be quite sure. These rings are first observable with certainty after heating at 169°C, but they are still much weaker than in the pattern of Fig. 4 and would not appear clearly in a reproduction.

Conclusions drawn from these four tests are summarized in the first four lines of Table III. The estimates of crystal size were obtained in the usual way from half-breadths of diffraction rings as determined from microphotometer traces. By designating mixing as "complete" we mean only that there was no clear evidence of increase of breadth of diffraction rings with diameter, and by "none" for ordering we mean that there was no sure evidence of the presence of superstructure rings. In some cases there were weak rings caused by corrosion or some foreign substance, and these decreased the delicacy of detection of possible extremely weak rings with mixed indices.

TABLE III. Various heat treatments of unmixed films.

Heat treatment Hours	Temp. °C	Mixing	Crystal size A	Ordering	Fig.	Calc. values from data of Jost $D\times10^{18}$ (cm²/sec.)	$\frac{h}{4(Dt)^{\frac{1}{2}}}$
16	127	Incomplete	25	None	—	1.2	1.2
16	148	Complete	—	None	8	7.	0.51
16	160	"	25	Uncertain	—	15.	0.35
16	160	"	25	Slight	—		
16	169						
16	194	"	—	Imperfect	4		
Quenched from 450°C		"	—	Uncertain	3		
16	270	"	60	Perfect	6, 7		
Slow cooled from 350°C		"	—	Perfect	5		

Giving most of the data of Table III only in qualitative form seems to be unavoidable. At the present time we do not know how to get a quantitative measure of degree of ordering from data obtained from broad superstructure rings. It seems, furthermore, to be quite impossible to obtain reliable estimates of diffusion coefficients from our experiments upon mixing in unhomogenized films, because the diffusion coefficient of copper into gold must change as the amount of copper in the gold increases and we obtain interpretable data only when this amount is large. We have, however, made some very crude comparisons of the observations given here with deductions from published data on diffusion rates.

To begin with, it is interesting to compare our observations with those made by Eisenhut and Kaupp[5] upon the mixing of gold and copper at temperatures from 100 to 300°C. They have expressed the results of some of their tests in the form of the expression $Z=10^{15.0}\exp(-T/16.0)$, where Z is the time in minutes at temperature T°K required to produce "complete mixing" in a film about 300A thick composed initially of a layer of copper lying upon a layer of gold in the atomic proportions of 70 to 30. In our experiments the mixing seems to be completed in 16 hours at a temperature of 148°C. According to their equation heat treatment for 16 hours ($Z=960$ min.) is just sufficient to give complete mixing at the temperature of 170°C and complete mixing at 148°C would occur in 64 hours. In view of the fact that our films differ from those of Eisenhut and Kaupp in being partially homogenized at the start (see the pattern of Fig. 2), as well as slightly thicker, this appears to be fairly good agreement.

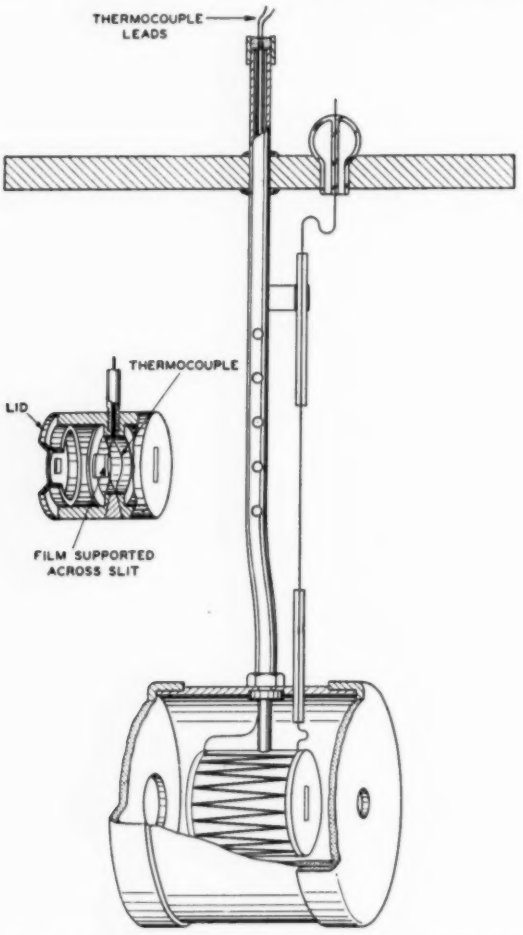

FIG. 9. Sketch of furnace in which alloy films have been heat-treated within the diffraction camera.

Other experiments which have been carried out upon the diffusion of copper into gold have been performed at higher temperatures and their results must be extrapolated before they can be compared with those reported here. Diffusion coefficients D vary with temperature in general according to the relation $D=D_0\exp(-Q/RT)$. For the diffusion of copper into gold in the range 301 to 616°C Jost[6] has found $D_0=91$ cm²/day ($=1.05\times10^{-3}$ cm²/sec.) and $Q=27{,}400$ calories/mole. For copper diffusing into a copper-gold alloy containing 10 weight percent of copper ($=31$ atomic percent) he finds the same value for Q and a value of D_0 smaller by a factor a little less than 2, which probably constitutes agreement almost within experimental error. The diffusion rate must, however, decrease considerably as mixing approaches completion, because self-diffusion rates of copper calculated from the data of Steigman, Shockley, and Nix[7] are very much lower than rates for the diffusion of copper into gold determined from the above constants. We have neglected this uncertainty and have compared our observations with deductions from values of D calculated from these constants. The calculated values of D for the temperatures 127, 148, and 160°C are given in next to the last column of Table III. In the last column are corresponding values of the function $h/4(Dt)^{\frac{1}{2}}$, where $t=57{,}600$ sec. (the duration of our heat treatments), and $h=1.3\times10^{-6}$ cm, the thickness which would be occupied by gold in one of our 400A films if the copper and gold atoms were completely segregated. Jost has plotted, for $h/4(Dt)^{\frac{1}{2}}$ equal to 1.0, 0.7, and 0.5, the percentage concentration of gold atoms throughout a layer of thickness h consisting initially of gold bounded on one side by copper of infinite thickness; and he has stated that mixing which would be judged from electron diffraction photographs to be complete would occur in finite layers for $h/4(Dt)^{\frac{1}{2}}$ equal to about 0.1. This latter value, $h/4(Dt)^{\frac{1}{2}}=0.1$ corresponds, for $t=57{,}600$ sec., $h=1.3\times10^{-6}$ cm, and the values of D_0 and Q reported by Jost, to $T=191$°C. According to his curves, the last trace of gold which is completely copper-free disappears at $h/4(Dt)^{\frac{1}{2}}=1.0$, and mixing is far ad-

[5] O. Eisenhut and E. Kaupp, Zeits. f. Elektrochemie **37**, 466 (1931).

[6] W. Jost, Zeits. f. physik. Chemie **B16**, 123 (1932); **B21**, 158 (1933).

[7] J. Steigman, W. Shockley, and F. C. Nix, Phys. Rev. **56**, 13 (1939).

vanced when this quantity equals 0.5. Our estimate that mixing is complete in the pattern of Fig. 8 ($h/4(Dt)^{\frac{1}{2}}=0.51$, see Table III) indicates more rapid mixing than predicted from Jost's data. On the other hand, our estimate of when mixing is complete is certainly very poor, and mixing is, furthermore, quite far advanced at the *beginning* of our experiments. It thus seems to us that our observations cannot be considered as disagreeing with those of Jost.

ALLOY FILMS AT ELEVATED TEMPERATURES

In the above section, we pointed out the desirability of obtaining diffraction patterns from alloy films at elevated temperatures, particularly above the alleged Curie point of order. To accomplish this a furnace has been designed which can be operated inside the diffraction camera. This furnace is a solid cylinder of copper 19 mm long and 20 mm in diameter in which there is an opening large enough to hold a molybdenum slit with its supported alloy film, as shown by the cross-sectional insert in Fig. 9. A heavy copper lid closes the furnace, and openings in the back and in the lid enable the primary electron beam of the diffraction camera to go through the alloy film and the resulting diffraction pattern to emerge into the main volume of the camera. The furnace is heated electrically by current through nichrome wire wound upon mica on the outside of the copper cylinder, and the winding as indicated in Fig. 9 is arranged to produce only a very slight magnetic field. An aluminum shield about the furnace decreases the heat lost by radiation, and the conduction loss is low because the only support is a tube of stainless steel which is long and thin. High over-all efficiency is indicated by the fact that 20 watts dissipated in the nichrome winding maintains the furnace at about 700°C. It is to the simplicity and convenience of the arrangement of this furnace within the diffraction camera that much of the success of the present technique must be attributed.

The temperature is determined by means of an iron-constantan thermocouple and a high resistance millivoltmeter. The thermocouple junction is pressed into a hole in the furnace wall by a copper plug, and the leads are taken out through the stainless steel supporting tube. The thermocouple was calibrated and found to be correct within the precision of the measurements which was about 1°C, and the furnace wall is so heavy

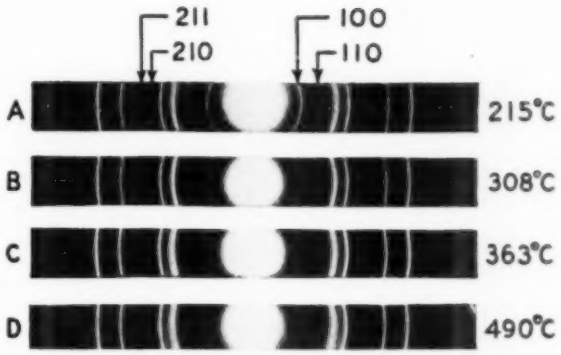

FIG. 10. Diffraction patterns at various elevated temperatures from films which had been initially ordered.

that no appreciable temperature gradient can exist in it. In order that the thermocouple shall register the temperature of the alloy film correctly, it is necessary that at equilibrium the film and wall temperatures be the same, and that sufficient time be allowed for equilibrium to be established.

Because the ratio of film width to film thickness is large (about 10^3), radiation may be more important than conduction in determining the temperature at its center; thus the openings in the furnace may cause the temperature of the film to be appreciably below that of the furnace wall, and a similar effect will be produced by the lid if its temperature is below that of the wall. A calculation of the magnitude of this error has been made from dimensions of the furnace and direct measurement of the amount δ by which the lid temperature is below T°K the temperature of the wall. On the assumption that the film is heated solely by radiation, it is easy to show that the amount ΔT by which its temperature is below T will be given by $\Delta T=C_1T+C_2\delta$, when T is much above room temperature and large in comparison with δ and ΔT. If the film were in the form of a sphere located at the center of the furnace, the constants C_1 and C_2 would have the values $\omega_1/4=0.0035$ and $\omega_2=0.20$, respectively, where ω_1 and ω_2 are the fractions of solid angle 4π subtended at the specimen, respectively, by the openings and by the solid part of the lid. For a flat film radiating according to the cosine law, these constants can be expressed as trigonometric functions of furnace dimensions, and have the numerical value $C_1=0.0070$ and $C_2=0.31$. In order to determine δ, a second thermocouple was pressed firmly against the lid by a copper plug driven into the opening. Simultaneous readings upon the two thermocouples, when the furnace was heated in the normal manner, gave $\delta=7$°C at $T=575$°K and $\delta=12$° at $T=830$K. From the equation $\Delta T=0.0070T+0.31\delta$ we find $\Delta T=6.2$° at 575°K and $\Delta T=9.5$° at 830°K. These values are upper limits, because in calculating them heating of the film by conduction has been neglected. In all of the work reported below, the temperatures given are those obtained from the thermocouple in the wall of the furnace, without correction;

it is realized that in many cases the film temperature is probably lower by as much as 5° and perhaps slightly more at high temperatures.

Estimates have been made of upper limits of the time required to bring the alloy film to temperature equilibrium with the furnace. In many experiments the temperature was changed at a rate of about one degree per minute. This rate is sufficiently low to maintain the film in temperature equilibrium. Whenever the heating or cooling rate was much greater than this, diffraction patterns were obtained only after the temperature had been maintained constant long enough for equilibrium to be established. It is believed that for all observations reported below the film and furnace were in thermal equilibrium, although as estimated above the film temperature was in many cases lower than that given here by as much as 5°.

Representative diffraction patterns from films at elevated temperatures are reproduced in Fig. 10. The first film had been heated to 490°C and then cooled in 55 minutes to the temperature of 215°C at which the pattern of Fig. 10A was obtained. The strength of the superstructure rings, the indices of the first four of which are given on the figure, indicates clearly that the crystals in the film were well ordered; but the superstructure rings are a little less sharp than the normal rings, and from visual inspection it appears that relative to the latter they are less intense in Fig. 10A than in Fig. 5. Although from microphotometer curves it was discovered that the apparent lower relative intensity of the superstructure rings is largely subjective, the increased widths are real, and thus it seems quite certain that order was not perfect in the film which produced the pattern of Fig. 10A. The imperfection of the order is undoubtedly to be attributed to the high rate of cooling. Somewhat sharper rings have been obtained from films cooled more slowly, but very low cooling rates are inconvenient in the furnace of Fig. 9 and superstructure rings indicative of apparently perfect order have never been obtained as a result of heat treatment in this furnace.

A film which had been ordered to about the same degree as that represented by the pattern of Fig. 10A was subsequently heated at the rapid rate of 140° per hour to 490°C and patterns were obtained from it at various temperatures. Three of these are reproduced as Figs. 10B, 10C, and 10D. From visual comparison of Figs. 10A and 10B one draws the conclusion, confirmed by microphotometer curves, that the superstructure rings in these two patterns are quite similar, and that therefore the thermal agitation of the atoms at 308°C was not sufficient either to decrease appreciably the slightly imperfect order obtaining initially or to permit a higher degree of order to be established in the short time involved. It is clear, however, from Fig. 10C that at 363°C the superstructure rings are markedly broader and apparently less intense, and evidence of superstructure is still poorer in the pattern of Fig. 10D obtained at 490°C.

From the examination of some hundreds of patterns, we have concluded that superstructure rings first appear considerably broadened between 325° and 350°C. On further heating the broadness increases up to about 370°C, but patterns obtained above this latter temperature exhibit only a slight and very gradual further change up to 560°C, which is the limit of our observations. On patterns produced by films at these high temperatures, one can always see a fuzzy ring located apparently between the positions of the (100) and the (110) superstructure rings. (Compare Figs. 10A and 10D.) On some patterns taken at about 400°C we have thought that we could see this fuzzy ring resolved into two rings and that we could detect other diffuse bands at the positions of (210) and (211) superstructure rings. It is interesting in this connection to compare the patterns of Figs. 3 and 10D. On the latter the diffuse ring is apparently intermediate between the positions of (100) and (110) rings, whereas in the former it agrees with the (100) ring (see Table I). On the original plate of the pattern of Fig. 3 there is a weak indication of another ring at the (110) position. The difference between the patterns of Figs. 3 and 10D seems to be attributable to the fact that the quenched film (Fig. 3) was slightly more highly ordered than the film at 490°C (Fig. 10D).

The possibility of diffraction evidence for short range order above the critical temperature has been explicitly predicted by Peierls and implicitly by Bethe[8] and others. Peierls says, "Above the critical temperature the x-ray pattern will, accordingly, not show any superlattice lines but in their place there might be very diffuse maxima of the continuous scattering, just as the

[8] R. Peierls, Proc. Roy. Soc. **A154**, 207 (1936); H. A. Bethe, Proc. Roy. Soc. **A150**, 552 (1935).

diffuse maxima in the scattering of liquids are an indication of the local ordering persisting above the melting point." We believe that the observation of the diffuse inner ring of Fig. 10D constitutes a verification of this prediction. Before this view can be accepted, however, it is necessary to rule out the possibility that this feature may be caused by corrosion products formed upon heating in the diffraction camera, and to show that the feature is not produced by alloys which do not form superstructures or by pure metals.

That the diffuse ring is not produced by pure metals is proved by many patterns which we have obtained from copper films and from gold films at various elevated temperatures. Patterns have also been obtained at temperatures up to 500°C from many alloy films of compositions corresponding to $CuAu_3$ and to CuAu. The patterns from $CuAu_3$ films, obtained after preliminary heating to produce thorough mixing, represent face-centered cubic crystals entirely without superstructure; there is no trace of such a diffuse ring as that of Fig. 10D. At temperatures up to 385°C the films of CuAu give patterns corresponding to ordered structures, the type of which depends upon the preceding heat treatment, but remarkably enough CuAu films above 400°C show no evidence of order; patterns from films above 400°C consist of the rings of a face-centered cubic structure only, with no additional rings and no trace of a fuzzy ring similar to that from Cu_3Au.

The evidence that the diffuse ring from Cu_3Au is not caused by corrosion is threefold. In the first place, the pressure of residual gas in the diffraction camera was many times lower when the patterns of Fig. 10 were produced than it was when patterns were produced which exhibited obvious evidence of corrosion. Furthermore, at these low pressures (1 to 5×10^{-5} mm Hg) the residual gas in the camera was known to be reducing. An unmixed alloy film always shows visual evidence of corrosion and on a diffraction pattern from such a film (see Fig. 2) one can often see weak rings which can be identified with Cu_2O; these rings caused by oxide disappear completely upon heating the film, which must be attributed to reduction of the oxide by the gold and the residual gases.

Probably the best evidence that the diffuse ring is caused by order and not by corrosion products is obtained from critical examination of a series of patterns from an initially ordered film as it is heated gradually to high temperature and then gradually cooled. These patterns exhibit a progressive change of the sharp (100) and (110) superstructure rings at low temperature into the single diffuse ring at high temperature, and a gradual reappearance of the sharp rings as the film is cooled, the pattern at the end of the experiment being identical with that at the beginning. Comparison of these patterns can best be made from their microphometer curves, and a representative set of such curves for *increasing* temperature is reproduced in Fig. 11. All of the curves, except that at 560°C which came from a second experiment, are from patterns from a film whose temperature was increasing at the rate of 69 degrees per hour. The abscissas are radii of the patterns in millimeters, and ordinates are proportional to photographic densities except near the (111) diffraction maximum where the photographic plate was considerably over-exposed. To facilitate comparison, the curves are plotted at equal intervals, one above the other, and the vertical scales are so adjusted that the difference between the background curve at the left and right of the figure is the same for all the curves. This adjustment of the scales of ordinates merely compensates for the variation of density of the original diffraction patterns, and one expects that the height of the (200) diffraction peak above the background will then be the same for all the curves. The solid lines for the (200) peaks have been arbitrarily drawn to have the same height, and the goodness of fit of the experimental points is thus a measure of the reliability of this density correction. Of the (111) peaks one only has been plotted on the figure, in order to avoid confusion.

Diffraction patterns from films which were being *cooled* progressively from high temperature have yielded microphotometer curves at various temperatures which are substantially identical with those at the same temperatures in Fig. 11. This observation proves that all of these curves are characteristic of equilibrium conditions in the film, except perhaps those at 247, 289, and

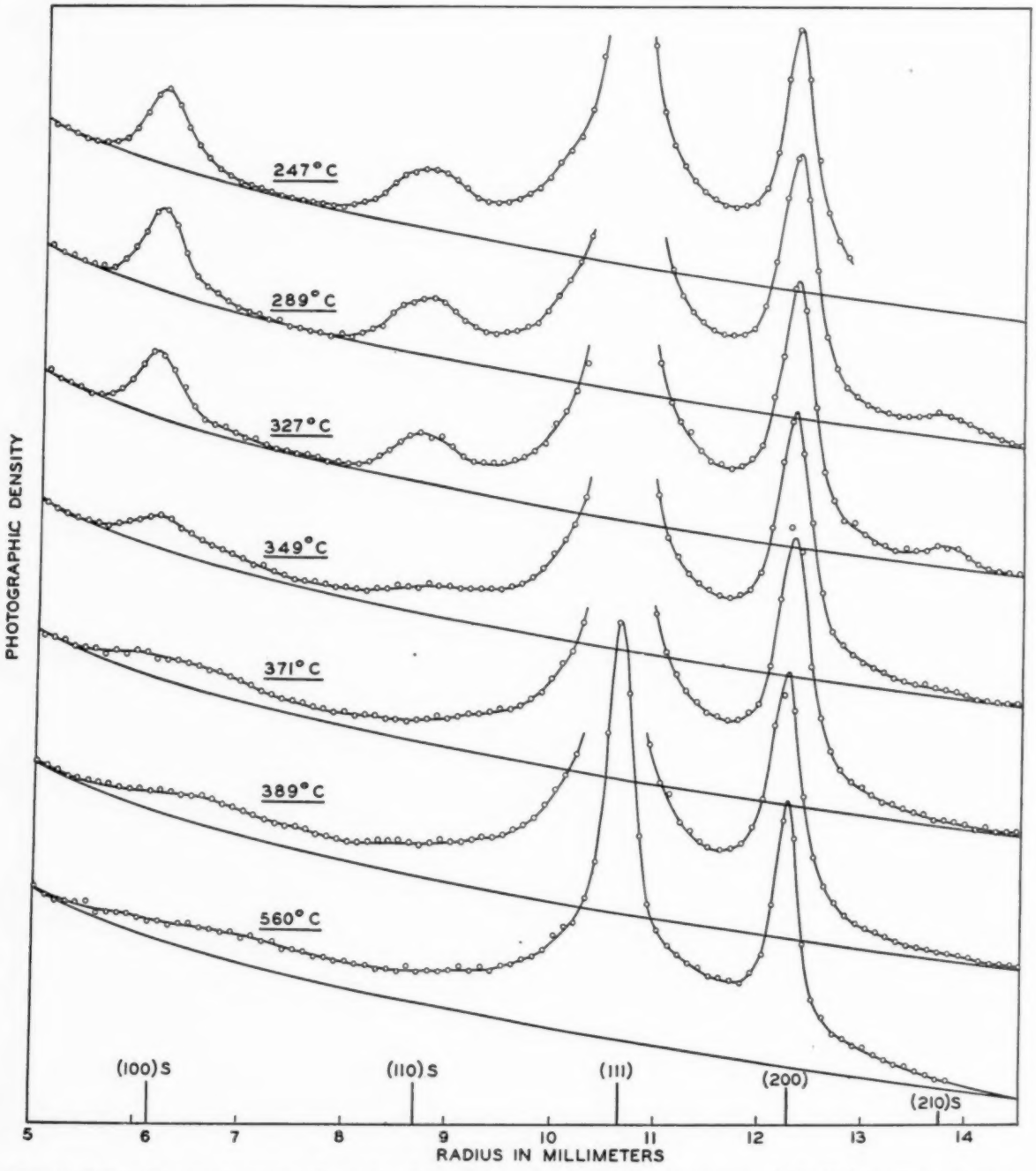

FIG. 11. Microphotometer curves of a series of diffraction patterns obtained at progressively higher temperatures.

327°C because the film was not perfectly ordered at the start of the experiment.

The curves of Fig. 11 illustrate clearly the statements made earlier in regard to changes in the superstructure rings as a film is heated. There is no obvious alteration in the (100) and (110) peaks in the microphotometer trace obtained at 327°C, but a marked change in the film had occurred at 349°, and a still further change at 371°; above 371° the (100) and (110) rings merge still further as the temperature is increased but the change is extremely gradual. It should be emphasized that from these curves one concludes that there is no large change in

order at any critical temperature, such as the alleged Curie point of order.

We have estimated the combined intensity of the (100) and (110) rings at different temperatures by obtaining the areas above the background curve of the corresponding segments of the curves of Fig. 11, after estimating the shape of the lower part of the (111) peak as well as we can. The values obtained are given in arbitrary units in the second column of Table IV. We think that the observed variation is probably attributable to experimental error, and that there is thus no clear indication of any change with temperature of the combined intensity of these two superstructure rings.

In the third column of Table IV are values of ΔR for the (100) peaks of Fig. 11, this quantity being defined in the present case as 0.2 mm less than the quotient of the area of the (100) peak and its height. (The subtraction of 0.2 mm is meant to correct roughly for the primary beam size.) The precision of ΔR is low for the 389° curve and very low for the 560° curve. Nevertheless this set of values of ΔR gives as good a quantitative indication as we have of the change of breadth of superstructure rings with temperature. Sykes and Jones[9] have calculated the mean size of domain in an ordered alloy from the breadth of superstructure rings by means of the Scherrer formula. If this procedure is correct, the mean sizes of domains at the various temperatures of Fig. 11 are given in the last column of Table IV. One expects that above the critical temperature order will extend scarcely beyond nearest neighbors and, as the two values of the last column of Table IV which were obtained above the critical temperature are of the order of 10A, these numbers of the last column are not unreasonable for mean domain size.

DISCUSSION

Sykes and Jones[9] have evidence from specific heat measurements that ordering in Cu_3Au begins to occur in a disordered specimen at temperatures below even 100°C, and Nix and MacNair[10] have concluded from dilatometer measurements that this alloy commences to order at a temperature somewhat below 200°C. Nevertheless, no direct diffraction proof of the production of order at these low temperatures has been obtained heretofore. We have observed that the ordering process in Cu_3Au goes on at an appreciable rate at a temperature as low as 169°C, and this must be taken as confirmation of the correctness of the interpretations given to the observations of Sykes and Jones, and of Nix and MacNair.

It is not entirely clear why x-ray evidence of ordering in Cu_3Au has been obtained only at temperatures above 320°C.[9] It is quite true that the superstructure rings on the pattern from the film which was heated at 169° in our experiments were more diffuse in angular measure relative to the wave-length than any rings which have been reported on x-ray patterns, and perhaps correspondingly diffuse rings on x-ray patterns could never be detected. This does not, however, explain the fact that we obtain diffraction evidence of *perfect* order after heating at a temperature (270°C, Fig. 6) much below that required to give the first x-ray indication of order. We are convinced that, if an x-ray test were made of one of our well-ordered films, it would give a result agreeing with the electron test. The conspicuous difference between samples tested by x-ray and by electrons lies in the mean crystal size, and we believe that it is to the smaller average size of crystal that we must attribute, in a considerable measure, the ease of determination of the beginning of the ordering process by means of electron diffraction. This is not, however, to be taken as suggesting an adequate understanding of the failure to obtain x-ray evidence of order in large specimens.

We feel that the difference between the elec-

TABLE IV. Superstructure rings at elevated temperature.

Film temp. (°C)	Combined intensity of (100) and (110) rings	ΔR for (100) ring (mm)	$L\lambda/\Delta R$ for (100) ring (A)
247	100	0.61	38
289	92	0.58	40
327	76	0.62	37
349	70	1.07	21
371	82	1.81	13
389	103	2.0	12
560	101	2.1	11

[9] C. Sykes and F. W. Jones, Proc. Roy. Soc. **A157**, 213 (1936).
[10] F. C. Nix and D. MacNair, Phys. Rev. **60**, 320 (1941).

tron diffraction patterns obtained at high temperatures from Cu_3Au and from CuAu is remarkable, and deserves emphasis and attention. Both are patterns of face-centered cubic structures; but, whereas the pattern from Cu_3Au exhibits a diffuse inner ring or rings due to vestigial order, there is no discernible trace whatever of such indication of order on patterns from CuAu films above 400°C. We believe that the difference may be fundamentally important, and certainly should be taken into account in any theory of the ordering process.

MAY 1 AND 15, 1942 PHYSICAL REVIEW VOLUME 61

The Optical Dispersion of Copper and Beryllium

M. P. GIVENS
Department of Physics, Cornell University, Ithaca, New York
(Received February 17, 1942)

The optical constants of copper and beryllium have been measured over a wave-length range from 2200A to 9800A. The observations were made by examining the state of polarization of light after reflection from a plane surface of the metal, the incident light having been linearly polarized. The surfaces were formed on a glass backing by evaporation. The absorption band of copper usually found in the neighborhood of 5000A was not found; copper oxide is believed to have been the source of that band. Positive values of the dielectric constant were also found. In the beryllium spectrum a strong absorption band was found near 3000A.

THE quantum mechanical development of a theory of solids has produced a new interest in the optical properties of metals, since a study of these properties provides some experimental evidence of the width of the conduction band and the position, widths, and density of states for the unoccupied bands immediately above the conduction band. This is one of the comparatively few direct checks on the theory of solids.

According to the theoretical picture,[1] the energy levels of the atom spread into bands when the atoms are brought together to form a solid. The low energy or "inner" levels are relatively unaffected, remaining quite narrow and not appreciably changed in position. For the levels containing the valence electrons and for the unoccupied levels of higher energy the situation is quite different. The level will, in the solid, become a band of levels, usually a few volts in width and containing as many "levels" as there are atoms in the solid. The bands may remain separate and distinct or may spread out to such an extent as to overlap.

If the electrons in the solid completely fill the valence band, and if the next band of higher energy is well separated from the valence band, then the solid is an insulator. When the valence band is only partly filled or overlaps an empty band, then the solid is a conductor allowing a net transfer of charge by some of the electrons moving from their equilibrium states into states of slightly higher energy. Under the influence of an alternating electric field, such as a light beam of low frequency, energy may be absorbed from the beam by raising the electron into a higher energy level in its own band. Such a process would give rise to an absorption rate which changes regularly with increasing frequency until the frequency is reached at which the electron is raised to the top of the conduction band. If the next band is well separated from the first, there will then be a portion of the spectrum for which the solid does not absorb energy. For incident light of frequency ν sufficiently great for a quantum $h\nu$ to move an electron from the valence band into the band above, there will exist the so-called anomalous absorption. Overlapping of the energy bands removes the transparent region of the spectrum and the regular and anomalous absorptions also

[1] For a general discussion of the theory see N. Sommerfeld and H. A. Bethe, *Handbuch der Physik* (1933), volume 24, part 2 or F. Seitz, *Modern Theory of Solids* (McGraw-Hill, 1940).

overlap. For still higher frequencies electrons may be raised from the inner or "x-ray" levels to unoccupied portions of the valence band or to higher bands; such frequencies are beyond the range of this work. Selection rules also influence the absorption.

Classical electrodynamics may be employed as a tool to evaluate, in terms of measurable quantities, the constants which a quantitative study of the theory would predict. The quantities are the conductivity σ and the dielectric constant ϵ. The quantities are related to the measurable optical constants n_0 and k_0 by means of the equations

$$\sigma = n_0 k_0 \nu,$$
$$\epsilon = n_0^2 - k_0^2,$$

where ν is the frequency.

There are two essentially different methods of measuring the optical properties of metals with reflected light. The first of these two methods requires the measurements of the relative phase shift Δ between the components of the light for which the electric vector is parallel to and perpendicular to the plane of incidence, and also the ratio of the reflectivities of these two components at some known angle of incidence ϕ. The ratio of the reflectivities is usually denoted as $\tan \psi \equiv R_p/R_n$, where R_p is the reflectivity for the component having its electric vector parallel to the plane of incidence, and R_n is for the perpendicular component. If the incident light is linearly polarized at azimuth 45°, then ψ represents the azimuth of the reflected light after the phase shift Δ has been compensated by a Babinet compensator or its equivalent. From the quantities Δ, ψ, and ϕ, the optical constants may be computed by simple equations.

The other method consists in finding R_p and R_n independently of each other at known angles of incidence. The relative phase shift is not necessary, but the difficulties of measuring absolute reflectivity compensate for this. An additional disadvantage of this method is the fact that there is no convenient calculating formula giving the optical constants as functions of the measured quantities, but the constants are contained implicitly in expressions giving the measured quantities. Also this method is more affected than the other by the surface condition of the metal.

The first method was used for this work and except for a few changes the apparatus is that designed by Voigt[2] and used by Minor[3] and others to study the optical properties of metals. The apparatus (Fig. 1) will be described briefly and the changes from Minor's apparatus will be pointed out. By means of a quartz lens L_1 an image of the source 0 was formed on the entrance slit of the monochromator. The exit slit of the monochromator was removed and this instrument so placed that the image formed at the customary position of the exit slit was formed on S, the entrance slit of the main polarograph. After passing the slit S the light was formed into a parallel beam by the quartz lens L and is linearly polarized by means of N_1, an air-spaced polarizing prism having its faces normal to the path of the light; this prism was mounted so that its azimuth could be determined by a vernier with a least count of 0.1°. The light is then reflected by the metal surface xx_1 (which is so

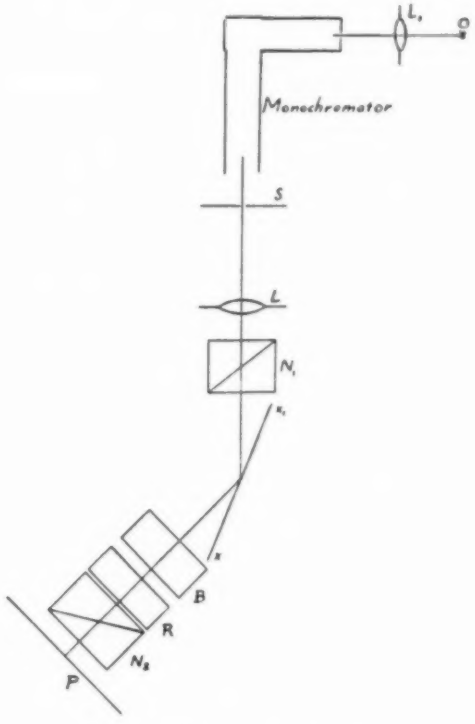

FIG. 1. Diagram of apparatus.

[2] W. Voigt, Phys. Zeits. **2**, 303 (1901).
[3] R. S. Minor, Ann. d. Physik **10**, 581 (1903).

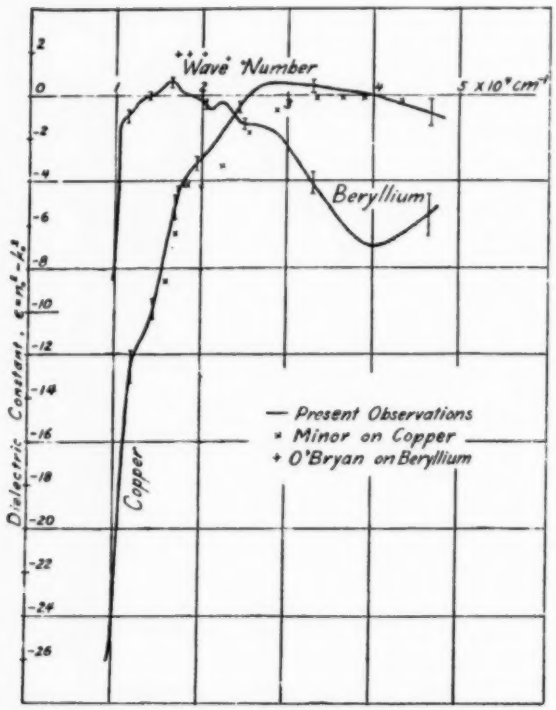

FIG. 2. Dielectric constant of copper and beryllium.

placed as to contain the axis of the polarograph) and enters the analyzing system. The analyzing system is similar to that designed by Voigt, the light first passes through a Babinet compensator (B) with its wedge edges horizontal. Next it passes through a pair of rotary wedges (R) having their wedge edges vertical; this pair of wedges is cut so that the path of the light is along the optic axis of the quartz, one of the pair being of right-handed quartz and the other of left-handed quartz. The two wedges are put together to form a parallel plate which rotates the plane of polarization by an amount which is a linear function of the distance across the plate. After passing the rotary wedges the light passed through an analyzing prism (N_2) similar in its construction to the polarizer N_1 except that the least count of the vernier for N_2 was 1′. The light then falls on a photographic plate P or a ground glass viewing screen to form a pattern of dark spots on a light background. The positions of the spots provide the necessary information about the relative phase and azimuth of the reflected light. The positions of the spots along a horizontal direction is a linear function of the restored azimuth of the polarized light, there being one spot every 180°. The positions of spots in alternate rows correspond to complementary angles so that the zero position and thus the azimuth of the light may be determined without the use of any reference plate. The positions of the spots along a vertical direction is a linear function of the phase difference, there being one spot every 360°. In this case a reference plate must be used. Immediately in front of the plate is a set of cross wires which cast shadows on the photographic plate, the shadows serving as reference lines when the plates are measured. The system employed a beam 2 cm in diameter. A telescope containing a Gauss eyepiece was mounted behind the photographic plate and by removing the plate holder this telescope could be used to line up the apparatus, or determine the angle of reflection. The whole analyzing system was mounted on one arm of the polarograph so that its position could be determined to 20″.

In Minor's apparatus a camera was used to photograph the pattern of spots. The camera, containing a pair of simple quartz lenses, was focused on the cross wires which in his work were placed between the B and R wedge systems. According to Minor,[4] the camera, when used at unit magnification, produced only negligible distortions. The distortions produced by a similar arrangement in this apparatus were not considered neglible and the camera was discarded in favor of this simpler arrangement which records a "shadow picture" of the wedge system. The cross wires were then moved back to be as close as possible to the photographic plate so they would cast a more distinct shadow. Although this method removes the distortions in the camera, it requires parallel light from a very small source and not the so-called parallel light which emerges from a collimator with a slit source. A pin hole was, therefore, indicated and some loss in intensity results. A good pattern could be obtained with a pin hole as large as 2 mm in diameter, but such an opening admitted too large a spectral range. In the final arrangement a slit 2 mm long and of adjustable width was used.

The apparatus was put into adjustment according to the same method described by Minor,[5] except that the zero position of the analyzing

[4] R. S. Minor, Diss. Gottingen (1902).
[5] R. S. Minor, Diss. Gottingen (1902).

prism was determined by the method due to Collins.[6] Several of the other adjustments depend upon this one.

The calculating equations for this procedure are

$$n_0k_0=\frac{\sin 2\psi \cos 2\psi \sin\Delta}{(1-\cos\Delta \sin 2\psi)^2}\sin^2\phi \tan^2\phi,$$

$$n_0^2-k_0^2=\sin^2\phi \tan^2\phi\frac{\cos^2 2\psi-\sin^2 2\psi \sin^2\Delta}{(1-\cos\Delta \sin 2\psi)^2}+\sin^2\phi.$$

These equations may be obtained by the application of electromagnetic theory.

Copper and beryllium were selected because theoretical calculations[7] have already been started for these metals. Copper had been examined before, but since that time the technique of evaporation in a vacuum has been developed, providing surfaces unaffected by mechanical or chemical polishing. Metallic films evaporated on glass were used. These films were of sufficient thickness so that the reflection phenomena were independent of the thickness.

COPPER

The copper used was obtained from the Bureau of Standards and contained 0.002 percent iron; 0.010 percent tin; no antimony; and no lead as impurities. Data were taken every 200A from 2200A to 9800A, and in some cases data were again taken after the film had aged in air. The data, obtained from photographs, consisted of the phase change Δ and the azimuth ψ of the reflected beam when linearly polarized light of 45° azimuth was reflected from the metal surface at an angle of incidence ϕ. The data so obtained were plotted on a graph and smooth curves drawn through the points (Figs. 2 and 3). From these curves information was taken allowing the calculation of the optical constants as a function of wave-length or frequency. The vertical lines about the curves indicate the probable error in the various regions of the spectrum.

These curves differ from the previous data in two important ways. First, the dielectric constant is positive near $\bar{\nu}=3\times10^4$ cm^{-1}. Second, previous data show a strong absorption band (increase in conductivity) near $\bar{\nu}=2\times10^4$ cm^{-1}. These differences probably result because the surface is free from copper oxide. One consequence of these differences is the color of the copper mirror, the fresh copper surface does not have the red copper oxide color usually associated with copper surfaces. The slight suggestion of a band obtained there may be due to traces of the oxide. A good vacuum during the evaporation is necessary if this copper oxide band is to be avoided.

Rudberg,[8] had previously suggested that this band might be due to copper oxide. He did not find the corresponding band in his experimental studies of the energy lost by electrons when scattered from copper.

If the anomalous band is assumed to be linear at its low frequency side it would begin at about 2.5 electron volts, and the conduction band, which is the remainder, is estimated to end at about 4.0 electron volts. These results are in qualitative agreement with the calculations by Rudberg and Slater[9] which indicate the conduction band should end about 4.0 electron volts and that the first anomalous band should begin about 2.9 electron volts. Slater[10] does not consider the

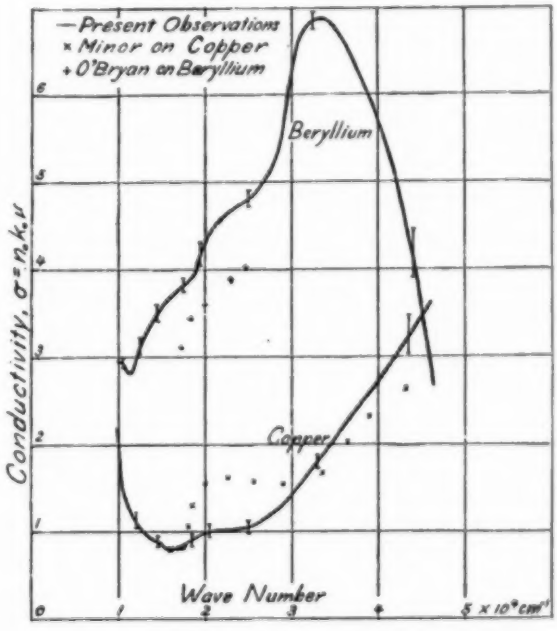

FIG. 3. Conductivity of copper and beryllium.

[6] J. R. Collins, Rev. Sci. Inst. **9**, 81 (1938).
[7] E. Rudberg and J. C. Slater, Phys. Rev. **50**, 150 (1936); C. Herring and A. G. Hill, Phys. Rev. **58**, 132 (1940).
[8] E. Rudberg, Phys. Rev. **50**, 144 (1936).
[9] E. Rudberg and J. C. Slater Phys. Rev. **50**, 155 (1936).
[10] J. C. Slater, personal letter.

results of the calculations to be more than qualitative, so that it is probably coincidence that the experiment and the theory agree as well as they do. From the theory[11] the quantity

$$f=\frac{4m}{n_0e^2}\int\sigma d\nu$$

represents the average number of electrons per atom contributing to the absorption in the frequency range over which the integration is carried out. m and e are the electronic mass and charge, respectively, and n_0 represents the number of atoms per unit volume. The integral is the area under the conductivity curve; for copper this was measured from the minimum ($\tilde{\nu}=1.5\times10^4$ cm^{-1}) to the high frequency end of the experimental range ($\tilde{\nu}=4.5\times10^4$ cm^{-1}). In that region the contribution to f was found to be 0.29. From the curve it would seem that this represents only a small portion of the band, since the conductivity is still increasing sharply at the end of the experimental range. For the whole band the f number is probably more than one (1). This band then probably does not arise by transitions from the 4s band to the 4p band because there is only one 4s electron per atom, and it already has an f number for the conduction band[12] of $f_0=0.37$. Therefore the band in the near ultraviolet may be due to transitions from the 3d band to the empty portion of the 4s band. There are ten 3d electrons per atom.

BERYLLIUM

The beryllium used was obtained from the Brush Beryllium Company. Two samples were used, one was "better than 99 percent pure," and the other was "99.9 percent pure" with impurities of iron, magnesium, and silicon. The data were worked up in the same manner as for copper and are presented in the figures.

The conductivity has a maximum near $\tilde{\nu}=3.3\times10^4$ cm^{-1} or $\lambda=3000$A and the dielectric constant has a minimum near $\tilde{\nu}=4.4\times10^4$ cm^{-1} or $\lambda=2500$A. The fact that the minimum of the dielectric constant is at a higher frequency than the conductivity peak indicates that there is no other absorption band near the high frequency side of the one at 3000A. The sharp decrease in conductivity near the end of the experimental range also agrees with this. The band is unusually narrow.

The irregularities in the curves for beryllium may not be real. However, judging from the probable errors as calculated from the experimental data, and also from the smoothness of the copper curves, one would conclude that the variations are probably real.

Theoretical calculations[13] which have been undertaken for beryllium are not yet sufficiently advanced that they may be checked by experiment.

In the range $\tilde{\nu}=1.1\times10^4$ cm^{-1} to $\tilde{\nu}=4.5\times10^4$ cm^{-1} the contribution to f is 0.63, which indicates that this is a fairly strong band of the beryllium spectrum.

In conclusion the author wishes to express his indebtedness to Professor J. R. Collins for his constant help and thoughtful criticism, to Professor D. H. Tomboulian for his advice and help during the preparation of the mirrors, to Professor H. A. Bethe for his assistance in interpreting the results, and to the Brush Beryllium Company for the donation of the necessary amount of beryllium.

[11] F. Seitz, *Modern Theory of Solids*, (McGraw-Hill, 1940), p. 646.

[12] N. F. Mott and H. Jones, *Properties of Metals and Alloys* (Oxford, 1936), p. 121.

[13] C. Herring and A. G. Hill, Phys. Rev. **58**, 132 (1940).

Magneto-Optical Properties of Ferromagnetic Suspensions

HANS MUELLER AND MORRIS H. SHAMOS*
George Eastman Research Laboratories of Physics, Massachusetts Institute of Technology, Cambridge, Massachusetts
(Received January 23, 1942)

Observations on the change of light transmission through magnetite suspensions under the influence of alternating magnetic fields show that the orientation of the particles is not exclusively of dipolar origin, as was assumed by Heaps and Elmore. Fields of frequencies between 500 and 15,000 cycles per sec. produce a steady change of absorption. In fields of lower frequencies ω the change consists of a steady and a fluctuating part. The wave form of the latter is studied with a photo-cell amplifier and an oscillograph. In general, it is given by an equation of the form: $A\cos\omega t+B\cos 2\omega t$. By varying the field intensity, the frequency or the viscosity, either A or B can be made to vanish. This behavior is shown to be characteristic of polar anisotropic particles, for which the torque on the induced dipole is of the same order of magnitude as that due to the permanent dipole. Included is a survey of the work done on the magneto- and electro-optical properties of numerous other colloids and suspensions.

INTRODUCTION

THE optical properties of many colloids and suspensions undergo marked changes under the influence of uniform magnetic or electric fields. Clear, transparent colloids made up of small particles with an average diameter less than about 0.1μ become birefringent, while the predominant optical effect in suspensions with large particles is a change in the intensity and angular distribution of the scattered Tyndall light. Frequently, when the integrated intensity of the scattered light is altered, the field changes the intensity of the transmitted light, i.e., it influences the absorption. In fine dispersions the latter effects are small, whereas the birefringence is negligible in coarse suspensions. An intermediate case arises when the linear dimensions of the particles are of the same order of magnitude as the wave-length of light. These sols show both an appreciable birefringence and a large change of absorption. Moreover, the change of absorption depends upon the state of polarization of the light, i.e., for light traveling normal to the direction of the field the colloid becomes dichroic, even when the micelles are not of a dichroic material. In coarse suspensions, however, this dichroism disappears.

The magnitudes of the various effects vary considerably with the sol concentration, the shape, and the optical, magnetic, and electrical properties of the micelles. Of the numerous colloids examined by one of us, only two, milk and a suspension of carbon-black in Nujol, show no effects. Electric birefringence is known to occur in suspensions of ground calcite, mica, and other minerals (see Procupju),[1] in various solvents, in smokes, in the metallic colloids of Au, Pt, Ag, and Hg, and it is especially large in the sols of bentonite, V_2O_5, and the mosaic virus proteins. It has also been observed in collagen, pseudo-globulin, soap solutions, inks, and diluted paints. The change of scattering and of absorption in an electric field is particularly large in aqueous suspensions of kaolin clays, of ZnO in Nujol, and in colloids of $PbCO_3$. The effects are readily observable in fields of 100 volts/cm, and, for the coarse suspensions, fields as low as 10 volts/cm produce noticeable changes. In many instances the effects are extremely large; for example, the intensity of Krishnan's H_h component[2] of the scattered light can be increased by a factor of 10, and, in the kaolin suspensions, the absorption coefficient can be decreased more than 30 percent.

The magneto-optical effects have been studied for only a few colloids. In fields of several thousand gauss they are usually much smaller than the corresponding electro-optical effects, with the following exceptions: Colloidal graphite (aquadag) shows a large change of scattering and of absorption in fields of less than 1000 gauss. Especially famous for their large magneto-

* Now at Washington Square College, New York University, New York, New York.

[1] S. Procupju, Ann. de physique **10**, 213 (1924).
[2] R. S. Krishnan, Proc. Ind. Acad. Sci. **7**, 91 (1938).

optical birefringence are colloidal solutions of the iron oxides, studied by Majorana,[3] Cotton and Mouton,[4] Schmaus,[5] and Heller and Zocher.[6] These solutions also exhibit a small change of absorption, and become dichroic in the magnetic field. Suspensions composed of larger particles of magnetite show a marked change of absorption. According to McKeehan,[7] this magneto-optical effect was discovered first by W. R. Grove in 1845. It was rediscovered by Heaps[8] in 1938, and has been the topic of a recent discussion by Elmore.[9] It is with the interpretation of this effect offered by the latter two authors that we should like to take issue here.

THEORETICAL

The magneto- and electro-optical effects in colloids are due to the orientation of anisometric particles. With increasing field intensity all the effects tend toward saturation, corresponding to complete orientation of all particles. Both Heaps and Elmore have assumed that, since Fe_2O_3 is ferromagnetic, we have to deal only with the orientation of permanent dipoles, i.e., that the torque on a single particle is given by

$$T=\mu H \sin\theta$$

where H is the applied field. The particles of all the other colloids studied are neither magnetic nor electric dipoles. In these colloids a major part of the torque arises from the action of the field on the induced rather than the permanent dipoles. Therefore, for particles with an axis of symmetry which forms the angle θ with the direction of the field, the torque is

$$T=\gamma H^2 \sin\theta\cos\theta.$$

Although the particles of Fe_2O_3 are oriented by very weak magnetic fields of one to ten Gauss (depending on particle size and heat treatment of the material) the possibility that the observed effect is not of ferromagnetic origin cannot be excluded. Hence the question arises: Is the magneto-optical effect in Fe_2O_3 due entirely to dipolar orientations, or is it in part due to the fact that the magnetic polarizability of the particles is anisotropic?

This problem can be solved on the basis of the following considerations: If the energy of orientation U is large compared to kT we must distinguish, as Elmore has pointed out, between two separate relaxation times. The short relaxation time $\tau_1=\rho/U$ is the time required for the absorption effect to reach a maximum when a steady field is applied suddenly, or when its direction is changed. However, when the field is removed, the decay of the effect is determined by the rotational Brownian motion, and thus the relaxation time is longer. This second relaxation time $\tau_2=\rho/kT$ (where ρ is the friction constant $8\pi\eta r^3$) will be called the decay time, and τ_1 the orientation time. The relaxation time τ_2 is used in Debye's theory. For dipoles $\tau_2/\tau_1=\mu H/kT$.

Now, if the suspension is subjected to an alternating field $H_0\cos 2\pi\nu t$ with period $1/\nu\gg\tau_2$ it is obvious, since the change of absorption depends upon H^2, that in the first approximation the intensity of the transmitted light will vary according to a law of the form:

$$\begin{aligned} I&=I_0+A\cos^2 2\pi\nu t \\ &=(I_0+A/2)+A/2\cdot\cos 4\pi\nu t \end{aligned}$$

where I_0 is the transmitted intensity when no field is acting, and A is the change for a steady field H_0. Actually, when saturation is approached the variation is not sinusoidal, although the period remains $1/2\nu$. When the frequency is increased, deviations from the above law are to be expected as ν approaches a critical frequency. The types of deviations and the frequencies at which they occur depend upon the origin of the orienting torque. In this respect, three possibilities will be considered.

(A) Dipolar Orientation

According to Debye's theory, the orientation and hence the optical effects disappear for high frequency fields. When $\mu H<kT$ the critical frequency is $1/\tau_2$, but in strong fields the critical period depends upon the orientation time τ_1, since the direction of the dipoles is reversed

[3] Q. Majorana, Comptes rendus **135**, 159, 235 (1902); Rend. Accad. Linc., [5], **11** (1), 374, 463, 531; (2), 90, 139 (1902); Physik. Zeits. **4**, 145 (1902).
[4] A. Cotton and H. Mouton, Ann. Chim. Phys. [8] **11**, 145, 289 (1907).
[5] A. Schmaus, Ann. d. Physik **10**, 658 (1903); **12**, 180 (1903).
[6] W. Heller and H. Zocher, Zeits. f. physik. Chemie **A164**, 55 (1933). (For a comprehensive study of these effects see: W. Heller, Kolloid Beihefte **39**, 1–4 (1933).)
[7] L. W. McKeehan, Phys. Rev. **57**, 1177 (1940).
[8] C. W. Heaps, Phys. Rev. **57**, 528 (1940).
[9] W. C. Elmore, Phys. Rev. **60**, 593 (1941).

after every half-cycle, and this reversal can take place in strong fields when $1/\nu > \tau_1$. In the first approximation, then, the intensity variation is of the form:

$$I = I_0 + B + C\cos(4\pi\nu t - \psi), \qquad (1)$$

where B and C approach zero at high frequencies. Notice that the periodic part has twice the frequency of the applied field, and is shifted in phase.

(B) Orientation of Anisotropic Non-Polar Particles

This case has been treated by Tummers[10] for small fields. In high frequency fields the particles are oriented, but the change of absorption is steady. The critical relaxation period is the decay time τ_2, for in this case the torque is proportional to H^2 and the orientation of the particles is not reversed. Hence the transmitted intensity can fluctuate only when the time between successive half-cycles is sufficiently large to allow the orientation to decay. Again, in the first approximation the intensity variation is given by Eq. (1), but, for nonpolar particles, only C vanishes at high frequencies, while the magnitude of the steady change B is equal to that produced by a steady field $H = H_0/\sqrt{2}$.

(C) Orientation of Anisotropic Polar Particles

For $1/\nu < \tau_1$, where the dipoles are ineffective, the alternating field creates a steady change in the transmitted light, as in case B. For $1/\nu > \tau_2$ the intensity is given by Eq. (1). In the intermediate case, however, where $\tau_2 > 1/\nu > \tau_1$, the particles are too sluggish to follow the variations of the torque $\gamma H^2 \sin\theta\cos\theta$, but they are sufficiently mobile to follow the variations of the torque on the dipoles. Since the quadratic torque creates a steady deflection, the combined effect of both torques is analogous to that produced in a polar colloid by the superposition of a steady and an alternating field:

$$H = H_1 + H_2\cos 2\pi\nu t.$$

This implies that, in the intermediate range, the transmitted intensity fluctuates according to a law which, in the first approximation, is of the form:

$$\begin{aligned} I &= I_0 + [\alpha + \beta\cos(2\pi\nu t - \psi)]^2 \\ &= (I_0 + \alpha + \beta^2/2) + 2\alpha\beta\cos(2\pi\nu t - \psi) \\ &\qquad + \beta^2/2\cdot\cos(4\pi\nu t - 2\psi). \end{aligned} \qquad (2)$$

Hence, if the influence of the anisotropy, i.e., the quantity α, is not small in comparison with the dipolar effect β, an appreciable fraction of the intensity variation has the same frequency as the applied field. In contrast to the two previous cases, the variation of the transmitted light may show no frequency doubling in strong alternating fields, when the dipole and the anisotropy play roles of equal importance—and when the frequency lies within the critical range.

Magneto- and electro-optical investigations in alternating fields, therefore, offer a very simple method for determining the origin of the torques on the micelles. Only when all the optical changes vanish at high frequencies can we be sure that the torque is of a purely dipolar origin. For most aqueous colloids frequencies of several kilocycles are to be considered high; for coarse suspensions in viscous media 60-cycle a.c. is sufficiently high. The numerous colloids for which the electro-optical effects have been investigated show the following changes: At high frequencies, steady changes in the birefringence, scattering, absorption, and dichroism occur. In fields of low frequency the change consists of both a steady and an alternating part, the latter having twice the frequency of the applied field. This behavior is characteristic of anisotropic nonpolar particles.

EXPERIMENTAL

Suspensions of Fe_2O_3 were prepared from a red powder, supplied to us by Dr. Benedikt of the magnetic laboratory of our Institute. This powder is derived from black Magnaflux powder No. 10 by annealing at 300°C in air. The particles were suspended in Nujol and the viscosity was varied either by heating or by diluting with CCl_4. The larger particles were allowed to settle out. From the decay time we estimate an average particle radius of about 10μ. The suspensions were placed in a rectangular glass trough of 5-cm length within a coil of 30 turns, and the radius of the coil was 3 cm. The current used was between 0.1 and 2 amp. Thus the range of field intensities was between

[10] J. H. Tummers, Diss. Utrecht, 1914.

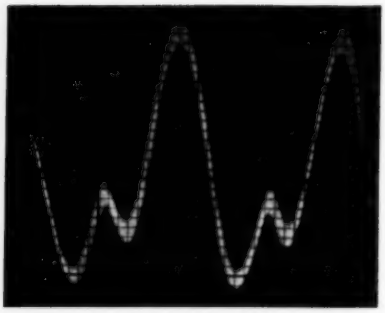

FIG. 1. Wave form of intensity fluctuations of the light transmitted by a suspension of magnetite in an alternating magnetic field of 90 cycles/sec.

$\frac{1}{2}$ to 10 gauss. Alternating current was supplied by an audio-amplifier and a beat frequency oscillator as source of constant frequencies. The light source was a d.c. operated incandescent lamp, the beam passing through the cell parallel to the magnetic field. In order to study the intensity variations of the transmitted light, a photo-tube amplifier was connected to a cathode-ray oscillograph, thereby obtaining a clear record of the alternating part of the photo-current.

RESULTS AND DISCUSSION

Visual observation showed an appreciable increase in the transmitted intensity when a steady field H was applied, and, except for the very viscous solutions, the change took place very quickly; i.e., the orientation time was a small fraction of 1 sec. The decay time, however, was noticeably longer; in most suspensions it was longer than 1 sec. The dependence of the effect on the field intensity is similar to that reported by Heaps, but our suspensions require a field of about 10 gauss for saturation,[11] whereas the more finely dispersed colloids used by Heaps become saturated in fields of 1 gauss. In spite of this difference it seems reasonably safe to assume that the origin of the optical effect is the same in both types of suspensions.

Alternating fields of frequencies up to 15 kc produced the same sort of visual changes as were observed for steady fields. For frequencies above 500 cycles the intensity change was steady, this fact alone indicating that for our suspensions the assumption of Heaps and Elmore is not tenable. The orientation of the particles is due, at least partly, to their anisotropic polarizability. On the other hand, this anisotropy is not sufficient to account for the observations in fields between 50 and 300 cycles, for in this range the transmitted intensity possesses a fluctuating component. Since the decay time is longer than 1 sec., this fact indicates that the particles are permanent dipoles. Hence, we conclude that we are dealing with polar anisotropic particles, for which the torque on the induced dipoles is of the same order of magnitude as that due to the permanent dipoles. This conclusion is supported by observations made upon the wave form of the intensity fluctuations. The shape of the oscillograph curve changes with the frequency, the field intensity, the temperature, and consequently the viscosity of the solution. It can be varied from a sine curve with twice the frequency of the oscillator to a sine curve with the same frequency as the applied field. In general, as shown by the photograph, Fig. 1, the curve represents the superposition of a sin ωt and a sin $2\omega t$ term. This type of curve can be explained very readily on the basis of Eq. (2), when the dipolar contribution β is somewhat larger than α.

Thus, for the more coarsely dispersed suspensions of Fe_2O_3, it is necessary to modify the theoretical considerations of Elmore by taking into account an additional term proportional to H^2 in the expression for the orientation energy. This introduces considerable complications into the theory: Several conclusions reached by Heaps and by Elmore must be invalidated, and the problem of the relaxation phenomena in strong fields becomes extremely complex. Observations in alternating fields can be used to decide whether a similar correction is necessary for the fine disperse suspensions. Since they are saturated by weaker fields it is possible that the quadratic term plays a negligible role for the smaller particles.

Recently, Benedikt[12] has devised a more direct method for measuring the magnetic torque on colloidal particles. His results on Fe_2O_3 and other ferromagnetic suspensions lead to conclusions which are identical with those derived from our optical investigation. We are indebted to Dr. Benedikt for supplying us with the magnetite powder.

[11] According to private communication this result agrees with observations of Dr. Elmore on similar suspensions.

[12] E. T. Benedikt, J. App. Phys. **13**, 105 (1942).

Excitation of the Anode Effect

PAUL L. COPELAND AND GERALD G. CARNE
Department of Physics, Illinois Institute of Technology, Chicago, Illinois
(Received December 2, 1941)

The accumulation of charges in the anode effect has been studied, and possible interpretations of the observed phenomena are suggested. The effects observed here are ascribed to a surface consisting of thorium on oxygen on nickel. For the purpose of making the analysis quantitative, an order of magnitude for the thickness of the film has been assumed and an arbitrary definition of electron capture has been introduced. Computations on this basis indicate that the probability of electron capture is surprisingly high. Although the quantitative interpretation must be considered tentative, some of the facts concerning the accumulation of the charge appear to be quite well established by the evidence. The likelihood of trapping an electron incident on the surface is relatively large when it has an energy corresponding to a few volts, and this likelihood falls at first slowly and then more rapidly as the energy of the incident electron is increased. The probability of electron capture falls rapidly as the temperature of the surface is raised. The electrons are trapped in states from which they escape at very different rates, and the states of short average life are especially numerous. When an equilibrium state is disturbed either by increasing or decreasing the current to the surface, the rate of contact potential shift is at first relatively rapid and it decreases very much as a new equilibrium is approached.

IN the anode effect charges are captured and held on the surface of a metal in such a way as to shift its apparent contact potential. S. A. Obolensky[1] observed that negative charges accumulating on a surface may remain for a considerable time. He noticed that the effect is most pronounced when relatively cool grids collect large space current and he reported evidence indicating that the negative polarization reduces the secondary emission from the grid. Studies by Nottingham[2] and by Copeland[3] emphasized facts concerning the decay of the trapped charge. Some information, however, was obtained concerning the relative effectiveness of electrons of various energies in the excitation process. W. B. Nottingham[2] found that low energy electrons produced a negative contact potential shift. The amount of this shift decreased as the kinetic energy of the collected electrons was increased, and for electrons of sufficiently high energy the resulting surface charge was actually positive. In none of the studies cited was the switching rapid enough to observe the building up of the charge on the surface in satisfactory detail, and it was primarily to obtain information of this sort that the present study was undertaken.

APPARATUS AND EXPERIMENTAL METHODS

The tube used was one of the triodes previously described.[3] Its geometry is cylindrical, and the source of electrons is a thoriated tungsten filament stretched along the common axis of the electrodes. The grid consists of thirteen strands of No. 35 nickel wire which are equally spaced elements on the surface of a circular cylinder 1.3 cm in diameter. The charges investigated are captured on the surface of this grid. The plate is a co-axial nickel cylinder 2.8 cm in diameter. Except for the arrangement of the grid structure, this triode is quite similar in design and in operation to commercial receiving tubes. Both of the separate tungsten wires supporting the grid at its ends are sealed through the Pyrex glass envelope of the tube. The temperature of the grid may be controlled by passing a current through it, and the temperature estimated through the use of the grid itself as a resistance thermometer, which had been calibrated with the aid of an optical pyrometer.

Both the circuit and the general method of obtaining data are quite similar to those indicated in the paper cited.[3] Figure 1 shows the essential features of the circuit used for making the measurements. The experimental tube is

[1] S. A. Obolensky, Vestnik Elektrotechn. **7**, 169–178 (1931). Not being familiar with this work, the senior writer regrettably failed to cite it in his previous paper (reference 3). Obolensky's title for the paper, "Negative grid polarization in a triode," is perhaps more descriptive than "anode effect," but to be consistent with previous publications in English, the name anode effect is used in this paper.

[2] W. B. Nottingham, Phys. Rev. **39**, 183 (1932).

[3] P. L. Copeland, Phys. Rev. **57**, 625 (1940).

shown in the circle. The filament is supplied by a storage battery as shown, the current through it and the potential difference across it being measured on A_f and V_f, respectively. The grid heating current is similarly supplied, and V_g and A_g are provided for the measurements. The plate potential is supplied by the storage battery shown in the lower part of the figure, and it may be reversed through the switch R_s. The grid bias is supplied by a potential divider

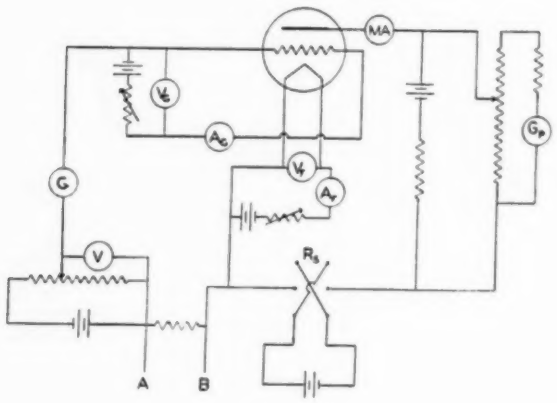

FIG. 1.

and is read on the accurate voltmeter V. The grid does not ordinarily collect a measurable space current, but when a potential impulse is applied between A and B in such a sense as to make the grid positive, electrons are collected by the grid, and the charge is measured by the low-impedance ballistic galvanometer G. The system for the measurement of the plate current changes, used as a measure of the contact potential shifts of the grid, contains a "compensator" which is a storage battery in series with 2 megohms of resistance. The "normal" plate current in the tube is thus of the order of one, two, or three microamperes depending on whether one, two, or three cells of the storage battery are used. The indicating instrument (G_p) is a Leeds and Northrup type R galvanometer connected to the compensator by means of an Ayrton shunt.

A set of observations was started with the grid at the contact potential which represents the equilibrium condition with negligible grid current and a desired grid temperature. The galvanometer was calibrated as a voltmeter for the measurement of the grid potential through determining the deflection of the galvanometer for several carefully measured grid potentials. The galvanometer was brought to zero by adjustment of the grid bias. Following this, the galvanometer was removed from the circuit by turning the Ayrton shunt to the zero position. Next the plate battery reversing switch R_s was thrown to make the plate negative. Finally the grid was made momentarily positive by applying a potential impulse between A and B. A large electron current was then collected by the grid, but the plate was protected by its negative bias, and the anode effect was thus confined to the grid wires. When the desired charge had passed to the grid wires, the application of the impulses was stopped. The decay time was measured from the final impulse. The plate reversing switch was then returned to its normal position, and the Ayrton shunt was operated to restore the galvanometer to full sensitivity. The deflection of the galvanometer was read and recorded as a function of the time. Because the rate of drift of the galvanometer was the greatest during the first readings, the shift of the contact potential was plotted as a function of the logarithm of the time just as in the previous work.[3]

A new feature of these studies was the use of an automatic switching arrangement to limit the time that the grid collected electrons to such short intervals that the excitation of the anode effect in steps could be studied. Preliminary experiments with a potential impulse applied from a rotating sector indicated that in order to study the building up of the charge in satisfactory detail the time during which the current was collected should be as small as 0.005 second. Desired conditions for the potential impulse are: (1) that it should be of short duration and accurately constant from measurement to measurement, and (2) that the value of the applied potential should be approximately constant throughout the duration of the impulse and conveniently adjustable for various tests. The electronic switching arrangement to be described, while not perfect, was reasonably satisfactory in these respects, and the convenience of its operation was sufficient to justify its use in the present study.

The wiring of the auxiliary circuit is shown in Fig. 2. The tube which acts as an electronic switch is the FG-81 thyratron. The potential drop across the thyratron is approximately constant during the time that the tube conducts. Thus when an alternating source of potential is used in the plate circuit, the drop across the load resistor varies too much to be used for the potential impulse. For this reason a second gas filled rectifier is introduced as a voltage regulator. The tube selected is the type 83 mercury vapor rectifier. This tube was designed as a full wave rectifier, and it has two independent plates which surround two different but electrically connected filaments. The potential difference between the filament and the plate in such a rectifier does not vary rapidly when the plate current changes. When no current is passed by the thyratron, the potential difference across the resistor in parallel with the tube is low enough to be negligible in its influence upon the collection of electrons by the grid of the experimental tube. This resistor, then, is a suitable source of potential impulses, and the potential difference applied to the grid of the experimental tube for short time intervals is tapped from it.

The right-hand side of the 83 tube is used as a rectifier for charging the condenser C. The potential difference across this condenser is applied as a grid bias for the thyratron. The resistance R is made large enough to keep the thyratron from passing current for about one minute after a single impulse is passed. A second resistor, with a switch for shunting it across the first, is provided for altering the time constant

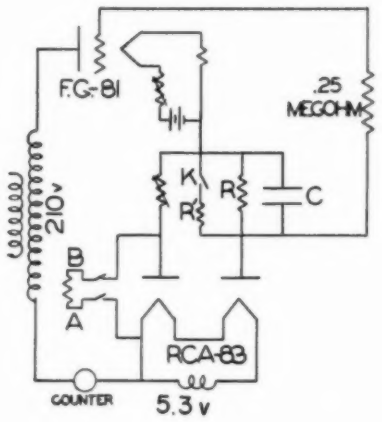

FIG. 2.

of the capacitance-resistance arrangement as desired. The 0.25-megohm resistor in the grid connection of the thyratron keeps excessive charge from passing to the grid while the thyratron is conducting. When used for applying timed impulses to the experimental tube, the circuit is operated from commercial 60-cycle power. A double pole switch is provided by means of which the auxiliary circuit may be connected to the experimental tube or insulated

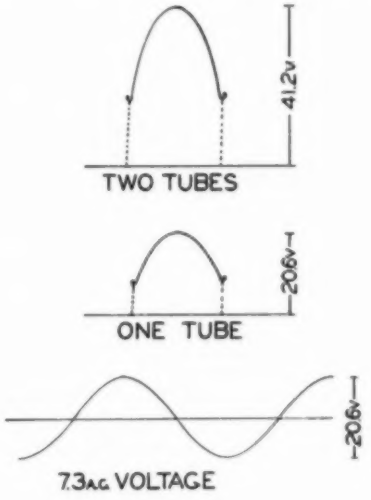

FIG. 3.

from it as desired. As soon as the a.c. is applied to the impulse circuit, the thyratron passes current, and the biasing condenser is charged. Since the charge on the condenser decreases gradually, the next impulse begins at or very near the peak of the a.c. potential in the plate circuit, and it continues for almost a quarter of a cycle or 0.00416 second.

Figure 3 shows an oscillogram of the potential impulse. It is seen that the potential is not really constant during the part of the cycle for which the current flows, but the regulation appears to be satisfactory for the present studies, and the electronic switching circuit was used in the bulk of the work.

When a single impulse is desired, the double pole switch connecting the auxiliary circuit to the grid of the experimental triode is left closed only for a single impulse. When several impulses are desired, the key K is depressed, so that the impulses occur at the rate of about 5 per second. The double pole switch at points A and B is

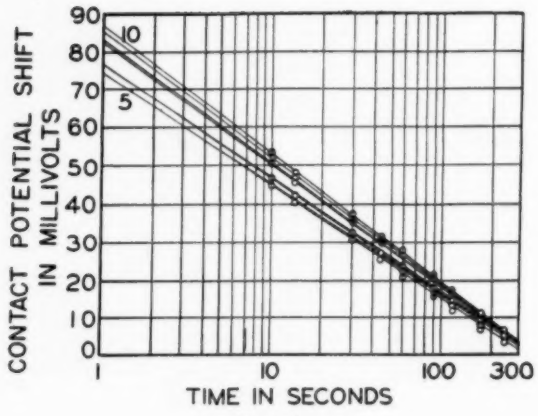

FIG. 4.

kept closed for just the desired number of impulses. As long as the time interval between the impulses is not made too large, the variation of the interval has a small but noticeable effect on the results obtained. Figure 4 illustrates this point. Here the time constant of the condenser-resistance arrangement in the auxiliary circuit was first made so short that the time between impulses was only 0.0166 sec. The four lower curves shown in Fig. 4 were obtained through the regular measurement routine previously described by using five impulses in each case. The top two of the lower group of four are barely distinguishable, and they resulted from impulses separated by only 0.0166 sec., while the lower two were observed after the grid had been excited by five impulses separated by approximately 0.2 sec. The four upper curves were taken with 10 impulses. The top two of the upper group were obtained after ten consecutive impulses had passed, and the lower two (almost identical) were taken after the application of ten impulses uniformly distributed over a 2-second interval. Differences appearing when the time interval between impulses is increased are probably significant, and they may be explained as an effect of the greater decay time between the earlier impulses and the observations. Differences thus introduced, however, do not appear to be sufficient to make the accurate control and measurement of the time elapsing between the impulses important.

DISCUSSION OF EXPERIMENTAL RESULTS

The first subject to be investigated was the building up of the charge on the grid as a

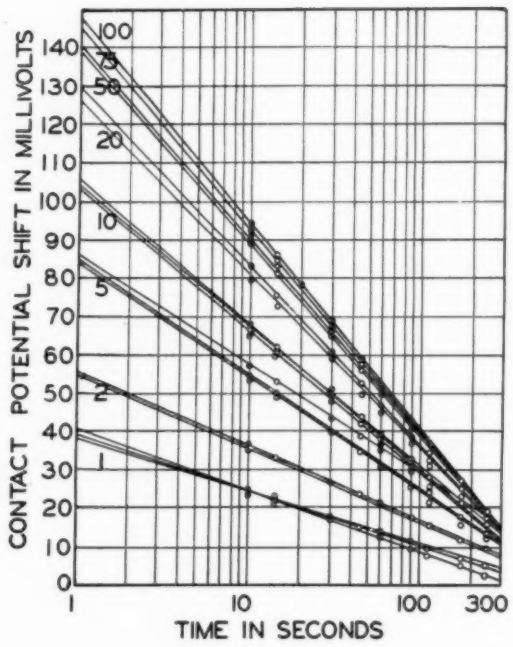

FIG. 5.

function of the number of impulses. These measurements were made at three different fixed temperatures for the grid, which were approximately 476°K, 548°K, and 586°K. It was convenient to change the filament temperature and with it the value of the impulse in the tests at the different temperatures. Figure 5 shows the results obtained with the grid at 476°K. Here the shift of the surface potential in millivolts relative to the normal state is plotted against the logarithm of the time in seconds measured from the final impulse. The plots, as in the previous paper,[3] are close to linear except when an equilibrium condition is approached. Observations could not be taken at the instant the impulse ceased, and the graphs consequently do not give the potential to which the grid surface was charged. The value given by extrapolating each line back to one second of time was taken as a measure of the potential to which the grid was charged. It must be admitted that this procedure is arbitrary, but it appears to be as good a choice as the data would justify, and comparisons based upon its consistent use should be valid. It thus appears that one impulse, which in this case was found by measurement to be 1.01 microcoulombs, charges the surface to about -37 millivolts. Two such impulses

charge it to −54 millivolts; five to some −84 mv, and so on. The proportion of the charge captured falls off rapidly as the number of impulses is increased, and in this test the potential to which the surface is charged appears to approach a limiting value somewhere in the neighborhood of −150 mv.

Figure 6 shows a similar set of data obtained with the grid at a temperature of about 548°K. The impulses used in this case were somewhat larger; their value as measured was 3.51 microcoulombs. In spite of the increase in the size of the impulses, the potential to which the grid is charged by a given number of impulses is lower than in the preceding case. The data plotted in Fig. 7 were obtained with the grid maintained at a temperature of about 486°K. By measurement a single impulse was found to contain 4.18 microcoulombs of charge. Again in spite of the increased impulse size the potential to which the grid is charged by a given number of impulses is still lower. The limiting potential in this case appears to be in the neighborhood of −85 mv. The variation of the surface charging with the temperature of the experimental surface appears to be consistent with that previously reported.[3]

These data are analyzed further in Fig. 8. Here the potential shifts indicated at the beginnings of the lines in Figs. 5, 6, and 7 are plotted as a function of the logarithm of the number of impulses. These plots are quite linear until an "equilibrium value," characteristic of

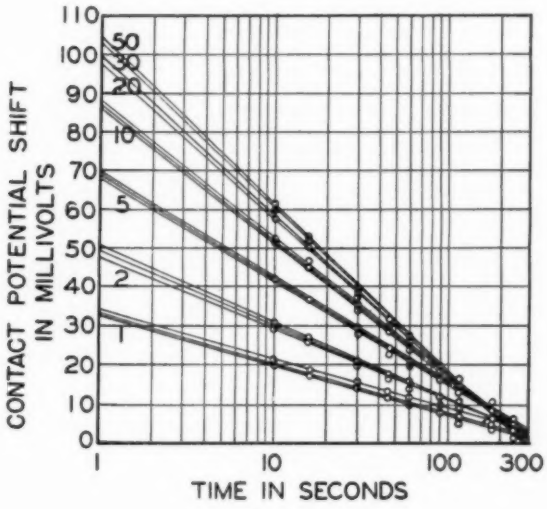

FIG. 6.

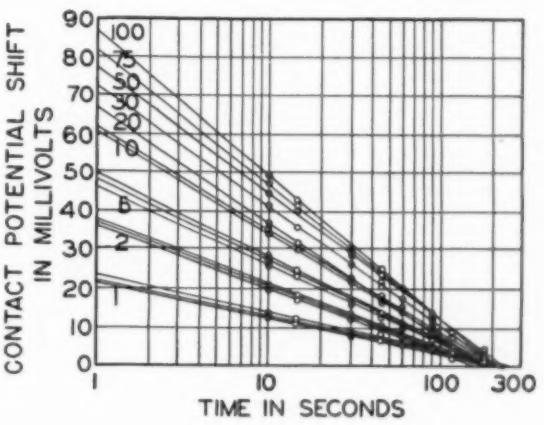

FIG. 7.

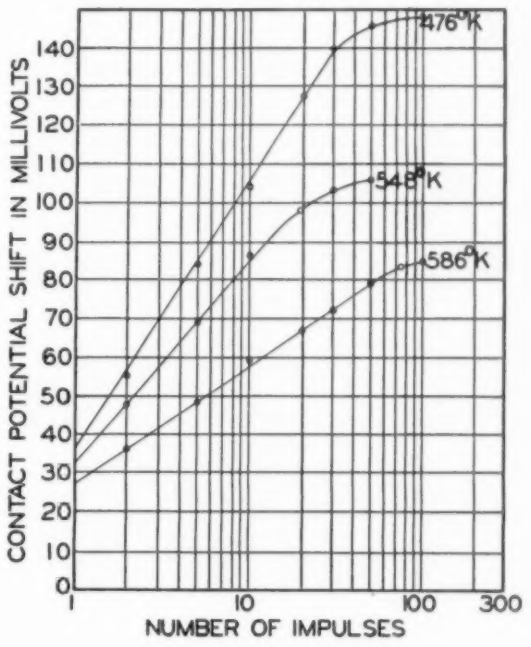

FIG. 8.

each grid temperature and incident electron energy and current density, is approached. This fact is interesting because it indicates that the behavior of the contact potential as the grid is charged resembles its behavior during the drift toward the normal state. The results shown both here and in a previous paper[3] indicate that when the potential shift is plotted as a function of the logarithm of the time after excitation, a very nearly linear plot results. Since the number of impulses is proportional to the time that the excitation current flows, Fig. 8 indicates that the potential attained in the process of excitation

is very nearly a linear function of the logarithm of this time until an equilibrium value is approached.

Another subject investigated was the manner in which the energy of the electrons incident on the grid influenced the probability of their capture. In all of the preceding observations the average energy of the electrons incident on the grid was estimated to be 14 volts. However, by putting a similar rectifier tube in series with the first in the auxiliary circuit, the available potential for the impulse was doubled as indicated by the upper oscillogram of Fig. 3. The resistor placed across the two tubes was divided into four equal parts for the purpose of varying the potential in equal steps. By allowing for the variation of potential during the impulse and for the potential drops across both the filament and the grid, the average energy of the electrons incident on the grid was estimated when each of four taps was used.

In these tests the grid was maintained at 485°K, and the contact potential shift resulting from five impulses containing equal numbers of electrons was observed for each of the electron energies. The results showed that the fraction of the electrons trapped varied with the energy of the incident electrons in a manner which was not unexpected in view of Nottingham's results.[4] The data obtained here are summarized in Table I where the proportion of the incident electrons of various energies trapped is compared with the proportion trapped when the energy of the incident electrons is 14 volts. It is seen that the likelihood of trapping electrons of energy less than 14 volts is relatively high, and that it decreases at first rather slowly as the energy of the incident electrons is increased. Above 14 volts the proportion of the electrons trapped drops off rapidly.

To obtain data for higher energy electrons, a rotating sector was used by means of which B batteries were thrown across the resistor AB for an interval long enough to allow the grid to collect a total charge equal to that in the five impulses supplied from the auxiliary circuit. The data obtained in this way were not quantitatively satisfactory, because in spite of a high internal resistance in the batteries, no oscillograms of the potential across AB were made, but they indicated that the likelihood of capturing electrons continued to fall rather rapidly as the energy of the incident electrons was increased. The contact potential shift became positive when electrons of much more than 60 electron volts were incident on the grid.

[4] W. B. Nottingham, Phys. Rev. **44**, 311 (1933).

TABLE I. Summary of data.

Energy (ev) of incident electrons	Relative number of trapped electrons
6	1.18
14	1.00
22	0.78
30	0.40

Although with the information at hand it is impossible to make an exact quantitative interpretation of these results, a start in this direction is useful, because it indicates interesting facts concerning the order of magnitude of the effect. For this purpose we assume that the layer on which the charges are trapped is 10^{-7} cm thick, and we neglect the polarization of the insulating layer.[5] Under these circumstances the capacitance of the film per unit area is 0.885 microfarad. The effective length of the grid structure is about 7 cm. Hence the total capacitance should be about 3.54 microfarads, and our estimate of the amount of trapped charge is this capacitance multiplied by the contact potential shift. Although the estimates of the charge are intended only to indicate the order of magnitude, relatively small differences between the various tests should be significant.

In the first test, the total charge Q_p collected by the grid in one impulse is 1.01 microcoulomb. The charge Q_c trapped by the grid in the first test is estimated to be 0.133 microcoulomb. It appears that about one electron in every 7.5 is trapped. For two impulses the trapping of charge falls to about one in 10.6, and for five impulses to one in 17. Although for the first impulse one electron in 7.5 is trapped on a grid

[5] Neglecting the polarization is very likely wrong, and it is to be taken merely as indicating lack of information concerning the properties of the film. Concerning the film thickness, it may be pointed out that W. B. Nottingham in Phys. Rev. **41**, 793 (1932) presented evidence for believing that the width of the potential barrier for a film of thorium on tungsten is about 4.5×10^{-8} cm. If to this we add 2.6×10^{-8} to represent the diameter of an oxygen atom, the thickness would be about 7×10^{-8} cm.

maintained at 476°K, of the second impulse only one in 19 is similarly trapped.

The change in the effect which is caused by varying the temperature of the grid is interesting. With the grid at 548°K, only one electron in 30.5 was captured from the first impulse, and for two impulses only one in 73 was trapped. With the grid maintained at 586°K, only one electron in 56 was captured from the first impulse, while of two impulses there is one in 67. Thus the magnitude of the anode effect falls off rapidly with increasing temperature as previously noted.

THEORETICAL CONSIDERATIONS

Some years ago Nottingham[6] proposed a potential barrier model for explaining the anode effect. The calculations described in a paper by one of us[3] were based upon this model. At the time this paper was being written, correspondence with Dr. Nottingham indicated that he was thinking in somewhat different terms, and it appears that a surface consisting of thorium on oxygen on nickel provides a better model for the understanding of the phenomena.

We consider that the nickel surface has on it sufficient oxygen to form at least a partial coverage. Upon this surface thorium, released in the activation of the filament, is deposited in such a way as to form a double layer surface with the thorium on the outside. We then assume that under normal conditions a certain fraction of the thorium atoms loses one of their valence electrons to the nickel, and that they therefore exist on the surface as ions. Low energy electrons falling upon this surface neutralize some of these ions, and we have various equilibrium states depending upon such factors as the energy of the collected electrons, the current density, and the temperature of the surface. When such an equilibrium condition is disturbed by cutting off the electron current, the return to the equilibrium state characteristic of zero incident current is quite gradual. Also, when the incident current is turned on, there is a more rapid but similar approach to the new equilibrium condition, and in these studies we have made the switching rapid enough actually to observe such phenomena.

The proposed model for the surface appears to be natural in view of the evidence that the effect is most pronounced in tubes with activated cathodes. In the tubes which we have used the temperature of the grids has been raised to approximately 850°K without altering the films responsible for the effect. In a tube with a tungsten grid the surface was rendered incapable of showing the effect at low temperatures only by raising it to a temperature at which thorium is known to evaporate from tungsten.[3] The hypothesis also offers the advantage of an easy explanation for the action of high energy electrons in leaving the surface more positive than normal. The high energy electrons are effective in removing electrons from some thorium atoms which would normally be neutral.

In this connection it is interesting to note the similarities between observations with the anode effect and with fluorescent and phosphorescent materials. The writers are indebted to Dr. R. P. Johnson for calling their attention to the very close resemblance of the decay curves in the anode effect to those observed with certain phosphorescent materials. The excitation curves, reported in this paper, also show similarities to the excitation curves for phosphorescence. The decrease in the likelihood of trapping electrons in the anode effect as the temperature of the surface is raised is closely analogous to the decreased efficiency of fluorescent materials at high temperatures. Such similarities are sufficiently impressive to make it seem likely that the mechanisms involved in the two types of phenomena are closely related.

The energy band picture[7] which has been proposed as a basis for understanding the behavior of the phosphors contains features which would be useful for the discussion of the anode effect. We would thus associate the localized energy levels with the thorium atoms on the surface. These levels are not all occupied. Electrons escape from these levels as a consequence of thermal agitation, and they are transferred to the conduction band in the nickel base. Such a model explains the relatively slow drift of a negatively charged surface toward the equilibrium condition just as it explains the

[6] W. B. Nottingham, Phys. Rev. **39**, 183 (1932).

[7] R. P. Johnson, J. Opt. Soc. Am. **29**, 387 (1939).

persistence of phosphorescence. This model also facilitates the explanation of the extremely low rate of drift of a positively charged surface[4] toward equilibrium.

Any satisfactory model must provide for the escape of the various trapped electrons to the base metal at widely varying rates. In this respect the anode effect resembles phosphorescence. This may be explained by picturing the localized levels as spaced various distances below an unoccupied conduction band.

The experimental data are sufficiently informative to lead us to some very definite conclusions in certain respects. It would seem necessary to make assumptions to account for the approximate linearity of the plots representing the contact potential shift as a function of the logarithm of the time. If the contact potential shift be assumed proportional to the trapped charge, this result means that the trapped charge itself is a linear function of the logarithm of the time. Neglecting any interaction between trapped charges, we assume that any electron trapped has a definite probability λ of being removed from the trap during each second of its stay. The values of λ associated with the various trapped electrons differ, and a certain distribution of the electrons will account for the observed curves. By calculation we have found that if the number of electrons trapped where the average life $\theta=1/\lambda$ lies between θ and $\theta+d\theta$ is $kd\theta/\theta$ where k is a constant of proportionality, the linear relationship between the number of electrons remaining and the logarithm of the time arises naturally from the summation of all the various decay curves.

The influence of the current density on the equilibrium value of the contact potential shift is of interest. The experimental evidence appears to indicate that, at a fixed grid temperature, the contact potential shift of the grid is proportional to the electron current collected by the grid until a definite limiting value, characteristic of the grid temperature, is approached.[3] The equilibrium condition is one in which the rate of trapping electrons is balanced by the rate of loss. If we neglect the influence of other factors, the rate of trapping electrons should be found proportional to the current density. The rate of loss of electrons having a particular average life should be proportional to the number of such trapped electrons. We should thus expect that so long as relatively few of the available traps are occupied, the contact potential shift of the grid in equilibrium should be proportional to the current density.

When equilibrium is disturbed by increasing or decreasing the current to the surface, it seems likely that the first states in which the population approaches equilibrium under the new conditions are those in which the average life is small. These states are relatively numerous, and they dominate the initial rapid shift of contact potential when an equilibrium condition is disturbed. States of longer life approach equilibrium much more slowly, and in the case of the decay curves it is these which account for the continuation of a slowly decreasing rate of drift over a period of an hour or so. Such considerations appear to be capable of accounting for the principal features both of the excitation and decay curves.

On a Paradox in the Theory of Heat Conduction

GEORGE JAFFÉ
Louisiana State University, University, Louisiana
(Received February 11, 1942)

The classical theory of heat conduction leads to infinite values for the heat current and for the propagation of temperature at $t=0$, if the initial conditions involve a discontinuity in the temperature distribution. These paradoxical results can be avoided if a method is applied which has been previously indicated by the author. In Section II the solution of a fundamental problem in gaseous heat conduction is given to a first approximation. This approximation holds for values of the distance from the discontinuity which are smaller than the mean free path, and for times which are smaller than the time required for a molecule to travel over a mean free path with the mean velocity. In Section III the new solution is compared with the classical one, and it is shown that all results of the latter which are devoid of physical sense disappear. Furthermore, it is indicated by graphical interpolation how the new solution changes into the classical one.

I. INTRODUCTION

IT is well known that the classical theory of heat conduction (or diffusion) leads to paradoxical results whenever the initial conditions involve a discontinuity in the distribution of temperature (or concentration). Not only does the current set in with an infinite value, but also the velocity with which any particular value of the temperature (or concentration) is propagated becomes infinite in the beginning.

These results are devoid of physical significance and are, evidently, caused by the fact that the fundamental assumption of a heat current proportional to the temperature gradient breaks down where there is no finite gradient. From the point of view of molecular theory there is no reason for any infinite values as long as the number of particles and the energies involved remain finite. Thus the problem presents itself of replacing the traditional solution, anyway for its initial stage, by a treatment which does not lead to singular values.

Now, in molecular theory, the mentioned law for the heat current is *deduced* from the fundamental conceptions. However, it must be emphasized that the traditional deduction holds only with certain restrictions, inasmuch as the velocity distribution is treated as almost isotropic, i.e., as slightly deviating from Maxwell's distribution law. This becomes an inadequate procedure when, in the initial state, the distribution is very far from isotropic, as in the case of a discontinuity of temperature or partial pressure across a surface.

The author has shown in a general way[1] that the integration of Boltzmann's fundamental equation has to proceed along entirely different lines in the two cases where the mean free path λ is short or long in comparison with the relevant linear dimensions. For the case "λ large" he has given a solution in terms of a series which proceeds with powers of λ^{-1}. The first term of this series corresponds to the case where collisions between molecules can be disregarded entirely and where the state of affairs becomes analogous to the conditions prevailing in the theory of heat radiation. This zero solution had previously been given by Smoluchowski[2] in connection with Knudsen's "molecular flow." The subsequent terms of the series render, with increasing accuracy, the influence of collisions between the molecules.

This solution is applicable to the present problem for sufficiently short intervals of time and for the immediate neighborhood of the surface of discontinuity. For, in a certain region, say within one-tenth of a mean free path from this surface, the case "λ large" prevails whatever the conditions of the problem are and wherever the boundaries are located.

We shall apply the method to one very simple problem only, which, however, for the reasons

[1] G. Jaffé, Ann. d. Physik **6**, 195 (1930). We shall refer to this paper in the text with J and indication of the pages.
[2] M. v. Smoluchowski, Ann. d. Physik **33**, 1559 (1910).

just stated, is typical for all such problems. The assumed initial conditions are that two portions of the same gas, but of different density and temperature, are brought into contact with each other along the plane $x=0$ at time $t=0$. No other boundaries are supposed to exist. These assumptions make the application of the method particularly easy because the main difficulty arises from the consideration of solid walls (J 241–248) and there are no such walls to be considered here. We shall be satisfied to give the zero-order solution only since it will be seen that it removes all the paradoxical results of the classical solution.

II. THE SOLUTION FOR "x SMALL" AND "t SMALL"

We shall make the simplifying assumption that the molecules of the gas, of mass m, have only translational energy. If the state is stationary up to $t=0$, Maxwell's law of velocity distribution will hold on either side of the plane $x=0$. In agreement with our method which considers "molecular beams" rather than volume elements as elementary units we write Maxwell's law in the form

$$dn_{c,\vartheta,\varphi}{}^{(i)} = n_i(m/2\pi kT_i)^{\frac{1}{2}} \times \exp(-mc^2/2kT_i)c^2dc \times \sin\vartheta d\vartheta d\varphi, \quad i=1,2. \tag{1}$$

Here, n_1, n_2 represent the number of molecules per cm³, and T_1, T_2 the temperatures, the subscript 1 being applied to the region $x\leq 0$. The $dn_1{}^{(i)}$ molecules represent a beam, of velocity between c and $c+dc$, progressing within the infinitesimal solid angle $d\Omega=\sin\vartheta d\vartheta d\varphi$ where ϑ is counted from the x axis ($0\leq\vartheta\leq\pi$) and φ from the x, y plane ($0\leq\varphi\leq 2\pi$).

Now we envisage an infinitesimal element of surface dS located at right angles to the x axis at a given *small* value of x, say $x=x_1$. Furthermore, we single out, for a given *small* value of t, say $t=t_1$, the $dn_{c,\vartheta,\varphi}$ molecules which are to be found per cm³ in an element of volume surrounding dS, their velocity being within the range $c\to c+dc$ and its direction inside the solid angle $d\Omega$. To be explicit let us assume that x_1 is positive and that ϑ is an acute angle ($0\leq\vartheta\leq\pi/2$).

Under these circumstances the number $dn_{c,\vartheta,\varphi}$, with x_1 and t_1 fixed, still depends on c as the "retarded values" have to be taken since the problem is not "stationary" (J 250). As long as c is smaller than the value c_1 given by

$$c_1t_1=x_1/\cos\vartheta, \tag{2}$$

the molecules originate in volume elements with $x>0$. Hence

$$dn_{c,\vartheta,\varphi}=dn_{c,\vartheta,\varphi}{}^{(2)} \quad \begin{cases} 0\leq\vartheta\leq\pi/2 \\ 0\leq c\leq c_1. \end{cases} \tag{3}$$

However, when c is larger than c_1 the molecules come from elements of volume with $x<0$, and, therefore,

$$dn_{c,\vartheta,\varphi}=dn_{c,\vartheta,\varphi}{}^{(1)} \quad \begin{cases} 0\leq\vartheta\leq\pi/2 \\ c_1\leq c<\infty. \end{cases} \tag{4}$$

For obtuse values of ϑ the molecules originate at values $x>0$ whatever the value of c. Hence in this case

$$dn_{c,\vartheta,\varphi}=dn_{c,\vartheta,\varphi}{}^{(2)} \quad \begin{cases} \pi/2\leq\vartheta\leq\pi \\ 0\leq c<\infty. \end{cases} \tag{5}$$

The three Eqs. (3), (4), (5) represent our zero approximation for the distribution. It will be seen that it is highly anisotropic. The solution as stated holds for positive values of x_1 only. It is easy to establish a similar solution for negative values of x_1.

A few remarks regarding the limits of validity of our zero-order solution must be made. The Eqs. (3) and (4) are based on the assumption that no collisions occur after the boundary $x=0$ has been crossed.[3] Consequently, (3) and (4) will certainly yield valid approximations as long as x_1 is a fraction of the mean free path. The time which the molecules require on the average to cover one free path is given by $t=\lambda/\bar{c}$. For values of time less than this (3) and (4) will hold. However, for values of $x_1\sim\lambda$ and $t_1\sim\lambda/\bar{c}$ the influence of collisions begins to make itself felt, and deviations from the zero solution must be anticipated.

Now we make use of our solution to calculate n, the number of molecules per cm³, integrating

[3] It is furthermore assumed that the "irradiated" values (1) do not change appreciably during the limits of time considered. This assumption will be fulfilled also as long as practically no collisions have occurred. The change in the irradiated values is considered, together with the influence of collisions, in the higher approximations.

first with regard to c for a given direction and then over all directions. The result can be stated in the following form:

$$n=(n_1/2)[1-\phi(\xi_1)]+(n_2/2)[1+\phi(\xi_2)]. \quad (6)$$

Here

$$\phi(x)=(2/\pi^{\frac{1}{2}})\int_0^x \exp[-x^2]dx \quad (7)$$

represents the error integral and the dimensionless variable ξ is given by

$$\xi=(m/2kT)^{\frac{1}{2}}(x/t)=(2/\pi^{\frac{1}{2}})(x/\bar{c}t). \quad (8)$$

In the result we have dropped the subscript 1 for x and t and it represents n as a function of space and time.

Calling the components of the velocity of a molecule u, v, w we obtain, in a similar way, for j_x, the mass current through dS per cm^2,

$$j_x=n\bar{u}=(n_1\bar{c}_1/4)\exp[-\xi_1^2] - (n_2\bar{c}_2/4)\exp[-\xi_2^2]. \quad (9)$$

Before we give the expressions for the energy density and the energy current density a general remark should be made. As long as the velocity distribution is almost isotropic it is rational to split the velocity into the ordered hydrodynamical motion $\bar{u}$, $\bar{v}$, $\bar{w}$ and the irregular heat motion $u-\bar{u}$, $v-\bar{v}$, $w-\bar{w}$ (J 218). This amounts to splitting the kinetic energy into the kinetic energy of translation and the thermal energy. Correspondingly, the energy current separates into various parts: heat current, convection current, etc.

However, when the velocity distribution is highly anisotropic, as in the initial stage of our problem, it seems more rational to consider the entire process as a uniform thermal process without separating the energy or the energy current into their traditional parts. It is for this reason that we have calculated the "total energy density" and the "total energy current density" using the components u, v, w of the total velocity. As the mean velocity is known from (9) and (6) (evidently we have $\bar{v}=0$ and $\bar{w}=0$), it would be easy to refer the "heat motion" to axes moving with the velocity $\bar{u}$ in the x direction.

Setting

$$\psi(\xi)=\phi(\xi)-(2/(3\pi^{\frac{1}{2}}))\xi\exp[-\xi^2], \quad (10)$$

we find for the energy density

$$U=(n_1/2)(3kT_1/2)[1-\psi(\xi_1)] + (n_2/2)(3kT_2/2)[1+\psi(\xi_2)], \quad (11)$$

and the energy current density becomes

$$W_x=(n_1\bar{c}_1/4)kT_1\exp[-\xi_1^2](2+\xi_1^2) - (n_2\bar{c}_2/4)kT_2\exp[-\xi_2^2](2+\xi_2^2). \quad (12)$$

Finally, we calculate the pressure tensor (J 221) using again the total components of velocity ($p_{xx}=nm\langle u^2\rangle_{\text{Av}}$, $\cdots$, $p_{xy}=nm\langle xy\rangle_{\text{Av}}$, $\cdots$). Thus these pressures would be observed on walls which are at rest. Calling the mean value of the normal pressure $\bar{p}$:

$$\bar{p}=nm\langle c^2\rangle_{\text{Av}}/3=2U/3, \quad (13)$$

we obtain

$$p_{xx}=\bar{p}+(2/(3\pi^{\frac{1}{2}}))[n_1kT_1\xi_1\exp(-\xi_1^2) - n_2kT_2\xi_2\exp(-\xi_2^2)],$$
$$p_{yy}=p_{zz}=\bar{p}-(1/(3\pi^{\frac{1}{2}}))[n_1kT_1\xi_1\exp(-\xi_1^2) - n_2kT_2\xi_2\exp(-\xi_2^2)] \quad (14)$$

and

$$p_{xy}=p_{xz}=p_{yz}=0. \quad (15)$$

We have indicated all these results to show how different the conditions are in the initial stage of our problem from what they become for larger values of the time variable. Neither is the expression for the diffusion current formally the same as that for the heat current, nor does a uniform hydrodynamic pressure exist.

It is easy to show that the results (6), (9), (11), (12), (14), (15) hold as well for negative as for positive values of x.

The zero-order distribution function being known, the higher approximations can be found successively by performing definite integrals only (J 251). However, the law of force for the interaction between two molecules in colliding must be known and the integrations become involved. It is of interest to note that the zero approximation does not require the knowledge of the force law and only assumes the validity of

Maxwell's distribution law on either side of $x=0$ before the thermal contact is established.

III. COMPARISON WITH THE CLASSICAL SOLUTION

First of all it should be noticed that the mass current and the energy current across the plane $x=0$ start with finite values as it should be. We find

$$j_x=n_1\bar{c}_1/4-n_2\bar{c}_2/4, \quad x=0,\ t\geq 0, \quad (16)$$

and

$$W_x=n_1\bar{c}_1kT_1/4-n_2\bar{c}_2kT_2/4, \quad x=0,\ t\geq 0. \quad (17)$$

These values are correct, i.e., they will not be affected by the higher approximations, for $t=0$. They are constant within the limits of validity of our solution which means that the curves representing j_x and W_x as functions of time start with horizontal tangents. The higher approximations will make these curves decrease and gradually turn into the classical solution which starts with an infinite value.

The second point of importance is that our formulae contain the variables x and t in the combination x/t only. Let g be any of the quantities describing the physical state, then g will be, for given initial conditions, a function of x/t

$$g=\varphi(x/t). \quad (18)$$

If we now assign to g any (possible) fixed value g_1 and ask with which velocity this value is being propagated, we can consider Eq. (18) giving g_1 solved with regard to x/t. Consequently x becomes proportional to t and dx/dt assumes a value which is constant within the limits of our approximation. Hence, the velocity of propagation for g_1 sets in with a finite value which, of course, still depends on the value of g_1.

In the classical solution of our problem[4] the physical variables are functions of $x/t^{\frac{1}{2}}$. This makes the velocity of propagation $\sim t^{-\frac{1}{2}}$ and the initial value is infinite, as mentioned in the introduction.

There is only one point where our solution, so far, retains a somewhat paradoxical aspect. If, e.g., we examine the expressions (9) for the mass current and (12) for the energy current we find that, for $x\neq 0$, the currents are zero for $t=0$ but assume values different from zero as soon as t is different from zero, no matter what the value of x is. The increase is very small for $t\ll\lambda/\bar{c}$ (much smaller than in the classical solution) but still this behavior involves some kind of infinitely quick propagation.

This result is evidently caused by the fact that, in integrating the distribution law with regard to the velocity c, we have tacitly taken the limits 0 and ∞, thus not excluding infinite velocities. It is customary, in handling Maxwell's distribution law, to take the limits as stated. This is perfectly legitimate as long as the distribution law is used to determine average values.

However, in our treatment, the actual maximum value of the velocity becomes of importance. It is, therefore, necessary to stress that this actual maximum value is finite as long as the number of molecules and the total energy in the system are finite. If, in our problem, we imagine the gas limited by a vessel with linear dimensions large compared with λ, our solution will still hold within the indicated limits sufficiently far from the walls. The maximum velocity now will be limited as it cannot possibly be larger than that resulting from the accumulation of the whole available energy on one molecule.

If the existence of a maximum velocity c_m is taken into account our solution (3), (4), (5) must be supplemented by the consideration of an initial stage in which no molecules at all have had time to travel from $x=0$ to $x=x_1$. As long as $t<x_1/c_m$ the velocity distribution will be isotropic and j_x as well as W_x will be strictly zero.

We do not consider it necessary to write down the somewhat lengthy expressions after correcting our solutions for a finite maximum value of the velocity. The correction affects, in a material way, only the period of time from 0 to $t\sim x_1/c_m$, whereas we are interested in the period near $t=x_1/\bar{c}$. However, from the point of view of principle it remains the fact that, for x_1 finite, the current cannot set in before a finite time ($t_1=x_1/c_m$) has elapsed.

To carry through the comparison between the classical and our solution in a numerical

[4] Ph. Frank and R. v. Mises, *Die Differential- und Integralgleichungen der Mechanik und Physik* (Friedr. Vieweg & Sohn, A. G. Braunschweig, 1927), Vol. 2, p. 190.

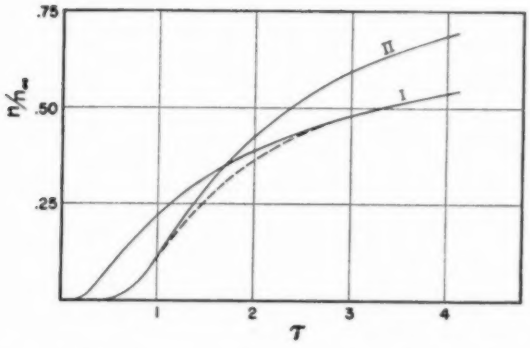

FIG. 1. The curves represent the relative number of particles n/n_∞ at the distance $\alpha=x/\lambda=1$ as function of the reduced time variable τ as defined by (19). Curve I represents the classical solution, curve II the solution here given. The broken line is a graphical interpolation.

way, we shall further simplify the problem by assuming $n_1 \neq 0$, $n_2=0$. These initial conditions correspond to the fundamental experiment in gaseous diffusion where, up to $t=0$, two different gases of constant temperature and pressure are separated by a plane wall.

We are going to introduce dimensionless variables α and τ for x and t setting

$$x=\alpha\lambda, \quad \bar{c}_1 t=\tau\lambda. \tag{19}$$

Thus α is measured in units of the length of a free path and τ in units corresponding to the time which a particle of velocity $\bar{c}$ takes to travel over one mean free path. For further discussion we assume the simple case of self-diffusion[5] and set for D, the coefficient of diffusion in the classical solution,

$$D=f\bar{c}\lambda, \tag{20}$$

where f is a numerical factor depending on the assumed law of interaction. In the elementary theory we have $f=\frac{1}{3}$.

The classical and our solution can now be written in the form

$$\eta=n/n_\infty=1-\phi(\xi), \tag{21}$$

if $n_\infty=n_1/2$ signifies the final value assumed after infinite time. The variable ξ has in the classical theory the value

$$\xi_{cl}=\alpha/(4f\tau)^{\frac{1}{2}}, \tag{22}$$

and in our theory the value

$$\xi=2\alpha/(\pi^{\frac{1}{2}}\tau). \tag{23}$$

In Fig. 1 we have drawn the two curves for $\alpha=1$ assuming $f=\frac{1}{3}$. Curve I represents the classical theory, curve II ours. It will be seen that n, the number of diffused particles per cm^3, becomes noticeable considerably later in our theory. Furthermore, it is seen from the diagram that the transition from II to I must occur somewhere between $\tau=1$ and $\tau=3$, approximately in the form indicated by the broken line. In agreement with our general argument the deviations from our solution should become noticeable (at the distance $x=\lambda$) for $\tau\sim 1$.

If α is different from 1 the curve II may still be retained if we take τ/α as abscissae. However, the abscissae for I will have to be multiplied by the factor α. Therefore, the point where I and II intersect will move to smaller values of τ/α if α is increased above $\alpha=1$, and to larger values of τ/α if α becomes smaller than 1. Thus, the classical theory will become correct for values of $\tau/\alpha=\bar{c}_1 t/x$ which are the smaller the larger, *ceteris paribus*, x.

As for the current we shall be satisfied to give its value for $x=0$. Calling $j_x{}^0=n_1\bar{c}/4$ the correct initial value, we obtain from the classical theory

$$j_x/j_x{}^0=(4f/(\pi\tau))^{\frac{1}{2}}, \tag{24}$$

whereas our theory gives the constant value $j_x/j_x{}^0=1$. Setting $f=\frac{1}{3}$ the two curves intersect for $\tau=4/3\pi$ which is, again, of the anticipated order of magnitude.

Calling ϕ^* the inverse function to ϕ and giving η a specified value $\eta=\eta_0$ we obtain from (21) and (23)

$$x/t=(\pi^{\frac{1}{2}}/2)\bar{c}_1\phi^*(1-\eta_0). \tag{25}$$

Hence, the velocity with which any value of n is propagated in the initial stage is proportional to $\bar{c}_1$ as should be expected.

[5] Cf. L. B. Loeb, *The Kinetic Theory of Gases* (McGraw-Hill, New York, 1934), Sections 70 and 73.

Self-Diffusion of Zinc*

P. H. MILLER, JR.
Randal Morgan Laboratory of Physics, University of Pennsylvania, Philadelphia, Pennsylvania

AND

FLOYD R. BANKS
Morgan State College, Baltimore, Maryland

(Received March 9, 1942)

Self-diffusion measurements in zinc single crystals of various known orientations and polycrystalline zinc have been made by a sectioning method with long-lived radioactive Zn^{65} as an indicator. Measurements on 18 single crystals in the temperature range of 340°C to 410°C enable an investigation of the anisotropy in the diffusion rate. Parallel to the C axis the diffusion rate was found to be $4\times10^{3}\exp(2.04\times10^{4}\text{ cal. mole}^{-1}/RT)$ cm² day^{-1} while that parallel to the basal plane was $8\times10^{6}\exp(3.1\times10^{4}\text{ cal. mole}^{-1}/RT)$ cm² day^{-1}. Polycrystals gave values between these extremes.

INTRODUCTION

THE use of radioactive isotopes as indicators in studies of self-diffusion was introduced by von Hevesy[1] and his collaborators, who studied self-diffusion in lead[1–3] and bismuth.[3] Subsequently self-diffusion studies have been made in copper,[4,5] gold,[6,7] silver,[8] and zinc.[9]

The usual method of studying self-diffusion is to electroplate or evaporate atoms of the radioactive solute onto the surface of the non-radioactive element and allow diffusion to proceed at fixed temperatures for predetermined periods. Diffusion measurements are then made either with the absorption or the sectioning technique. In the absorption technique, developed and used by Hevesy,[1] Seith,[2] Keil,[3] McKay,[7] and Steigman, Shockley, and Nix,[5] measurements of radioactive decay (or of the emanations of the recoiling parent atoms) are made before and after the diffusion and the diffusion coefficient obtained, by taking into account the half-life of the indicator, the range, and absorption of the emitted radiation in the substance employed. In the sectioning technique, introduced by Sagrubskij[6] and developed to greatest advantage by Johnson,[8] the impregnated sample is sectioned (mechanically or chemically) after diffusion and the activity of each section measured. This method of obtaining the diffusion coefficient is independent of the half-life of the indicator, the range, and the absorption of the emitted radiation. Since it is mechanically difficult to cut sections conveniently and with reasonable accuracy thinner than 4×10^{-3} cm, the absorption measurements are more useful for small rates of diffusion because of the short ranges of alpha-particles (10^{-3} cm) and recoil particles (5×10^{-7} cm).

Bismuth and zinc are the only non-cubic crystals in which self-diffusion has been studied, and therefore are the only ones which can reveal structure dependence of diffusion. Anisotropy in bismuth[3] has already been observed.

In a previous paper[9] the measurement of the coefficient of self-diffusion in zinc single crystals parallel to the C axis, with radioactive Zn^{65} as indicated and the sectioning technique, was reported. The present work is a continuation of the investigation for various orientations of single crystals (to study anisotropy) and polycrystalline zinc.

EXPERIMENTAL PROCEDURE

The single crystals were grown by withdrawing the melt at a rate of 3 cm per hour through a

* This investigation was started with the cooperation of Lt. Harry M. Day of the Naval Research Laboratory while he was still associated with the Research Laboratories of the General Electric Company, Schenectady, New York. Table I indicates the crystals which he so skillfully prepared and carefully heat treated.

[1] Hevesy, Seith, and Keil, Zeits. f. Physik **74**, 197 (1932).
[2] W. Seith, Zeits. f. Elektrochemie **39**, 538 (1933).
[3] W. Seith and A. Keil, Zeits. f. Metallkunde **25**, 104 (1933).
[4] B. V. Rollin, Phys. Rev. **55**, 231 (1939).
[5] Steigman, Shockley, and Nix, Phys. Rev. **56**, 13 (1939).
[6] A. Sagrubskij, Physik. Zeits. Sowjetunion **12**, 118 (1937).
[7] H. A. C. McKay, Trans. Faraday Soc. **34**, 345 (1938).
[8] W. A. Johnson, Trans. A.I.M.E. **143**, 107 (1941).
[9] F. R. Banks, Phys. Rev. **59**, 376 (1941).

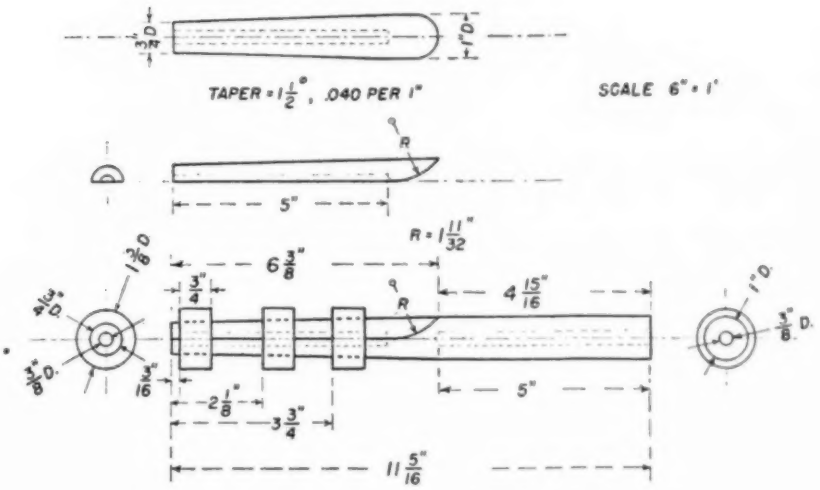

FIG. 1. Spit graphite crucible for growing metal crystals.

vertical temperature gradient of 80°C per cm in a split graphite crucible, shown in Fig. 1, which facilitated greatly their removal. The crystals, cylindrically shaped (⅜ to ½ inch in diameter and about ½ to 1 inch long), were prepared with end faces as plane as possible by a process of alternate etch and polish in such a manner as to ensure no recrystallization on heat treatment. The orientation of the *C* axis with respect to the plane end of the cylinder was determined after heat treatment from the gnomonic projection of a back reflection Laue photograph. Figure 2 is a typical projection, and the intersection of the three planes in the zone of the *C* axis gives the orientation directly with an accuracy of 0.5°. The polycrystalline samples were cast, then heat treated at 380°C for several hours, and the plane ends prepared as in the case of the single crystals. The grain size was about 0.05 inch, or about 12–15 grains per end of the cylinder.

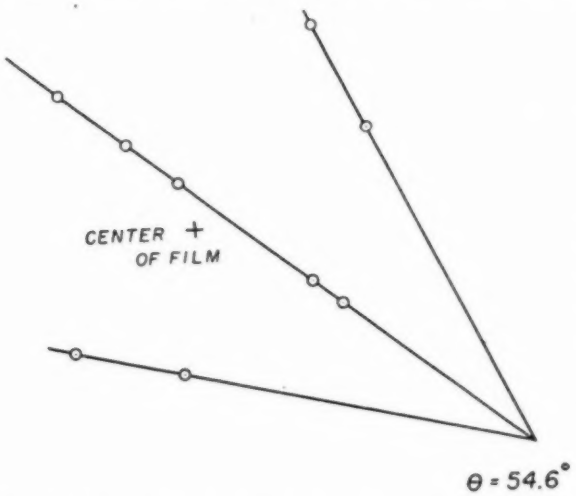

FIG. 2. Gnomonic projection of a back reflection Laue photograph used in measurement of crystal orientation.

The sides of the samples were masked with wax before electroplating from Zn^{65} solution[9] (either cyanide or chloride) with some nonactive zinc present as carrier. The samples were sealed off in a Pyrex tube for heat treatment. In those heat treated by H. Day the temperature control was good to 0.1°C while for those heat treated by Miller and Lasof the temperature variation was 2°C. The time of heat treatment (6 to 75 hours) was selected so that the last section (usually the eighth) had an activity of one-fourth of the background, enabling a reasonable accuracy to be obtained without unduly long counting times.

The sections, usually eight, were turned in a lathe after the diffusion interface had been set perpendicular to the axis of rotation. Sections approximately 0.002 inch thick were removed; the exact thickness was determined from the weight of the sample, the known density of zinc (taken here to be 7.10 g/cc), and the area of the face from which the sections were turned. General freedom from edge effects was ensured by turning off the cylindrical surface of the crystal to a depth of 0.015 inch before the sections were removed.

The activity of each section was measured

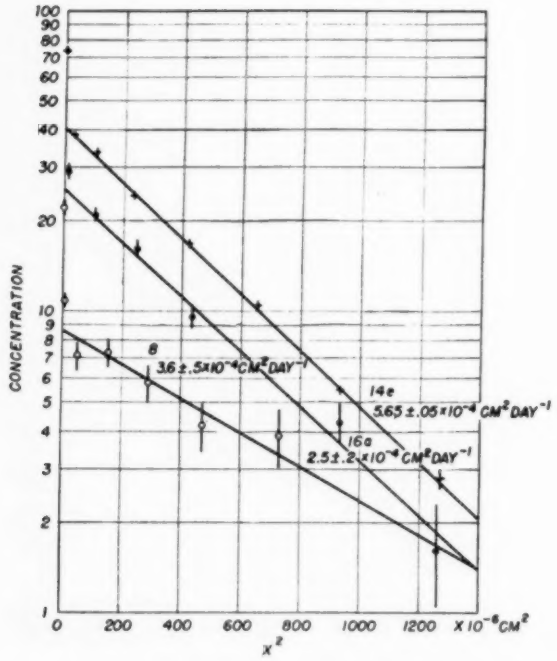

FIG. 3. Logarithm of concentration in arbitrary units *vs.* the square of the average distance of the sections from the diffusion interface. The length of the vertical lines through the experimental points represents the probable error based on the square root of the total number of counts. Lines 14*c* and 16*a* and 8 are examples of typical measurements of the three classes A, B, C.

with a Geiger-Mueller counter. Care was taken to place the turned sections for a particular crystal in the same position relative to the counter. Two separate series of measurements on the same crystal gave identical values of Dt within an experimental error of 2 percent, indicating that errors from this source are negligible. The total activity after heat treatment was about 300 counts per minute above the background of 15 counts per minute. About 2400 counts per section were taken, and thus the precision ranged from about two percent for the first section to ten percent for the last.

The appropriate solution of the diffusion equation

$$\partial c/\partial t = D(\partial^2 c/\partial x^2)$$

when there is no evaporation from or blocking at the surface on which has been deposited a negligibly thin layer of total activity c_0, is

$$c = c_0(\pi Dt)^{-\frac{1}{2}} \exp(-x^2/4Dt);$$

c is the concentration of the Zn^{65}, t is the time of heat treatment, x the axial coordinate in the sample, and D the diffusion coefficient. If $\ln c$ is plotted against $(\bar{x})^2$, which represents the square of the average distance of the section from the diffusion interface a straight line results of intercept $-\ln c_0(\pi Dt)^{-\frac{1}{2}}$, and of slope $-1/4Dt$. Thus Dt is obtained directly from the graph.

RESULTS

The experimental results are shown in Table I. The value of D is obtained by least-square methods in which all the experimental points except the first in the $\ln c$ *vs.* x^2 plot are used. The accuracy is arbitrarily put in one of three classes: A, 0 to 3 percent; B, 3 to 10 percent; C, 10 to 20 percent. All crystals having a total activity of at least 300 counts per minute are in classes A and B. Some of the crystals having a smaller total activity, whose last section possesses an activity which is a small fraction of the background, are in class C. Figure 3 is a typical curve for each of the three classes.

TABLE I. Data on crystals.

Point No.	D	$1/T$		Accuracy	Grown and heat treated
1	9.9×10^{-4} cm² day⁻¹	1.463×10^{-3} c⁻¹	90°	*B*	H. Day
2 *a*	7.9	1.485	90°	*B*	H. Day
b	7.7			*B*	H. Day
3 *a*	4.5	1.544	90°	*A*	H. Day
b	4.3			*A*	
4 *a*	4.0	1.567	90°	*C*	H. Day
b	3.6			*B*	
5 *a*	2.5	1.592	90°	*B*	H. Day
b	2.7			*C*	
6 *a*	10.0	1.480	70°	*B*	P. Miller and
b	8.0			*C*	S. Lasof
7 *a*	5.1	1.527	70°	*B*	P. Miller and
b	5.4			*C*	S. Lasof
8	3.6	1.557	70°	*B*	P. Miller and S. Lasof
9	3.0	1.528	15°	*B*	P. Miller and S. Lasof
10	5.0	1.528	60.5°	*B*	P. Miller and S. Lasof
11	2.2	1.582	46°	*B*	P. Miller and S. Lasof
12	1.0	1.645	54.5°	*B*	P. Miller and S. Lasof
13 *a*	1.0	1.458	90°	*C*	H. Day
b	1.1			*C*	
c	1.6			*C*	
d	1.6			*C*	
14 *a*	4.2	1.523	Poly.	*A*	H. Day
b	4.8			*B*	
c	5.5			*A*	
d	6.1			*A*	
e	5.6			*A*	
f	5.7			*A*	
15 *a*	3.5	1.575	Poly.	*B*	H. Day
b	2.2			*B*	
c	2.3			*B*	
16 *a*	2.5	1.609	Poly.	*B*	H. Day
b	1.2			*B*	
c	1.6			*B*	
17	9.8	1.475	Poly.	*A*	P. Miller and S. Lasof
18	3.1	1.536	Poly.	*A*	P. Miller and S. Lasof
19	2.3	1.595	Poly.	*B*	P. Miller and S. Lasof

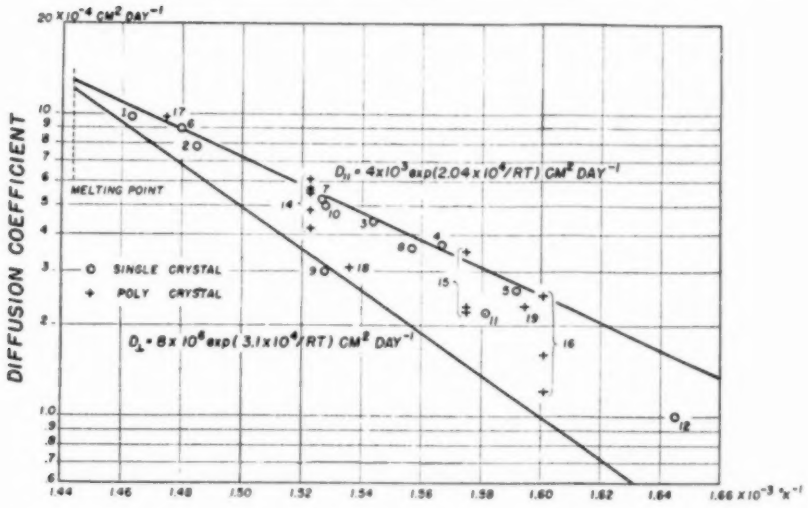

FIG. 4. Logarithm of diffusion rate *vs.* the reciprocal of absolute temperature. Points 1 to 5 (see Table I) are for crystals with the *c* axis parallel to the direction of diffusion and should lie on the upper line. Points 6 to 12 are for crystals with random orientation. Points 13*a* to 13*d* were not shown, since they were discarded from the calculations because of their large experimental error. Points 14 to 19 are for polycrystals. Their large spread of values for a fixed temperature results from their large grain size.

The diffusion coefficients are assumed to have the following temperature dependence:

$$D_1 = A_1 \exp(-Q_1/RT)$$

and

$$D_2 = A_2 \exp(-Q_2/RT),$$

where D_1 represents the diffusion coefficient parallel to the C axis, D_2 that perpendicular to the C axis, A_1 and A_2 are the respective activation constants, and Q_1 and Q_2 the respective activation energies. If the C axis is inclined at an angle θ to the diffusion interface the observed value of the diffusion constant is

$$\ln D_{\text{obs}} = -(Q_1/RT)\sin^2\theta - (Q_2/RT)\cos^2\theta + \sin^2\theta \ln A_1 + \cos^2\theta \ln A_2.$$

The twelve points (number 1 to 12, Table I) were used to determine the values of Q_1, Q_2, A_1, A_2. The values obtained, from least-square methods, are

$$Q_1 = 2.04 \pm 0.09 \times 10^4 \text{ cal./mole},$$
$$Q_2 = 3.1 \pm 0.3 \times 10^4 \text{ cal./mole},$$
$$A_1 = 4 \times 10^3 \text{ cm}^2\text{/day},$$
$$A_2 = 8 \times 10^6 \text{ cm}^2\text{/day}.$$

Points 1 to 5 were reported previously[9] and from them the activation energy Q_1 was estimated to be 1.96×10^4 cal./mole, within the possible error as determined by the method of least squares.

DISCUSSION OF RESULTS

Three important sources of error arise in obtaining Dt in the manner described, *viz.*, the effect of evaporation, the effect of blocking on the surface, and non-parallelism of the sections with the diffusion interface. It is found that during heat treatment as much as 30 percent of the activity is lost by evaporation. Calculations indicate that for our value of Dt, with the exception of the first two points, a reasonable straight line is obtained with a slope 3 percent lower than the one obtained if there were no evaporation. If blocking at the surface occurs because of poor contact of the plated zinc on the surface, the first point will be high, but the remaining points will not be affected, as is indicated by the agreement between the experimental and the theoretical curves. In almost every case the fraction of radioactive atoms "stuck" on the surface was less than 10 percent. It is to be noted that blocking or evaporation in an absorption technique would lead to serious error.

After heat treatment it was found that in some of the samples the original plane face was not flat by 0.001 inch. Calculations indicate, never-

theless, that the ln c *vs.* x^2 curve is still a straight line whose slope is not more than 7 percent high for our range of values of Dt.

The total error of a single point, because of the errors just mentioned and statistical fluctuations, does not exceed 10 percent. We agree with Johnson[8] in that the diffusion coefficient can be determined to within one percent provided reasonable care is taken to cut the sections parallel to the accurately plane diffusion surface.

In the polycrystalline samples the total thickness of the sections used was usually 0.016 inch. Therefore, no large change in the effective diffusion constant for a single sample, because of orientation of the individual grains, is to be expected (the grain size was 0.05 inch, as indicated above). Statistical fluctuations from one sample to another are caused by the small number of grains, but the value of the diffusion rate should lie between the values of D_1 and D_2 at the same temperature.

In zinc, a hexagonal crystal, $a=2.67$A and $c=5.04$A at 380°C, the average temperature at which the observations were made. The axial ratio is 1.89, or 15 percent greater than that for a hexagonal close packed lattice, and Q_1 and Q_2 are the same order of magnitude. Thus, the anisotropy is not as pronounced as in bismuth where the diffusion rate near the melting point is a million times more rapid perpendicular to the C axis than parallel to it.[3]

For vacancy diffusion the distance of closest approach for an ion moving past its neighbors, which are at a minimum equilibrium distance of 2.67A, into a hole is 2.31A for motion in the basal plane and 2.40A for motion between basal planes. One would therefore expect the activation energy to be considerably higher for diffusion in the plane of the a axis. From the simple theory[10] we would expect A to be of the order of 10^4 cm^2/day and to be roughly independent of crystal direction, for the value of A depends essentially on the square of the jump distance and the vibrational frequencies of the lattice. Consequently, the difference of 10^3 is rather surprising at first sight. However, thermal vibrations cause the ions to be displaced a considerable amount from their equilibrium positions, and the average displacement is about 8 percent of the distance between nearest neighbors. Since the change in distance during a jump is the same order of magnitude, it follows that the actual motion is very complicated. Furthermore, a jump in the basal plane involves two nearest ions, while one between two basal planes involves four nearest ions. The probability that two ions are favorably displaced because of thermal vibrations and thus encourage a third to make the jump is considerably higher than the probability that four atoms are simultaneously favorably displaced enabling a fifth ion to make the jump. This cooperative phenomena, which Huntington[11] has treated in more detail, might explain the large anistropy in the values of the activation constant. No special significance is attached to the tendency for the anisotropy in the diffusion rate to vanish at the melting point.

[10] R. M. Barrer, *Diffusion In and Through Solids* (Cambridge University Press, 1941), Chapter 6.

ACKNOWLEDGMENTS

We are indebted to Professor Luis W. Alvarez, Radiation Laboratory, University of California, for the gift of radioactive zinc, to the workers of W.P.A. project No. 21637 for assistance, to the Faculty Research Committee of the University of Pennsylvania for grant No. 451, to Professor F. Seitz and to Louis L. Ridenour for their helpful suggestions, to Mr. H. Lister, who prepared the sections for measurement, and to Mr. Gerald Edmunds of the New Jersey Zinc Company, Palmerton, Pennsylvania, for the gift of the 99.999 percent purity zinc from which the single crystals were prepared. We are especially grateful to Mr. Sol Lasof who grew and found the orientation of some of the single crystals (see Table I), and to Dr. Harry M. Day without whose cooperation this investigation would never have been undertaken and who so skillfully prepared and heat treated the accurately oriented, strain-free single crystals and some of the polycrystals (see Table I).

[11] H. B. Huntington, Phys. Rev. **61**, 325 (1942).

Thermal Expansion of Single and Optically Mosaic Zinc Crystals

WILLIAM PAUL STAKER
Department of Physics, State University of Iowa, Iowa City, Iowa
(Received February 24, 1942)

Thermal expansions of sixteen zinc single crystals have been measured in the temperature range, 25° to 100°C by an optical lever method. The dependence on orientation followed the expected cosine-squared symmetry relation. The principal coefficients, parallel and perpendicular to the hexagonal axis, were found to be: $\alpha_0 = 64.2$ and $\alpha_{90} = 14.1 \times 10^{-6}$ per degree C. Slight differences in purity did not affect the values of the expansion coefficients, nor did optically mosaic crystals differ from true singles. Permanent strain lowered the coefficients slightly.

SEVERAL previous determinations of the linear coefficients of expansion of zinc single crystals have been made, but because of poor agreement in these, new measurements were thought desirable. Grüneisen and Goens[1] measured directly the thermal expansion of two crystals of very different orientation and by extrapolation obtained values of the two principal coefficients, α_0 and α_{90}. Their results covered a considerable temperature range. Bridgman[2] also made measurements on two crystals, using an optical lever system and crystals approximately 2.5 cm in length. His temperature range was from 15° to 25°C. His results were approximately ten percent lower than those of Grüneisen and Goens for the same region. Crystal lattice measurements have been made by x-ray methods, and the so-called "lattice-coefficients" calculated, by McLennan and Monkman[3] at low temperatures and Owen and Yates[4] from 20° to 100°C. Measurements by Austin,[5] who used an interferometer method and very small crystals, yielded results varying greatly from those of previous determinations. He used five single crystals in his temperature range of from 0° to 350°C.

An optical lever system was used in the present work because of its extreme sensitivity, accuracy, and ease of use. Not only is a large magnification easily obtainable, but there is an additional advantage due to the fact that long specimens can be used. The crystals were from nine to twelve centimeters in length. The apparatus was designed also to do away with any excess handling of the crystals previous to the measurement, such as cleaving, or smoothing of the surface. Since it was the differential expansion between a fused quartz rod and the zinc crystals that was measured, the value of α for the zinc was obtained by adding to the observed value the linear expansion coefficient of the quartz, 0.5×10^{-6} per degree C. The apparatus is shown in Fig. 1. Small collars *B* were fitted to the crystals and held by three small set screws. A collar was put over each end of the

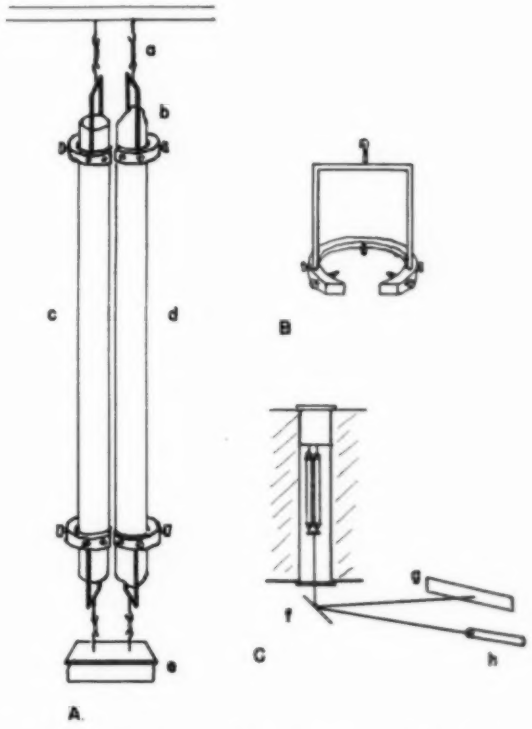

FIG. 1. Arrangement of apparatus. A. Crystal, *d*, and quartz rod, *c*, suspended side by side; mirror, *e*. B. Detail of collar. C. Sketch of complete assembly.

[1] E. Grüneisen and E. Goens, Zeits. f. Physik **29**, 141 (1924).
[2] P. W. Bridgman, Proc. Am. Acad. **60**, 305 (1925).
[3] J. C. McLennan and R. J. Monkman, Trans. Roy. Soc. Can. [3] **23**, 255 (1929).
[4] E. A. Owen and E. L. Yates, Phil. Mag. **17**, 113 (1934).
[5] J. B. Austin, Physics **3**, 240 (1932).

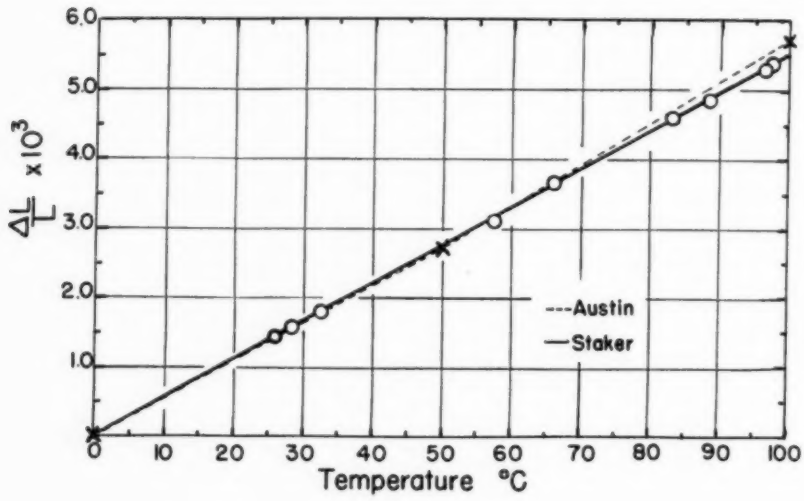

FIG. 2. Change in length per unit length at 0°C, as function of temperature. The x's and broken line are Austin's data for a 0° crystal. The circles and solid line are the writer's for a 24.4° crystal.

crystal *d* Fig. 1A, and by means of a small hook and small wire loops *a* the crystal was suspended from a cross-bar in the furnace. The fused quartz rod *c* was suspended in like manner. The collars were flattened on one side in order that the crystal and quartz rod could hang as close as possible without touching. From the hooks on the collars at the lower end of the crystal and quartz rod there was hung a small plane mirror, *e*, by means of loops attached to hooks in the mirror holder. The image of a scale *g* Fig. 1C, was observed in the mirror by means of a telescope *h*. A magnification of 480 was realized with a light path from scale to mirror of 234 cm and lever arm of mirror equal to 0.975 cm. The bottom of the furnace had a glass plate covering it. Below this was a plane mirror *f* set at 45° with the horizontal to reflect the light in from the scale and then out again to the telescope. With this magnification there was at the highest temperature, a total scale deflection of approximately 5 cm for the high orientation crystals and as much as 20 cm for the low orientation crystals. This corresponds to a total expansion of about 0.1 mm for the high orientation crystals and 0.5 mm for low orientations. If we assume that the scale could be read accurately to 0.2 mm, the corresponding error would be 0.4 percent for the high orientation crystals, or 0.1 percent for the low orientations. Otherwise stated, the $\Delta L/L$ corresponding to 0.2 mm scale reading is 4×10^{-6}.

The collars and all metal parts used were made symmetrical in order to avoid any possible error. To remove any possibility of extraneous effects due to uneven expansion of the furnace and base, the average of two runs was used between which the crystal and quartz rod were interchanged.

Chromel-alumel thermocouples were used with a Leeds and Northrup type K potentiometer to determine the temperature. Because of the length

TABLE I. Summary of results.

No.	Material	Condition	Orientation	$\cos^2\theta$	Observed α_θ ($\times10^6$)	Calculated* α_θ ($\times10^6$)	Deviation ($\times10^6$)
1	BH^3	mosaic	90.0°	0.000	13.9	14.1	0.2
2	BH^3	mosaic	84.1	.0106	14.2	14.6	0.4
3	BH^3+Cd	single	80.3	.0284	15.7	15.5	0.2
4	BH^3+Cd	single	76.0	.0586	17.0	17.0	0.0
5	BH^3+Cd	mosaic	75.5	.0625	17.05	17.2	0.15
6	BH^3	mosaic	72.3	.0924	18.7	18.7	0.0
7	BH^3	single	70.6	.110	19.5	19.6	0.1
8	BH^3	single	58.5	.273	27.7	27.8	0.1
9	BH^3+Cd	single	51.9	.381	33.2	33.2	0.0
10	HH	mosaic	44.5	.510	39.2	39.6	0.4
11	BH^2	single	28.2	.776	52.5	52.9	0.4
12	BH^2	single	27.0	.794	53.8	53.9	0.1
13	BH^3	single	25.1	.820	54.9	55.2	0.3
14	BH^3	single	24.4	.829	55.5	55.6	0.1
15	BH^3	mosaic	23.7	.838	57.1	56.0	1.1
16	BH^3	single	22.0	.859	57.8	57.1	0.7
9**	BH^3+Cd	single	51.9	.381	31.1	33.2	2.1
17**	BH^3	mosaic	55.3	.324	28.1	30.3	2.2
17***	BH^3	mosaic	55.3	.324	29.1	30.3	1.2

* $\alpha_\theta=\alpha_{90}+(\alpha_0-\alpha_{90})\cos^2\theta$; $\alpha_\theta=(14.1+50.1\cos^2\theta)\times10^{-6}$.
** Strained.
*** Annealed.

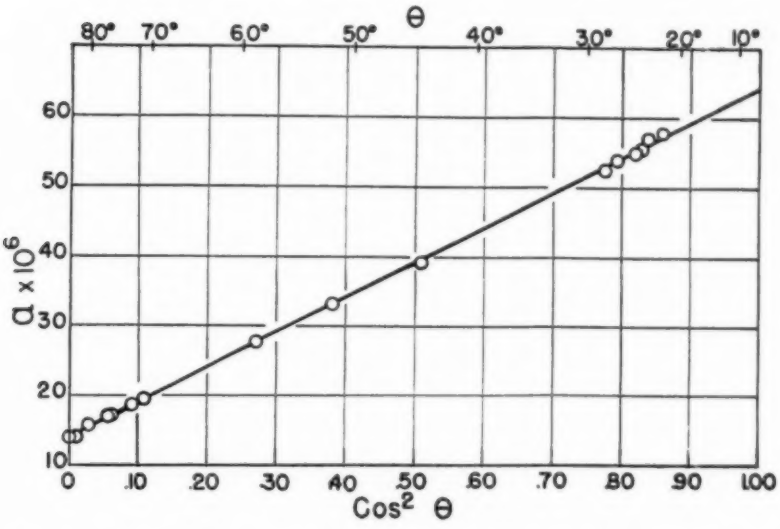

FIG. 3. Mean coefficients of expansion (25°–100°C) of sixteen crystals as function of square of cosine of orientation angle.

of the specimen, two thermojunctions were used, one placed near each collar on the crystal. The temperatures at these two points rarely differed by more than 0.25°C, and since different localities along the crystal showed no greater variation, the average of these two points was considered to be the temperature of the specimen.

Each run consisted of readings taken at five or six temperatures from room temperature up to 100°C and back again. Each rising temperature reading was made by increasing the furnace current an appropriate amount and then waiting until temperature equilibrium was surely reached, a matter of several hours. Readings with falling temperatures were taken similarly. The two sets of readings, when plotted, lay within experimental error, on the same straight line. (See Fig. 2.) The expansion coefficient was computed from the slope of this line. A complete run took about twenty-four hours.

Measurements were made on sixteen crystals of various lots of zinc. Details are given in the second, third, and fourth columns of Table I. The designations BH[2] and BH[3] refer to two lots of Bunker Hill[6] zinc; BH[3]+Cd means that approximately 0.2 percent cadmium was added to the zinc; HH stands for Horsehead special zinc;[6] mosaic indicates that the crystals were "optical mosaics."[7] The specimens made of BH[3] zinc were circular in cross section and were grown by a modified Bridgman method, as described by Good.[8] The BH[2] and HH specimens were trapezoidal in cross section and were grown by Professor E. P. T. Tyndall by the method described by Cinnamon.[9]

The measurements are summarized in Table I and are shown graphically in Fig. 3. The inter-

TABLE II. Mean principal expansion coefficients.

Observer	α_{90} (×10⁶)	α_0 (×10⁶)	Method	T (°C)
Staker	14.1	64.2	Optical lever	25 to 100
Grüneisen and Goens	14.1	63.9	Direct measure	20 to 100
Bridgman	12.6	57.4	Optical lever	15 to 25
Owen and Yates	14.3	60.8	X-ray	20 to 100
Austin	19.0	57.0	Interferometer	0 to 100
Grüneisen and Goens	9.4	65.0	Direct measure	20 to −180
McLennan and Monkman	11.3	49.5	X-ray	18 to −190

[6] Bunker Hill and Horsehead special are commercial zincs of very high purity (about 99.99 percent zinc). For some estimate of impurities in BH[3] and HH see H. E. Way, Phys. Rev. **50**, 1181 (1936) and A. W. Hanson, Phys. Rev. **45**, 324 (1934).

[7] H. K. Schilling, Physics **5**, 1 (1934), and W. J. Poppy, Phys. Rev. **46**, 815 (1934).

[8] W. A. Good, Phys. Rev. **60**, 605 (1941).

[9] C. A. Cinnamon, Rev. Sci. Inst. **5**, 187 (1934).

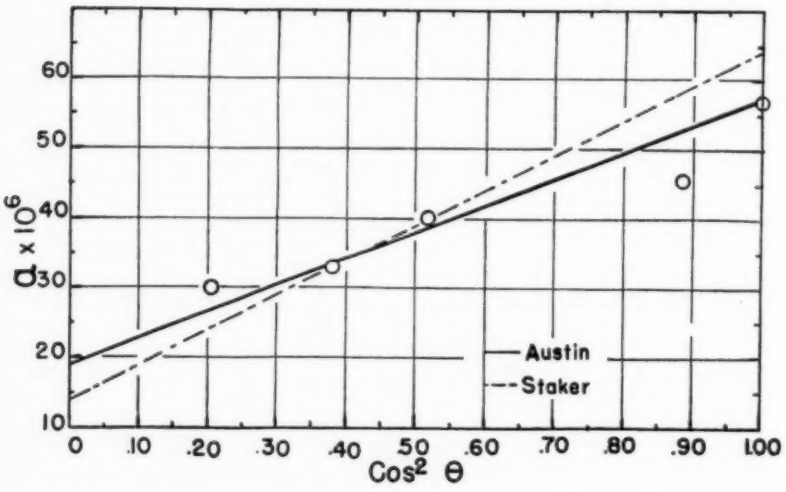

FIG. 4. Mean coefficient (0°–100°C) as determined by Austin as function of square of cosine of orientation angle. The dotted line is the writer's line of Fig. 3.

cepts of the line, 14.1×10^{-6} and 64.2×10^{-6}, are α_{90} and α_0, respectively. The line was fitted to the data by the method of least squares. It may be seen in Table I that the observed values lie very close to the line. The largest deviation is 1.1×10^{-6} for crystal No. 15. The mean (absolute) deviation is 0.27. No significant difference is evident between the various lots of zinc nor for the crystals which contained cadmium, nor for those which were optically mosaic.

The coefficient of expansion for a crystal (No. 17) known to have been strained was also found. It was 28.1×10^{-6}, but, after annealing, rose to 29.1×10^{-6}. In order to get an independent check on this supposed effect of strain, another crystal (No. 9), which had originally given a value falling on the line, was strained. After straining, it gave a value of 31.1×10^{-6} instead of the original 33.2×10^{-6}.

The present and previous results are summarized in Table II by giving the two mean principal thermal expansion coefficients, α_0 and α_{90}, for the temperature ranges indicated. The writer's results agree most closely with those of Grüneisen and Goens. Although Bridgman's results are lower, the ratio of principal coefficients is the same ($\alpha_0/\alpha_{90}=4.55$). The fairly good agreement with Owen and Yates seems to indicate that the lattice expansion and macroscopic expansion are not significantly different. Moreover, what difference there is may perhaps be ascribed to the fact that the x-ray measurements were made on filings of the polycrystalline material and there might well be, under such circumstances, enough constraint to reduce the large expansion parallel to the axis, particularly as this is the direction of lowest Young's modulus. The present results do not throw any direct light on the large disagreement of McLennan and Monkman with Grüneisen and Goens for low temperatures. The writer's disagreement with Austin, whose work was done by a very sensitive method and apparently with great care, warrants some discussion. Austin's data for the temperature range 0° to 100°C are plotted in Fig. 4. By comparison with Fig. 3, it is seen that his results are more scattered than the writer's. Austin also considered his results to show that the mean coefficients of expansion, taken for successive 50° intervals, alternately increased and decreased. The writer found no such effect between room temperature and 100°C. This is shown in Fig. 2, in which the three points indicated by x's are Austin's values of $\Delta L/L$ for a zero-degree orientation crystal. These determine two straight lines with a noticeable difference in slope, whereas the writer's points (0) for a 24° crystal lie, within experimental error, on a single straight line. No run on any crystal showed any sign of a noticeable difference in slope between the low and high temperature ends. The writer believes that the two largest sources of error in Austin's work were

the use of such short lengths and the complicated method used to measure temperature. His measurements were of the transverse expansion on crystal rods 2.5 mm in diameter.

In conclusion, the writer wishes to express his sincere appreciation to Professor E. P. T. Tyndall for suggesting this problem and for his encouragement and advice throughout the work.

MAY 1 AND 15, 1942 PHYSICAL REVIEW VOLUME 61

Field Emission from Tungsten and Thoriated Tungsten Single Crystals*

J. H. DANIEL
George Eastman Research Laboratories, Massachusetts Institute of Technology, Cambridge, Massachusetts
(Received March 13, 1942)

A reproducible time sequence of different pattern types has been found to appear in electron projector images of field emission from tungsten single crystals when the crystals are kept at temperatures above 1100°K. These pattern types, some of which have been observed before and attributed to migrations of surface tungsten atoms, can best be explained (with a single possible exception) as the result of rearrangement of adsorbed gas atoms on certain crystallographic surface areas under the influence of temperature and field. Their classification by means of their relation to surface conditions provides a sensitive test for a clean tungsten surface. The relative variation of emission intensity with crystallographic direction observed in thermionic emission is duplicated in field emission from clean tungsten, but the magnitudes of the variations are greater in field emission. These magnitudes seem to be greater than can be accounted for by the dependence of field emission on the exponential third power of work function which is indicated by some experiments. Such experiments in turn are at variance with theory, which predicts only an exponential three-halves power dependence. Attempts to extend electron projector methods of investigation to the simple composite surface of thorium on tungsten have uncovered no positive tests for surface conditions. Distinctly different types of field emission patterns were obtained from thoriated points formed from thoria-incorporated tungsten wire than from points of pure tungsten upon which thorium was evaporated externally. These differences disappeared, however, when the former patterns transformed into the latter after outgassing of the points for one or two hours at temperatures between 2700°K and 2900°K. In this final pattern, thorium adsorbs chiefly on the regions around but not including the 100 direction, and on a triangular region about and including the 111 direction. Once deposited, the thorium could not be completely removed from the tungsten surface.

INTRODUCTION

WHEN applied to the Fermi-Sommerfeld picture of a metal, the conception of wave mechanical penetration by electrons of a surface potential barrier lowered and thinned by an intense, externally applied, electrostatic field leads to the field emission equation first derived[1] by Fowler and Nordheim:[2,3]

$$J = 1.55\times10^{-6}(F^2/w)10^{-2.98\times10^7(w^{\frac{3}{2}}/F)\phi(y)}. \quad (1)$$

In this equation J is the field emission current density in amperes per square centimeter, F the surface potential gradient in volts per centimeter, w the work function[4] in electron volts, $y=3.62\times10^{-4}(F^{\frac{1}{2}}/w)$, and $\phi(y)$ is a function containing the ratio of two elliptic integrals which has been tabulated for values of y from 0 to 1 by Nordheim.[3]

Although the general features of Eq. (1) have been confirmed experimentally,[5-8] difficulties resulting from the extremely high surface fields required have prevented conclusive establish-

* Part of a thesis presented for the degree of Doctor of Science, from The Department of Physics, Massachusetts Institute of Technology, October, 1940.

[1] Errors in the original derivations may be avoided by consulting the complete derivation given in A. Sommerfeld and H. A. Bethe, *Handbuch der Physik* (1934), Vol. 24, Part 2, Sec. 3, Art. 19, p. 436.

[2] R. H. Fowler and L. Nordheim, Proc. Roy. Soc. **A119**, 173 (1928).

[3] L. Nordheim, Proc. Roy. Soc. **A121**, 626 (1928).

[4] Defined as the difference in potential energy of an electron in the highest occupied energy level allowed by quantum statistics at 0°K, and that of the electron when removed from the metal and carried to a distance large compared to the lattice constant, so that the image force becomes practically zero, but small compared to the dimensions of the crystal face.

[5] E. W. Müller, Zeits. f. Physik **102**, 734 (1936).

[6] J. E. Henderson and R. K. Dahlstrom, Phys. Rev. **55**, 473 (1939).

[7] F. R. Abbott and J. E. Henderson, Phys. Rev. **56**, 113 (1939).

[8] G. M. Fleming and J. E. Henderson, Phys. Rev. **58**, 887 (1940).

ment of the power to which w is raised in the exponential term.[5, 9–12] The variation of field emission with crystallographic direction seems to be larger than can be accounted for by the corresponding work function variation with crystallographic direction, if the work function dependence given in Eq. (1) is assumed.[10, 11]

Finally, changes occurring at high temperatures in patterns produced by field emission from single crystals in electron projectors have recently been attributed[9, 11] to changes in the position distribution of metallic surface atoms caused by the large electrostatic forces involved. The experiments reported here describe such pattern changes as were found reproducible with tungsten single crystal surfaces. They indicate that, with one possible exception, these changes are due to position changes of impurity atoms adsorbed on the surface rather than to position changes of surface tungsten atoms.

EXPERIMENTAL PROCEDURE

A. Apparatus and Vacuum Technique

The type of tube used is shown in Fig. 1. Following the suggestion of K. K. Darrow,[13] it will be called an "electron projector." With several thousand volts on the collector ring, field emission electrons, proceeding radially through the high field immediately about the point, strike the fluorescent screen (whose potential is maintained slightly below that of the collector ring by secondary emission) and thus produce on the screen a highly magnified emission image of the surface of the point, bright regions corresponding to areas of large emission from the point. The construction of the fluorescent screen and its treatment with a potassium silicate coating have been described in detail by Martin.[14] The high voltage used to produce the field in quantitative measurements was held constant to better than 0.01 percent by an electronic voltage stabilizer of the amplification-bridge type described by Hunt and Hickman.[15]

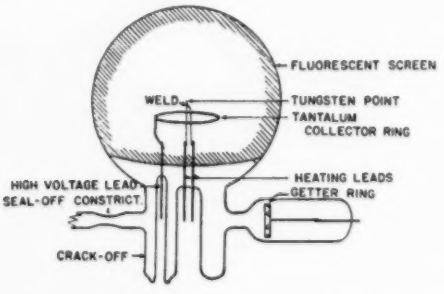

FIG. 1. Spherical electron projector.

To obtain projector patterns at all stable, vacua of 10^{-8} mm Hg or better were essential. Because of the extreme dependence of field emission on vacuum conditions,[7] great care was taken in the preparation of glass and metal parts. An evacuation schedule (on a mercury diffusion pump backed by a mercury jet pump and a mechanical pump) similar to that described by Nottingham[16] was used, with alternations between oven-baking (at 500°C) and metal outgassing (liquid nitrogen having been placed around the liquid-air trap with the tube oven hot) continuing until the pressure read by an ion gauge failed to improve. The tubes were gettered with Ba-Al getter, and special attention paid to long and thorough outgassing of the getter ring and to pre-heating of the seal off constriction (losing one-half its cross section) before sealing the tube off. After standing for about twelve hours, tubes sealed off with the ion gauge attached showed pressures as low as 5×10^{-9} mm Hg.

B. Preparation of Points

Electrolytic etching of the end of a 0.003-inch diameter General Electric "218" tungsten wire in a 30 g/liter NaOH solution to produce a sharp, microscopically smooth point seemed to give superior and more reliable results than chemical etching with molten sodium nitrite. The use of 60-cycle a.c. seemed to give more uniform macroscopic shapes than could be obtained with d.c. The initial determination of proper conditions was a matter of somewhat tedious trial and error. Excellent and consistent results were obtained by using 4.4 volts, 60 cycles, applied through a

[9] E. W. Müller, Zeits. f. Physik **108**, 668 (1938).
[10] E. W. Müller, Naturwiss. **49**, 820 (1939).
[11] M. Benjamin and R. O. Jenkins, Proc. Roy. Soc. **A176**, 262 (1940).
[12] R. Haefer, Zeits. f. Physik **116**, 604 (1940).
[13] K. K. Darrow, Rev. Sci. Inst. **12**, 53 (1941).
[14] S. T. Martin, Phys. Rev. **56**, 947 (1939).
[15] F. V. Hunt and R. W. Hickman, Rev. Sci. Inst. **10**, 6 (1939).
[16] W. B. Nottingham, J. App. Phys. **8**, 762 (1937).

20-ohm resistor in series with the electrolytic cell. Figure 2 shows typical points.

Although these points could be made so fine as to be unresolved by the microscope (magnification 315×), heating[17] to 2900°K for several minutes in vacuum always dulled them to estimated diameters of about 4 to 10×10^{-5} cm. Observations of the voltages required to produce given currents in projection tubes indicated by their reproducibility that if a point were flashed at 2900°K for a minute, it could be held at 2600°K for long periods without altering its diameter or shape. The relative sizes and intensities of crystallographically identical parts of the projector pattern were good indicators of symmetry of point shape. Heating the point for long periods (of the order of ten hours) at 2700°K was found to remove asymmetries without appreciably changing the diameter of the point as measured under the microscope, or its emission for a given voltage. About nine out of ten points so constructed proved to be perfect single crystals.

With the aid of the electron microscope, it has been established by Heafer[12] that the surfaces of points thus "heat smoothed" exhibit no faceted structure, and are smooth down to atomic irregularities. These should not affect field emission because of their smallness compared to the surface potential barrier thickness.

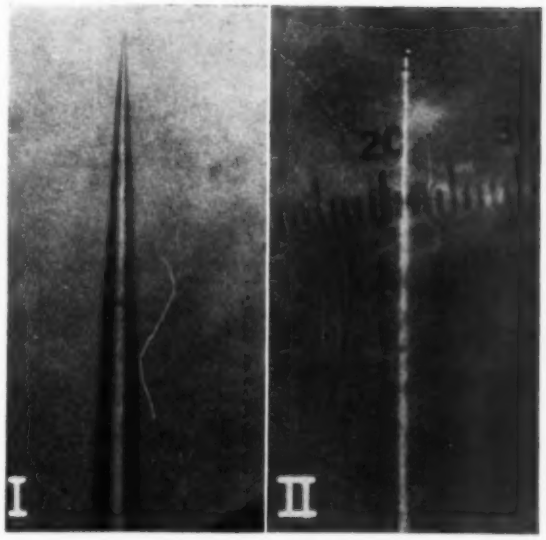

FIG. 2. Top illumination photomicrographs of typical electrolytically-etched tungsten "points." Ten scale divisions = 7×10^{-3} cm. I. Blunt-shaped point immediately after etching. Note glassy-smooth appearance. II. Long, thin point (not the same point shown in I) after heating in vacuum to 3300°K for 4 minutes has produced a ball-like tip. Before heating, the tip was so fine as to be unresolved by the microscope (magnification 315×).

OBSERVATIONS ON TUNGSTEN SINGLE CRYSTALS

Figures 3-I and 3-II show the field emission pattern of an almost clean single crystal tungsten point. The central dark region is along the 110 direction, which normally lies parallel to the axis of drawn tungsten wire. The three smaller dark spots arranged on vertices of an equilateral triangle to the right and also to the left of the 110 region are the 211 directions, with the bright 111 directions of threefold symmetry at the center of the triangles. The two large bright areas immediately above and below the 110 direction are symmetrical about the small 100 dark spots.

The pattern of a clean tungsten surface differs from that of Figs. 3-I and 3-II only in its completely smooth texture, and in the disappearance of the suggestion of dark areas forming a cross which is centered at the 110 spots and connects the adjacent 211 spots. Under the best vacuum

[17] Heating of the point was accomplished by passing current through the point wire and another wire of the same diameter welded on about a millimeter distant from the point tip, as shown in Fig. 1. Temperatures, calculated from the Jones-Langmuir tables [H. A. Jones and I. Langmuir, Gen. Elec. Rev. **30**, 310, 354, 408 (1927)], with the wire diameter and current input, could be checked at the junction of the wires with a micropyrometer. This method cannot be relied upon for wire diameters less than 10^{-3} cm, however, and it is thus impossible to measure the temperature of the emitting surface of the point. This might well be appreciably below that of the junction since the conduction area along the wire decreases as the square of the point radius, while the radiation area decreases roughly only as the first power, and it is chiefly by conduction that the temperature of the tip is maintained against radiation losses. Rough calculation [J. H. Daniel, "Studies of field emission," Sc.D. Thesis, Massachusetts Institute of Technology (1940), Appendix II], with approximations in the direction to increase the effect, show that at worst the temperature drop between junction and tip would amount to 6°, 100°, and 500°K for junction temperatures of 1000°, 2000°, and 3000°K, respectively. Since radiation from the tip has been assumed to take place with the tip at junction temperature, the calculations made for a blackbody, and the effect of Joule heating by field currents as well as the effect of radiation in heating the tip neglected, we can expect this temperature difference for temperatures below 2000°K to be negligible for the purposes of this article. The flashing temperatures quoted, however, since they are uncorrected for any such temperature differences, are probably one or two hundred degrees too high as given. In view of such considerations, Haefer's reported temperature measurements may well be too low, perhaps by several hundred degrees at reported temperatures of 2400°K.

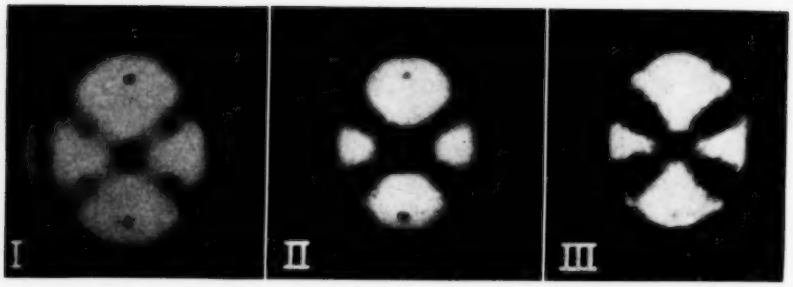

FIG. 3. Field emission patterns from tungsten single crystals at room temperature. I. "Almost clean" pattern. Photograph was taken immediately after "flashing" the point at 2800°K. Exposure time 10 seconds. II. Same pattern as in I, but different crystal and 15-second exposure. III. Pattern of II 30 minutes after flashing.

conditions ever attained in these experiments this clean pattern could be maintained at room temperature only for a period of a second or so immediately after flashing the point at high temperature.

Following this short-lived clean state, a dancing commotion of fine bright spots spreads over the light areas. After a number of seconds this commotion becomes less in evidence, the activity decreasing, and the bright spots appearing somewhat larger. After a minute or less a sort of background with the mottled appearance of Fig. 3-III sets in, and finally, after several minutes, this background becomes fairly stable, with, however, some motion still taking place. After ten minutes or less the pattern appears completely stable insofar as this "atomic" motion is concerned.

If the pattern of a point which has not been previously heat treated be observed between periods of heating at successively higher temperatures, the erratic phenomena of "anomolous" field emission occurring before "blackout," described elsewhere,[18] will appear up to temperatures of 2000°K. Around this temperature, electro-positive surface impurities causing the anomolous emission are removed. The relatively stable patterns occurring immediately after blackout exhibit a large dark region around the 100 direction. This transforms into the brightest region of the pattern of Fig. 3-I only after several minutes heating at 2800°K (see Fig. 4). This same phenomenon, as well as the comparative darkness of the 111 region evidenced in Fig. 4, was noted in Nichols' quantitative measurements of thermionic emission from tungsten as a function of crystallographic direction.[19]

If before such severe heating has caused the area around the 100 to change to a good emitter (and, therefore, presumably while the point surface is strongly contaminated by adsorbed gases, but probably not by electro-positive impurities[18]), the temperature be raised while the field producing the pattern remains on, the following will be observed: At 1100°K, the mottled spots of the pattern begin to stir sluggishly, quickly reaching a state of violent agitation at 1200°K which becomes more and more rapid until smoothed into a restless haze at 1500°K. From 1500°K to 2000°K, where the pattern is finally obliterated by the light of thermionic emission from other parts of the wire, a perfectly smooth appearance is presented. During this temperature rise, however, the striking changes illustrated in Fig. 4 take place. The transfer from the pattern of Fig. 4-II to that of Fig. 4-IIA occurs in the neighborhood of 1150°K. At any time during these phenomena, the existing pattern may be "frozen" in position by reducing the point to room temperature. Figure 4-IIB represents the "freezing" of Fig. 4-IIA, and the mottled aspect again appears. If, however, the field be removed before the temperature is reduced, and then applied again with the point at room temperature, the pattern of Fig. 4-II is found. Such phenomena can be explained by the assumption that surface atoms which change emission properties have one set of more stable positions on the crystal in the absence of the field, and another in its presence, a temperature

[18] J. H. Daniel, J. App. Phys. 12, 645 (1941).

[19] M. H. Nichols, Phys. Rev. 57, 297 (1940).

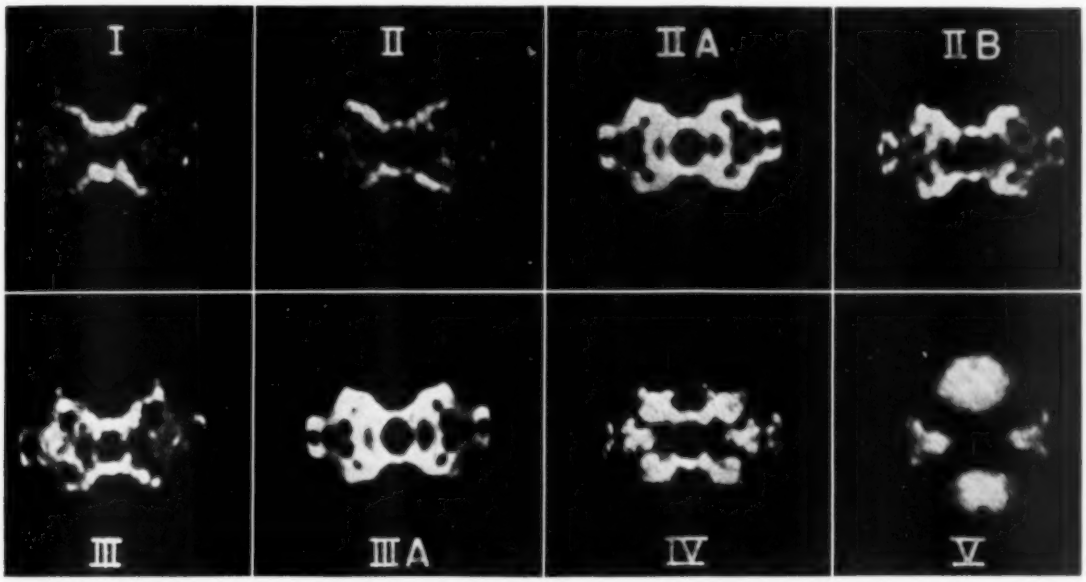

FIG. 4. Field emission patterns illustrating successive stages in "clean up" of a tungsten crystal by heat treatment. Electro-positive impurities were removed by temperatures in excess of 2000°K before the getter was flashed and the tube sealed off. I. Point at room temperature 20 hours after seal off of tube. II. Point at room temperature after 20 seconds at 1700°K and 20 seconds at 2100°K. IIA. Point raised to 1700°K from condition of II. If the field be removed and the point then reduced to room temperature, the pattern of II returns. IIB. Point reduced to room temperature from condition of IIA, field remaining on. If the field now be removed and reapplied, the pattern of IIB will still be found. The pattern of IIA and IIB is designated as the "temperature pattern" of the "normal pattern" II. III. Point at room temperature after 20 seconds at 2600°K. IIIA. Point raised to 1400°K from condition of III. IV. Point at room temperature after 20 seconds each at 2760°K, 2840°K, and 2900°K. V. Point at room temperature after 3 minutes (including 20 seconds in IV) at 2900°K.

of between 1100°K and 1200°K being necessary to allow the atoms to change from one set to the other. That the temperature at which the "reorientation" occurs is so definite is due to the fact that the field necessary for producing a pattern for observation is relatively constant; a slight lowering of the transition temperatures in the case of strong fields is believed to have been detected.

To promote further discussion, a "normal pattern" will be defined as that pattern existing before temperature (in excess of 1100°K) and field have been applied simultaneously; e.g., Fig. 4-II. A "pattern change" is then the change of pattern occurring when temperature and field are applied simultaneously to give what will be defined as the "temperature pattern" corresponding to the normal pattern. Figure 4-IIA (or Fig. 4-IIB) is thus the temperature pattern corresponding to the normal pattern Fig. 4-II. The normal pattern may be returned by heating to 1200°K in the absence of field.

Figures 5-IA, 5-IIA, 5-IIIA, and 4-IIA in that order illustrate the typical time sequence found in temperature patterns. The patterns of this sequence were much more striking in their differences than the corresponding normal patterns.

DISCUSSION

A. Mechanism of Pattern Changes

The change of projector pattern with heating in external field has been attributed[9, 11, 12] to a surface migration of tungsten atoms over the underlying crystal. The following considerations suggest that such changes are due instead to reorientation or migration of surface impurity atoms:

With increasing pressures in the tube, the time sequence of temperature patterns is speeded up, the patterns themselves remaining the same. The pattern of Fig. 4-IIA is obtained easily with points which have not been thoroughly outgassed. With points which have been thoroughly outgassed, this pattern can be obtained only by leaving the point at room temperature for weeks or months. The better the vacuum, the longer the time before the pattern returns.

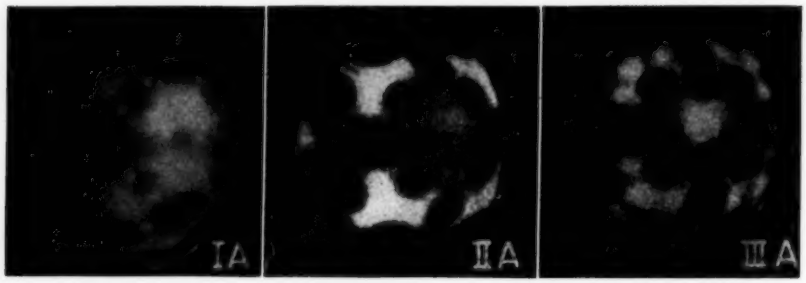

FIG. 5. Time sequence of temperature patterns observed with tungsten crystals. The crystal of this point is unusual in having the 100 region rather than the 110 region near the center of the pattern. The faint dark line running horizontally through the 100 region is an imperfection due possibly to twinning. Areas below this line are displaced slightly to the right of corresponding areas above. The bright 111 region of the threefold symmetry in the extreme left of IIA and IIIA appears where the 100 would be expected if the entire point surface were composed of a single crystal. The crystal boundary was visible in the actual pattern. The pattern of IA offers a striking illustration of how asymmetry of point shape can be detected by the variation in size of crystallographically identical dark spots. IA. Temperature pattern obtained a few seconds after thorough flashing. This pattern would become practically identical to that of clean tungsten if the bright lines connecting the 110 spots to adjacent 211 spots were absent. IIA. Temperature pattern obtained 30 minutes after flashing. IIIA. Temperature pattern obtained 2 hours after flashing. The final temperature pattern of this sequence is that of Fig. 3-IIA, and can only be obtained weeks after flashing.

If the various temperature patterns were caused by migration of tungsten atoms under the influence of temperature and field, rather than by accumulation of adsorbed atoms, comparatively little change in any existing temperature pattern should occur over a reasonable time with the field removed and with the point below 1100°K. Instead, the sequence of temperature patterns proceeds at substantially the same speed whether the point is at room temperature or well above 1100°K, and whether the field remains on or off (i.e., off except when observing the pattern).

If pattern change were due to the migration of surface tungsten atoms under the influence of temperature and field, a temperature pattern well advanced in the time sequence should be present immediately after reducing the point from a high temperature, with field applied, to room temperature. Instead, each flashing, with or without field, for any length of time, starts the pattern sequence over from its beginning.

The dependence of the speed of temperature-pattern sequence on pressure, its relative independence of temperature (below 1500°K) and of field, and the effect of high temperatures (above 2000°K) in returning a temperature pattern occurring early in the sequence—all are consistent with the gas adsorption hypothesis and not easily explained by the tungsten migration hypothesis.

To fit the findings of Benjamin and Jenkins[11] into the picture presented here, it is necessary to conclude that their surface conditions were considerably more stable than those considered here, although total gas pressures are presumably of the same order of magnitude. Total pressure, of course, cannot be relied upon for a true indication of surface condition since the partial pressures of active gases responsible for contamination may be many orders of magnitude less than the total pressure. Recently Moore[20] has shown that the evacuation schedule used here, while excellent for thermionic work, is not suitable for low temperature work. Thus the relatively rapid appearance of successive temperature patterns in the sequence observed here is explained.

Such vacuum conditions made the pattern sequence quite apparent when it might otherwise have escaped attention. They do not allow the arguments (given above) against migration of surface tungsten atoms to be applied with certainty to the pattern of Fig. 5-IA, however, because of the rapid appearance (within about a second under the most stable conditions obtained) of this pattern. Thus the possibility

[20] N. H. Moore, Ph.D. Thesis, Massachusetts Institute of Technology (1941).

that the bright lines of Fig. 5-IA may be due to repositioning of surface tungsten atoms instead of adsorbed gas atoms cannot be excluded on the evidence presented here.

It has been suggested[11] that the crystal-symmetric, step-like structure often observed in projector patterns of field emission is due to etched ridges which are subsequently removed by heating. Such structure was obtained in these experiments (e.g., Figs. 5-IIA and 5-IIIA) from points which had been heated many hours at 2800°K—enough to remove all ridges. It was obtained, however, only with the temperature pattern of gas contaminated surfaces. It might be inferred that such structure occurs because of layer-like gas adsorption on a smooth surface.

It is probable that the large dark region about the 100 direction in early stages of heat treatment (see Figs. 4-I through 4-IV) is due to adsorbed atoms rather than to etching effects which are removed by surface tension at high temperatures. The dark region occurs with points which have not been outgassed in sealed-off and gettered tubes, but which have been thoroughly heat treated previous to sealing off, so that any etched flat surfaces have been removed if they are ever to be removed by heat treatment. The dark region was also observed to return in the space of a month to two points which had been sealed off in a vacuum of not so low a pressure as was usually the case.

B. Other Aspects of Single Crystal Field Emission

On the strength of the adsorbed gas hypothesis, the temperature pattern sequence may be used as a sensitive indicator of surface and of vacuum conditions. From the normal pattern it appears that regions connecting the 110 to adjacent 211 directions are first contaminated. Whether contamination then spreads to the 111 regions and finally to the regions around the 100, as might be suggested by the greatly enhanced temperature-pattern emission from these regions, cannot be determined with certainty until what takes place in the "repositioning" of adsorbed atoms is understood in detail.[21]

Rough tests seemed to indicate that the amount of gas contamination occurring in four hours on a thoroughly outgassed point held at temperatures above 1600°K was not of sufficient importance to affect the total emission more than five percent, although the effect on the projector pattern was quite apparent for temperatures below 2000°K. Points left at room temperature for long periods first showed a rapid decrease (for perhaps half an hour), then a gradual increase (several days) over the "almost clean" tungsten emission.

Aside from any explanation of pattern change, there is the perplexing problem of accounting for the apparently excessive variation in field emission between bright and dark areas of the normal pattern. A quantitative measurement of the emission variation would be more satisfactory than estimates based on the brilliancy of the projector image. However, Benjamin and Jenkins[11] (as well as Müller[9]) have estimated this variation to be of the order of at least 100 to 1, and have given several suggestions in attempting to account for such large variation. In this connection, the following comments are in order: In confirmation of Benjamin and Jenkins' objections to Müller's proposed theory of internal reflection of electrons between the crystal atomic lattice planes, it might be pointed out that in extending the theory to Martin's thermionic pattern for a clean tungsten single crystal, Müller was able to explain results (concerning relative brilliancy in projector patterns of the 110, 211, and 100 directions) attributed to Martin[14] which are not the results Martin obtained, and which are irreconcilable with those results. This theory has never been supported by the discovery of band structure in energy distribution measurements in thermionic, photoelectric, or field emission measurements.

The field emission pattern of clean tungsten is identical in configuration to the thermionic pattern Martin obtained from a polished single-crystal tungsten ball, but the light contrast is much greater. There is also strict qualitative or relative agreement between field emission pattern intensities in various crystallographic directions and the thermionic emission in the corresponding directions determined quantitatively by Nichols.[19] As will be seen in the next section, the transformations produced in the clean tungsten

[21] It might be pointed out, however, that a darkening of these areas does occur in the contaminated normal pattern.

pattern by evaporation of thorium on the crystal are qualitatively the same in thermionic[14] and in field emission. Such agreement[22] may be considered to strengthen the evidence that field emission, like thermionic, is predominantly a surface phenomenon, and not governed by reflection of electrons within the metal.

OBSERVATIONS ON THORIATED TUNGSTEN SINGLE CRYSTALS

A. Experimental

To extend electron projector investigations of field emission to simple composite surfaces, the same tubes described above were used. In two of these were mounted points formed by electrolytic etching from 0.005-inch diameter tungsten wires in which about one percent thoria had been incorporated during manufacture (981328 Westinghouse "B" wire). These points will be referred to as "thoriated tungsten points." The third tube contained a close spaced coil of this 0.005-inch thoriated tungsten wire about an inch and a quarter in length and a tenth of an inch in diameter, mounted just within the collector ring, on the level of the General Electric 218 "pure" tungsten point. Electrical connection and mechanical support were furnished by an extension of one filament lead and by an extra lead incorporated in the tube stem. From this coil thorium could be evaporated externally on more than half the surface of the tungsten point. This type of point will be designated as a "thoriated 218 point."

The vacuum technique described above was again employed, and observations made only on gettered tubes with total pressures less than 10^{-8} mm Hg. As shown above, under such conditions no appreciable contamination takes place on simple tungsten surfaces above 2000°K. It is therefore possible, though by no means certain, that in the 15- or 20-minute period required for activation of thoriated tungsten points (during which the points were held at 2100°K following a "flash" at 2900°K) there was little chance for contamination.

As compared to the simple tungsten patterns described above, all patterns from both thoriated tungsten and thoriated 218 points were remarkably stable. It was not found possible to produce any marked changes by rearrangement of adsorbed atoms upon application of the field at high temperatures. About the only effect ever produced was to form or intensify a sort of dark ring around the 111 region which is evident in Fig. 6-IV.

B. Thoriated Tungsten Points

Figures 6-I through 6-VIII are explained by their captions. Activation for long periods at temperatures below 2100°K produced no essential changes in the patterns. It was found impossible by any amount of flashing to obtain a pure tungsten pattern.

The patterns of Figs. 6-I through 6-V were obtained many times, and were reproducible and comparatively stable until the points had remained at temperatures in excess of 2700°K for a total time of between one and two hours. Then a change took place, and these patterns were not again obtained. Instead, the pattern of Fig. 6-VIII appeared. As will be seen presently, this is the same pattern as was obtained from thoriated 218 points. Figures 6-VI and 6-VII show transition stages. Such a transition suggests the elimination, by a process of decomposition and diffusion to the surface, of metallic impurities which are not present in the 218 wire.

C. Thoriated 218 Points

In evaporating thorium on the pure tungsten 218 point, a schedule developed by Coomes[23] to give an oxygen-free layer of thorium, and one to give an oxygen-impregnated layer were used. Differences in resulting patterns were too minor to warrant any conclusions.

Before the evaporating coil had been raised

[22] It appears that Benjamin and Jenkins are not justified in stating that they do not find similar agreement between thermionic and field emission work functions. First, their estimated order of increasing work function based on field emission patterns is actually the order of decreasing field emission intensities, and agrees perfectly with Nichols' experiments if compared with his order of decreasing thermionic emission intensities. Second, in referring to the work function of the 100, 111, and 110 regions, Benjamin and Jenkins must actually mean for what they call the 100 region, the region surrounding the 100 dark spot, since if this spot itself were taken as the 100 region, their order of increasing "work function" would surely have been given as 111, 100, and 110 instead of 100, 111, and 110. However, they compare this region surrounding the 100 spot with Nichols' data for the 100 spot itself.

[23] E. A. Coomes, Phys. Rev. **55**, 519 (1939).

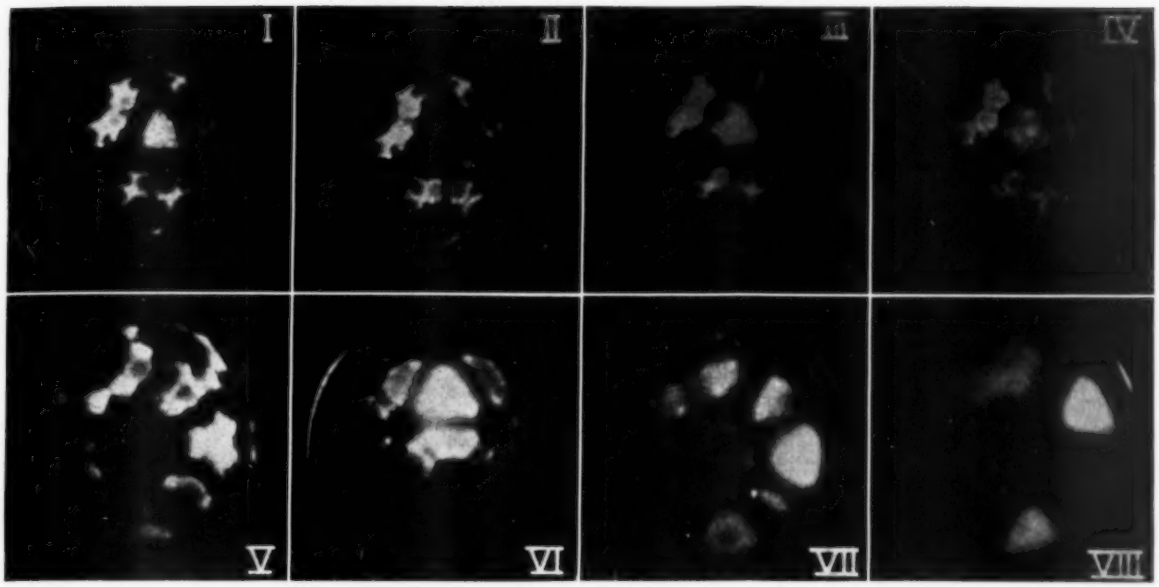

FIG. 6. Field emission patterns from a thoria-incorporated tungsten point which has been activated at 2100°K, thus giving a thorium coverage corresponding to maximum thermionic emission in the polycrystalline state. I. Initial semi-permanent pattern, point at room temperature. The bright 111 triangle is at the center. The three 100 regions resemble dark centers of a daisy with twelve bright radial petals, the four petals bordering the 211 regions being much darker than the rest, so that eight bright petals are symmetrically arranged in four groups of two's (better seen in V). II. Pattern of I after 3 hours at room temperature. The bright 111 region has been completely blacked out. III. Pattern of I after 15 minutes at room temperature. In the meantime the point has been flashed at temperatures in excess of 2700°K for about 10 minutes total. After such treatment, the bright 111 triangle could not be blacked out by long standing at room temperature as in II, but developed instead a six-sided star appearance as in III. IV. Pattern of III when point is raised to 1200°K. The dark circle appearing in the 111 triangle is the only evidence found of anything suggesting a "temperature pattern" differing from the "normal patterns" with thorium coverages. V. A second thoriated tungsten point, not a single crystal, but exhibiting one 100 area and one 111 area, the regions affected by thorium adsorption. The pattern is a late stage of III. VI. Crystal of I at room temperature, showing an early stage of transition to the final permanent pattern of VIII and Fig. 7. This transition occurred after approximately one and one-half hours total at temperatures in excess of 2700°K. VII. Crystal of V showing a later stage of the transition of VI. VIII. Final pattern of crystal of V. Point at room temperature after activation for one hour at 2100°K.

above 1800°K in the presence of the point, simple tungsten patterns with their characteristic time sequence were obtained. After evaporation of thorium, however, attempts to remove it from the point by severe heating[24] gave rise to a pattern not greatly different from that of Fig. 7-I, though with less marked separation of the 111 region into three bright spots. While this pattern was very similar to the normal pattern of contaminated tungsten (Fig. 4-V), it was much more stable, and over a period of days showed none of the striking temperature pattern variations (except for the presence of slight bright ridges along the dark cross connecting the 211 spots through the 110) through which a simple tungsten surface is transformed by adsorption of gases.

[24] Periods as long as 18 hours at 2600°K with intermittent flashes amounting to a total of thirty minutes at 2850°K were tried.

DISCUSSION OF RELATED PHENOMENA

Placed in logarithmic form, Eq. (1) becomes:

$$\log_{10}(I/V^2) = \log_{10}[1.55\times10^{-6}(\beta^2 A/r^2 w)] - 2.98\times10^{7}(rw^{\frac{1}{2}}/\beta V)\phi(y), \quad (2)$$

where I is the field emission current in amperes from an area $A=kr^2$, r being the point radius in centimeters, and k a proportionality constant; V is the applied voltage, giving a surface field $F\doteq\beta V/r$, where β is a constant depending on the shape or smoothness of the point; w is the work function in electron volts; ϕ is a function of $y=3.62\times10^{-4}(\beta V/rw^2)^{\frac{1}{2}}$. Thus a plot of $\log_{10} I/V^2$ *vs.* $1/V$, which will be termed a field emission characteristic, should give a straight line, the

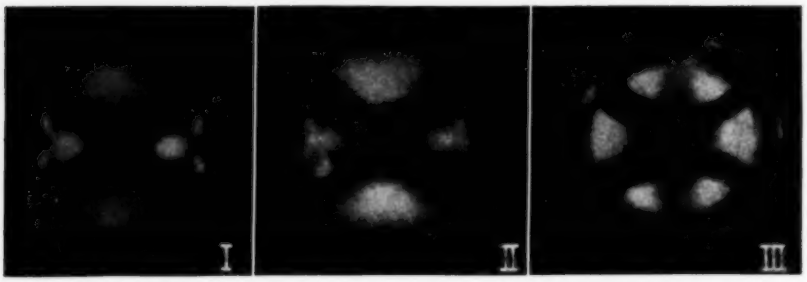

FIG. 7. Field emission patterns from a tungsten single crystal point upon which thorium has been evaporated externally from a coil of thoria-incorporated tungsten wire. Unsymmetrical light flares near the 111 area on the left are caused by stray field emission from the evaporating soil. The evaporation schedule: With point at 1600°K, the evaporating coil is held at 2500°K, flashed at 2850°K for two minutes every three hours. I. After evaporation for 1 hour, point at room temperature. II. After evaporation for 5 hours, point at room temperature. III. After evaporation for 30 hours, point at room temperature.

effect of $\phi(y)$ being, to close approximation, a vertical displacement of the line.[7] The slope is given by:

$$S=\frac{d(\log_{10} I/V^2)}{d\,V^{-1}}=-2.98\times10^7\frac{r}{\beta}\phi(y)w^{\frac{1}{2}}. \quad (3)$$

In an extensive series of experiments, Müller[5] varied w by evaporating layers of different materials on the surface of both points and wires, measured w thermionically, and plotted $\log_{10} S$ *vs.* $\log_{10} w$, where S is the slope of the field emission characteristic obtained for the corresponding value of w. From Eq. (3) this should give a straight line with slope equal to $\frac{3}{2}$. However, for films of Ba, Mg, Th, and O_2 on tungsten, and Cs on WO_3, in thicknesses ranging from zero ("pure" tungsten) to layers having the properties of the "massive" film material, Müller consistently obtained a linear relation with slope magnitude equal to three.[25]

To account for the discrepancy on the basis of a variation in β, it is necessary that β be proportional to $w^{-\frac{1}{2}}$ over the entire range of work function used by Müller—a factor of at least ten in β. Müller ruled out this possibility on the ground that the w^3 law held in the transition from a tungsten surface over to sufficient atomic layers of adsorbed material to give in effect "massive" metal of the material. Under such conditions no orientation or repositioning of adsorbed dipoles, which might give an effective β variation, would be expected.

On the other hand, assuming values for the average work function and width of the Fermi band in tungsten, calculating the field from the shape of the point as observed with the electron microscope, and estimating the emitting area, Haefer[12] found the experimentally obtainable numerical values in Eq. (2)[26] to agree with the theoretical values to within 10 percent. This he takes as confirmation of the $w^{\frac{1}{2}}$ law for pure tungsten. The significance of such agreement becomes less clear in view of Benjamin and Jenkins' finding[11] from a rubber membrane potential model that β may be about $\frac{1}{2}$ instead of unity[27] on account of the presence of the heating wire and the point wire itself.

Haefer's experiments with Ba, K, and Cs layers on tungsten appear to confirm the $w^{\frac{1}{2}}$ law. He suggests that Müller's results were due to crystallite formations of the evaporated materials which effectively altered β, and which he avoided by careful evaporation. In view of the picture of adsorption well-established by thermionic experiments on activation of thoriated tungsten,[28] however, it does not seem probable that such crystallites could exist, unless by "crystallite" is meant a grouping of adsorbed atoms only one

[25] That Ahearn [A. J. Ahearn, Phys. Rev. **50**, 238 (1936); see also footnote 2 of reference 18] found no change in field emission upon activation of a thoriated tungsten wire would seem to indicate that thorium atoms were not present on the sharp irregularities which must have comprised the emission centers.

[26] A simplified equation was used.

[27] β = unity for a geometrically perfect and microscopically smooth sphere.

[28] I. Langmuir, J. Frank. Inst. **217**, 543 (1934).

atom thick in the dimension perpendicular to the surface. There is good evidence[29] that such a grouping (patch effect) does exist, particularly at low temperatures, and it seems to offer an explanation of the "mottled" pattern aspect often observed with adsorbed layers.[30] However, because of the small thickness of such a group relative to the thickness of the surface potential barrier, it does not seem probable that such atomic irregularities could affect field emission through a local intensifying of field (or change in β).

It is difficult to see how the apparently excessive variation of field emission with crystallographic direction could be directly concerned in giving a high exponent for w in Müller's experiments. However, there are objections to all field emission experiments so far reported which, though they might not be expected to have great influence on the results, nevertheless should be removed in order to establish conclusively the exponent of w in Eq. (1). Müller's measured thermionic work function presumably did not apply to the comparatively minute single-crystal area giving rise to field emission, but rather to a much greater area. Haefer used values from the literature for w which were obtained for large polycrystalline surfaces. Nichols has found[31] that the average thermionic work function of a single crystal wire differs from that of a polycrystalline wire. Measurements should be made under proper vacuum and surface conditions upon a well-defined area of a single-crystal surface small enough to have an essentially constant value of w and uniform value of surface field,[32] so that a value of w obtained as a thermionic average will not be compared with one obtained by a field emission averaging process.

The writer wishes to thank Professor W. B. Nottingham for his advice and criticism during the progress of this work, and for his suggestions in the preparation of the manuscript. Grateful acknowledgment is also made to Dr. N. H. Moore for discussion of his recent work in field emission, to Mr. L. W. Ryan for invaluable aid in glass-blowing operations, and to Mrs. E. C. Montague (National Institute of Health) for typing of manuscripts.

[29] W. B. Nottingham, Phys. Rev. **49**, 88 (1936).

[30] Benjamin and Jenkins (see reference 11) give a calculation, based on diffraction effects, which relates the size of a spot on the fluorescent screen of a projector to the number of atomic diameters across the "aperture" of a group of atoms on the point surface which might be causing the spot. Their implicit assumption that the emerging parallel electron beam, at the "aperture" of surface atoms, has a wave-length corresponding to the energy attained after falling through the total potential difference between point and screen, seems unjustifiable.

[31] M. H. Nichols, Phys. Rev. **59**, 944 (1941).

[32] The non-uniformity of field produced by certain types of surfaces has been shown by calculation [C. C. Chambers, J. Frank. Inst. **218**, 463 (1934); also reference 7] to be relatively unimportant, merely introducing a higher power of V in the first term of Eq. (2). This results in a slight curvature of the field emission characteristic, which, as in the analogous case of the effect of the temperature exponent in plots of Richardson's thermionic equation, is difficult to detect experimentally.

The Nature of Reactions Occurring in the Production of the Afterglow of Active Nitrogen and the Effect of Temperature on the Phenomena

DAVID E. DEBEAU
Department of Physics, University of California, Berkeley, California
(Received February 24, 1942)

THE nature of the processes occurring in N_2 activated by high frequency discharge has not been clearly understood owing to the many diverse and apparently contradictory phenomena occurring. Recent work by Lord Rayleigh has thrown important light on the phenomena but has not led to a clear interpretation in terms of reactions. Recent study by the writer of a phenomenon observed long ago by J. J. Thomson,[1] which indicated that one component of active N_2 was frozen out at liquid-air temperature, has led to a picture of the mechanism which accounts for the puzzling observations.

The application of an electrodeless discharge to one of two connected glass bulbs filled with N_2 at a pressure of about 0.5 mm of Hg gives rise to an easily visible yellow green afterglow in the second bulb. At the same time the pressure of the system was nearly doubled with only a slight increase in the temperature of the glass walls. The application of liquid air on the second bulb to less than one percent of the area of the whole system reduces the pressure to the value it had before the discharge was started. The intensity of the afterglow in the immediate vicinity of the cooled surface greatly increases, and then, within thirty seconds, disappears from the entire chamber. After the liquid air has evaporated, the increase in pressure is accompanied by a reappearance of the afterglow, first at the cooled surface then spreading to fill the bulb. A similar set of phenomena was observed when solid CO_2 and acetone were used as the cooling agent. This is what Thomson termed the freezing out of an active component. It is obvious that the pressure differences set up gas currents of considerable magnitude carrying activated nitrogen to the cooled surface.

The pressure changes are too large to be accounted for by the small average temperature changes of the system, but can be attributed to the nearly complete dissociation of N_2 in the discharge. Rayleigh[2] was able to obtain about 10 ev per molecule from active N_2 in interaction with gold. This energy corresponds to that of completely dissociated N_2 with half the atoms in the metastable ^2D and the rest in the normal ^4S state.

The afterglow is known to originate in the high vibrational levels on the $B^3\Pi$ state of N_2 and to result in the formation of metastable $A^3\Sigma$ molecules of nitrogen. Nitrogen in the B state must then be one of the products of the recombination of atomic nitrogen.

The first step in the recombination is the formation of a collision complex.

$$N+N=(NN) \tag{1}$$

If one of the atoms is in the ^2D state and the other in the ^4S, the complex will have 9.84 ev energy above the ground state of N_2, approximately the energy of the levels which give rise to the afterglow.

The collision complex will be destroyed by one of the following mechanisms

$$(NN)=N+N, \tag{2}$$

$$(NN)+M=N_2(B)+M \tag{3a}$$

$$N_2(B)=N_2(A)+h\nu \text{ (afterglow)},$$

$$(NN)+M=N_2(^1\Sigma)+M \text{ (energy dissipated as heat, radiation not in the afterglow region, or in excitation of the third body).} \tag{3b}$$

In general the energy radiated as afterglow is known to be small compared with the energy present in the activated N_2, so that most impacts result in (3b) but the few impacts resulting in (3a) cause the afterglow.

The rapid pressure drop observed after the application of liquid air indicates that the over-all rate of destruction of the nitrogen atoms (reac-

[1] J. J. Thomson and G. P. Thomson, *Conduction of Electricity through Gases*, volume 2 (Cambridge University Press, 1933), p. 444.

[2] Lord Rayleigh, Proc. Roy. Soc. **A176**, 1 (1940).

tion (1)+reaction (3)) increases with *decrease* in temperature. Reactions (1) and (3) are bimolecular and their rates would normally *decrease* with a decrease in temperature. Assuming no change in the rate of reaction (2), we would expect the over-all rate of destruction of nitrogen atoms to decrease with a decrease in temperature. However, if a decrease in temperature greatly increases the lifetime of the collision complex, that is if the rate of (2) is reduced much more than is the rate of (1) there will be a material increase in the concentration of (NN). Thus despite a small decrease in the *rate constant* of reaction (3), a lowering of the temperature will result in a large increase in the total rate of (3) and the destruction of nitrogen atoms with and without radiation to form N_2 and a corresponding decrease in pressure. In what manner the stability of the complex (NN) could be increased as regards spontaneous dissociation as a result of the decrease in energy of the N atoms cannot be specified. It is, however, not unnatural to find that where the heat of formation of a molecule is near the average energy of the components, a small reduction in energy of the components will result in a great increase in the molecule formation. In this system the change in concentration of (NN) is more than sufficient to reverse the expected effect of temperature on the rate of reaction causing a negative temperature coefficient for the over-all reaction.

The changes in the intensity of the afterglow allow us to follow the progress of the reaction. The transitory increase in intensity immediately on cooling is the result of the increased concentration of (NN) and the increased rate of (3a). However, the increased rate of (3) leads to a more rapid destruction of atoms and eventually to a decrease in the concentration of (NN) and the extinction of the afterglow. The reduction in pressure causes a continuous streaming of activated gas to the cooled surface preventing an increase in concentration of atoms until the liquid air evaporates. The afterglow reappears only after the concentration of atoms and of complexes is increased, and appears first at the cooled portion of the chamber where the rate of (3a) is the greatest.

Warming the gas should decrease the intensity of the afterglow without diminishing the concentration of atoms, and therefore the energy available for transfer to a metal surface by reaction (3b) or for excitation of Hg atoms by a collision of the second kind. A dark modification of active nitrogen with these properties has been observed.[3,4]

This picture is in excellent agreement with the high degree of dissociation and activation energy of Rayleigh, the negative temperature coefficient observed by Rayleigh, the data on energy transferred to Hg and other metal atoms by collisions of the second kind, and the available kinetic data.[5,6,7]

The writer wishes to thank Professor Loeb, who suggested this problem and whose helpful guidance was invaluable.

[3] J. Okubo and H. Hamada, Phil. Mag. **15**, 103 (1932).
[4] E. J. B. Willey, J. Chem. Soc., 2837 (1927).
[5] E. J. B. Willey, J. Chem. Soc., 1620 (1928).
[6] E. J. B. Willey, J. Chem. Soc., 336 (1930).
[7] H. O. Kneser, Ann. d. Physik **87**, 717 (1928).

Letters to the Editor

PROMPT publication of brief reports of important discoveries in physics may be secured by addressing them to this department. The closing date for this department is the third of the month. Because of the late closing date for the section no proof can be shown to authors. The Board of Editors does not hold itself responsible for the opinions expressed by the correspondents. Communications should not in general exceed 600 words in length.

Stars and Slow Protons at 14,125 Feet

WILSON M. POWELL*
Kenyon College, Gambier, Ohio
April 6, 1942

A LARGE number of heavily ionizing particles appeared in a Wilson cloud chamber containing five horizontal lead plates each one cm thick. The plates were six cm apart and the gas in the chamber was argon at a pressure such that the range of a particle in the gas is approximately the same as that in dry air at 20°C and 76-cm Hg pressure.

Stars containing heavily ionizing particles appear both coming out of the lead and arising in the gas. Many of the particles start in one lead plate and stop in the next. If there were equilibrium in the chamber, then the ratio of the stars produced in the lead to those produced in the gas should be equal to the ratio of the particles stopping in the lead (i.e., traversing the space between the plates) to those stopping in the gas. These two ratios are found to be 14.7 and 13.2, respectively, which makes them equal to each other well within the experimental error. It can be concluded that equilibrium is established. By multiplying the average path of a particle in the gas, namely 7 cm, by this ratio, we find the average range of the particles to be 100 cm in air. This corresponds to a kinetic energy of about 10 Mev, which agrees closely with the maximum in the energy distribution curve for particles appearing in photographic emulsions left at high altitudes.[1]

The range in lead of a 10-Mev proton amounts to approximately 0.02 cm, and since the plates are one cm thick, the rays of only one star in fifty produced in the plate will appear leaving the lead plate. The average number of particles in a star in the gas is three, and there are probably as many neutrons as ionizing particles ejected. If we assume that it takes about eight Mev to eject a neutron or proton from the nucleus then the total energy necessary to produce an average star is a little over 100 Mev.

In a set of 19,000 pictures there appear 156 stars and 9840 penetrating particles. The penetrating particles make slightly more than two traversals per particle and thus are responsible for 2×10^4 traversals. Since there are fifty stars created inside the lead for one appearing leaving the lead, the total energy for all the stars at 100 Mev per star is $156\times50\times100$ Mev or 7.8×10^5 Mev. The penetrating particles lose approximately 13 Mev in traversing one lead plate. The total energy of all the traversals is $2\times10^4\times13$ Mev or 2.6×10^5 Mev. The startling fact appears that the energy used in creating stars is three times greater than the energy lost by the penetrating component in the same amount of material. If instead of using only the stars we make the same type of comparison with short range heavily ionizing particles which leave one lead plate and stop in the next one without penetrating a lead plate, we get dissipation of energy of the same order of magnitude.

Practically all of the stars are produced by non-ionizing radiation, and since they are hardly ever accompanied by cascade showers it seems reasonable to assume that the producing agent is neutrons. The average energy of the neutrons, as we found above, is in the neighborhood of 100 Mev. If their average angular distribution is similar to that for the penetrating particles, they will make two traversals of one cm of lead on the average. If the nuclear cross section is 3×10^{-24} cm^2 per lead atom and if they pass 6×10^{22} lead atoms in penetrating two cm of lead, then approximately five out of six neutrons will pass through the chamber without producing a star. This means that there are $156\times50\times6$ or 4.7×10^4 energetic neutrons while 9840 penetrating particles pass through the chamber. This is nearly a ratio of five to one in favor of neutrons.

There is a group of slow protons which stop in the chamber and at the same time have enough energy to penetrate one or more lead plates. On comparing these protons with the faster penetrating particles, it is at once apparent that the protons have a maximum range very nearly equal to five cm of lead. Only two protons out of 400 stopped with a range of five cm of lead, whereas a total of 40 particles would be expected to pass through the five plates on the basis of the geometry of the chamber and the statistics of more energetic penetrating particles. This indicates that the protons are of secondary origin and we should expect to find them in equilibrium. Actually we find that the ratio of protons created in the chamber to those stopped, instead of being one, was one to twenty. We are forced to conclude that for this group of protons capable of penetrating one or more cm of lead, equilibrium is not established. None of the usual assumptions can be applied with any satisfaction to explain this situation.

The explanation appears to lie in the action of the energetic neutrons. We have just seen that the neutrons have an average energy around 100 Mev. Inside the chamber there are no free protons. All the nuclei present are heavy. The neutrons produce disintegrations and low speed protons inside the chamber. On the other hand, outside the chamber there are free protons in the wood of the trailer-laboratory and in the observer. There the neutrons can transfer their energy to protons without degradation and the protons will appear passing through the lead plates of the chamber. One cm of wood in the neighborhood of the chamber bombarded by these neutrons would be sufficient to account for the number of fast protons observed. This explains completely the large number of fast protons entering the chamber and their maximum range, and at the same time reconciles this fact with the small number of fast protons produced inside the chamber.

I wish to take this opportunity to thank Professor

Oppenheimer for many valuable suggestions in interpreting the results, and to acknowledge the support of the Rumford Fund of the American Academy of Arts and Sciences, the Fund for Astrophysical Research, and the American Philosophical Society.

* Guggenheim Memorial Fellow.
[1] A. Widhalm, Zeits. f. Physik **115**, 481 (1940).

On the Virtual State of the Deuteron

LAMEK HULTHÉN
University of Lund, Lund, Sweden
March 6, 1942

IN a previous paper[1] it was shown that

$$\frac{d^2\phi}{d\xi^2}+\left(a+b\frac{e^{-\xi}}{\xi}\right)\phi=0, \tag{1}$$

being the simplest possible form of the Schrödinger equation for the deuteron in the ^1S and ^3S states,[2,3] has no discrete eigenvalue, if $b<B_1=1.6798$, one eigenvalue a—i.e., one stable energy level—if $B_1<b<B_2=6.44_7$, etc.[4] Putting $b=B_1-\beta$, $|\beta|\ll B_1$, and supposing a to be of the same order of size as β^2, we can with great accuracy write the normalized solutions of (1) for the continuous spectrum ($a>0$) as follows

$$\phi(\xi)=\frac{(1-e^{-\xi}-c(1-e^{-\xi})^2)}{(1-c)\pi^{\frac{1}{2}}a^{\frac{1}{4}}}\sin(a^{\frac{1}{2}}\xi+\delta) \tag{2}$$

with the constants c and δ ($=\delta_\infty$) given by

$$c=0.3489-0.0296\beta, \quad \operatorname{tg}\delta=2.2655a^{\frac{1}{2}}/\beta.$$

A natural definition of the virtual eigenvalues for an equation like (1) is obtained by requiring the average of the potential energy to be minimum for the state in question. Thus, in our case, a is a virtual eigenvalue, if it makes the expression

$$S(a)=b\int_0^\infty \frac{e^{-\xi}}{\xi}\phi^2 d\xi \tag{3}$$

a maximum. An equivalent definition, quite analogous to the definition of the discrete eigenvalues, is given by the condition: $\operatorname{tg}^2\delta=1$.

For small β we then get

$$a_{\text{virt}}=0.1948_4\beta^2 \tag{4}$$

for positive *and* negative β. From a purely mathematical point of view there is in general an infinite number of virtual eigenvalues for equations of the type considered here, but in our case even the second maximum is far too flat to possess any physical importance. Moreover, the first and lowest virtual state is strongly pronounced only when b is very close to one of the critical values B_1, B_2, etc.

For small negative β there exists a discrete eigenvalue a_1:

$$a_1=-0.1947_9\beta^2. \tag{5}$$

The obvious symmetry of (4) and (5) with respect to the zero level seems to be a general feature of problems of this kind: exact validity has been verified for the rectangular potential well and the potential function $e^{-\xi}/(1-e^{-\xi})$.

Although the virtual state of a system described by an equation like (1) can thus be calculated exactly, one cannot, of course,—apart from the question of the strict validity of (1) for the deuteron—expect any corresponding accuracy in experiments, because the breadth of the energy level is of the same order of size as the energy itself.

As (4) agrees surprisingly well with the relation suggested by Belinfante,[5] the determination of the fundamental constants g_1 and g_2 of the meson theory is not appreciably influenced by the results presented here.[1,3,6]

Further details will be published elsewhere.

[1] L. Hulthén, Arkiv för mat. astr. och fysik, **A28**, No. 5 (1942).
[2] A. H. Wilson, Proc. Camb. Phil. Soc. **34**, 365 (1938).
[3] C. Møller and L. Rosenfeld, Danske Vidensk. Selsk. math.-fys. Meddelelser **17**, No. 8, 57 (1940).
[4] Cf. also Wilson, reference 2, besides R. Sachs and M. Goeppert-Mayer, Phys. Rev. **53**, 991 (1938).
[5] F. J. Belinfante, Dissertation (1939), p. 45.
[6] C. Møller, Danske Vidensk. Selsk. math.-fys. Meddelelser **18**, No. 6 (1941).

Secondary Scattering of Electrons in Silicon

R. P. JOHNSON AND W. R. GRAMS
Research Laboratory, General Electric Company, Schenectady, New York
April 1, 1942

IN electron diffraction patterns of polycrystalline CuCl Germer[1] finds the (222) ring roughly 200 times as strong as it should be, though the (200) ring has its expected very low intensity. He explains this anomaly by supposing that most of the electrons reaching the (222) ring have actually suffered two successive first-order (111) reflections in the same crystal. His experiments show, in support of this view, that the (222) ring is practically absent if the crystals are sufficiently small, and increases in relative prominence with increasing crystal size until it is approximately as strong as the (400) ring.

We can offer, as another instance of the same effect, our observation that the (222) ring appears prominently in electron diffraction patterns of polycrystalline silicon, where it should be not merely weak but entirely absent. We have examined transmission samples made by settling powdered Si from air suspension onto Formvar films, and reflection samples prepared by rubbing bulk polycrystalline Si on emery paper—here the diffracting microcrystals are in a dust layer adherent to but not continuous with the bulk Si crystals. In every pattern the (222) ring has the same intensity, estimated by eye, as the adjacent (400) ring. Contrastingly, no trace of a (200) ring can be found.

The (222) ring, in our patterns, contains several distinct spots, each spot arising from a single crystal of the sample. We find that every prominent (222) spot is associated with a prominent spot on the (111) ring, while the reverse correspondence is not nearly complete. This fact seems to us to speak decisively in favor of Germer's explanation, and against the alternative view that the diamond type extinction rule is here for some reason relaxed with respect to (222). If the observed (222) spots were true second-order reflections from (111) planes, the correspondence either should be complete in both directions or should fail as often in one direction as in the other. On the other hand, if the (222) spots are actually due to twice-reflected electrons, each pseudo-(222) ray should be accompanied by its parent (111) ray, though (because some crystals are too

thin for secondary scattering and others are unfavorably malformed) not every (111) ray should have accompanying progeny.

[1] L. H. Germer, Phys. Rev. **61**, 309 (1942).

Absence of High Energy Beta-Rays from Br^{82}

MARTIN DEUTSCH
Massachusetts Institute of Technology, Cambridge, Massachusetts
April 23, 1942

J. ROTBLAT[1] has reported a group of high energy beta-rays from the disintegration of Br^{82}, in addition to the main group of maximum energy 0.46 Mev. From absorption measurements the end point was estimated to occur at about 1.2 Mev, and the abundance to be about 3 percent of the main group. These findings were in contradiction to the author's previous beta-ray spectrometer measurements.[2] Since the disintegration of Br^{82} is accompanied by three gamma-rays, the hardest of which has an energy of 1.35 Mev,[3] the high energy electrons could be Compton recoil or photoelectrons due to these gamma-rays.

The widespread use of this isotope in biological studies as well as the fact that its disintegration scheme is otherwise quite well understood,[3] made it appear desirable to determine the origin of the high energy group. An absorption experiment was therefore performed with a view to reducing the secondary effects due to gamma-rays to a minimum. The source was prepared by the method of Roberts and Irvine[4] from $C_2H_2Br_4$ irradiated by slow neutrons from the M. I. T. cyclotron. It was deposited as a thin layer of AgBr on a small piece of filter paper which, in turn was suspended on a narrow strip of paper at least 10 cm from all solid material with exception of the collimating diaphragm as shown in Fig. 1A. The number of secondaries from this diaphragm should not be materially affected by the addition of absorber. The curve marked "good geometry" in Fig. 1 represents the data obtained in this arrangement and shows no evidence of a high energy group. The dotted line indicates approximately the result expected in the presence of such a group of 3-percent abundance.

In order to increase the accuracy of the experiment further, it was repeated in the arrangement shown in Fig. 1B. The beta-rays had to pass through the lower counter into the upper one and only coincident counts in both counters were recorded. This reduced the relative gamma-ray background by a factor of four compared to the arrangement shown in Fig. 1A, the remaining gamma-ray counts being due to recoil electrons produced in one counter passing into the other. The curve marked "coincidences" in Fig. 1 shows the results after correcting for absorption in the counter windows. The dotted line again indicates the "tail" expected from a high energy group. We may conclude that no such group is present with an abundance as high as 0.5 percent of the main group. This is in agreement with the disintegration scheme proposed by Roberts, Downing, and Deutsch.[3]

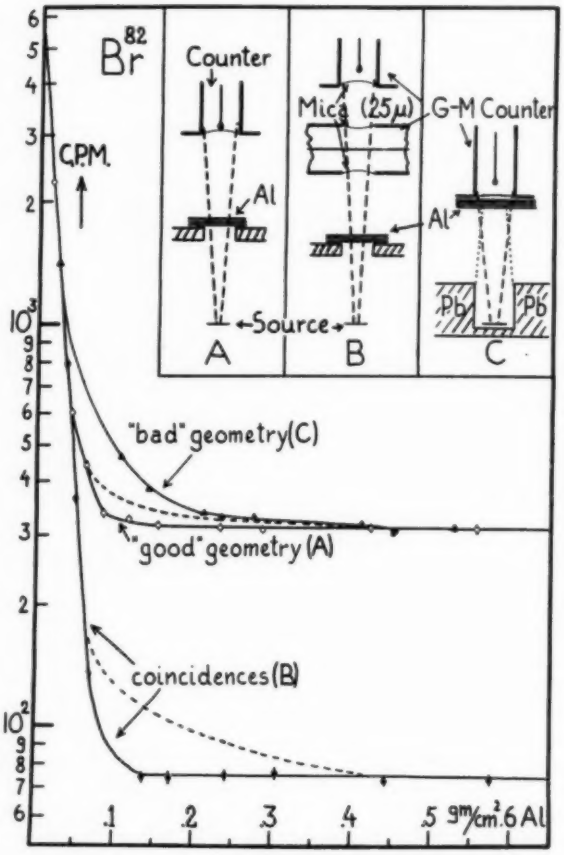

FIG. 1

Finally an absorption experiment was performed under conditions favoring effects due to secondary electrons. In this arrangement, shown in Fig. 1C, a considerable number of secondary electrons produced in the lead "well" surrounding the source, should be absorbed by addition of aluminum absorbers. The curve marked "bad geometry" in Fig. 1 does indeed show a shape very similar to that expected from a high energy beta-ray group. Rotblat's results are therefore probably best interpreted by assuming that his experimental arrangement was intermediate between those shown in Fig. 1A and C.

This effect is to be expected whenever beta-rays are accompanied by gamma-rays whose energy is greater than the maximum energy of the beta-rays. We have found the high energy electrons from Fe^{59} reported by Livingood and Seaborg[5] to be also due to secondary effects. A detailed study of this latter disintegration will be published shortly.

[1] J. Rotblat, Nature **148**, 371 (1941).
[2] M. Deutsch, Phys. Rev. **59**, 684A (1941).
[3] A. Roberts, J. R. Downing, and M. Deutsch, Phys. Rev. **60**, 544 (1941).
[4] A. Roberts and J. W. Irvine, Jr., Phys. Rev. **53**, 608 (1938).
[5] J. J. Livingood and G. T. Seaborg, Phys. Rev. **54**, 51 (1938).

Proceedings of the American Physical Society

METROPOLITAN SECTION MEETING, MARCH 27, 1942

THE second meeting of the Metropolitan Section of the American Physical Society for the season 1941–1942 was held on Friday, March 27, 1942 at Brooklyn College. The following papers were presented:

Afternoon session, 3:00 P.M.

Counters, Their Characteristics and the Theory of Their Discharge. S. A. KORFF

The Polarization of Electrons. CLIFFORD SHULL

The Concept of Entropy. K. K. DARROW

Evening session, 7:30 P.M.

Electric Fish (with demonstration). R. T. COX.

The following officers were elected for the season 1942–1943:

Chairman,	RICHARD T. COX
Vice Chairman,	HELEN A. MESSENGER
Secretary-Treasurer,	W. S. GORTON
Elected Members of the Executive Committee	L. H. GERMER
	JOHN A. WHEELER

W. S. GORTON,
Secretary-Treasurer

Information For Contributors

THE Editors of THE PHYSICAL REVIEW would be aided in their task if the following items were used as a guide by all contributors.

MANUSCRIPTS

Send manuscripts to J. W. Buchta, Department of Physics, University of Minnesota, Minneapolis, Minnesota.

Papers must be in English, typewritten double spaced with wide margins on a durable white paper, preferably lettersize. The original copy, not the carbon, should be submitted.

For general style, spellings, abbreviations and form, recent issues of this journal should be consulted.

ABSTRACTS

An abstract must accompany each article. It should be adequate as an *index* and as a *summary*. As an index it should give all subjects, major and minor, concerning which new information is presented. As a summary it should give the conclusions of the article and all numerical results of general interest.

MATHEMATICAL EXPRESSIONS

Make all expressions clear to the typesetter. Identify in the margin of the manuscript Greek letters and unusual symbols.

Use fractional exponents instead of root signs.

Avoid complicated exponents and subscripts. Should it be necessary to repeat a complicated expression a number of times it should be represented by some convenient symbol.

The solidus (/) should be used wherever possible for fractions.

REFERENCES

References should appear as footnotes, numbered consecutively, and arranged thus:

[1] A. B. Smith, Phys. Rev. **41**, 852 (1932).
[2] G. R. Harrison, *Atoms in Action* (William Morrow & Company, New York, 1939), first edition, p. 30.

FIGURES AND TABLES

Legends for figures must accompany manuscript. Each table should have a caption. These in all cases should be complete in themselves so as to make the data intelligible to the reader without reference to the text. Each figure and table should be cited in sequence in the text.

LINE DRAWINGS AND PHOTOGRAPHS

Plan figures for reduction to one third or one fourth the original size. Wherever possible arrange figures so that after reduction they will not be wider than three inches. Lettering must be large enough to be readable (about 3 mm high) after reduction. The figures should be so arranged that the space is used efficiently.

Line drawings must be made with India ink on white paper or tracing cloth. Coordinate paper is not desirable, but if used must be blue-lined and all coordinates to be reproduced drawn with India ink.

Drawings which cannot be used will be returned to the author.

Photographs of drawings seldom are satisfactory. They often do not show clear black and white contrasts and are not suitable for relettering which is sometimes necessary. Photographs of apparatus seldom give as much information as drawings.

Please avoid round or oval photographs.

ALTERATIONS

Take great care that each manuscript is typographically accurate. A limited number of alterations in proof are unavoidable, but the cost of making extensive alterations after the article has been set in type will be charged to the author.

Proof and all correspondence concerning papers in the process of publication should be addressed to the Publications Manager, American Institute of Physics, 175 Fifth Avenue, New York, New York.